Multi-hazard performance of steel moment frame buildings with collapse prevention systems in the central and eastern United States

Johnn Paul Judd

Dissertation submitted to the faculty of the Virginia Polytechnic Institute and State University in partial fulfillment of the requirements for the degree of

Doctor of Philosophy
In
Civil Engineering

Finley A. Charney, Chair
Martin C. Chapman
Matthew R. Eatherton
Roberto T. Leon
Adrian Rodriguez-Marek

May 4, 2015
Blacksburg, Virginia

Keywords: Earthquake Engineering, Wind Engineering, Nonlinear Dynamic Analysis, Structural Steel Buildings, FEMA P-695, FEMA P-58, Risk

Multi-hazard performance of steel moment frame buildings with collapse prevention systems in the central and eastern United States

Johnn Paul Judd

ABSTRACT

This dissertation discusses the potential for using a conventional main lateral-force resisting system, combined with the reserve strength in the gravity framing, and or auxiliary collapse-inhibiting mechanisms deployed throughout the building, or enhanced shear tab connections, to provide adequate serviceability performance and collapse safety for seismic and wind hazards in the central and eastern United States. While the proposed concept is likely applicable to building structures of all materials, the focus of this study is on structural steel-frame buildings using either non-ductile moment frames with fully-restrained flange welded connections not specifically detailed for seismic resistance, or ductile moment frames with reduced beam section connections designed for moderate seismic demands.

The research shows that collapse prevention systems were effective at reducing the conditional probability of seismic collapse during Maximum Considered Earthquake (MCE) level ground motions, and at lowering the seismic and wind collapse risk of a building with moment frames not specifically detailed for seismic resistance. Reserve lateral strength in gravity framing, including the shear tab connections was a significant factor. The pattern of collapse prevention component failure depended on the type of loading, archetype building, and type of collapse prevention system, but most story collapse mechanisms formed in the lower stories of the building. Collapse prevention devices usually did not change the story failure mechanism of the building. Collapse prevention systems with energy dissipation devices contributed to a significant reduction in both repair cost and downtime. Resilience contour plots showed that reserve lateral strength in the gravity framing was effective at reducing recovery time, but less effective at reducing the associated economic losses. A conventional lateral force resisting system or a collapse prevention system with a highly ductile moment frame would be required for regions of higher seismicity or exposed to high hurricane wind speeds, but buildings with collapse prevention systems were adequate for many regions in the central and eastern United States.

ACKNOWLEDGEMENTS

Many people have contributed to this research. I am grateful most of all to my advisor, Dr. Finley Charney, for providing an opportunity to do earthquake and wind engineering research that is both exciting and meaningful, and for the mentoring he has provided throughout my doctoral studies.

I sincerely appreciate the support of my graduate committee. Thanks to Dr. Roberto Leon for many thoughtful discussions, for introducing me to forensic engineering and civil engineering failures, for encouraging me in the field of disaster resilience, and for providing the opportunity to meet many leaders in our profession. Thanks to Dr. Matthew Eatherton for helping me to be a better structural engineer, for several insightful comments, and for helping me to be successful in full-scale experimental testing. Thanks to Dr. Adrian Rodriguez-Marek for introducing me to risk analysis—it has been both challenging and rewarding. And thanks to Dr. Martin Chapman for help understanding seismology and earthquake hazards and for his friendship along the way.

I would also like to acknowledge the support of the ASCE/SEI Ad-Hoc Wind Performance-Based Design Committee, chaired by Don Scott and Larry Griffis. I appreciate the guidance provided by Larry Griffis of Walter P. Moore Inc. in Austin, Texas on wind engineering and for driving a big truck with me in Canada. I appreciate the assistance on understanding wind tunnel testing given by Daryl Boggs of Cermak Peterka Petersen (CPP Inc.) in Fort Collins, Colorado, and Peter Irwin and Bujar Morova of Rowan Williams Davies and Irwin (RWDI) Inc., in Guelph, Ontario. I am grateful for the generous assistance of Nicholas Luco (USGS in Golden, Colorado) in risk analysis, and for Dimitrios Vamvatsikos (National Technical University of Athens) in supplying hysteresis parameters developed in FEMA P-440A (FEMA 2009b).

This research would not have been possible without time and assistance provided by friends and family. As in the past, my brother Glenn Judd was an excellent resource for computational questions. The scheduler he wrote was a life-saver. My wife Sharon spent countless hours proofreading and giving constructive comments. I also appreciate the support of my graduate colleagues, Ebrahim Abbas, Adam Phillips, and Chris Galitz in the experimental research, and Armen Adekristi in furnishing the spectral matching algorithm. I especially appreciate the support of my research group, Jeena Jayamon, Andy Hardyneic, Francisco Flores, and Jordan Jarrett. Your help has been invaluable.

This research was supported by the National Institute of Standards and Technology (NIST) grant No. 60ANB10D107. Financial support was also provided by the Charles E. Via, Jr. Doctoral Fellowship endowment at Virginia Tech, the Department of Civil and Environmental Engineering, and Simpson Strong-Tie, Inc. in Pleasanton, California. I would like to express appreciation to Steven Pryor of Simpson Strong-Tie, and to Igor Marinovic of BlueScope Steel Ltd., in Memphis, Tennessee, for their support.

I have attempted to eliminate errors, but it is inevitable that there are deficiencies in this dissertation. Those, along with the opinions and recommendations expressed, are my responsibility, and do not necessarily reflect views of people and organizations acknowledged.

TABLE OF CONTENTS

LIST OF TABLES

LIST OF FIGURES

Chapter 1

INTRODUCTION

This chapter describes the motivation for the research, provides background on seismic design, multi-hazard performance, and performance-based wind design. The objective and scope of research are defined. The chapter also summarizes the organization and content of the dissertation.

1.1 Motivation and Background

Extensive regions of the United States are at risk from multiple hazards. Earthquakes are a serious threat not only in the western United States, but in much of the central and eastern United States. For example, the 5.7-magnitude 2011 Virginia earthquake—felt by more people in the United States than any previous quake—caused damage in excess of $100 million. But large seismic events are not the only concern. Since 2009, for example, Oklahoma has had over twenty magnitude 4.0 to 4.8 tremors (USGS-Oklahoma Geological Survey 2014), making the state more seismically "active" per square mile than California.

Windstorms and related coastal inundation have caused over 4,000 casualties and led to property losses in excess of $250 billion over the past 16 years (NIST 2014b). The 2012

derecho, an intense fast-moving windstorm, is a recent case in point. The windstorm caused substantial damage and cut power to millions of people in the eastern United States.

Tornadoes alone have devastated communities and caused over 5,000 casualties since 1950—more casualties than for earthquakes and hurricanes combined during the same period (NIST 2014a). The 2011 Joplin, Missouri Tornado, one of 1,691 tornadoes in the United States that year, was especially damaging. The Enhanced Fujita (EF) 5 intensity tornado carved a mile-wide path of destruction, caused 161 fatalities, injured over a thousand, and produced approximately $3 billion in property losses.

1.1.1 Seismic Design

The conventional practice in seismic resistant design of new buildings in the United States (FEMA 2009c; ASCE 2010) is to proportion and detail ordinary (Occupancy and Use Category II) structures such that there is no more than a 10% probability that the structure will collapse when subjected to the risk-based Maximum Considered Earthquake ground motions (MCE_R) (ASCE 2010, Table C.1.3.1b), which generally have a return period, or mean recurrence interval (MRI), of approximately 2,475 years, and that risk of collapse does not exceed 1% in 50 years (FEMA 2009c). While no explicit calculations are required to assess the true likelihood of collapse performance, safeguards are provided by well-established system configuration and detailing rules and by limits on computed drift.

The seismic performance expectations for new buildings subjected to ground motions that occur more frequently than the MCE are loosely stated in the commentary for current design standards [e.g. ASCE (2010) 7-10; 2009 NEHRP Recommended provisions], but no calculations are required to assess the adequacy of the building's performance under such motions. However,

there is significant historical evidence that earthquakes along the west coast of the United States that occur more frequently than the MCE ground motions, and which produce less severe ground shaking than the MCE ground motions, can cause significant and unacceptable levels of damage. The 1994 Northridge California Earthquake, which caused an estimated $57 billion in losses (Seligson and Eguchi 2005), is a case in point. This earthquake had a magnitude of 6.7, and earthquakes of equivalent size are expected to reoccur once every 35 to 40 years in that area. Although it is technically incorrect to associate a single event with a return period, Northridge was one of many moderate-magnitude quakes that caused extensive economic loss in California during the span of only a few decades (Hamburger et al. 2012). The predicted recurrence of the ground motions that resulted from these earthquakes was lower than the design recurrence intervals yet the damage was above acceptable levels. Thus, a significant shortcoming of the current practice for designing new buildings is that it does not explicitly address the lower hazard-level ground motions.

1.1.2 Wind Design

The conventional practice in wind resistant design of new buildings in the United States (ASCE 2010) is to proportion and detail ordinary structures to remain elastic when subjected to strength-level design wind speeds, which have a 700-year MRI. The design wind speeds accounts for synoptic wind (regional atmospheric circulation due to high low pressure regions, including hurricanes). Non-synoptic wind (local wind from thunderstorms and derecho downbursts and tornado vortices) is not typically accounted. Conventional wind design does consider more frequently occurring wind speeds, but the probability of wind collapse is not calculated. Although no target collapse risk for wind has been established, it is assumed that the

building code provisions (ASCE 7-10) provide a target annual probability failure rate of $5x10^{-6}$ collapses/year to $7x10^{-7}$ collapses/year for ordinary structures (ASCE 2010, Table C.1.3.1a).

1.1.3 Multi-Hazard Performance

A broadened design philosophy called performance-based engineering has emerged as a potential remedy, where the goal is to meet or exceed predefined performance objectives under different levels of hazard (FEMA 2006, 2012a; ICC 2012b). Typical performance objectives for buildings are provided in Table 1.1. The objectives described in Table 1.1 were adapted in part from the *International Performance Code* (ICC 2012b) rubric and define how a building structure is expected to perform during an event (earthquake or windstorm) in terms of the impact, described in terms of a maximum tolerable level of damage.

Table 1.1 Performance objectives in terms of tolerable impact (adapted from ICC 2012b)

Seismic or Wind Hazard			Building Occupancy and Use (Risk Category)			
Event	Occurrence	Probability of Exceedence	Infrequent (I)	Ordinary (II)	Critical (III)	Essential (IV)
Small	Frequent	50% in 30 years (43-year MRI)	**Moderate**	**Mild**	**Mild**	**Mild**
Medium	Occasional	20% in 50 years (225-year MRI)	**High**	**Moderate**	**Mild**	**Mild**
Large (DBE)	Rare	10% in 50 years (475-year MRI)	**Severe**	**High**	**Moderate**	**Mild**
Large	Rare	7% in 50 years (700-year MRI)	**High**	**Moderate**	**Mild**	**Mild**
Very Large	Very Rare	3% in 50 years (1,700-year MRI)	**Severe**	**High**	**Moderate**	**Moderate**
Very Large (MCE)	Very Rare	2% in 50 years (2,475-year MRI)	**Severe**	**Severe**	**High**	**Moderate**

- **Mild** impact means there is no loss of structural strength and stiffness, and the building is safe to occupy. Nonstructural systems are fully operational, and the overall extent and cost of damage is minimal.

- **Moderate** impact means there is some structural damage, but such damage is limited and repairable. There may be delay in occupancy. Nonstructural systems are operational but may require repair. Emergency systems remain fully operational. The extent and cost of damage is significant in some areas.

- **High** impact means there is significant damage to structural components (but "no large falling debris"). Repair is possible, but significant delays in occupancy are expected. Nonstructural systems are inoperable; emergency systems are significantly damaged, but remain operational. Severe Impact means there is significant structural damage, but the gravity-load carrying system is still intact. Occupancy and repair may not be possible or feasible. There may be multiple casualties.

Although there is general agreement for the recurrence intervals assigned to the large, Design Basis Earthquake (DBE), and the very large, Maximum Considered Earthquake (MCE) ground motion events, various performance-based design provisions assign different recurrence intervals for lower (serviceability and immediate occupancy) level ground motion. [See commentary on the *International Performance Code* (ICC 2012b).] These intervals can vary anywhere from a 25-year MRI to a 72-year MRI. Similarly, wind design of ordinary building occupancy and use (Category II) structures is associated with large (rare) wind events (700-year

MRI). Critical and essential (Category III and IV) structures are associated with very-large (very rare) wind events (1,700-year MRI). Typical recurrence intervals used for serviceability wind design vary from 100-year MRI on the high end to 10-year MRI or even less (a 1-year MRI is often used in design of high-rise buildings).

Traditional performance-based seismic analysis is often based on the characteristics of the seismicity of tectonic plate boundaries, like the western United States, where it has been the experience that frequent and occasional earthquakes can be very significant, as was the case with Northridge. [See, for example, steel frame, reinforced concrete frame, and masonry building performance assessments reported by Haselton and Churapalo (2012).] While this expectation is appropriate for the western United States, it is not necessarily correct in the central and eastern United States. The nature of the overall seismic hazard is quite different in the central and eastern United States. Large magnitude earthquakes are possible outside the west, but they are rare.

The implication is that in many areas of the central and eastern United States, the only seismic limit state of importance is collapse prevention. Ground shaking associated with more frequently occurring events is not likely to be damaging, and in fact, the gravity and wind system is going to be capable of resisting the most probable motions (Judd and Charney 2014b). Of course it is not prudent to ignore the likelihood of a major earthquake, and collapse prevention is still essential.

Thus, while the goal of less than 10% probability of seismic collapse given the MCE ground motion is equally applicable in both the western and the central and eastern United States, and the desire for good performance at lower level shaking is also equally applicable, it seems that the very distinct differences in the temporal distribution of the level of shaking in the

different portions of the country would lead to different conceptual bases for providing acceptable performance. However, this is not the case because for a given ground motion intensity, buildings in the central and eastern United States are designed in essentially the same manner as buildings in the western part of the country.

1.1.4 Performance-Based Wind Design

Performance-based wind engineering has been identified as a national research priority (CTBUH 2014; NIST 2014b). To date, several performance-based frameworks have been developed for wind engineering (van de Lindt and Dao 2009; Ciampoli et al. 2011; Griffis et al. 2012; Kareem et al. 2013) and hurricane engineering (Barbato et al. 2013). Aswegan et al. (2015) developed a procedure for nonstructural damage control of steel buildings under serviceability-level wind. Nonlinear analysis has been used to determine the structural reliability of tall concrete buildings (Hart and Jain 2013), and to determine inelastic damage accumulated in tall buildings during hurricanes (Chen 1999; Chen and Davenport 2000; Gani and Légeron 2011). Muthukumar et al. (2012) evaluated the performance of an existing concrete shear wall building. Still, general application of nonlinear analysis to performance-based wind analysis is undeveloped.

One motivation for a performance-based nonlinear wind analysis is that conventional wind-designed buildings may be overly conservative. Member stresses are limited to the linear elastic range for strength-level events (700-year MRI for typical occupancy and usage). An additional motivation for a nonlinear analysis is to determine collapse capacity of buildings—especially storm shelters (e.g. FEMA 2008a,b) and critical facilities in tornadoes or other extreme events.

Another motivation is that the possibility of employing buildings designed for wind to achieve adequate seismic performance is economically appealing. More than 80% of the cost of constructing a new steel building may be attributed to material costs, fabrication labor costs, and erection labor costs (Carter et al. 2000). The remaining construction costs include special inspections and other additional costs, such as scheduling constraints. Ductile connections and detailing drive up construction costs (e.g. Batt and Odeh 2005), and invoking "R=3" provisions leads to increased demands (and costs), but not necessarily increased performance (Hines and Fahnestock 2010).

1.2 Objectives and Scope

The objective of this research was to determine the potential for using a conventional main lateral-force resisting system, combined with the reserve strength in the gravity framing and/or auxiliary collapse-inhibiting mechanisms deployed throughout the building, or enhanced shear tab connections—collectively termed a collapse-prevention system—to provide adequate serviceability performance and collapse safety for seismic and wind hazards in the central and eastern United States.

While the concept is intended to be applicable to building structures of all materials, the focus of this study was on structural steel-frame buildings using either non-ductile moment frames not specifically detailed for seismic resistance, or ductile moment frames designed for moderate seismic demands. The focus of the research is a proof-of-concept and global behavior (i.e. building, or region behavior). Design and detailing of specific collapse prevention devices is outside the scope of this research.

The applicability of the concept to steel moment-frame buildings commonly constructed in the central and eastern United States was determined using a set of archetypical short period (1-story and 2-story) and long period (4-story, 8-story, and 10-story) office buildings that employed either a non-ductile moment frame with directly welded flange fully-restrained moment connections (i.e. AISC 2011a, Figure 12-4a), or a ductile moment frame with a reduced beam section (RBS) fully-restrained moment connection (i.e. AISC 2011b, Figure 5.1) designed for moderate seismic demands. The reserve lateral strength in the gravity framing was considered and collapse inhibiting devices (slack-cables, loose-linkages, or telescoping braces) were deployed throughout the building. Alternatively, shear tab connections to the strong axis of the column were enhanced by installing T-stub type flange connectors.

The vulnerability of the archetype structural systems to seismic and wind side-sway collapse (collapse fragility) was determined by conducting gravity, frequency, nonlinear static "pushover" analyses, followed by conducting a series of nonlinear dynamic response history analyses of increasing seismic or wind intensity until side-sway collapse, following the FEMA P-695 (FEMA 2009a) methodology. Uncertainty in the collapse assessments was considered by treating separately the inherent variability of seismic and wind hazards (aleatory uncertainity) and the variability due to imperfect structural modeling, testing, and construction (epistemic uncertainty) (Ang and Tang 2006). Aleatory uncertainty of seismic and wind demands for the ground motion and wind record sets was determined directly using record-to-record dispersion in the structural analysis results. Epistemic uncertainty was determined subjectively, using qualitative rating systems.

Seismic performance was evaluated using a Monte Carlo simulation using the FEMA P-58 (FEMA 2012a,b,c,d) framework. The sensitivity of the collapse assessments was evaluated for several key aspects of analytical modeling and hazard uncertainty.

The risk of collapse was determined by integrating collapse fragility and hazard, accounting for directional effects and site response for seismic hazards, and accounting for non-synoptic events for wind hazards. The combined seismic and wind (multi-hazard) risk of collapse was determined and compared with societal levels of acceptable risk.

1.3 Dissertation Organization

This dissertation is organized into nine chapters and three appendices.

- Chapter 1 provides background for the research, and explains the motivation for the current study. The objectives and scope of the research are defined. The chapter also gives an overview of the organization of the dissertation.

- Chapter 2 briefly describes important features of seismic and wind hazards in the context of structural engineering. For seismic hazards, ground motions, earthquake rate, ground motion attenuation, site response, and spectral shape are discussed. For wind hazards, basic wind speeds and non-synoptic wind hazards are discussed. Finally, a comparison is made between elastic seismic and wind base shear forces and multi-hazard performance of hypothetical buildings.

- Chapter 3 describes the collapse prevention system concept and the selection and development of archetype structural systems. The archetype systems were intended to be prototypical building configurations with or without collapse prevention mechanisms, in order to determine the applicability of the CP system concept to steel moment-frame buildings commonly constructed in the central and eastern United States. Reserve lateral strength in the gravity framing system is discussed. Delayed-stiffness collapse inhibiting mechanisms are described, as well as optional energy dissipation devices. Enhanced shear tab connections, using T-stub type structural fuses, are discussed. The analytical modeling and nonlinear analysis approach are also included.

- Chapter 4 assesses the seismic collapse safety of the archetype structural systems with and without collapse prevention systems. The collapse vulnerability (collapse fragility) was determined using a sequence of gravity, frequency, nonlinear static "pushover" analyses, followed by nonlinear dynamic response history analyses incrementally scaled, with respect to a target spectrum, until side-sway collapse. The risk of seismic collapse was determined by integrating collapse fragility and hazard, accounting for directional effects and site response. Results of selected archetype systems are discussed. Finally, a comparison with the seismic collapse assessment of traditional structural systems is included.

- Chapter 5 assesses the wind collapse safety of the archetype structural systems with and without collapse prevention systems. The wind collapse vulnerability (collapse fragility) was determined using a sequence of gravity, frequency, nonlinear static "pushover"

analyses, followed by nonlinear dynamic response history analyses incrementally scaled, using an equivalent single-degree-of-freedom model and with respect to a reference wind speed, until side-sway collapse. The results of selected archetype systems are discussed.

- Chapter 6 discusses the results of parametric studies used to determine the sensitivity of seismic and wind collapse assessments to changes in hazard or structural vulnerability via analytical modeling. The seismic hazard parameters include ground motions, site response, regional risk, and intensity measures. The seismic modeling parameters include column panel zone representation, the method used to account for second-order (P-Delta) effects, column splices, risk integration method, and damping. The wind hazard parameters consider duration of wind. The wind modeling parameters include type of lateral system, static overstrength, fundamental building period, and structural system degradation of stiffness and strength.

- Chapter 7 discusses the seismic performance of archetype structural systems. Performance, in terms of repair costs and downtime, was assessed at serviceability and design hazard levels based on the structural and non-structural component fragility using floor accelerations and inter-story drift from nonlinear response history analyses. Resilience was quantified by calculating the probable loss in functionality during a reference time interval. Resilience contours were used to characterize the tradeoff between construction and repair costs, and the ability to recover rapidly after an earthquake.

- Chapter 8 assesses the multi-hazard (combined seismic and wind) risk of collapse. The multi-hazard risk was calculated by assuming that the cumulative seismic risk and the cumulative wind risk are statistically independent. The acceptable level of risk, including social amplification, is discussed. The results for selected archetype structural system are used to illustrate a multi-hazard assessment.

- Chapter 9 summarizes the findings of this research study. Conclusions and recommendations based on the results are discussed, and areas for future research are identified. The potential impact of the research is suggested.

- Appendix A contains standard analysis examples and benchmark problems to evaluate the performance of computer software used in this study for structural analysis. Appendix B discusses the design of the archetype Type I non-ductile moment frame buildings. Appendix C contains excerpts of the *OpenSees* (PEER 2012) scripts and selected modeling results for the Type I non-ductile moment frame 4-story building with enhanced shear tab connections.

Chapter 2

SEISMIC AND WIND HAZARDS

This chapter describes salient features of seismic and wind hazards as they pertain to structural engineering for buildings. For seismic hazards, ground motions, earthquake rate, ground motion attenuation, site response, and spectral shape are discussed. For wind hazards, basic wind speeds and non-synoptic wind hazards are discussed. Finally, a comparison is made between elastic seismic and wind base shear forces and multi-hazard performance of hypothetical buildings.

2.1 Seismic Hazards

2.1.1 Uniform Hazard Ground Motions

The US Geological Survey (USGS) provides ground motions (spectral accelerations) in the United States and corresponding maps for various probability levels. This data was based on the ground shaking from potential earthquakes identified in workshops. The recommendations from the workshops were then peer-reviewed by several science organizations and two expert panels. The USGS updates the ground motion values periodically (the latest version of ground motion values was released in late 2014). The 2008 United States National Seismic Hazard Maps were adopted by ASCE 7-10 and the 2009 NEHRP provisions. The maps provide 0.2-second and 1.0-

second spectral accelerations, respectively, that have a 2% probability of being exceeded in 50 years—corresponding to the MCE ground motion for the "B/C" boundary soil site classification and 5% of critical damping. Spectral accelerations for other periods and recurrence intervals are provided (but not mapped).

By way of comparison, in Europe, the Swiss Seismological Service coordinates a collaborative project—called Seismic Hazard Harmonization in Europe (SHARE)—that provides ground motion values similar to those provided by the USGS. The SHARE project involves a core team of over 50 scientists from institutions across Europe, North Africa, and Turkey, along with additional experts participating in workshops (Giardini et al. 2013a). The European map provides peak ground accelerations that have a 2% probability of being exceeded in 50 years. Ground motion values for other probability levels can be accessed through the European Facility for Earthquake Hazard and Risk (EFEHR) (Giardini et al. 2013b).

Ground motions for seismic design have traditionally been defined to provide a uniform hazard. Typically the ground motions have a 2% to 10% probability of being exceeded in 50 years, depending on occupancy and use of the structure, and the building code and region involved (ASCE 2005; FEMA 2009c; Bommer and Pinho 2006). However, it is the probability of structural collapse that is of paramount concern (ATC 1978; ATC 1984; FEMA 2009c) and, as a result, the goal of a uniform risk of collapse has replaced uniform hazard in recent design. The chief example of this is the current ASCE 7-10 ground motion maps for the United States, which are intended to provide a uniform risk of collapse of 1% probability in 50 years (Luco et al. 2007; FEMA 2009c; ASCE 2010). Another example of uniform risk design is the ASCE 43-05 approach for designing nuclear power plants (Kennedy 2011).

The difference between uniform-hazard and uniform-risk design ground motions depends on the convolution of two factors: the shape of the ground motion spectral acceleration versus annual frequency of exceedence curve (termed the "seismic hazard curve") and the structural sensitivity or vulnerability of collapse to ground motion (termed the "fragility curve"). For *new* construction it is implied that the design using uniform-hazard maps of ground motion leads to structures with fragility curves where the probability of collapse is consistent at a given hazard level. Thus, the difference between uniform-hazard and uniform risk *design* maps is primarily a reflection of the underlying differences in seismic hazard, discussed in the following section for the United States.

Seismic hazard varies within many regions of the world. In the United States differences between hazard curves in the western United States (tectonic plate boundary area) and hazard curves in the central and eastern United States (intra-plate area) are well documented (FEMA 2009c; Levendecker et al. 2000; Judd and Charney 2014a). Similar but less dramatic differences exist in Italy (tectonic plate boundary area) (Crowley et al. 2009). Of course, within some regions—especially smaller regions—the seismic hazard curves do not vary greatly. In France, for example, the shapes of the seismic hazard curves are similar (Douglas et al. 2013), and thus the distinction between a uniform-hazard and uniform-risk map is less pronounced.

2.1.2 Earthquake Rate

The rate of earthquake recurrence varies across the United States. In general, earthquakes of a given magnitude occur more frequently in the western United States than in the central and eastern United States. The cumulative earthquake rates and seismic hazard curves for four high-seismic locations shown in Figure 2.1 are used to illustrate this fact. The earthquake rate (Figure

2.1a) is estimated using the Gutenberg-Richter relationship (1944) and the magnitude and number of events in 4° latitude by 2° longitude regions based on seismic events recorded in the Advanced National Seismic System (ANSS 2013) global earthquake catalog. The earthquake rate for Memphis is approximately corrected by removing double events.

The difference in earthquake recurrence rate is also evident in the shape of seismic hazard curves (Figure 2.1b), which graphically depict the annual rate of exceeding a ground motion. Based on the 2008 USGS National Seismic Hazard Map data for 5% damping on rock (soil site class B/C boundary), the 0.2-second spectral acceleration during very large events (2,475-year MRI) in Memphis and Charleston is comparable to San Francisco and Los Angeles. Yet the intensity of shaking for small and medium events in the central and eastern United States is only a small fraction of that in the western United States.

The lower recurrence rates in the central and eastern United States mean that the dominate contributions to the overall seismic hazard come from smaller-magnitude events, compared to western United States. This difference is thought to be a reflection of a wider distribution of faults in the intra-plate region compared to tectonic boundaries.

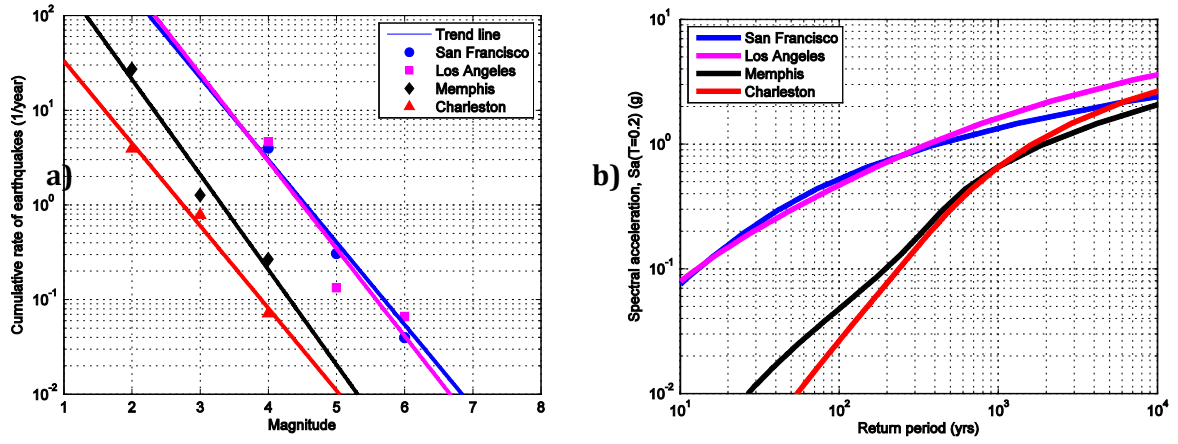

a) Cumulative earthquake rate (b) Seismic hazard curves

Figure 2.1 Regional differences in earthquake rate

The impact of the difference in earthquake rate is further illustrated in Figure 2.2, which shows the probability over the next 100 years of a 6.7-magnitude earthquake occurring in Los Angeles, California compared to Charleston, South Carolina, calculated using the USGS 2009 earthquake probability mapping application (USGS 2010). A Northridge-sized earthquake (M6.7) is expected in California within the next 30 years (SCEC 2007) and the probability over the next 100 years of a 6.7-magnitude earthquake occurring in Los Angeles is extremely high (as high as 100% in many locations), but is less than 15% in Charleston, South Carolina, although strong quakes of this size are possible in both locations. For comparison, a Mineral, Virginia-sized earthquake (M5.8) is expected to occur in the northern Virginia area every 752 years or so (Chapman 2015).

Differences between seismic ground shaking are plainly evident in many regions and across a wide range of low-intensity hazard levels (Judd and Charney 2014a). For example, Figure 2.3 to Figure 2.6 shows maps (contour lines of constant values) of the ratio of spectral accelerations for different MRI compared to the MCE (2,475-year MRI) ground motion. The top map compares the 0.2-sec spectral accelerations (S_s), and the bottom map compares the 1.0-sec spectral accelerations (S_1).

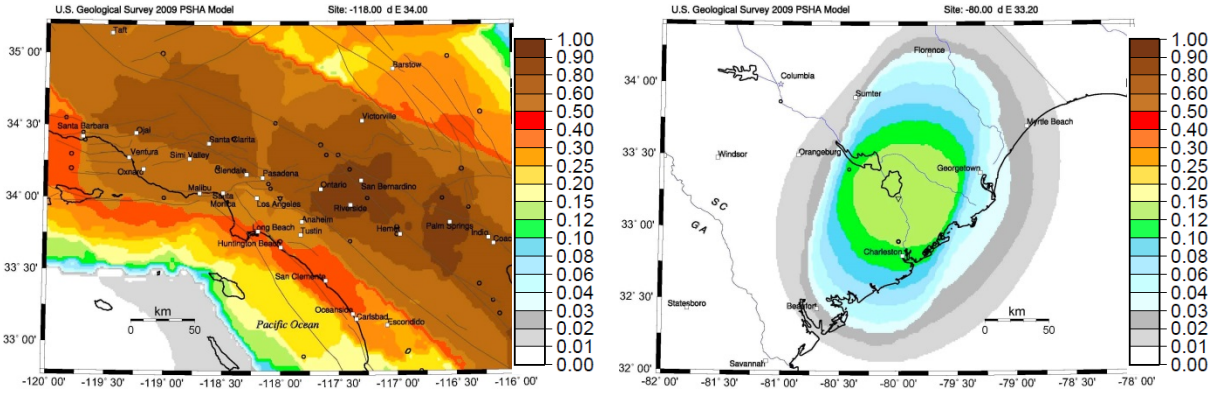

a) Los Angeles, California b) Charleston, South Carolina

Figure 2.2 Probability of exceeding a 6.7-magnitude earthquake in 100 years

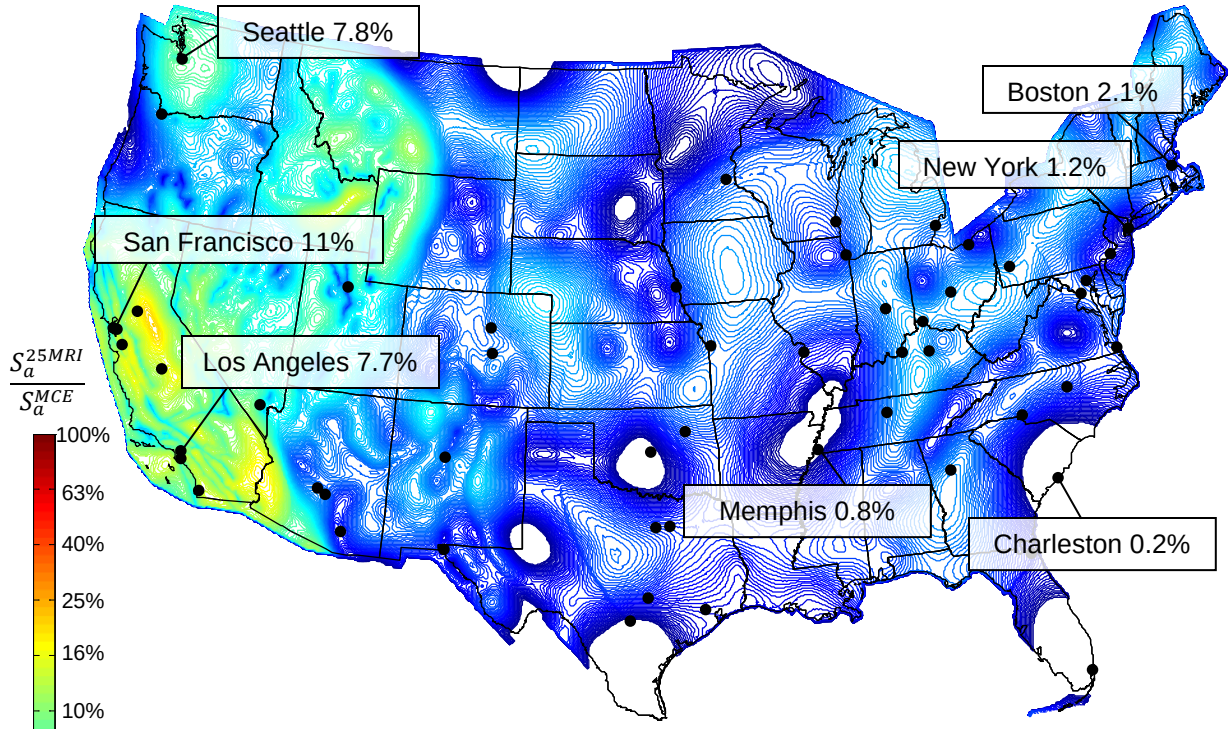

a) 0.2-second spectral acceleration (S_s)

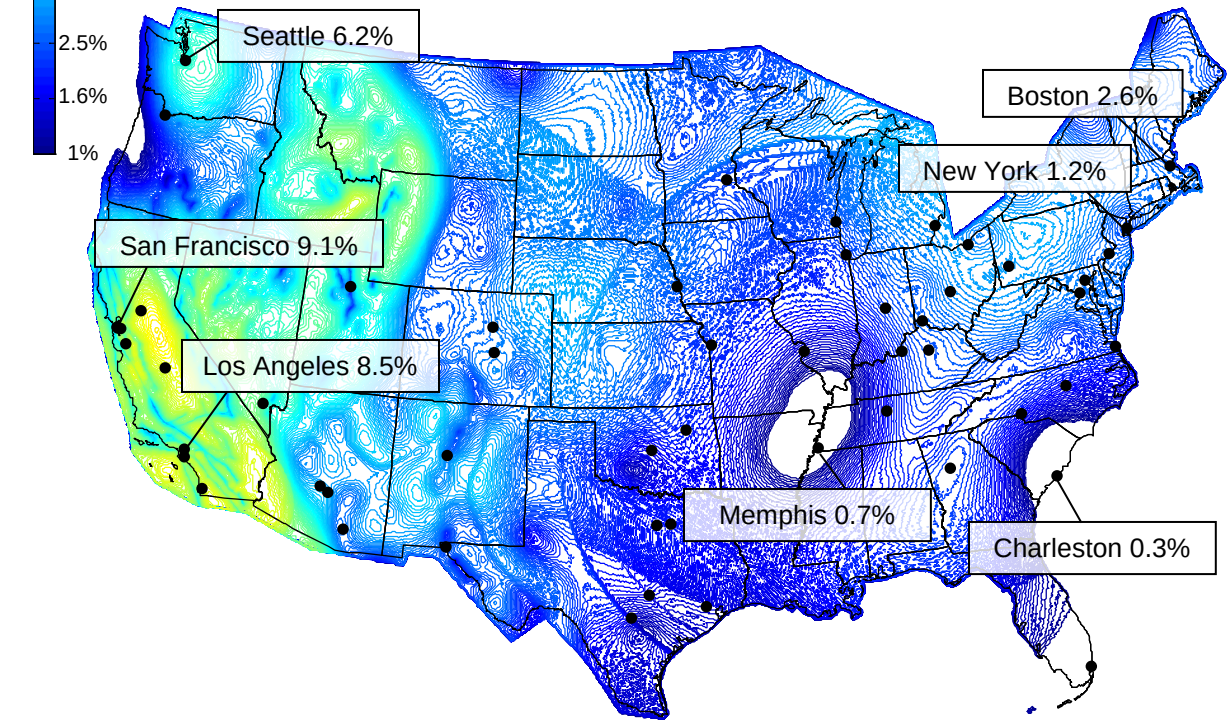

b) 1.0-second spectral acceleration (S_1)

Figure 2.3 Ratio of 25-year MRI spectral acceleration compared to MCE ground motion

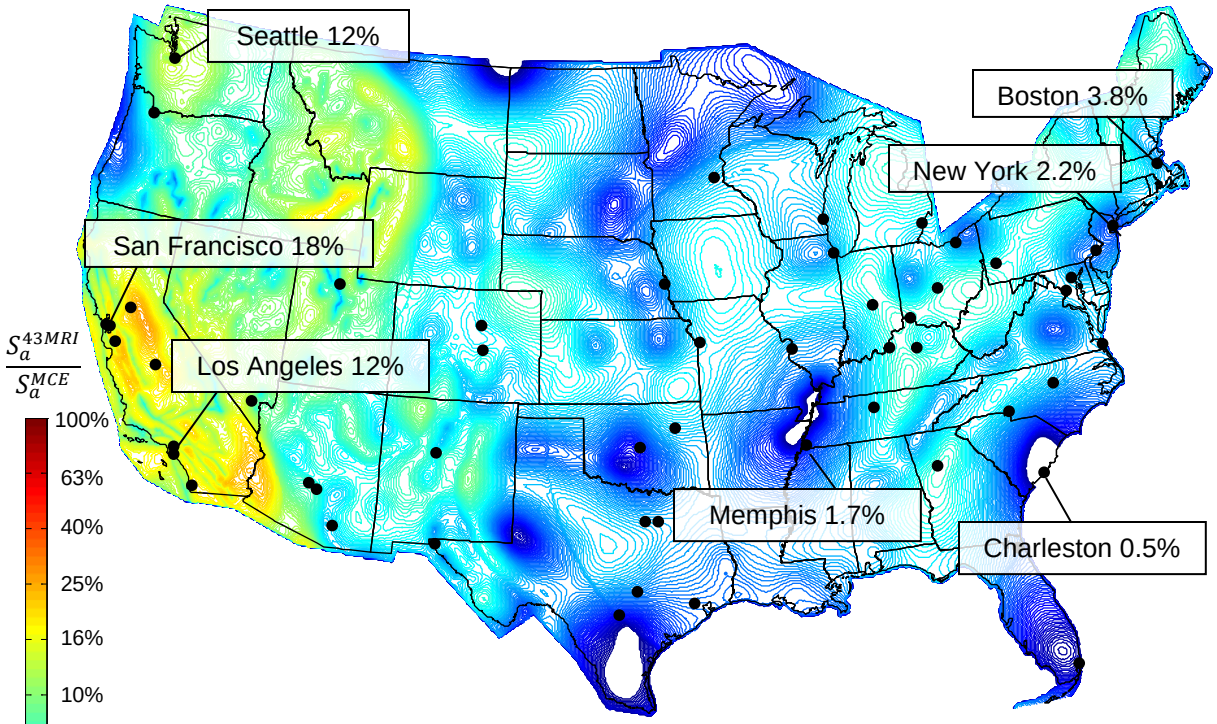

a) 0.2-second spectral acceleration (S_s)

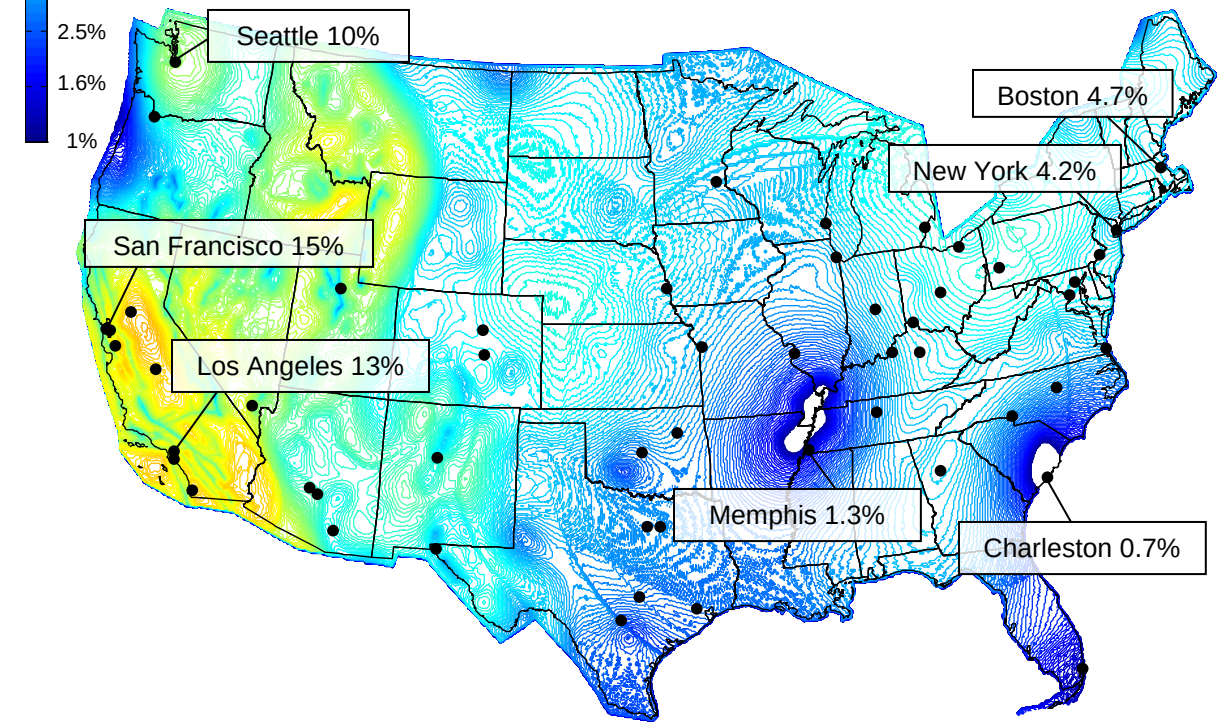

b) 1.0-second spectral acceleration (S_1)

Figure 2.4 Ratio of 43-year MRI spectral acceleration compared to MCE ground motion

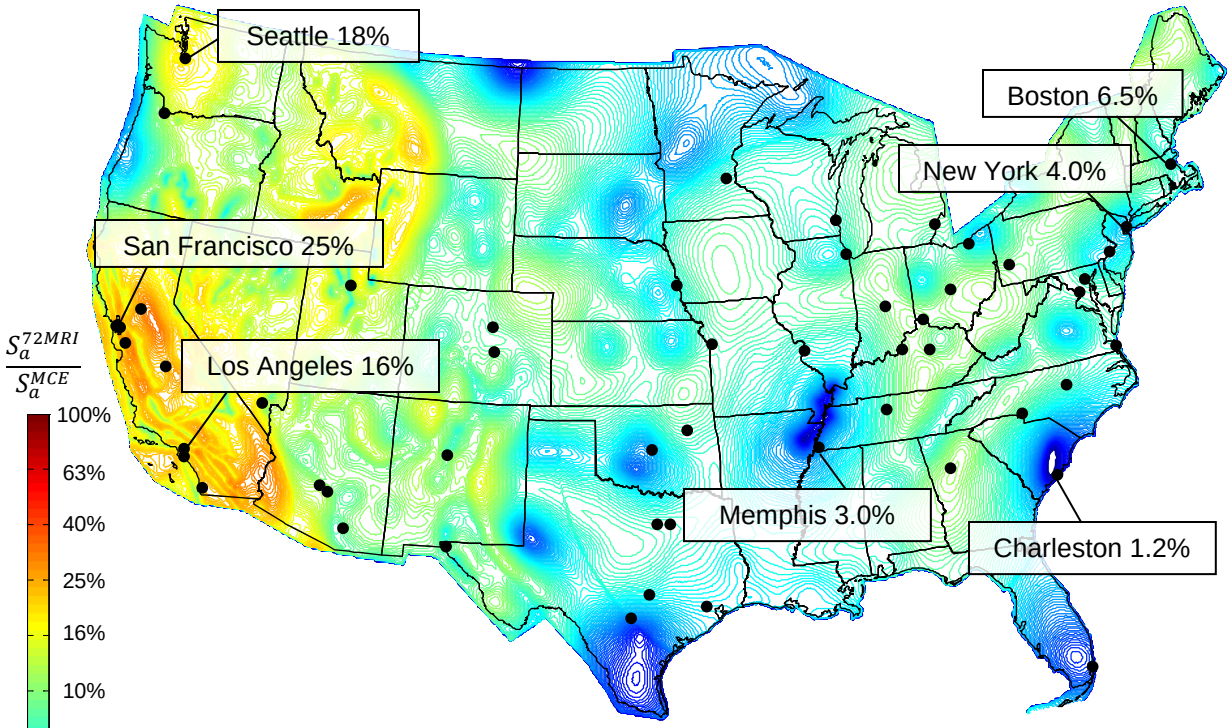

a) 0.2-second spectral acceleration (S_s)

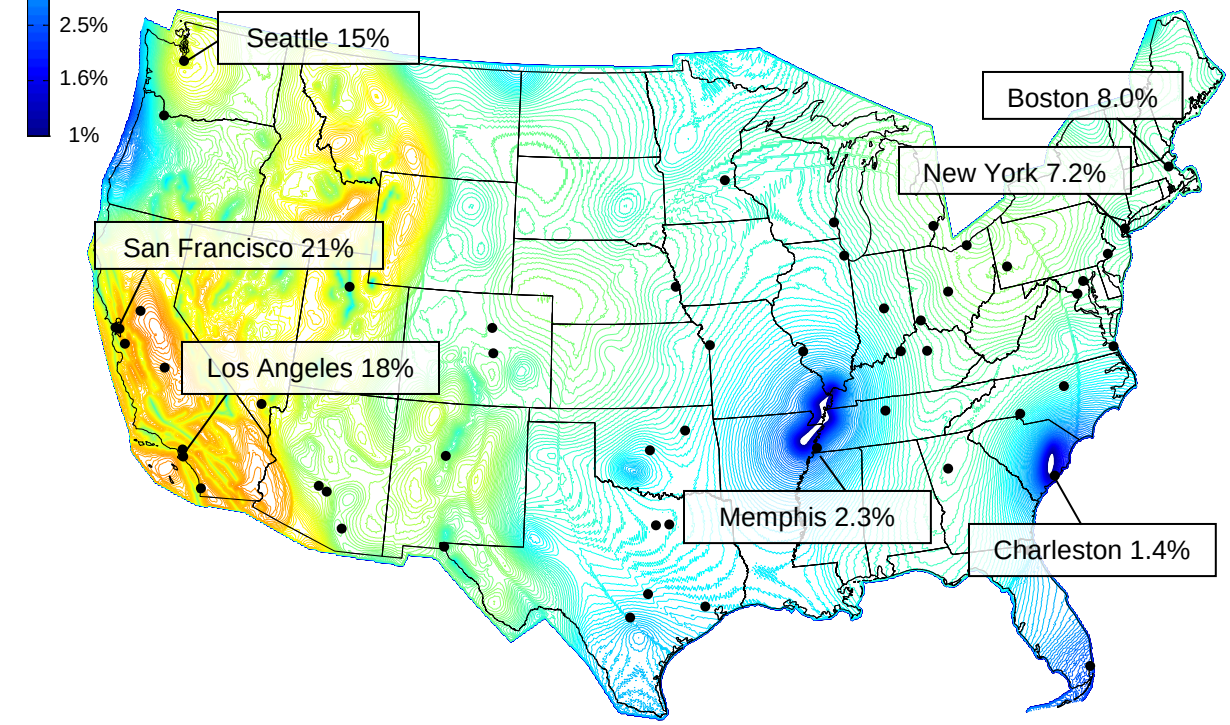

b) 1.0-second spectral acceleration (S_1)

Figure 2.5 Ratio of 72-year MRI spectral acceleration compared to MCE ground motion

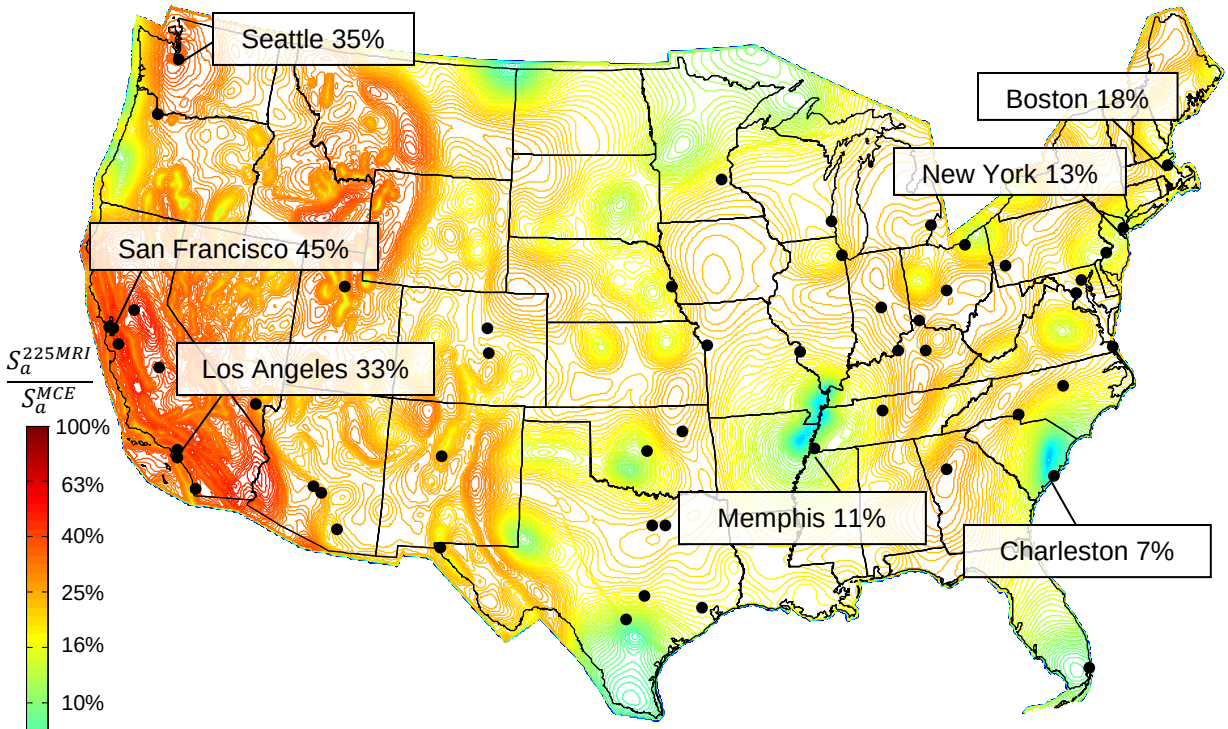

a) 0.2-second spectral acceleration (S_s)

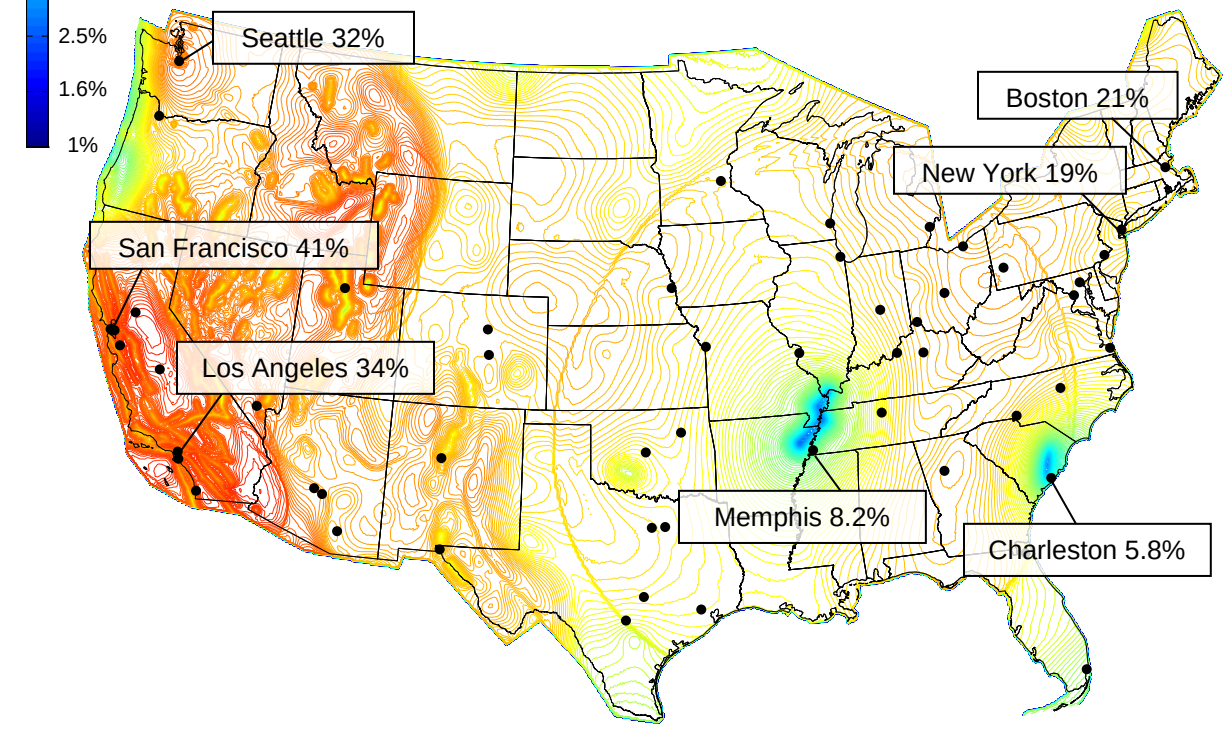

b) 1.0-second spectral acceleration (S_1)

Figure 2.6 Ratio of 225-year MRI spectral acceleration compared to MCE ground motion

Generally speaking, spectral demand with a 72-year MRI, is approximately 10% of the MCE ground motion for the central and eastern United States, and 20% of the MCE ground motion for the western United States. Of course, for soft soil (site classes D and E), low-frequency ground motion is amplified more compared to high-frequency ground motion. The effect of site response is considered later in this chapter.

A summary of average spectral acceleration compared to the uniform-hazard MCE-level spectral acceleration is given in Table 2.1. Ratios for all map grid locations (every 0.05°) was defined using 106° W longitude as the boundary between western United States and central and eastern United States regions (Wald and Allen 2007). Deterministic limits on the ground motion were not considered because the focus of the comparison was on probabilistic demands (and not on design demands). The summary shows that ratios in the central and eastern United States were roughly half that of the western United States. Comparing only population centers in the west coast with the central and eastern United States, and not including the intermountain region and outlier locations (e.g. Charleston, Memphis, and Miami), the ratios in the central and eastern United States were 3 to 4 times smaller than the western United States.

Table 2.1 Average ratio of spectral acceleration (for different MRI) compared to MCE ground motions

MRI (years)	All map (gridded) locations		Population centers	
	Western United States	Central and Eastern United States	West Coast of the United States	Central and Eastern United States
25	0.07	0.03	0.08	0.02
43	0.12	0.06	0.13	0.04
72	0.19	0.11	0.19	0.07
225	0.44	0.34	0.36	0.20

Based on these results, for most locations in the central and eastern United States the spectral demand associated with the 43-year event is approximately 5% of the MCE, compared to 13% of the MCE for the western United States. The service-level (43-year MRI) spectral acceleration of 13% of the MCE ground motion for population centers in the western United States confirms that used in previous seismic performance studies (Atlayan and Charney 2014; Jarrett et al. 2015). For the 72-year event, spectral demand is approximately 10% and 20% for the central and eastern United States and western United States, respectively.

2.1.3 Ground Motion Attenuation

In general, the newer, more fractured and jointed bedrock in the western United States dissipates seismic waves more over a given distance compared to the older central and eastern United States bedrock. As well, there are significant regional aspects to ground motion attenuation. Figure 2.7 shows major geological regions and their Quality (Q) factors, which are inversely proportional to attenuation. The western United States generally has a low Q factor (e.g. sedimentary basins). Seismic waves attenuate less in the Great Plains, where there is a high Q factor, and generally in the Midwest, although this region is complex and difficult to generalize (Conn 2013; PEER 2013).

Ground motion is attenuated somewhat less along the Atlantic Coastal Plain (moderately-high Q factor), but considerably damped along the Gulf Coastal Plain (low Q factor). Indeed, differences in regional attenuation of ground motion were dramatic during the 2011 Mineral, Virginia earthquake. Ground motion propagated efficiently in the northeast, but was sharply attenuated in the Gulf States (Chapman 2015).

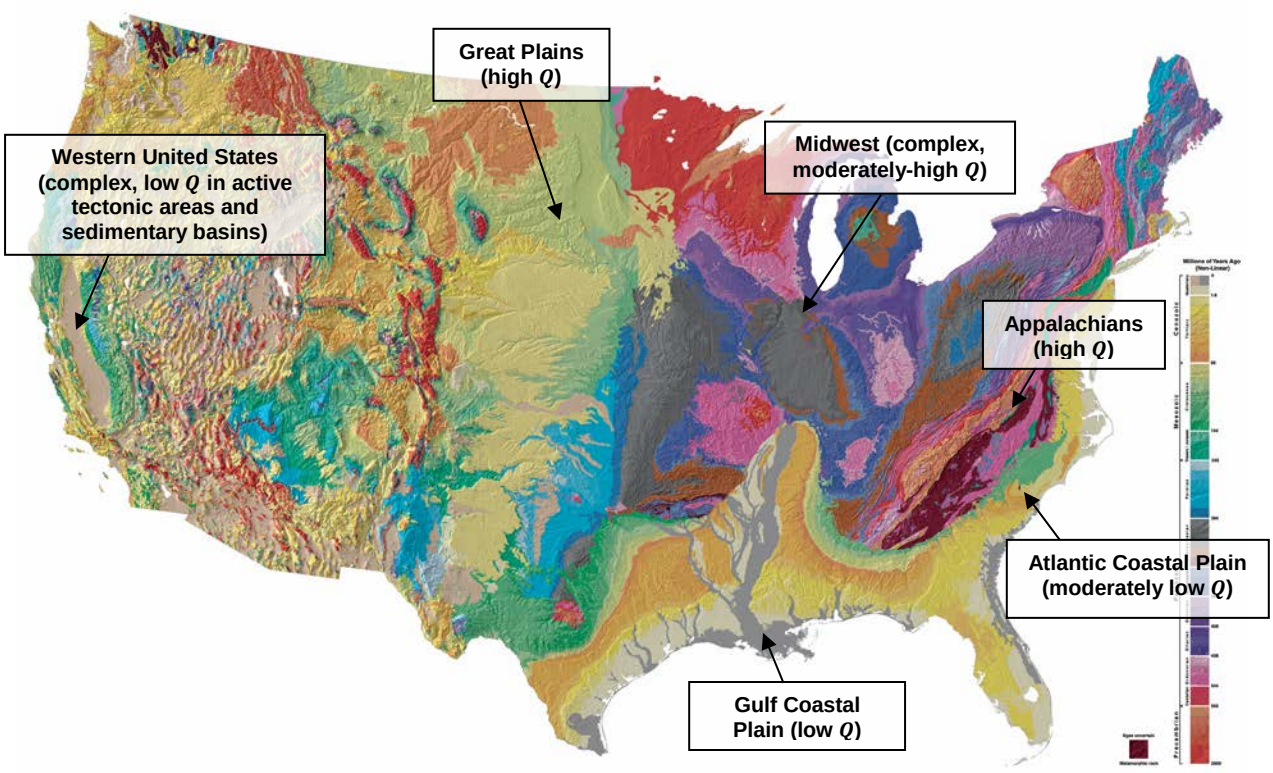

Figure 2.7 Geological regions of United States (background map of geology adapted from map by Vigil et al. 2000)

Thus, earthquakes of a given magnitude attenuate much less rapidly in the central and eastern United States compared to the western United States. This leads to a larger "felt area" and potential for a more damaging impact. The difference between the geographic extents of perceived ground motion is shown in Figure 2.8 for the 2011 Mineral, Virginia earthquake and a similar magnitude earthquake in California (the 2004 Parkfield earthquake). The Virginia earthquake was felt by more people in the United States than any previous quake in an area encompassing a third of the country's population (Horton 2012). The larger felt area in the central and eastern United States is noteworthy, considering that half of the U.S. population lives within 600 miles of Tennessee.

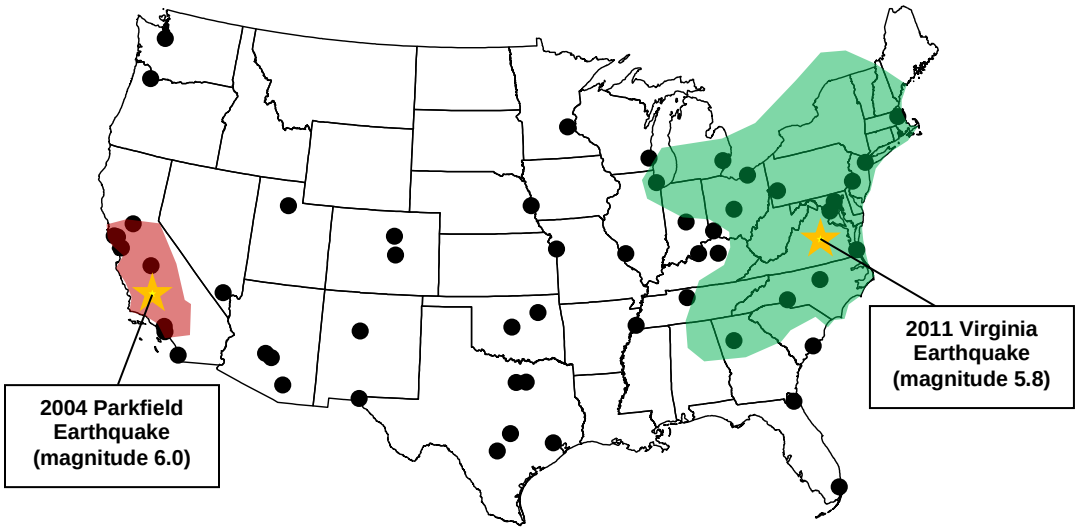

Figure 2.8 Geographic extent of perceived ground motion (adapted from USGS 2012)

The difference in ground motion attenuation also affects the way earthquakes contribute to the hazard at a location, in terms of magnitude and distance. Table 2.2 shows the mean distance and magnitude of events that contribute to MCE ground motion (2,475-year MRI) for selected locations, based on the 2008 USGS Interactive Deaggregation Tool (USGS 2013). In the western United States, the hazard is dominated by earthquakes that are close by, due to a higher density of faults. By contrast, in the central and eastern United States, as the spectral period increases, the seismic hazard is increasingly dominated by distant earthquakes, sometimes as far away as 300 miles or more. There are more known faults in western United States than in the central and eastern United States, and these known sources have high seismic potential. For these reasons, distributed seismicity contributes little to the hazard in the western United States but is a strong contributor in the central and eastern United States.

Table 2.2 Mean Distance (Magnitude) contributing to MCE ground motion

Location		Spectral Period (s)		
		0.2	1.0	2.0
Western US	Los Angeles	5 km (6.66)	6 km (6.72)	12 km (6.87)
	Las Vegas	16 km (6.14)	41 km (6.59)	77 km (6.96)
Central and Eastern US	Chicago	115 km (5.86)	376 km (7.09)	455 km (7.38)
	Nashville	203 km (7.41)	221 km (7.52)	226 km (7.57)
	Boston	62 km (5.97)	165 km (6.61)	229 km (6.8)
	New York	36 km (5.81)	119 km (6.44)	212 km (6.7)
	Philadelphia	56 km (5.89)	169 km (6.53)	290 km (6.8)
	Washington, D.C.	126 km (6.16)	286 km (6.77)	386 km (6.97)
	Charlotte	143 km (6.77)	196 km (7.1)	242 km (7.21)

Another consideration is that ground motion attenuation is more uncertain in the CEUS. This uncertainty is manifest by the dispersion in response spectrum, especially in the high frequency (very short period) range for ground motion prediction equations. For example, Figure 2.9 shows the mean response spectrum (conditioned for 1.0-second spectral period) for Las Vegas and Nashville using different ground motion prediction equations based on the 2008 USGS Interactive Deaggregation Tool (USGS 2013).

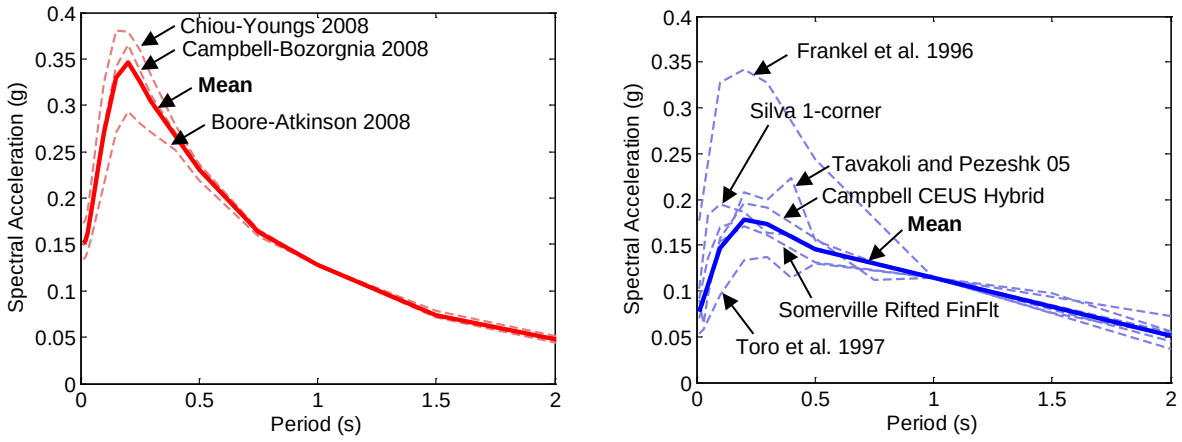

a) Las Vegas b) Nashville

Figure 2.9 Conditional mean response spectrum (conditioned on 1.0 second) for different ground motion prediction equations

In the western United States, the ground motion prediction equations are well defined, compared to the central and eastern United States. The underlying cause of uncertainty in the central and eastern United States is the lower earthquake rates and scarcity of strong motion data (Nikolaou et al. 2012).

The likely duration of ground motion is longer in the central and eastern United States. For example, Figure 2.10 compares synthetic ground motions that are generated based on the most likely (modal magnitude and distance) event for Las Vegas and Nashville. The ground motions are generated using a stochastic model and deaggregation analysis (for 1.0-second spectral period in Table 2.2).

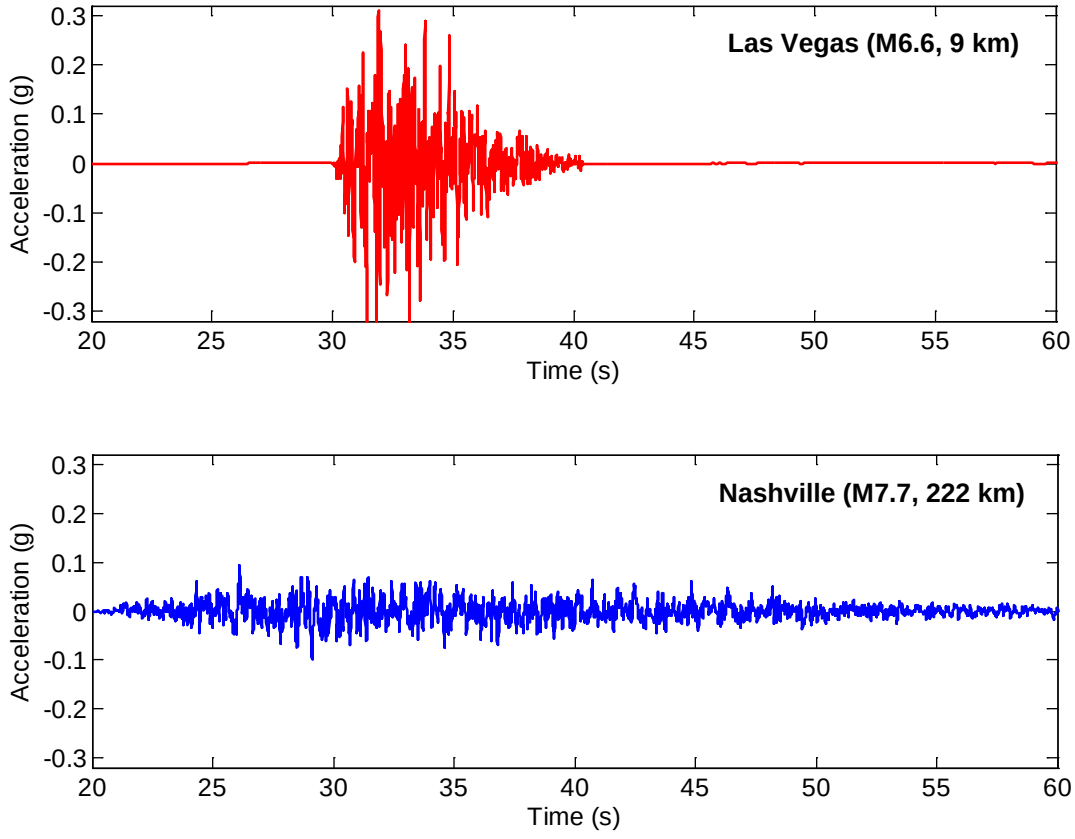

Figure 2.10 Synthetic ground motions for most likely event based on a hazard deaggregation

Although a more realistic physics-based model (e.g. that by Somerville et al. 2001) is needed to realistically represent source and path effects, including near-fault directivity (NIST 2011), the comparison shows that the overall duration of ground motion in the central and eastern United States is predicted to be significantly longer than in the western United States. The difference in duration is primarily due to the different distances from the fault sources.

The implication for performance-based design is that, all other factors being equal, the longer duration of strong ground motion will likely mean: (1) structural components will be subjected to additional cycles of deformation; and (2) collapse capacity will be lower (Chandramohan et al. 2013). This is especially important for components susceptible to low-cycle fatigue, such as pre-Northridge beam-to-column connections (Kanvinde and Deierlein 2004) and steel frames in buildings not specifically detailed for seismic resistance.

2.1.4 Site Response

The conventional NEHRP and ASCE 7 procedure to account for local site soil response (amplification) is based on correlating shear wave velocity in the top 30 meters of the soil, V_{s30} with ground motion records in the San Francisco bay area (Borcherdt 1994). Response resolution was limited to two spectral period bands, short periods (near 0.2 seconds) and medium range periods (near 1.0 seconds), because the design spectra was anchored these two periods. Although a finer resolution of spectral periods, updated attenuation relationships, or similar refinements have been proposed (Huang et al. 2010b; Seyhan and Stewart 2012), the original two-band method has been shown to be adequate for the western United States (Borcherdt 2002). For example, Figure 2.11 shows a comparison of the uniform hazard spectrum for a location in San Francisco using the NEHRP/ASCE 7-10 procedure and the Huang et al. (2010b) procedure.

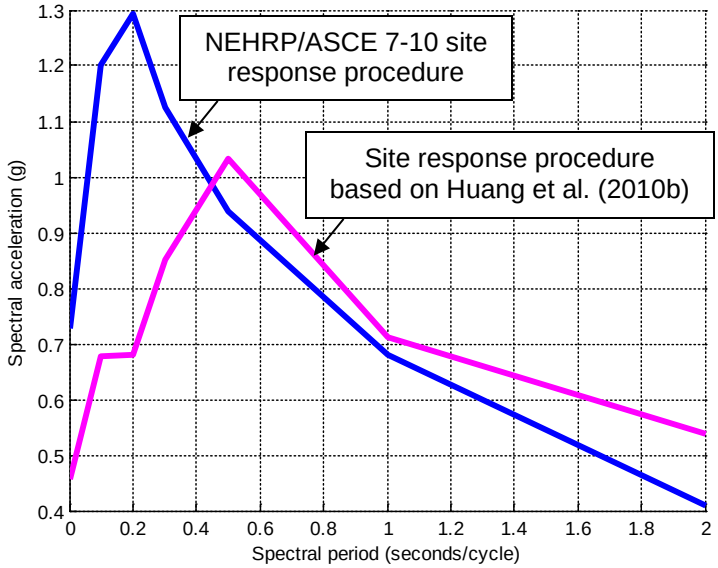

Figure 2.11 Uniform hazard spectrum for a location in San Francisco (38.0º latitude, -121.7º longitude) with soil site class D (average V_{s30} = 180 m/sec)

The Eurocode 8 procedure is similar to the NEHRP procedure, except that site response factors are applied to the entire spectrum (instead of period bands), and that there are some differences in defining soil classifications. Improvements have been suggested for both the classifications and the amplification factors (Pitilakis and Riga 2012), and for incorporating some knowledge of the type and depth of the soil column (Pitilakis and Riga 2013).

Nevertheless, site response is complex. Ground motion amplification depends on the shear wave velocity profile and thickness of the soil column, bedrock characteristics, the magnitude and depth of the soil-to-bedrock impedance contrast, and topographic effects, among other factors (Kramer 1996). This is especially true in the central and eastern United States. As a consequence, various alternative site response procedures have been proposed (Rodriguez-Marek and Bray 2001; Pitilakis and Riga 2013; Kottke et al. 2012).

Bedrock Characteristics

Bedrock in the western United States sedimentary basins exhibits V_s of generally 2,000 m/s. Bedrock in the central and eastern United States is typically harder, with V_s consistently higher than 3,000 m/s (Nikolaou et al. 2012). The implication for seismic performance-based design is that site response in the central and eastern United States is better represented using V_s = 2,000 m/s data (i.e. 2010 Revision III update of the 2008 USGS data) for bedrock motion, instead of the conventional V_s = 760 m/s data corresponding to the "B/C boundary" assumed for the western United States.

Soil-Bedrock Impedance Contrast

An important consequence of bedrock characteristics is that the soil-bedrock impedance contrast is typically larger in the central and eastern United States, compared to the western United States. As seismic shear waves move upward through a layer contrast, the transmitted wave is amplified. (See Kramer 1996; Aki and Richards 1980; Schnabel et al. 1972.) The response at the free surface (ground) is the compounded effect of transmitted up-going waves and reflected down-going waves. In the absence of resonance,

$$\text{Ground / bedrock motion} = \frac{2\rho_{bedrock}V_{s,bedrock}}{\rho_{soil}V_{s,soil}} \quad (2.1)$$

Assuming a single layer contrast, no attenuation in the soil layer, and no damping (Q equal to ∞), the minimum amplification is 2.0 at the free surface. For a typical rock (V_s = 1,000 m/s and density, ρ = 2 gm/cc) and bedrock (ρ = 2.5 gm/cc), the maximum amplification at the ground would be 5.0 in the western United States and 7.0 or greater in the central and eastern United States. Resonance occurs in proportion to the location of the layer contrast relative to the

surface. An actual soil profile has multiple layers and a finite Q, so the amplification is damped out after the first harmonic.

Thus, site response is simply an application of the principle of conservation of energy. One way to think of site response is to consider that seismic waves traveling towards the ground surface are like ocean waves approaching the shoreline. As the ocean wave slows down, the ocean wave amplitude increases. In California most of the population is in sedimentary basins and active tectonic areas, and the velocity contrast is roughly 2. In the central and eastern United States the velocity contrast can be much higher. In fact, a high impedance contrast is true for many locations along the east coast and in the Midwest.

The velocity profile is also gradual in the western United States, but in the central and eastern United States the contrast is often sudden. Site response studies in Washington, D.C. following the Virginia earthquake showed "sharp velocity contrasts" (Godfrey et al. 2012).

Short and mid-range period amplification are consistently higher along the eastern Coastal plains than the conventional procedure predicts (Nikolaou et al. 2012; Amine et al. 2012). Generally speaking, there is a 20% increase in high-frequency motion and no increase in low-frequency (long period) motion in central and eastern United States compared to the western United States (Hashash and Moon 2011; Amine et al. 2012).

Depth of Soil-Bedrock Impedance Contrast

It is not uncommon in the central and eastern United States to have a significant impedance contrast located within the top 100 feet. In such locations, the shallow depth of a high impedance contrast can generate damaging surface waves during an earthquake, much like a tsunami. Thus, even if most of the soil profile can be generalized (bedrock characteristics,

contrast between bedrock and lower layers) the last layer to the surface can govern site response. As a result, it may not be practical to generalize site response. South Carolina is a case in point. Site response is very different in Columbia and Charleston, but even within Columbia, response is very different west of the fall line in the Piedmont, compared to the Coastal Plain in the east (Amine et al. 2012).

As previously mentioned, the USGS uniform-hazard ground motions reference a shear wave velocity, V_s = 760 m/s. This corresponds to the boundary of the ASCE 7-10 soil classification of "rock" (site class B) and "very dense soil and soft rock" (site class C). Although the actual bedrock shear wave velocity in the central and eastern US is much higher—three times or more (Nikolaou et al. 2012)—site class B was selected because it represented an average of the rock sites used in the western United States attenuation relationships (FEMA 2003).

Soil-Structure Interaction

The importance of soil-structure interaction may be indicated by the superstructure-to-soil "velocity" ratio, expressed in Equation 2.2.

$$velocity\ ratio \quad = \quad \frac{H/T_1}{V_{s30}} \tag{2.2}$$

where H is taken as 2/3 of the building height and T_1 is the fundamental period of vibration of the building.

When the ratio is on the order of 0.1, soil-structure interaction is an important factor in site response (NIST 2012a). In general, for braced frame or shear wall structures, the ratio is between 0.1 and 0.5. For moment frames on stiff rock, the ratio will be less than 0.1 (Stewart et al. 1999). Thus, soil-structure interaction is not expected to be significant for the buildings analyzed in this research.

2.1.5 Spectral Shape

The combined effect of earthquake rate, ground motion attenuation, and site response results in a central and eastern United States spectral shape that is distinguished from the western United States by added high-frequency content (NIST 2011).

For example, Figure 2.12 shows the characteristic uniform hazard spectrum for 12 major population centers in the western United States (and the average spectrum) and for 25 major population centers the central and eastern United States (and the average spectrum) for both the 43-year MRI (upper plots) and the 2,475-year MRI MCE ground motion (lower plots). The spectra in Figure 2.11 were normalized with respect to the peak ground acceleration and plotted on a log-log scale. The spectra demonstrate both the spectrum shift toward higher frequencies (especially at the MCE-level) and the wider variability in the central and eastern United States.

The difference in spectrum is significant because high frequency content in ground motion affects building performance. Existing buildings, wind-designed buildings, and braced-frame buildings—all common in the central and eastern United States—are sensitive to high frequencies due to high stiffness and lack of ductility. For example, an analytical study of a 9-story low-ductility chevron braced frame building (Hines et al. 2011) indicated that higher-mode effects caused significant damage. In general, short-period buildings exhibit poor collapse safety performance (NIST 2012b).

An implicit assumption of the uniform-hazard response spectrum is that a single event may produce the spectral values (ordinates in the response spectrum). As an alternative, the conditional mean spectrum (Baker 2011), which is the probabilistic expected (mean) response spectrum conditioned on a target period and corresponding spectral acceleration, can be used.

If all ordinates in the uniform hazard response spectrum were dominated by the same very-large event, the uniform hazard and conditional mean spectrum would be essentially the same (Baker 2011). Unlike the western United States, in the central and eastern United States often a small close event dominates the high-frequency while a large distant event dominates low-frequency. For these reasons, and due to the fact that multiple modes often contribute (NIST 2011), the uniform hazard response spectrum is thought to be a suitable (i.e. not an overly conservative) target for ground motion selection and scaling (Lin et al. 2013) in the central and eastern United States. Nevertheless, the further research is required to confirm this statement.

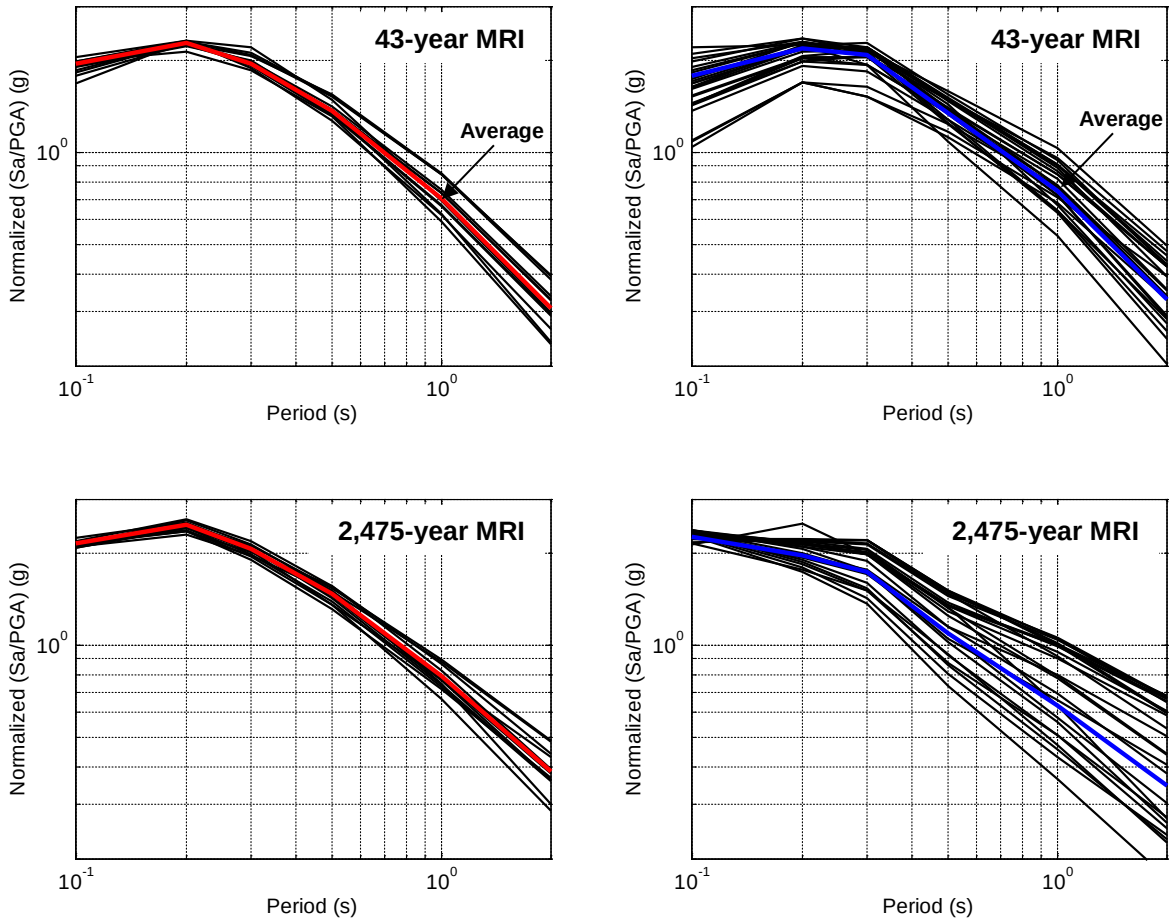

a) Western United States b) Central and eastern United States

Figure 2.12 Characteristic uniform hazard response spectra

2.2 Wind Hazards

2.2.1 Uniform Hazard Wind Speeds

Uniform hazard wind speed values for the United States and corresponding maps for selected probability levels are provided in ASCE 7-10 and in digital format by the Applied Technology Council (ATC 2011). These values correspond to a synoptic basic wind speed (in mph) for a 3-second gust at 33 feet above the ground for terrain exposure category C (unobstructed, open country) and, as a consequence, they do not account for topographic effects. Non-synoptic wind, especially tornadic wind, is not accounted for in the ASCE 7-10 mapped values. The basis is twofold. First, spatially the probability of occurrence of a tornadic wind speed is significantly lower compared to the basic wind speed. Second, measurements of wind speed during actual tornados indicate that the wind speed is often (more than half the time) lower compared to the basic wind speed (ASCE 2010). The effect of tornados is considered in more depth in the next section, and the effect of tornados on the collapse risk of building is examined in Chapter 5.

Figure 2.13 shows the design wind speed for a 700-year MRI (used for ordinary occupancy risk category II structures). The figure resembles Figure 26.5-1.A in ASCE 7-10 and includes "special wind regions," where a design value is not provided. Figure 2.14 shows the corresponding wind hazard map used in this research, which is identical to Figure 2.13 except regional values of wind speed were applied to the special wind regions. (In design special wind regions should be examined for unusual wind conditions.) Figure 2.15 compares service-level wind speeds to the design wind speed (700-year MRI) for the central and eastern United States. In contrast to ground motion, service-level wind is a significant percent of the design-level.

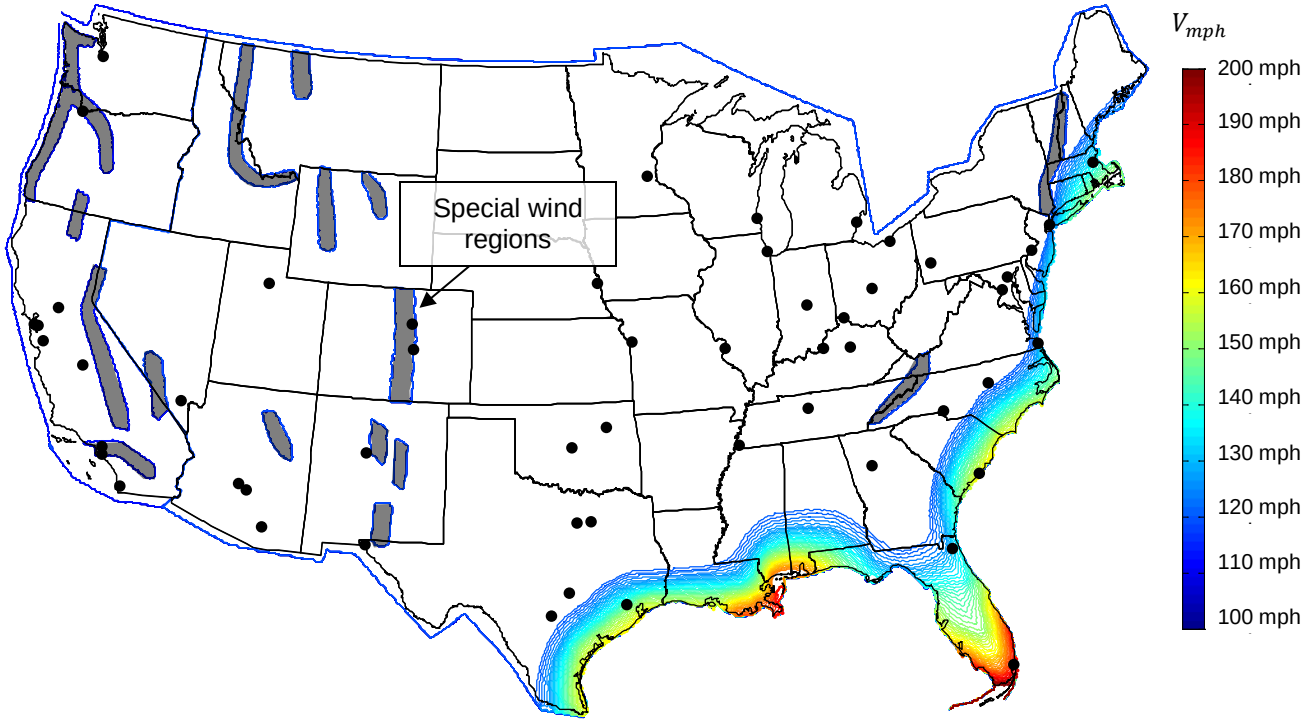

Figure 2.13 Design wind speed contours with a 700-year MRI (special wind regions included)

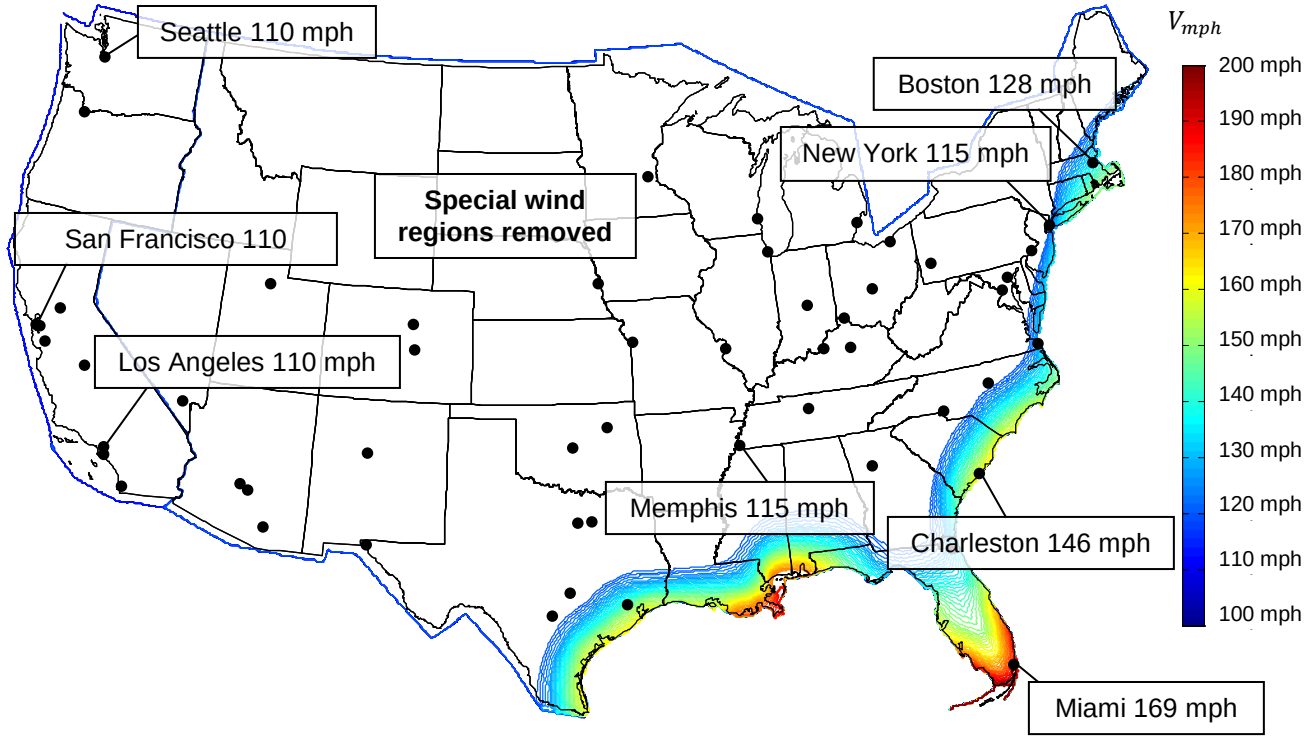

Figure 2.14 Design wind speed contours with a 700-year MRI (special wind regions removed)

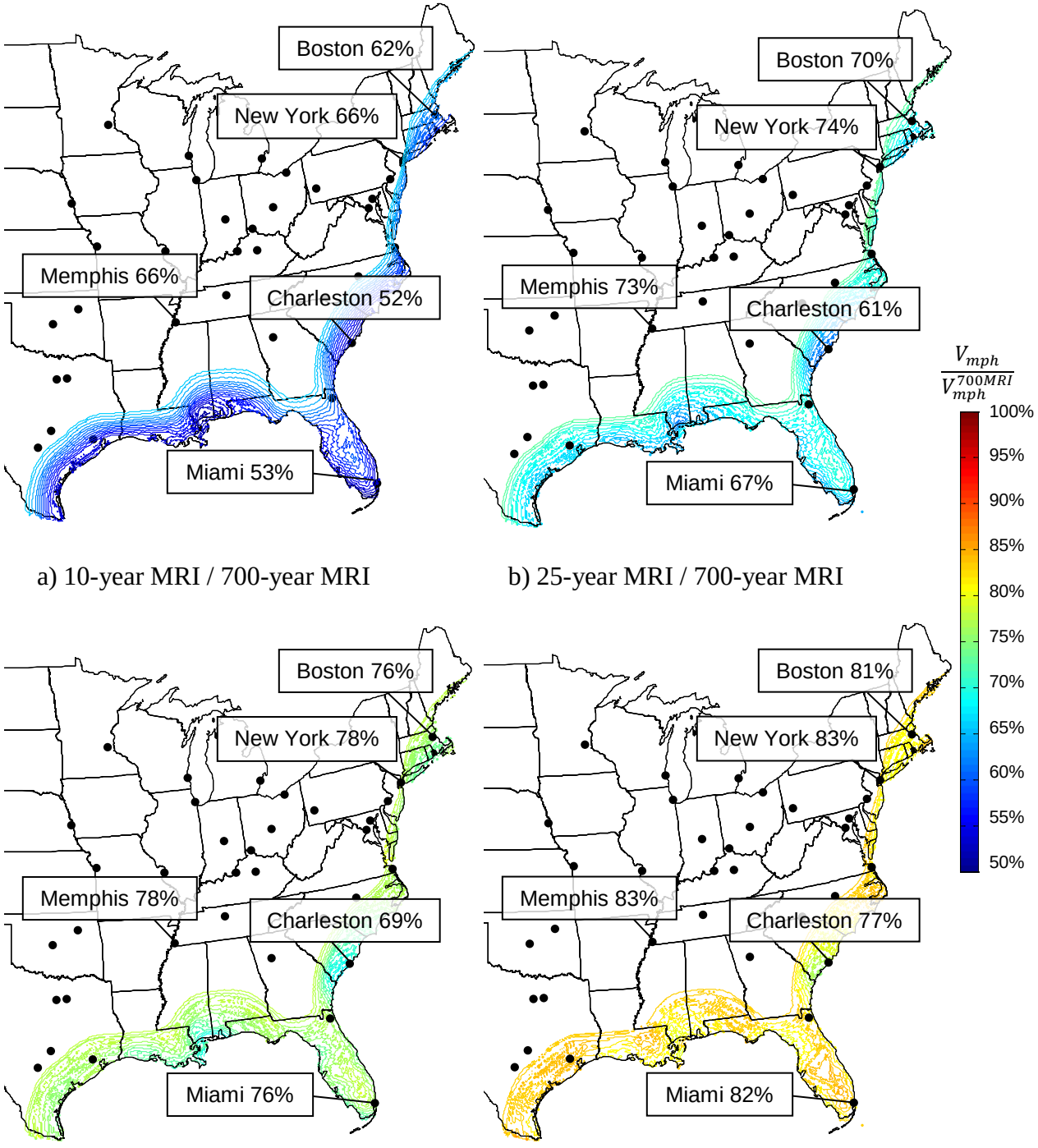

a) 10-year MRI / 700-year MRI

b) 25-year MRI / 700-year MRI

a) 50-year MRI / 700-year MRI

b) 100-year MRI / 700-year MRI

Figure 2.15 Ratio of service-level wind speed to design wind speed for ordinary occupancy and use structures (risk category II)

2.2.2 Wind Hazards

Wind hazards are inherently different compared to seismic hazards. Wind loads are generated by wind pressures applied to the building envelope, whereas seismic loads are inertial forces generated by ground movement. The characteristics of wind pressure depend primarily on the shape of the building and the terrain exposure. Wind loads also depend on the type of windstorm (e.g. hurricane, extra-tropical cyclone, downburst, and tornado). This differs from seismic load characteristics which depend largely on the mass and stiffness of the building and the tectonic environment, fault mechanism, and epicenteral distance.

Wind load is a random phenomenon that is stationary in the short term, and is often described as mean load with superimposed random fluctuations (gusts) that tend to increase during a windstorm in a ratcheting pattern. By contrast, earthquake ground motion is non-stationary and reflects combinations of compression and shear seismic waves. As a result, seismic loads are essentially symmetric, but the average along-wind load is non-zero. Cross-wind loads generated by vortex shedding and harmonic effects are not symmetric, and are important in taller structures.

Another difference is that a wind event is significantly longer in duration than an earthquake. A typical strong windstorm (excepting tornados) may be 45 to 60 minutes long or even longer (e.g. Gani and Legeron 2012). A particular building model may sustain extreme wind loads for an hour prior to collapse (as shown through analysis in this study), but the same building model subjected to earthquake ground motions may sustain only 10-20 seconds of strong shaking.

Additionally, the frequency content of wind loads is typically broader compared to the earthquake load spectrum, but contains less high-frequency content (Boggs and Dragovich

2006). Structural damage during an earthquake lengthens the fundamental period, which in turn can lower demands or increase demands, depending on the shape of the response spectrum (Naga and Eatherton 2014). In a windstorm, softening of a structure induces greater flexibility and demands. On the other hand, wind-borne debris (missile impact) can likewise change the character of the wind load.

2.3 Multi-Hazard Comparison

2.3.1 Seismic and Wind Elastic Base Shear Forces

A comparison between elastic seismic and wind base shear forces generated by equal likelihood events indicates that steel frame buildings designed for wind may have the essential strength required for small and medium seismic events. A hypothetical 8-story building with a height of 100 feet, assuming a 12.5-ft story height, is used for illustration. The building width (dimension perpendicular to the wind direction) is taken as 90 feet, to represent three 30-ft long bays. The building length (dimension parallel to the wind direction) is taken as 60 feet, to represent two 30-ft long bays. The building "density" is assumed to be 8 pounds per cubic foot. The building structural system is assumed to employ steel moment frames for lateral resistance, and to provide about 1% damping for dynamic wind forces. The building is assumed to be located on rock (ASCE 7-10 soil site class B) and in open terrain (ASCE 7-10 wind exposure terrain type C).

Elastic seismic base shear force was calculated using the equivalent lateral force procedure (ASCE 7-10 Chapter 12.8), where the minimum base shear requirements were not invoked, and the response modification factor was set to 1.0. Spectral accelerations were based on the 2008 USGS National Seismic Hazard Map data.

The wind base shear force was calculated using the directional procedure ("all heights" method) for the main wind force resisting system (ASCE 7-10 Chapter 27). Basic wind speeds were based on the digitized version (ATC 2011) of the ASCE 7-10 wind speed maps (Figures 26.5-1.A through C, and Figures CC1 through CC4), except that regional values were applied to "special wind regions." For wind forces, the fundamental period of vibration was estimated using the wind procedures. As a result, the period calculated was slightly longer compared to the estimated values used for seismic forces.

Spectral accelerations and basic wind speeds with return periods in between mapped data return periods were interpolated or extrapolated based on the nearest interval. (For a given probability of exceedence, the corresponding return periods for wind and seismic hazards differ slightly, but not significantly.)

Figure 2.16 to Figure 2.21 compare elastic seismic and wind base shear forces for the hypothetical 8-story building in the conterminous United States for the range of event return period, or median return interval (MRI), used for wind serviceability design. The maps show contour lines of constant values (white space does not represent zero). The value of the base shear ratio is indicated by the color (exponential scale). This comparison indicates that for serviceability applications, the wind elastic base shear force is 10 times the seismic force or more, outside the western United States.

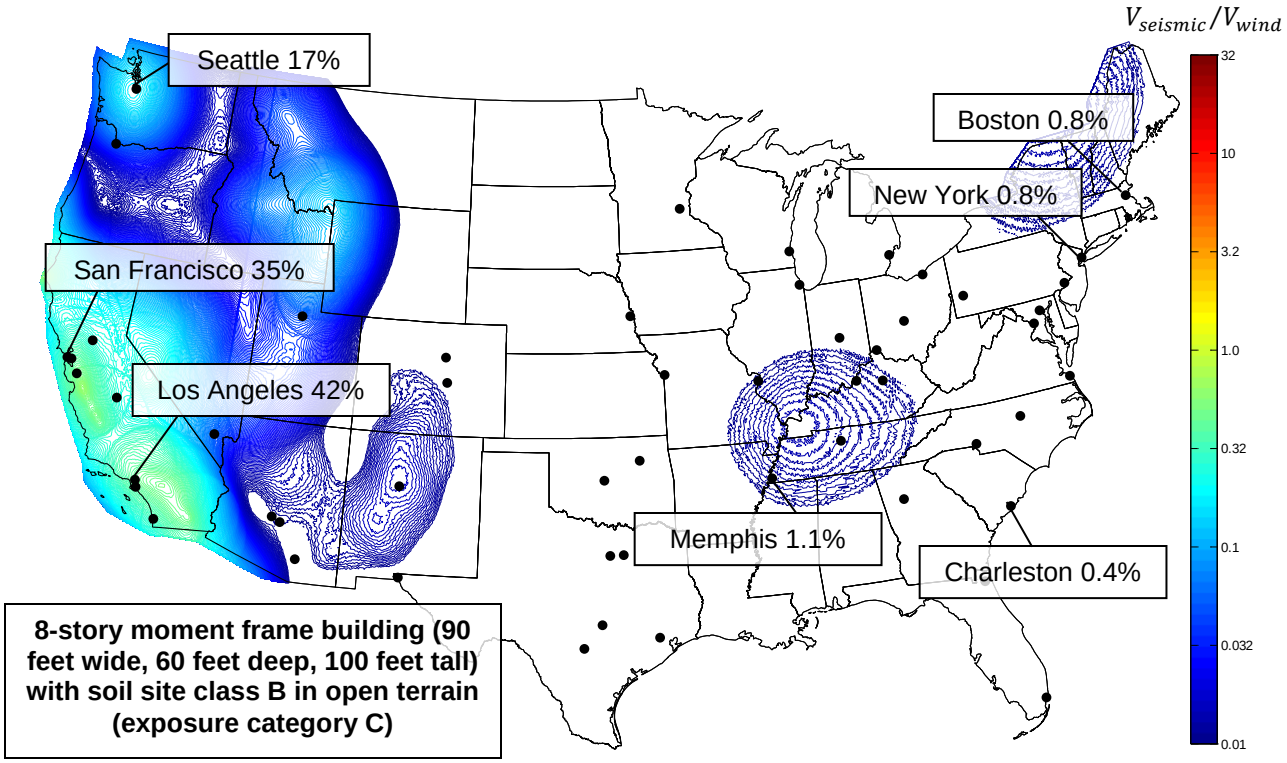

Figure 2.16 Ratio of seismic to wind elastic base shear for 10-year MRI

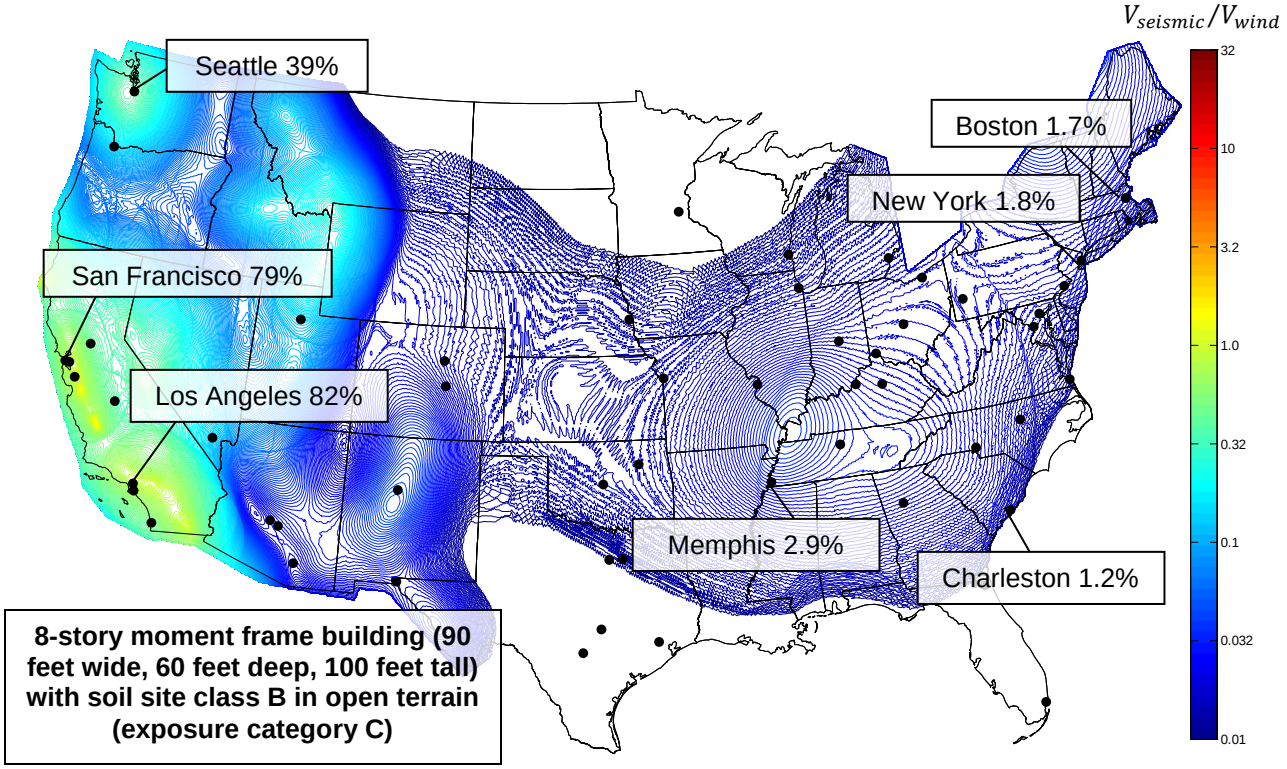

Figure 2.17 Ratio of seismic to wind elastic base shear for 25-year MRI

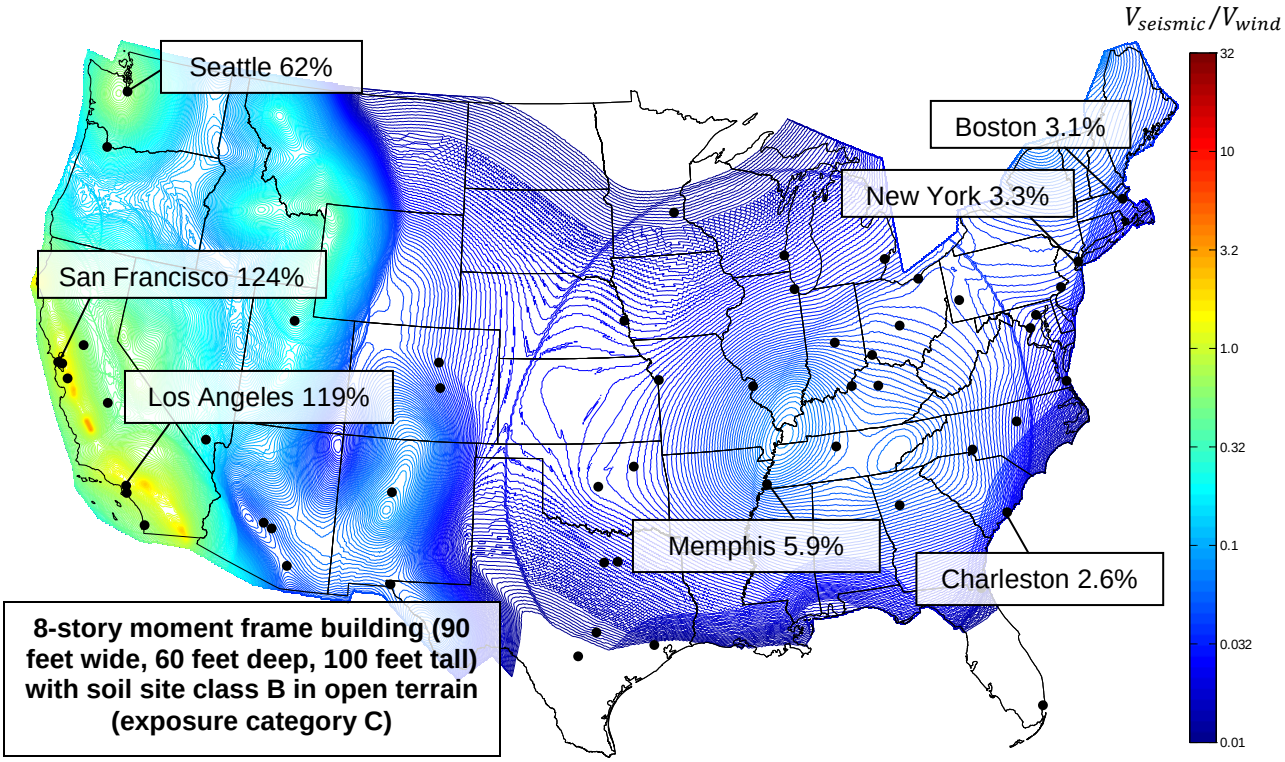

Figure 2.18 Ratio of seismic to wind elastic base shear for 50-year MRI

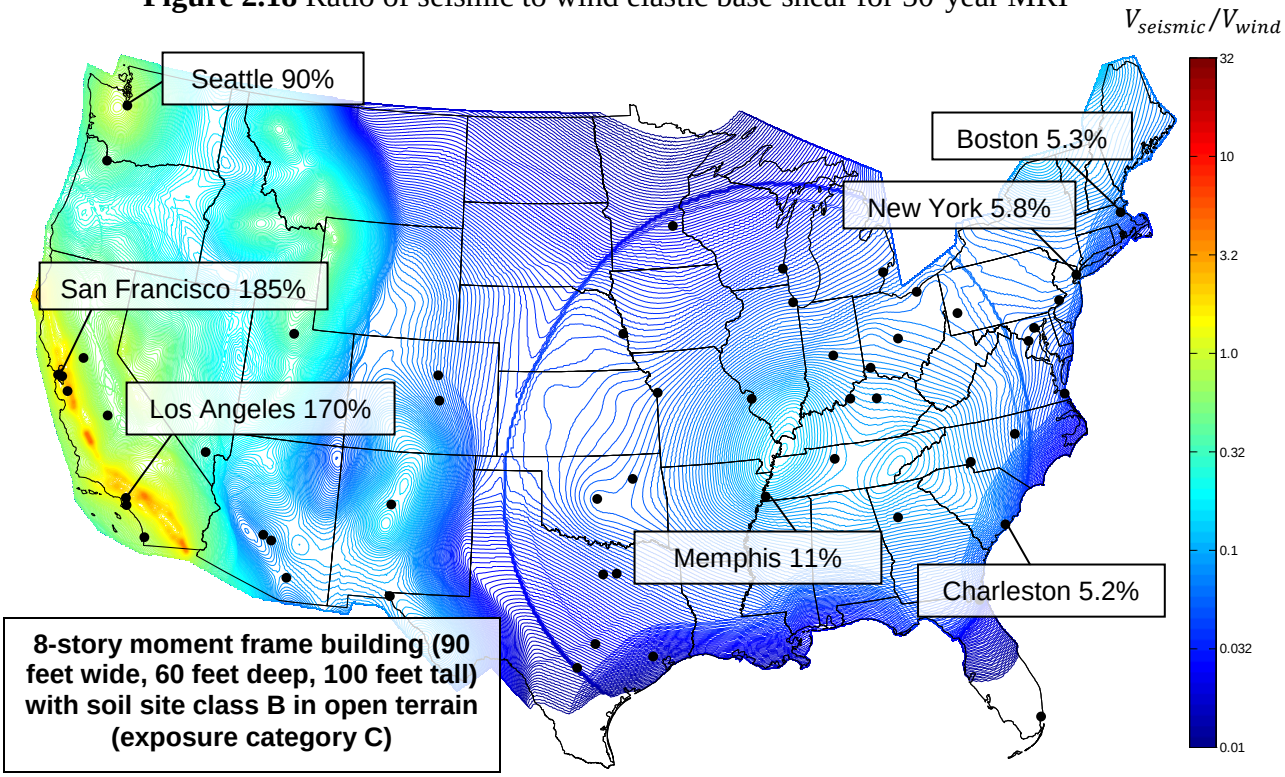

Figure 2.19 Ratio of seismic to wind elastic base shear for 100-year MRI

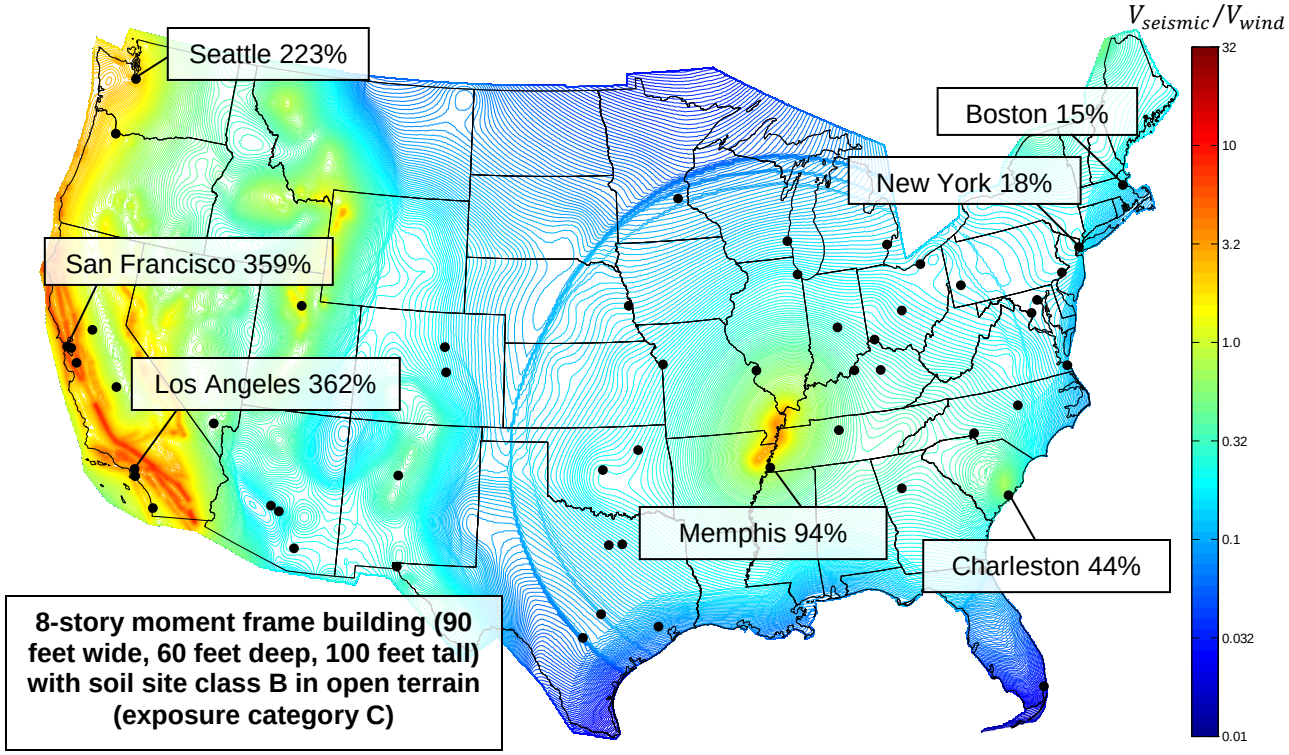

Figure 2.20 Ratio of seismic to wind elastic base shear for 700-year MRI

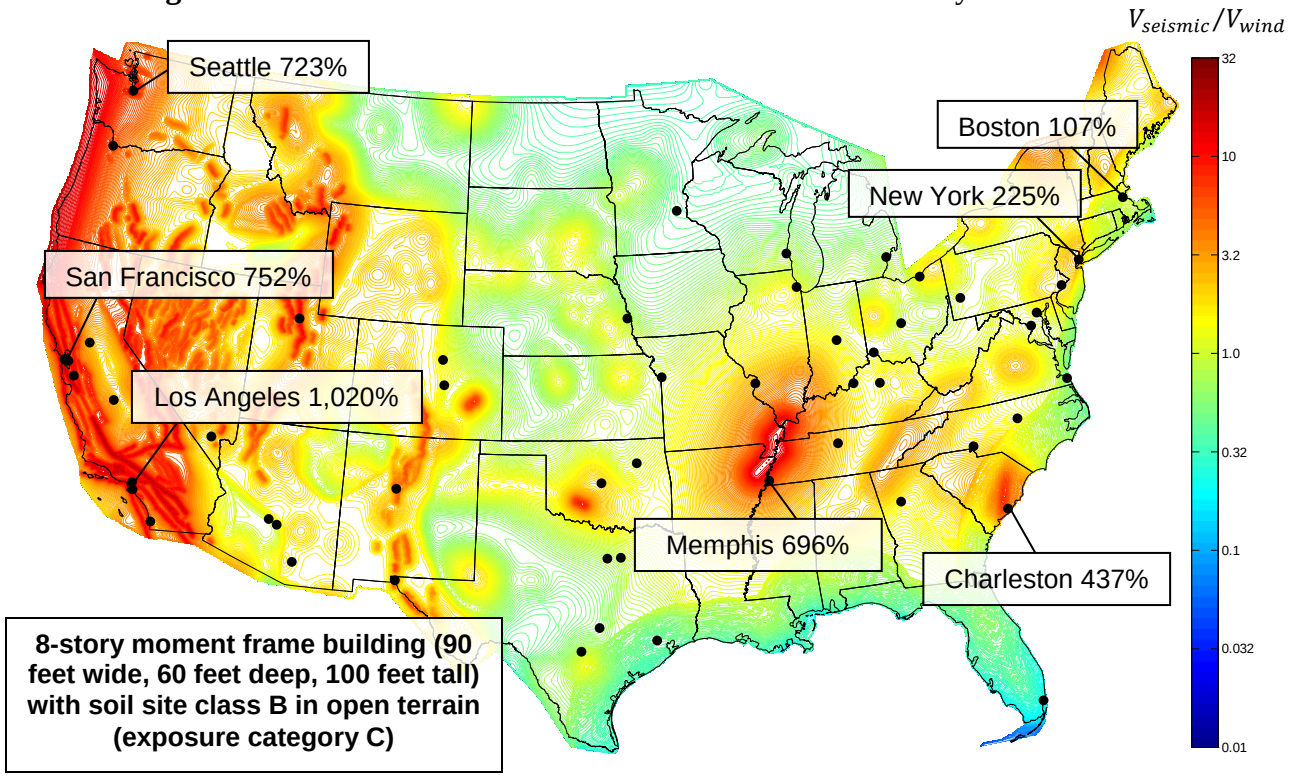

Figure 2.21 Ratio of seismic to wind elastic base shear for 100,000-year MRI

The sensitivity of the conclusions to building period, soil type, and terrain exposure is shown in Figure 2.22 to Figure 2.25, where a constant 100-year MRI (39% probability of exceedence in 50 years) and assuming stiff soil (site class D) is used for comparison. Seismic design controls in many areas for short-period buildings, but wind design controls for long-period buildings. The effect of terrain on the wind pressure is less significant. The effect of hurricane wind is evident along the southern and eastern coastlines.

Figure 2.26 shows the comparison of the base shear for seismic activity, assuming soft soil (site class D) with the base shear for extreme winds estimated by extrapolating ASCE wind speed data. Figure 2.27 shows the same comparison of the base shear, except that the extreme wind speeds are based on tornados. Tornado wind speed was estimated by using the number of tornados that have been cataloged for 2°×2° regions and correlating the tornado intensity factor with a wind speed (Ramsdell and Rishel 2007). For rare events (MRI much greater than 100 years), seismic force controls. Using tornado data was conservative for locations in the interior of the United States (such as in Memphis), but extrapolated wind data was more conservative for non-tornado prone regions or regions with exposed to hurricane wind speeds.

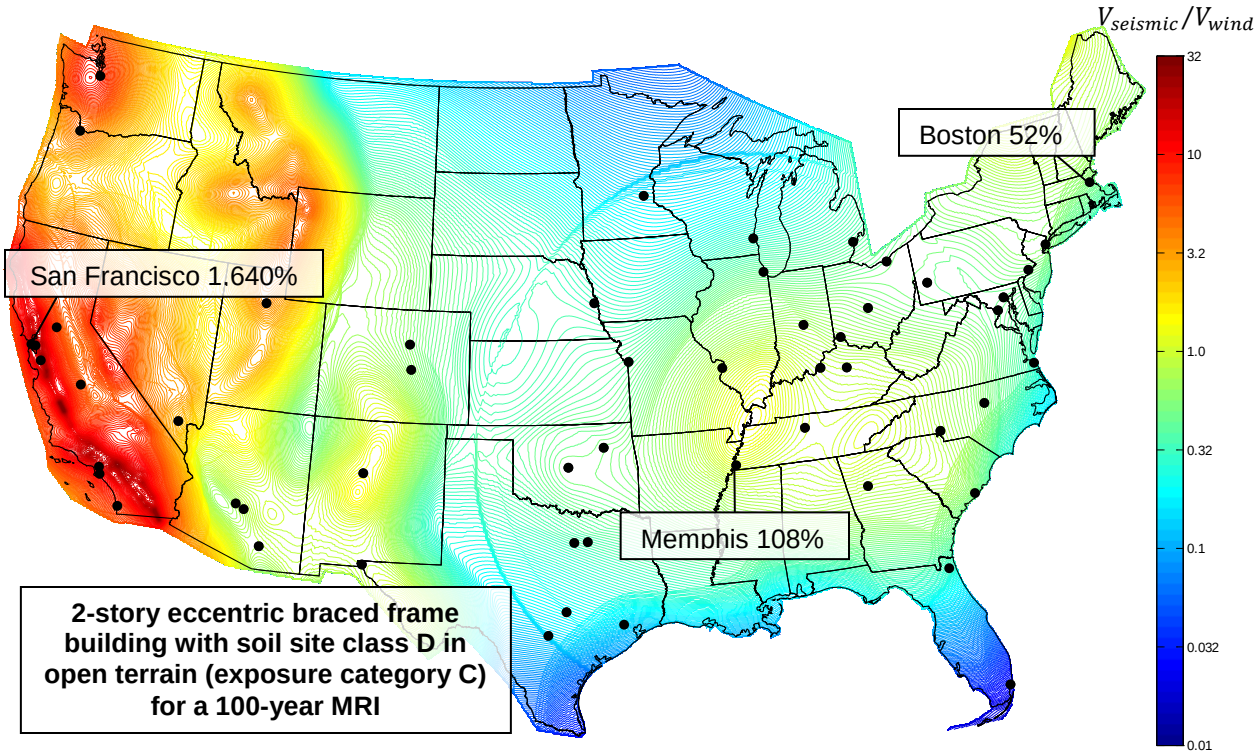

Figure 2.22 Ratio of seismic to wind elastic base shear for a short-period building

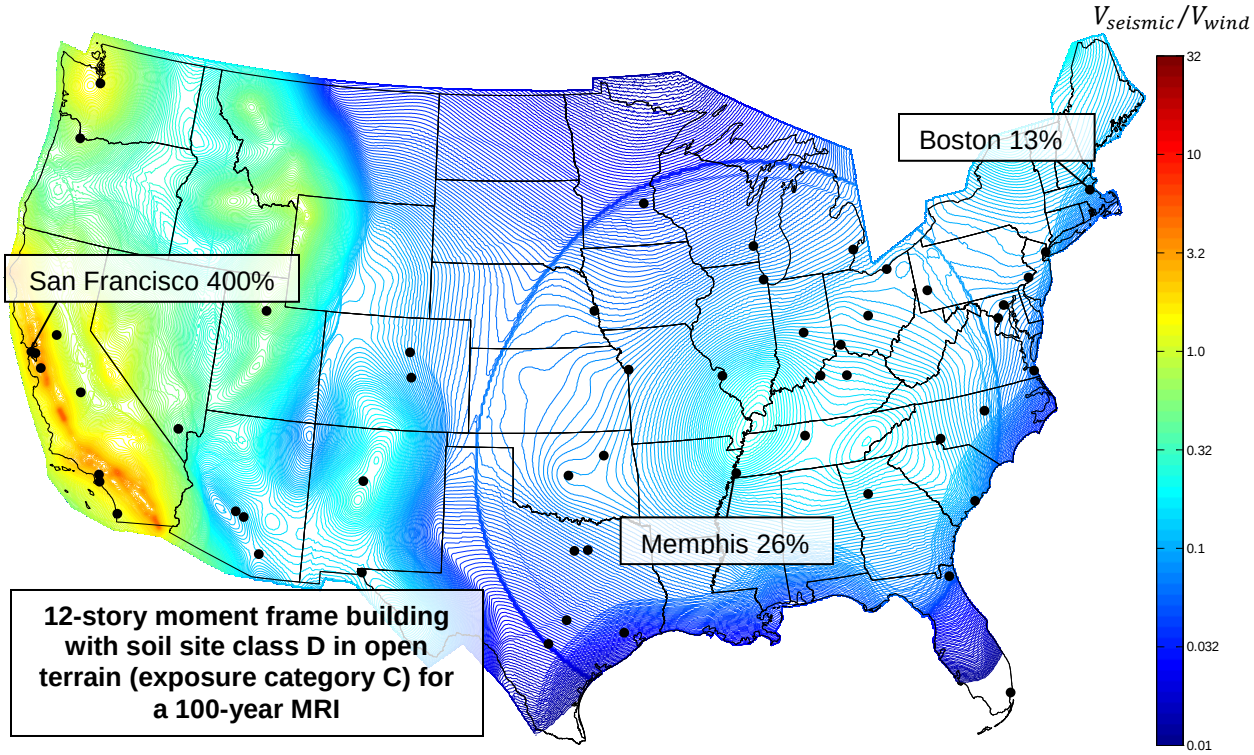

Figure 2.23 Ratio of seismic to wind elastic base shear for a long-period building

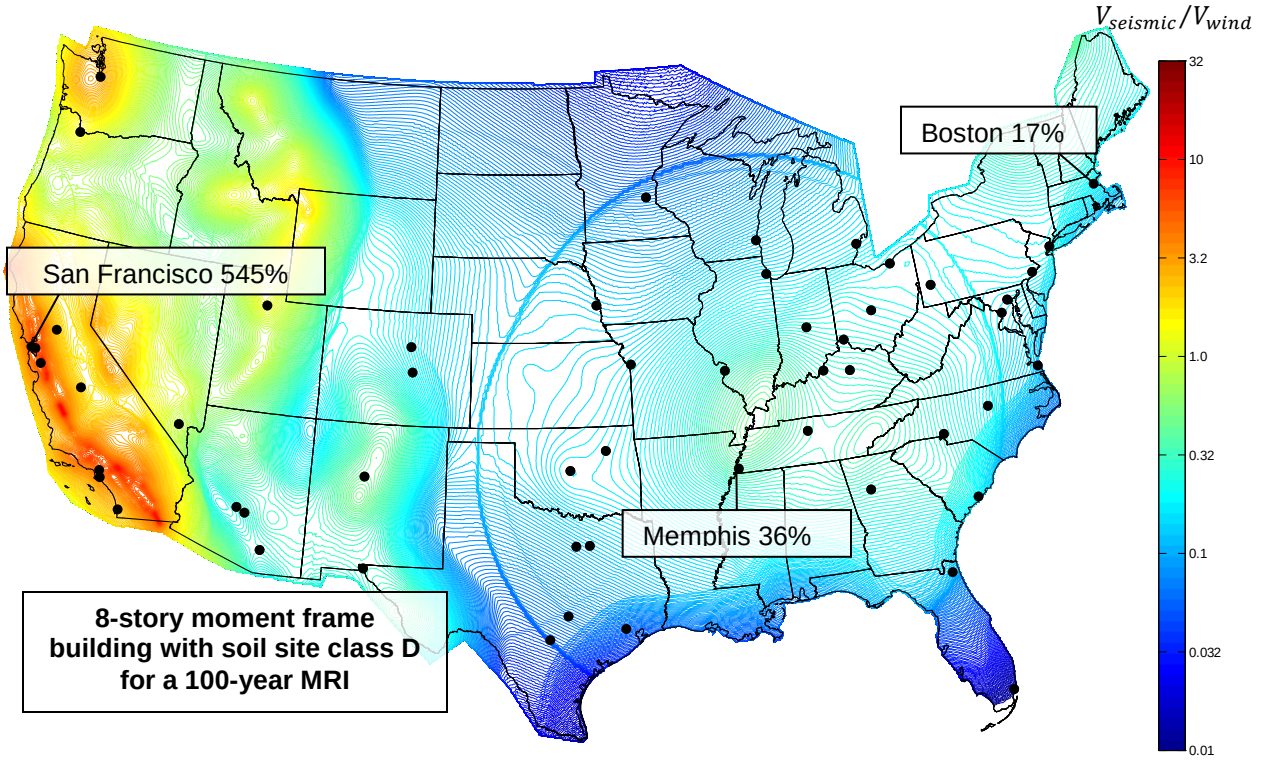

Figure 2.24 Ratio of seismic to wind elastic base shear for urban terrain (exposure category B)

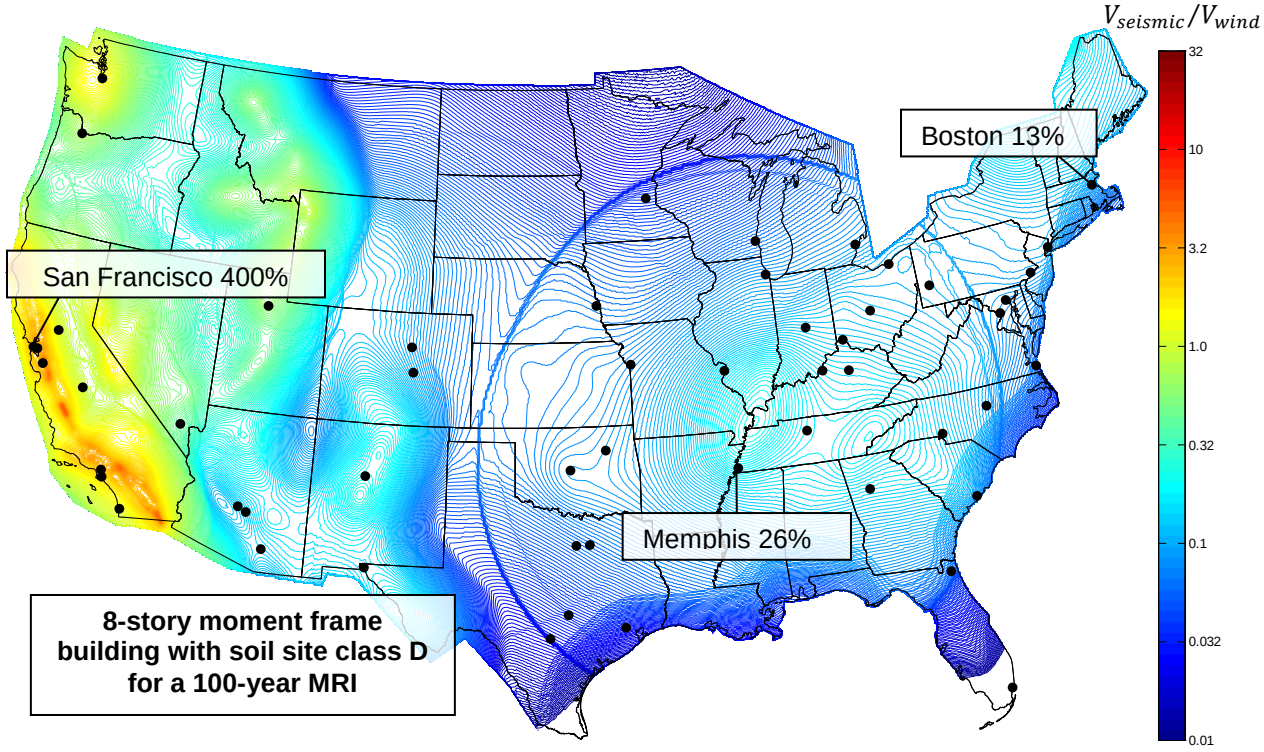

Figure 2.25 Ratio of seismic to wind elastic base shear for open terrain (exposure category C)

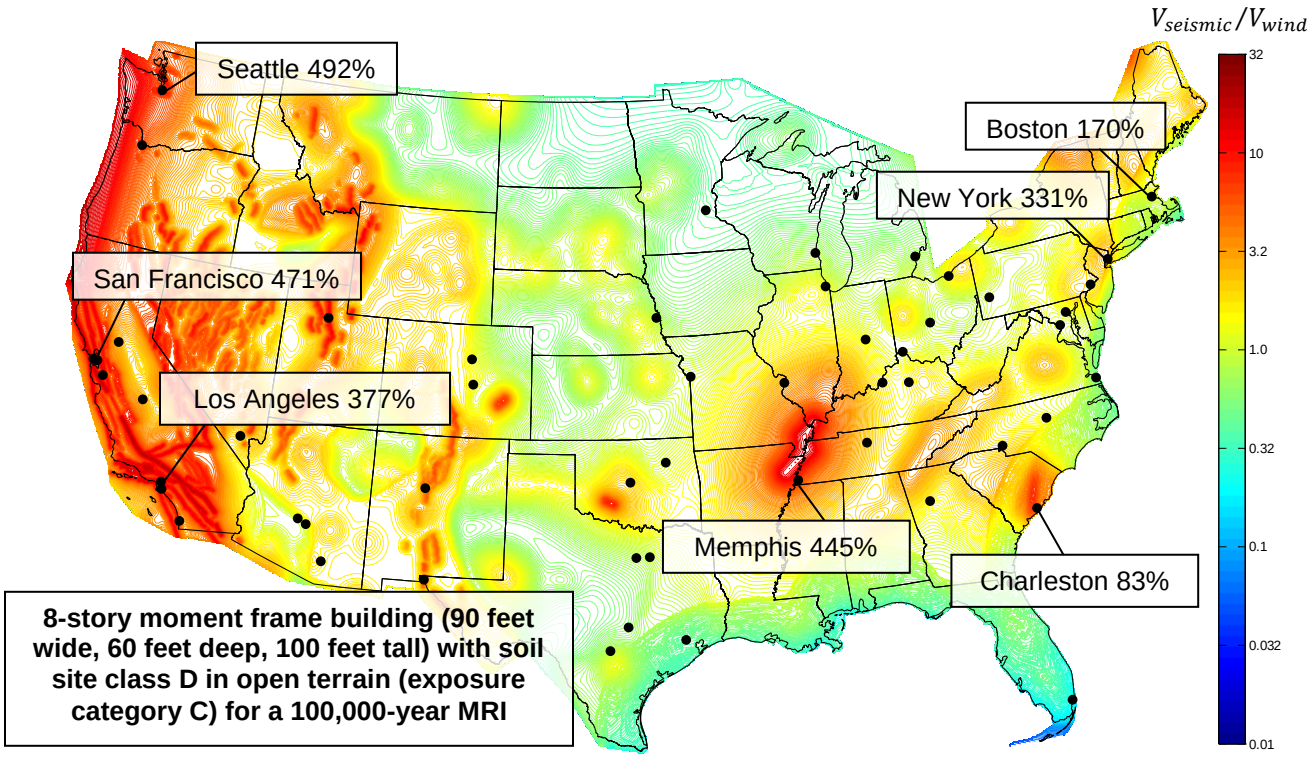

Figure 2.26 Ratio of seismic to wind elastic base shear for extrapolated ASCE 7-10 wind speeds

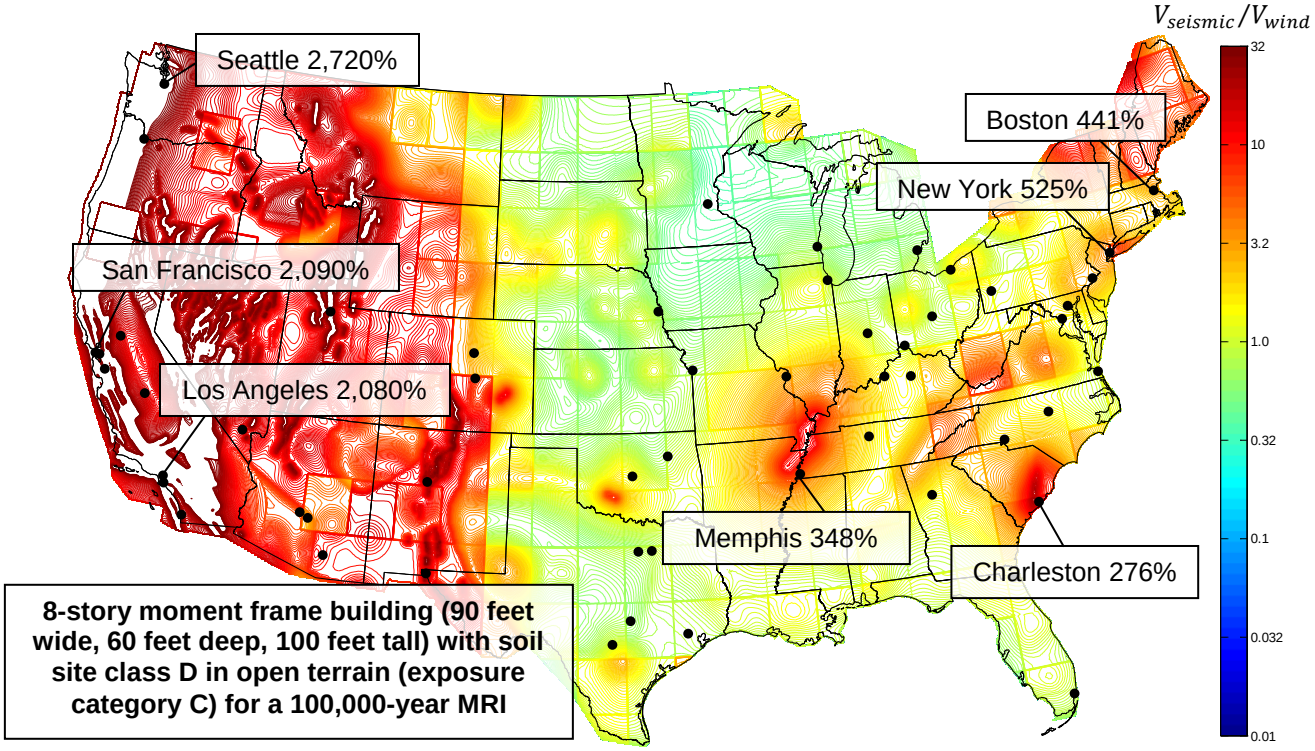

Figure 2.27 Ratio of seismic to wind elastic base shear for tornado wind speeds

2.3.2 Multi-Hazard Performance Example

An example structure is used to illustrate the multi-hazard performance of a building located in the central and eastern United States for a variety of structural systems. The example (hypothetical) structure is a children's hospital located to be located in Cape Girardeau, Missouri (37.3º latitude, -89.52º longitude) with soil site class D. A discussion of site response in Cape Girardeau is provided by Hoffman (2001).

The hospital has six stories above grade with one basement level (15 feet below grade). The building is 125 feet wide (N-S direction), 175 feet deep (E-W direction) and 85 feet tall. The first story height is 17.5 feet and upper story height is 13.5 feet. The design live load is 60 psf on the main floors, and 20 psf on the roof.

Performance Objectives

The set of performance goals (objectives) selected for the hospital are summarized in Table 2.3. It is assumed that the seismic and wind hazard levels, defined in terms of the mean-recurrence interval (MRI), were set by the stakeholders. In this example, the MRI for small and medium magnitude events was longer (i.e. conservative) compared to the 2012 *International Performance Code* (ICC 2012b). Mild damage is tolerated for most hazard levels (43-year to 475-year MRI). Moderate damage is tolerated for the maximum considered earthquake (MCE) ground motion hazard level (2,475 MRI). High damage is not tolerated for any hazard levels. It is intended that the structural design will prevent collapse and protect the life of the occupants. Since the children's hospital is an essential facility, the overarching performance objective goes beyond safeguarding life to reducing damage and ensuring that the hospital is operable during earthquakes and windstorms.

Table 2.3 Performance criteria: tolerable impact in terms of hazard level

Earthquake Event (Hazard Level)			Maximum Damage Limit (Tolerable Impact)
Magnitude	Occurrence	MRI (years)	
Small	Frequent	43	Mild
Medium	Less Frequent	225	Mild
Large	Rare	475	Mild
Very Large	Very Rare	2,475	Moderate

Seismic Hazards

The USGS national seismic hazard maps and data (Petersen et al. 2008) and seismic deaggregation tools were used to determine the seismic hazards. Figure 2.28 shows the contribution potential of earthquakes (described by magnitude and distance from the source to site) for the spectral acceleration at 1.0 seconds/cycle [$S_a(T_n = 1.0\ s)$] for each hazard level. This long-period spectral response is nearest the estimated fundamental period of the building (approximately between 1.0 and 1.5 seconds/cycle).

The seismic hazard is dominated by a magnitude 7.7 rupture on the New Madrid fault at a distance of less than 50 km from the children's hospital, except for small levels of hazard (frequent seismicity, 43 MRI) where a 5.4 magnitude quake farther away (124 km) is the primary contributor along with widespread background seismicity.

Table 2.4 summarizes the spectral acceleration, modal event, and source for each earthquake hazard level. The epsilon values for each magnitude (M) and distance (D) pair indicate the degree of uncertainty (values within -0.5 to 0 are less uncertain). Contributions of the hazard not arising from the New Madrid fault are from the central and eastern United States (CEUS) area source. Taken together, Figure 2.28 and Table 2.4 show that ground shaking was not expected to be significant, except for a rare earthquake.

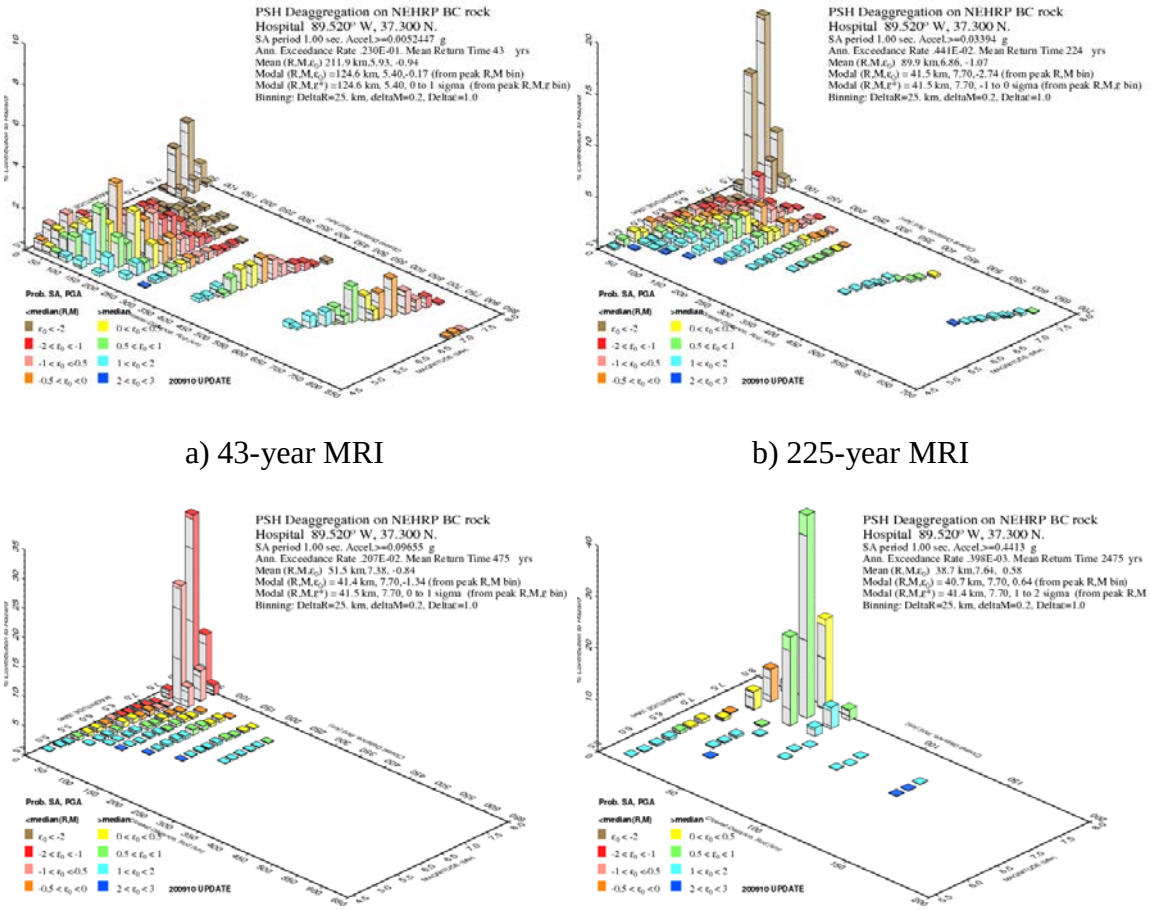

a) 43-year MRI

b) 225-year MRI

c) 475-year MRI

d) 2,475-year MRI

Figure 2.28 Contribution of potential quakes to spectral acceleration, $S_a(T_n = 1.0\ s)$

Table 2.4 Primary contributions to seismic hazard

Sa(Tn=1.0 s)		Modal Event (Earthquake)				
MRI (years)	(g)	Contribution	M	D (km)	Epsilon	Source
43	0.005	3%	5.4	124	-0.5 to 0	CEUS (91%)
225	0.034	20%	7.7	43	less than -2	New Madrid FZ (43%)
475	0.097	35%	7.7	43	-2 to -1	New Madrid FZ (75%)
2,475	0.441	40%	7.7	41	0.5 to 1.0	New Madrid FZ (94%)

Wind Hazards

Windstorm hazards were determined using the ASCE 7-10 methods. Figure 2.29a shows the basic wind pressure values for design of the structural system. The location of the children's hospital is in an area of the United States that has historically been very susceptible to tornadoes. Figure 2.29b shows the predicted 3-second gust wind speeds (mph) for the contiguous United States (corresponding to a 100,000-year MRI), based on a typical structure size and the number of tornado events that have been cataloged for 2°×2° regions (Ramsdell and Rishel 2007).

An examination of the seismic and wind hazards for this location reveals that the magnitude of expected earthquake hazards is unlikely to be significant, and that windstorms may actually dominate the most performance levels (i.e. the lower performance levels, serviceability).

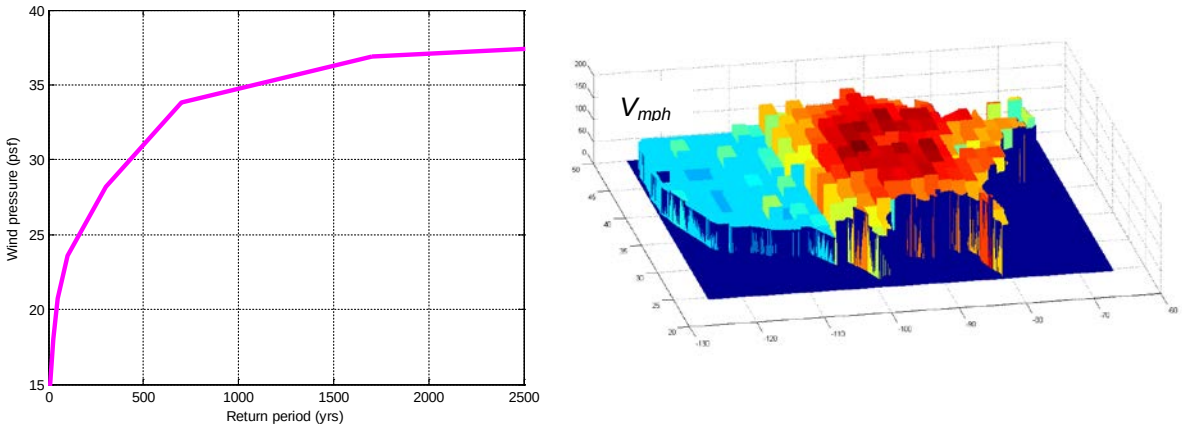

a) Design MWFRS wind pressure (psf) b) 3-second tornado gust wind speed (mph)

Figure 2.29 Wind pressure and tornado hazards for example structure

Comparison of Structural Systems

Four types of structural systems (defined in general terms) were considered for the children's hospital:

- Steel moment frames
- Reinforced concrete (R/C) moment frames
- Steel eccentrically braced frames (EBF), steel buckling restrained braced (BRB) frames
- All other systems. Broadly includes a variety of materials and systems (e.g. shear walls)

An optimal structural system is to selected based on (1) reducing the spectral demands on the structural system; (2) comparing the relative structural performance based on seismic and wind drift analyses; and (3) considering the historical performance, cost-effectiveness, and architectural viability of the system.

Table 2.5 demonstrates how the choice of structural system effects the spectral demands in terms of the estimated spectral acceleration at the fundamental period of the hospital. Since the approximate fundamental period of the hospital (based on the ASCE 7-10 empirical method) is a function of the structural system, stiffer systems lead to lower periods and higher seismic design demands.

The corresponding values of spectral acceleration account for bidirectional effects of ground shaking (maximum-direction spectrum instead of geometric mean spectrum) as well as ground motion amplification at the site based on the soil (using the NEHRP/ASCE 7 factors). Although the amplification factors in NEHRP/ASCE 7 were developed for the western United States, recent analysis (Hashash and Moon 2011) suggests that the magnitude of amplification is appropriate for long period structures in the Mississippi embayment, such as the hospital.

Table 2.5 Effect of structural system on spectral demands

Structure				Spectral Acceleration, Sa(Ta)			
System	Ct	x	Ta	43 MRI	225 MRI	475 MRI	2,475 MRI
Steel moment frame	0.028	0.8	0.98	0.012	0.077	0.222	0.745
R/C moment frame	0.016	0.9	0.87	0.014	0.089	0.251	0.855
Steel EBF	0.03	0.75	0.84	0.015	0.092	0.257	0.882
Steel BRB	0.03	0.75	0.84	0.015	0.092	0.257	0.882
All other	0.02	0.75	0.56	0.019	0.113	0.308	1.066

Figure 2.30 compares the seismic hazard curves for each structural system. The curves include the geometric mean spectrum hazard (gray line), maximum-direction spectrum hazard (red line), and the soil-amplified maximum-direction spectrum hazard (blue line), discussed in detail in Chapter 4. Seismic hazard levels are indicted by horizontal lines (from top to bottom, 43-year, 225-year, 475-year, and 2,475-year MRI) and MCE values are indicated by vertical lines.

Compared to a steel moment frame system, concrete moment frame or braced frame systems "attract" 13% to 22% more spectral acceleration, depending on the hazard level and system. This increase in spectral acceleration is due to the shape of the response spectrum and the flexibility of the system. All other factors aside, this comparison supports the selection of a steel moment frame system.

A simple analysis was used to compare the relative performance of potential structural systems. Table 2.6 shows the estimate of roof drift based on the drift-controlled structural system being designed using ASCE 7-10, and based on a linear relationship between drift and spectral acceleration. Damage is based on approximate drift ratio limits adapted from Griffs (1993), Galambos and Ellingwood (1986), and ASCE (1986). In Table 2.6, "high damage" is indicated in orange.

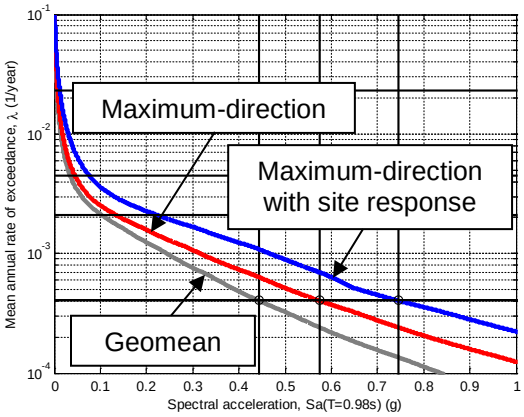

a) Steel moment frame

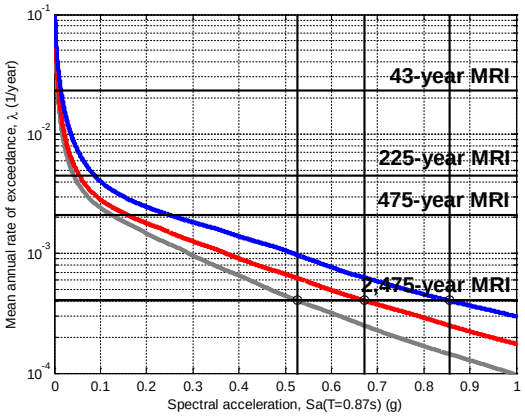

b) Reinforce concrete (R/C) moment frame

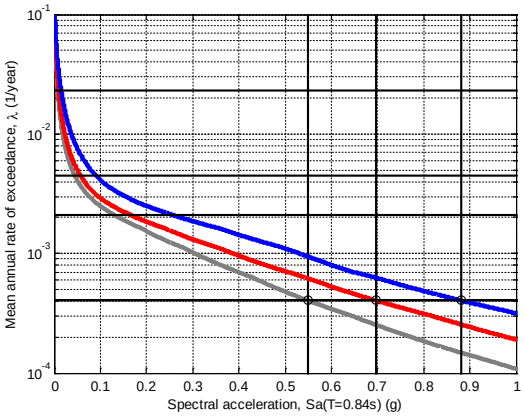

c) Steel EBF or BRB

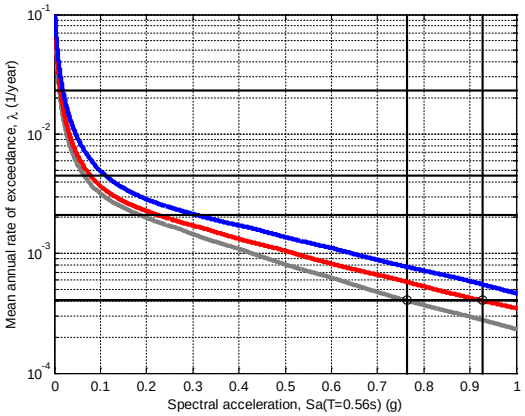

d) "All other" structural systems

Figure 2.30 Seismic hazard curves for potential structural systems

Table 2.6 Estimated drift ratio and probable damage for seismic hazards

System	Drift Ratio			
	43-year MRI	225-year MRI	475-year MRI	2,475-year MRI
Steel moment frame	0.000246	0.001554	0.00447	0.015
R/C moment frame	0.000253	0.001565	0.004395	0.015
Steel EBF	0.000254	0.001567	0.004365	0.015
Steel BRB	0.000254	0.001567	0.004365	0.015
All other	0.000266	0.001596	0.00434	0.015

The analysis suggests that the hospital is unlikely to experience any kind of significant damage due to earthquakes. Yet, should the New Madrid fault have a very-rare large magnitude rupture at the MCE hazard level, high damage is expected. The hospital is expected to survive, but likely it will be badly damaged. It may be difficult to repair and there may be significant downtime during those repairs.

The analysis method for this example is manifestly approximate, and is not intended to provide a precise or final assessment. Yet given that limitation, the analysis would suggest there is no advantage in terms of seismic drift control for one structural system above another. However, wind drift control is another matter.

Table 2.7 shows an estimate of the damage expected due to windstorms. The estimate is based on the ratio of wind base shear to seismic base shear, where the seismic base shear is calculated including the R value and importance factor, but not the 2/3 factor for the design basis earthquake demands. Tornadoes are a threat for this area of the country, but the effects do not alter the projected wind speeds until longer return periods.

Table 2.7 Estimated drift ratio and probable damage for windstorm hazards

Structural Lateral Force-Resisting System				Drift Ratio			
				43 MRI	225 MRI	475 MRI	2,475 MRI
Type	Ct	x	Tw	89 mph	103 mph	110 mph	122 mph
Steel moment frame	0.045	0.8	1.57	0.0021	0.0028	0.0032	0.0035
R/C moment frame	0.023	0.9	1.25	0.0018	0.0025	0.0028	0.0031
Steel EBF	0.030	0.75	0.84	0.0018	0.0024	0.0027	0.0030
Steel BRB	0.030	0.75	0.84	0.0018	0.0024	0.0027	0.0030
All other	0.013	1	1.13	0.0015	0.0020	0.0023	0.0025

The results indicate that it is very possible for the children's hospital to experience mild damage, especially for more flexible structures. Steel moment frames are especially vulnerable. Thus, a realistic selection of a structural system requires an evaluation of the likely damage due to windstorm hazards. Steel moment frames are favorable in terms of historical performance in earthquakes. Steel moment frames are especially cost-effective for 6-story to 9-story structures, compared to other systems, if the gravity system is utilized (Elnashai and Di Sarno 2008).

2.4 Discussion

In many ways, seismic hazard in the central and eastern United States is different compared to the western United States. Although earthquakes of a given magnitude occur less frequently in the central and eastern United States, ground motion is felt over a much broader area. Strong ground motion in the central and eastern United States is likely to be of long duration, which is important for non-ductile structures and components that are prone to low-cycle fatigue. Also, the uniform hazard response spectrum is likely a conservative target for ground motion selection and scaling. Large magnitude earthquakes are rare outside the western United States. As a consequence, even for communities in the New Madrid high-seismic area, the impact of frequently occurring earthquakes (serviceability-level seismic hazard) is the primary concern, not life safety (Olshansky et al. 2003).

Of course it is recognized that any "micro-zonation" or generalization concerning seismic hazard is inherently inexact. There are significant regional aspects to ground motion attenuation, and, in addition to topographic effects, site response is dependent on bedrock characteristics, the soil velocity profile, and the magnitude and depth of the soil-to-bedrock impedance contrast.

Bedrock in most of the central and eastern United States is harder than the bedrock in populated areas of the west coast, and in evaluating site response, ground motion data corresponding to V_s = 2,000 m/s is more appropriate compared to B/C boundary data. Soil-structure interaction is important for stiff buildings located on a stiff soil site, and should be considered in the site response of braced-frame and shear wall buildings on hard rock sites, common in the central and eastern United States. Although site response informed by regional geology may provide a first-order estimate (e.g. Kottke et al. 2012), a geotechnical site investigation is recommended where feasible.

The spectral demands associated with the 43-year and 72-year events in the central and eastern United States are approximately 5% and 10% of the MCE, respectively, roughly half of the comparable demands in the western United States. This is noteworthy considering that in ASCE 7-10 drift limit is 0.02 for the DBE (defined as two-thirds of the MCE) for buildings with ordinary use and occupancy.

For example, assuming a structure was designed using ASCE 7-10 and a linear relationship between drift and ground motion intensity, a building in the western United States would experience, on average, an inter-story drift ratio of approximately $0.10 \times 0.02/(2/3) = 0.003$ in the 43-year event. According to typical observed behavior (i.e. Griffis 1993) this magnitude of drift ratio would be visible and would cause architectural damage. The drift ratio corresponding to the 72-year event is 0.006, and could be expected to damage many nonstructural components, including partition walls and windows. The latter is especially significant for wind engineering, where penetration of the building envelope can lead to water infiltration and serious habitability problems (Kwok et al. 2015).

In the central and eastern United States, the same building would experience, on average, a 43-year MRI drift ratio of only $0.05 \times 0.03 = 0.0015$ times the story height, which is near the threshold of expected damage for nonstructural components (Griffis 1993). Thus, in contrast with the western United States, ground motions during small and medium events, used to design for serviceability limit states, are unlikely to be significant for new buildings in the central and eastern United States. In contrast, service-level wind loads are expected to be significant.

As a consequence, it is possible that buildings designed for wind can provide adequate performance in many regions. In high-seismic zones, like New Madrid and Charleston, where very large rare quakes are possible, a structural system (i.e. a collapse prevention system) could be devised to exploit the unique shape of seismic and wind hazard curves in the central and eastern United States. Of course it should be recognized that large events are possible not only in New Madrid and Charleston, but all over the central and eastern United States. The historical events in New Madrid and Charleston stand out in the catalog because of the scarcity of large-magnitude events, but the earthquakes were not exceptional in terms of magnitude. In fact, almost all of the central and eastern United States is capable of generating a magnitude 7.5 earthquake (Chapman 2014).

Chapter 3

ARCHETYPE STRUCTURAL SYSTEMS

This chapter describes the collapse prevention system concept and the selection and development of archetype structural systems. In order to determine the applicability of the collapse prevention system concept to steel moment-frame buildings commonly constructed in the central and eastern United States, the archetype systems were intended to be prototypical building configurations with or without collapse prevention mechanisms. Reserve lateral strength in the gravity framing system is discussed. Delayed-stiffness collapse inhibiting mechanisms are described, as well as optional energy dissipation devices. Enhanced shear tab connections, using T-stub type structural fuses, are discussed. The analytical modeling and nonlinear analysis approach are also discussed.

3.1 Collapse Prevention System Concept

The concept of a collapse-prevention system consists of two aspects. First, the main lateral-force resisting system is designed for wind (or low to moderate seismicity), and, where required, together with the gravity framing system it is used to provide adequate performance under low to moderate level ground motions and service-level wind events. Second, the main lateral-force resisting system (and the reserve lateral strength in the gravity framing where applicable) is used

in tandem with a back-up collapse-inhibiting mechanism, or enhanced shear tab connections, to provide life safety under extreme ground motions (i.e. the MCE-level ground motions) and extreme wind events. When necessary, serviceability performance is improved by augmenting collapse-prevention systems with auxiliary energy dissipation devices.

3.1.1 Reserve Lateral Strength in Gravity Framing

The concept of utilizing gravity framing as a back-up or "reserve" lateral system is a concept that has emerged in post-Northridge years (Liu and Astaneh-Asl 2000; Ariyaratana and Fahnestock 2011; NIST 2012c).

Gravity framing can serve as a reserve lateral system for two reasons: First, gravity frame connections have lateral strength. Composite concrete-slab and steel beam-to-column (shear tab) connections are partially restrained and inherently have lateral strength and stiffness. Liu and Astaneh-Asl (2000, 2004) showed that simple gravity beam-to-column connections may provide significant lateral strength and act as a ductile back-up system by engaging the concrete slab. Similarly, reserve lateral strength also exists in braced frame systems where gusset plates at pinned ends of braces create rotational restraint at the beam-to-column connection (Stoakes and Fahnestock 2011; Ariyaratana and Fahnestock 2011).

Second, the quantity of gravity connections in a moment-frame building can be significant compared to the number of fully-restrained (moment) connections, depending on the building column layout and the gravity column orientation. Thus, although the lateral strength of a shear tab connection is typically a fraction of the moment-frame connection strength (on the order of 10% to 30%), taken in aggregate the gravity framing strength may be significant.

Analytical studies have shown that the gravity system may contribute in a significant way to the performance of steel moment frame structures, in terms of strength and stiffness (Eatherton and Hajjar 2011), serviceability (Flores and Charney 2014), and collapse resistance (NIST 2010b; Flores and Charney 2014; Judd and Charney 2014b; Flores 2015). Incorporating the gravity system in a non-linear response history analysis (at 3 times the MCE) of a 4-story building (NIST 2010b), for example, reduced median roof drift ratio from 4.9% to 3.4%, and reduced the number of collapses in 44 analyses from 22 to 11. Post-earthquake reconnaissance has also confirmed the concept of reserve lateral capacity in gravity framing. Observations of two low-rise steel buildings after the 1994 Northridge quake concluded that the perimeter moment frames had failed, but the gravity framing likely had prevented collapse (Leon 1998). An analytical study after the quake also confirmed that this might be the case (Astaneh-Asl et al. 1998).

The availability of reserve lateral strength in the graving framing has led to the idea of using dual systems for lateral resistance, such as a conventional lateral force resisting system (i.e. a moment or braced frame) for primary resistance, and a gravity framing system as a back-up lateral resisting system (Nelson et al. 2006; Hines et al. 2009; Hines and Fahnestock 2010). The effect of reserve strength in the gravity framing has been shown to be greater for non-ductile lateral systems than for ductile lateral systems (Wen et al. 2013). This study considers the reserve strength due to the gravity framing columns and gravity framing beams (shear tab connections).

3.1.2 Collapse Inhibiting Mechanisms

Literature Review

Collapse mechanisms with delayed strength and stiffness mechanisms are an attractive back-up system. The intent of such a mechanism is to not add stiffness to the structure prior to the time the mechanism is needed. In terms of seismic design, added stiffness reduces the period of vibration, and in turn, a reduced period of vibration typically increases the base shear demand (depending on the ordinate of the response spectrum).

Delayed-stiffness collapse inhibiting mechanisms have been used in the past, particularly in large-scale seismic experiments where conventional structures are tested to near collapse, but for safety and other reasons it is not acceptable for the test specimen to fully collapse. For example, slack cables were used to prevent full collapse of a full-scale 4-story steel moment-frame structure that was tested on a shake table at the E-Defense facility in Japan (Lignos et al. 2013).

Research using delayed stiffness is limited compared to other types of lateral protection schemes. Saunders (2004) investigated brace devices made of hyper-elastic materials used to provide passive seismic protection of buildings. As the term suggests, hyperelastic materials deform nonlinearly, stiffen under load, and unload elastically. Hyperelastic devices behave similar to the way nonlinear fluid viscous dampers perform (Oesterle 2002). Thus, while hyperelastic braces may not increase base shear forces at service level loads, they are able to stabilize a structure and prevent collapse. Saunders employed two sets of cubic polynomial functions to define the hyperelastic material stress-strain relationship. The first set exhibits higher early stiffness. The second set exhibits higher later stiffness. Saunders' cubic polynomial functions were based on a preliminary study by Jin (2003). Jin examined the effect of

hyperelastic elements on maximum displacement, residual displacement, and maximum base shear, and combined these results to determine the optimum cubic polynomial functions. Saunders' analytical results showed that delayed-stiffness devices (e.g. a slack-cable) are effective at controlling the behavior of unstable systems, while at the same time avoiding too much contribution to stiffness (and thus higher component force demands).

Saunders work was also the basis for subsequent research by Chittur Krishna Murthy (2005) who investigated one of two prototype hyperelastic devices proposed by Saunders. In Chittur Krishna Murthy's study, a visco-hyperelastic device consisting of motorcycle tires was placed between two steel rings. The results showed the device successfully dissipated energy.

Ryan (2006) investigated structures using double-braided synthetic fiber ropes to improve the seismic performance of steel moment frames. The investigation included experimental tests, 1:3-scale dynamic tests and 1:6-scale shake-table tests and nonlinear dynamic analytical studies. The 1:6-scale experiments suggested the ropes considerably improved performance, since maximum and residual drift were reduced with minimal increase to the maximum base shear. Although the original intent of Ryan's work was to evaluate the "cable snapping" energy-dissipation potential of the ropes, the upshot was that ropes could stabilize structures that have significant residual drift. In a related application, used slack chains to prevent displacement in a "beyond-design level earthquake" of a building located in Los Angeles County (Kelly 2004).

Ibrahim, et al. (2005) developed an energy dissipation device called a "viscoplastic" damper. This device consisted of two steel plates that were pre-bent (pre-buckled), so when loaded axially in tension or compression, the axial stiffness was reduced. Between the plates was a high damping viscoelastic solid material that was stressed in tension when the plates were in compression, and stressed in compression when the plates were in tension. The changes in

strain (deformational velocity) in the viscoelastic material provided damping at low-level displacements, and the flexural yielding in the plates at higher levels of deformation provided the needed energy dissipation under strong ground shaking. The device had a nonlinear force-displacement relationship while the steel was still elastic, with the stiffness increasing with axial force.

Marshall (2008) and Marshall and Charney (2010a, 2010b, 2012) developed a device that acts like a low-axial stiffness viscoelastic damper at low levels of deformation, and then stiffens to act like a steel buckling restrained brace at higher levels of deformation. This device was tested both analytically and experimentally, and proved to be very effective in controlling low-level response (via damping) and high level response (via inelastic yielding). A similar device was also tested by Yamamoto and Sone (2014). These devices are a prototype of one of the "advanced telescoping brace" collapse prevention mechanisms described in this study.

A variety of designs could form a collapse inhibiting mechanism (Figure 3.1 and Figure 3.2). [See also Judd and Charney (2014e).] The simplest mechanisms consist of a pair of slack cables (Figure 3.1a,b) or loose linkages (Figure 3.2a) that provide no resistance or stiffness until the building story deformation reaches some limit, such as 2% interstory drift. Then, at the predefined deformation, the slack cable (SC) or loose linkages (LL) become taut and augment the residual building system strength to prevent dynamic instability. This study will consider slack cables in knee-brace arrangement and loose linkages.

Selected mechanisms can be equipped with energy dissipating devices, such as small viscous fluid dampers or viscoelastic solid high-damping rubber material, to enhance serviceability performance under wind or small seismic events. Energy dissipating devices are effective for seismic design (Symans et al. 2008). In fact, a previous investigation of steel

moment-frame buildings (Atlayan and Charney 2011) indicated that adding even a small amount of damping is advantageous (e.g. increasing the equivalent system damping from 5% to 10% critical). In the case of collapse-prevention systems, this added damping would primarily be used to control behavior up until the point that the collapse inhibiting mechanism engages.

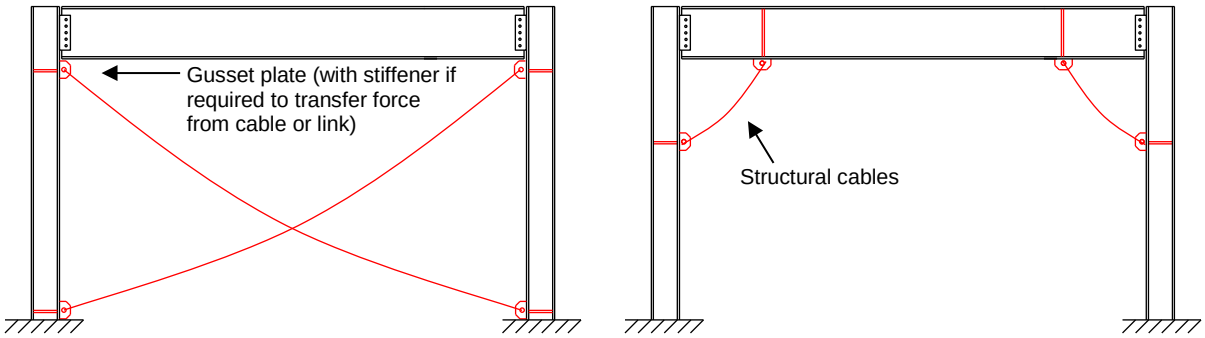

a) Full-bay slack-cable X-bracing b) Slack-cable (SC) knee bracing

Figure 3.1 Prototypical collapse inhibiting mechanisms

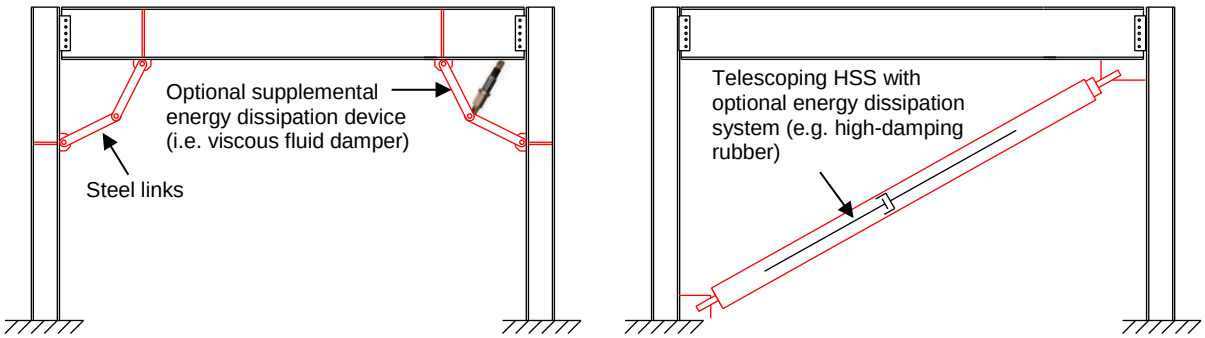

a) Loose linkages (LL) b) Telescoping brace (TB)

Figure 3.2 Prototypical collapse inhibiting mechanisms equipped with energy dissipating devices

Loose linkages may be used alone as a collapse inhibiting mechanism (left corner in Figure 3.2a) or may be used in association with a damper (right corner in Figure 3.2a), to act as a true toggle brace damper system. In fact, the loose-linkage mechanism can be thought of as a toggle brace without the damper. The idea behind a toggle brace is that deformations acting parallel to the braces are amplified in the transverse direction, thereby increasing the efficiency of dampers (Constantinou et al. 2001).

The toggle brace system is useful in stiff structures, for reduction of wind vibrations, or to reduce the size of the damper device. By amplifying displacement and velocity, smaller and lower-cost dampers may be used. The amplification allows dampers to be used in the short-period range, as well as for wind applications. Amplification systems may use gear mechanisms (Berton and Bolander 2005) or "toggle braces" and "scissor jacks" (Whittaker and Constantinou 2004).

Charney and McNamara (2008) show that a toggle system is "generally more efficient when compared to the diagonal system." Huang and McNamara (2006) investigated both toggle-brace and scissor-jack systems. The conclusion was that the effectiveness of the system is directly related to the stiffness of the brace. Hwang et al. (2008) derived new design formulas for structures with supplemental viscous dampers by modifying the existing design formulas to account for the effects of combined shear and flexural deformation of the structure. Constantinou et al. (2001) demonstrated the use of three types of toggle brace mechanisms that may be utilized effectively in application of small structural drift, using shake table testing of a large scale steel modal structure and analysis, and discussed some applications.

Huang (2004) derived the amplification factor by including the brace elongation, and discussed configurations for different design parameters, including target story drifts, brace

stiffness, joint reduction, and damping value. The conclusion was that "conventional placed damper device may be not efficient under normal wind condition due to small story drift" and "the efficiency of [toggle brace damper] devices is very sensitive to the design parameters, such as geometric configuration, relative brace stiffness and damping values, and other parameters." Also, "the stronger and stiffer brace members always have better performance for the [toggle brace damper] system. The larger viscous damper force may not produce larger energy dissipation." Hwang et al. (2005) provided design procedures for "upper" and "lower" toggle-brace-damper systems with dampers directly installed to beam-column joints, and performed shake table tests on a scaled-down three-story steel model. The result is the system was more efficient in controlling the seismic response of the model structure compared to a diagonal-braced damper system.

Hwang et al. (2006) showed that viscous toggle-braced dampers are effective in reinforced concrete structures with walls, as well as such structures without walls. Lee et al. (2007) studied toggle brace systems using magnetorheological dampers. Based on analytical and experimental results, the study concluded that structural performance is enhanced compared to magnetorheological dampers not installed in an amplifying brace system. Di Paola and Navarra (2009) propose a "pendulum" type toggle brace damper system.

A more complex collapse inhibiting mechanism is the telescoping brace (TB) shown in Figure 3.2b. In this mechanism two steel tubes telescope over each other and can elongate without resistance until a "stop" mechanism causes the brace to go into tension. The brace cannot carry compression. The telescoping brace described here is an adaptation of the hybrid passive energy dissipation device developed by Marshall and Charney (Marshall and Charney 2010a,b; Marshall and Charney 2012) discussed in the previous section.

A key aspect of the collapse-prevention system concept is the size of the mechanisms: the slack-cable and loose-linkage configurations can be compact and unobtrusive. Where a compact configuration is used, the collapse inhibiting mechanisms could be distributed throughout the building. A larger mechanism, such as the telescoping brace, on the other hand, would likely be installed in only selected bays. Another important aspect of the collapse-prevention system is that the mechanisms may be deployed in both the moment frame and the gravity frame. Indeed, collapse inhibiting mechanisms are envisioned to work as a supplement to the conventional lateral-force resisting system (e.g. moment frame or braced frame) in conjunction with reserve lateral strength in the gravity framing system.

3.1.3 Enhanced Shear Tab Connections

As discussed previously, the lateral force-resisting capacity of a conventional gravity-frame beam-to-column connection is often small, on the order of 10% - 30% of a comparable moment-frame connection, and is not typically utilized for seismic protection. An alternate collapse-prevention system (in lieu of utilizing the existing reserve lateral strength in shear tab connections and a collapse inhibiting mechanism) is proposed in this section that enhances the lateral-force resisting capacity of conventional gravity-frame connections.

The method consists of modifying the existing shear tab connection (as a retrofit or in new construction) and installing T-stub type flange connectors in order to create a ductile partially-restrained beam-to-column connection (Figure 3.3). The existing beam flanges and the T-stub connector are used to form a buckling-restraint mechanism that allows a reduced-width segment of the T-stub stem, or “yield-link” (Figure 3.4), to act as a structural fuse in a seismic or extreme wind event. The application is based on the Yield-Link™ components used in Strong-

Frame® special moment frame system (Pryor and Murray 2013; ICC-ES 2013). Such enhanced shear tab connections have the added benefit that beam flange bracing is not required. Moreover, the connection is highly repairable because damage is limited to the fuses while other components of the connection remain elastic.

In the enhanced shear tab connection, a single plate shear connection is used to transfer shear, and a pair of buckling restraint mechanisms (one at the top beam flange, one at the bottom) is used to transfer flexure. The single plate shear connection uses a coped beam web, a center standard bolt hole, and upper and lower slotted bolt holes, to permit a true hinge mechanism (Figure 3.5).

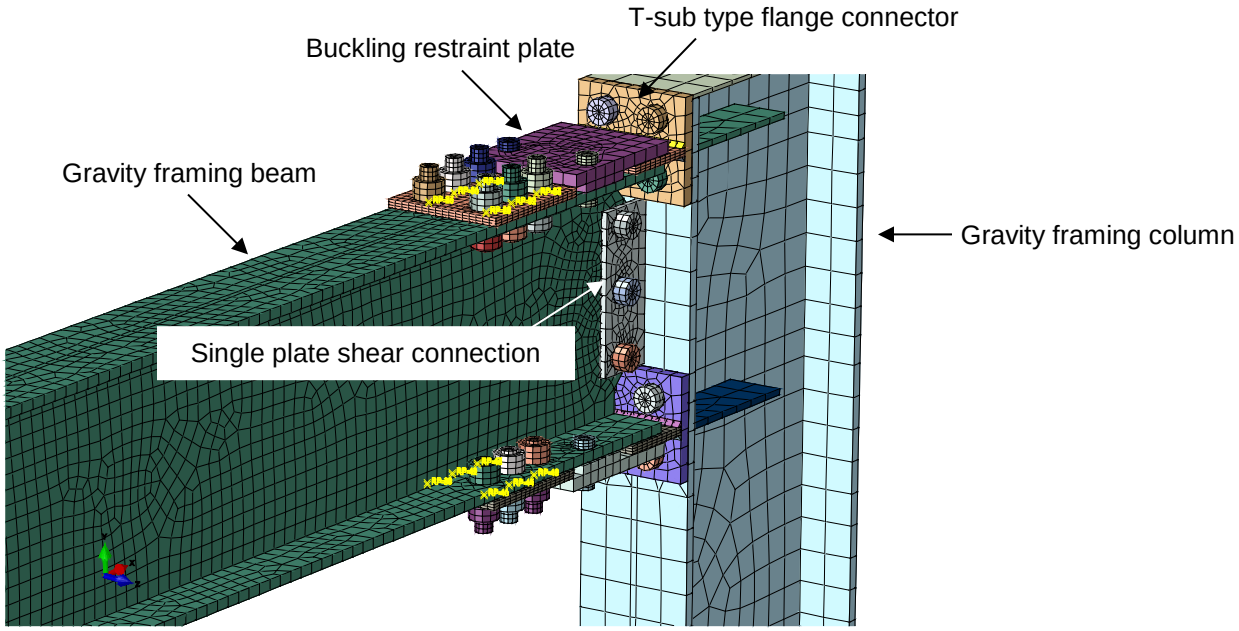

Figure 3.3 Finite element model of enhanced shear tab connection

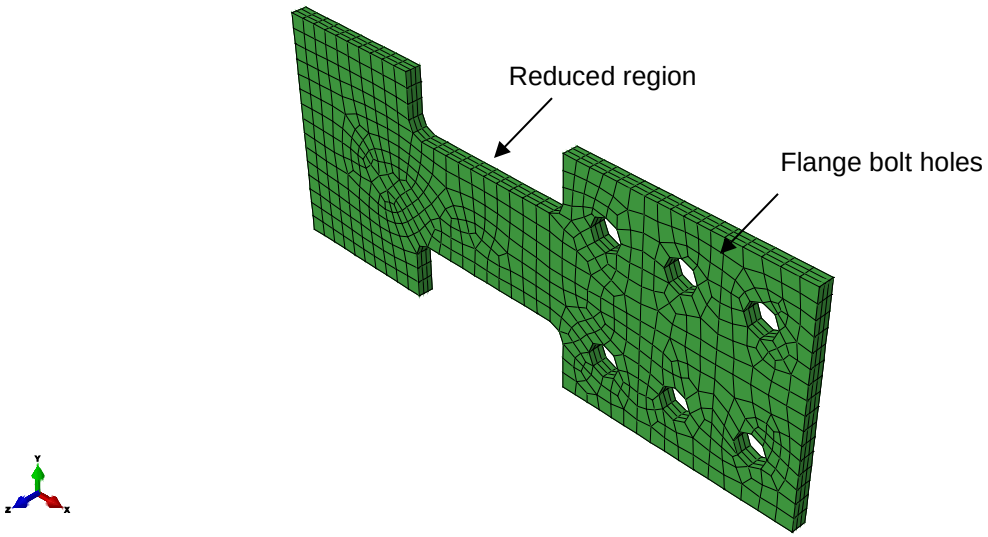

Figure 3.4 Finite element model of yield link (T-stub stem)

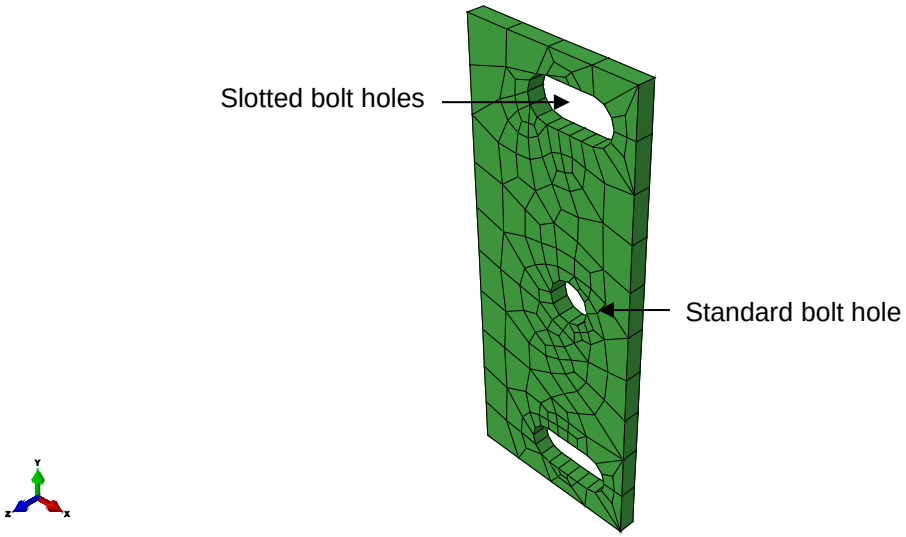

Figure 3.5 Finite element model of shear tab with slotted upper and lower bolt holes

The buckling restraint mechanism consists of the T-stub type flange connectors, an outer restraining plate, inner spacer plates, and restraint bolts. Figure 3.6 shows a finite element representation of the enhanced shear tab connection during a monotonic load analysis. The T-stub structural fuse is bolted to the beam flange, it has a flange that is bolted to the column flange, and a stem (with a reduced region) designed to yield in both tension and compression. Compression yielding of the T-stub stem is achieved by using the beam flange and the outer restraining plate to force the reduced region of the link stem into high-mode buckling (rippling). Figure 3.7 shows a finite element model representation enhanced shear tab connection with a buckling restraint plate that is too thin to constrain the buckling of the reduced region, during a monotonic load analysis.

The inner spacer plates limit friction between the restraint plate and the T-stub stem, and limit transverse movement of the T-stub stem during yielding. Snug-tight bolts pass through the restraint plate, each spacer plate, and the beam flange to encapsulate the mechanism. The remaining bolts are fully pre-tensioned. In concept, the buckling restraint mechanism provided by the restraint plate and beam flange is similar to that used in all-steel buckling restrained brace (BRB) frames (Genna and Gelfi 2012a,b, 2014).

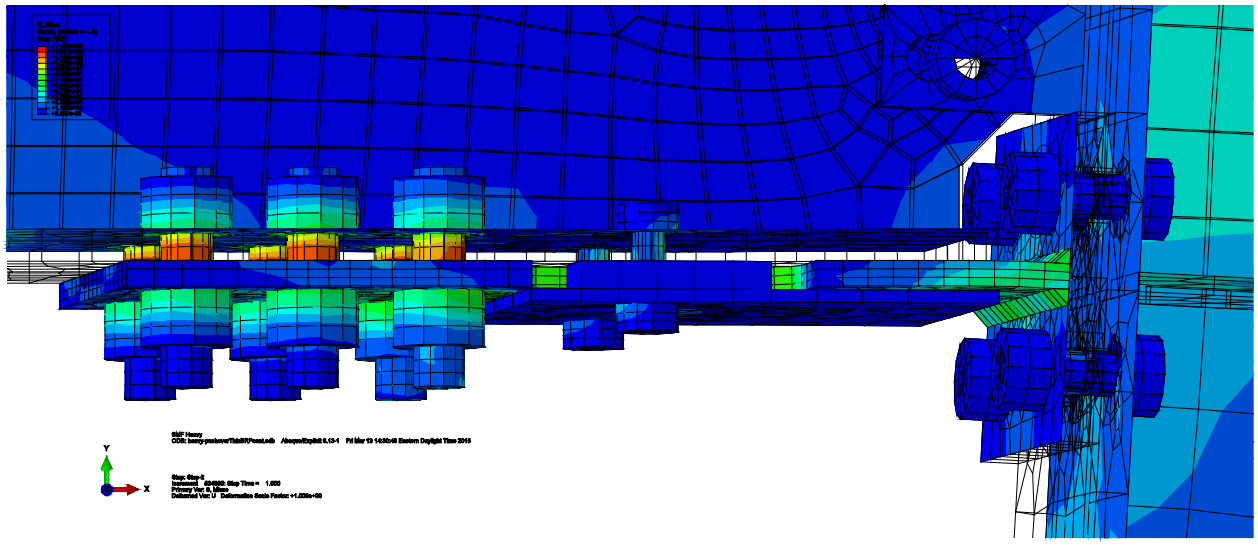

Figure 3.6 Finite element model of enhanced shear tab connection

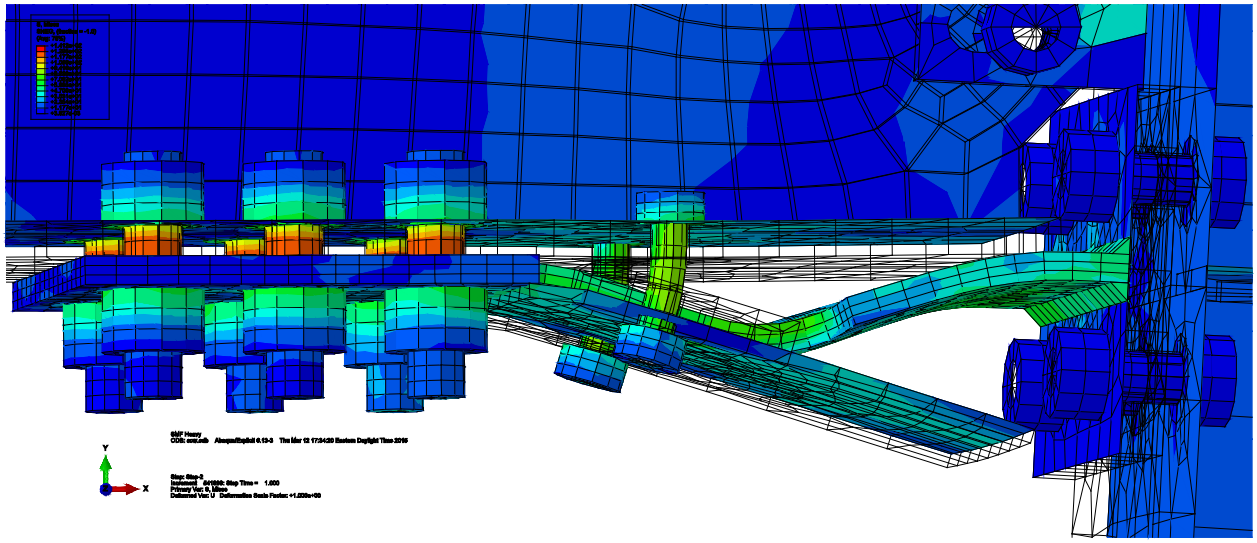

Figure 3.7 Finite element model of non-constrained buckling restraint mechanism

3.2 Archetype Buildings

Table 3.1 summarizes the building archetypes. Three types of archetypical structural systems were included. The buildings employed either a non-ductile moment frame, or a ductile moment frame designed for moderate seismic demands. Building design criteria was based on the building codes and standards in current use (described in detail in Appendix B).

Table 3.1 Archetype structural systems

Archetype (Seismic Design Category)	Total Number of Stories	Reserve lateral strength in shear tab connections	Enhanced shear tab connections	Slack Cables	Loose Linkages	Loose Linkages with Viscous Fluid Dampers	Telescoping Braces with High-Damping Rubber
Type I							
Non-ductile (SDC B_{min})	1	●	●	●	●	●	●
	2	●	●	●	●	●	●
	4	●	●	●	●	●	●
	8	●	●	●	●	●	●
Ductile (SDC D_{min})	1	●	●	●	●	●	●
	2	●	●	●	●	●	●
	4	●	●	●	●	●	●
	8	●	●	●	●	●	●
Type II							
Non-ductile (SDC B)	4	●					
Type III							
Non-ductile (SDC B)	10	●					

3.2.1 Type I Archetype Buildings

The first type ("Type I") was archetypical short period (1-story and 2-story) and long period (4-story and 8-story) office buildings that employed either a non-ductile moment frame, with fully-restrained flange welded connections, or a ductile moment frame with reduced beam section (RBS) connections. The building configuration and overall plan layout for Type I are shown in Figure 3.8 and Figure 3.9. The building plan used 20-ft bays and perimeter moment frames. The first story height (measured to the top of the beam) was 15 ft. Upper story height was 13 ft. 1-story and 2-story moment frame columns were considered pinned at the base, taller columns were considered fixed. The layout, story heights, and gravity loads match the special steel moment framing building archetypes developed in the ATC-76 project (NIST 2010a).

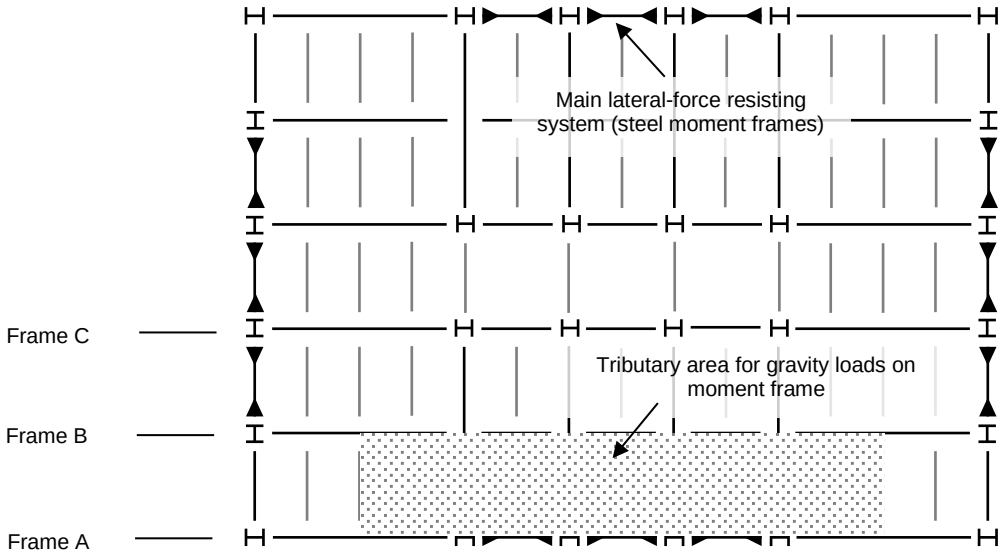

Figure 3.8 Type I non-ductile and ductile moment frame 1-story, 2-story, 4-story, and 8-story building framing plan

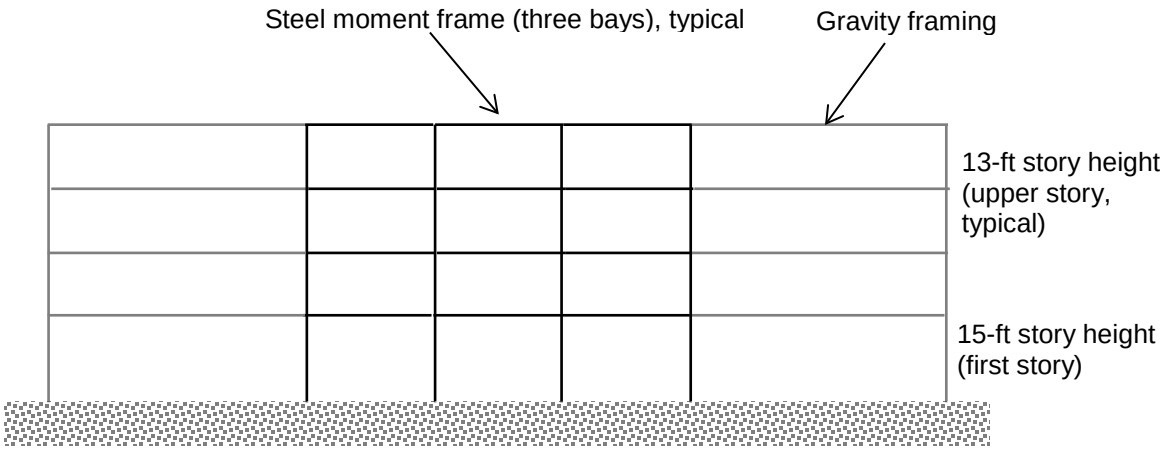

Figure 3.9 Type I archetypical building elevation view of structural framing in longitudinal direction (4-story building shown)

Gravity columns were considered pinned at the base, and were spliced 4 ft above the third and sixth floors. The ATC-76 evaluation (NIST 2010a) did not model gravity framing and, as a result, the gravity framing layout shown, including the direction and spacing of filler beams every 10 ft, column splices, and gravity column orientation, were developed in this study. The gravity frame columns were oriented with the strong axis in the same direction as the moment frames (the longitudinal direction), and thus the reserve lateral strength observed in this study represents an upper bound on the gravity framing contribution for this building configuration.

The first building type was developed following the procedure recommended in FEMA P-695 (FEMA 2009a). The non-ductile steel moment frames were not detailed for seismic resistance and were designed for a wind hazard corresponding to non-coastal location in the United States and low seismicity [Seismic Design Category (SDC) B_{min}, meaning the lowest spectral accelerations corresponding SDC B].

Table 3.2 provides the structural members for the non-ductile moment frame buildings. Moment frame design was based on meeting drift requirements and providing a column moment of inertia between 1 and 2 times the beam moment of inertia (Hamburger et al. 2009; Bruneau et al. 2011). The frame was designed without considering the collapse prevention system. Initial beam and column sizes were adjusted when required to meet strength and stability requirements. Column sizes were selected from W14, W18, and W24, depending on the loads. To reduce cost, column sizes were increased to avoid specifying double plates.

The gravity framing selection (Table 3.3 and Table 3.4) was based on considering both composite and non-composite (construction) strength. Gravity members were not designed for lateral loads, except members that form part of the steel moment frames were subsequently designed for lateral loads. The final column member sizes used match the gravity columns used in a related study (Flores 2015).

Table 3.2 Type I archetypical building non-ductile moment frames

No. of stories	Story	Beam size	Column size		Controlling criteria
			Exterior	Interior	
1	1	W18X35	W14X82	W14X82	Stability
2	1	W21X44	W18X71	W18X76	Stability
	2	W16X31	W18X71	W18X76	
4	1	W16X40	W18X76	W18X86	Stability
	2	W21X44	W18X76	W18X86	
	3	W18X35	W18X40	W18X46	
	4	W16X31	W18X40	W18X46	
8	1	W21X48	W24X146	W24X146	Wind strength
	2	W24X68	W24X146	W24X146	
	3	W24X76	W24X76	W24X103	
	4	W24X55	W24X76	W24X103	
	5	W24X55	W24X55	W24X62	
	6	W21X48	W24X55	W24X62	
	7	W18X35	W24X55	W24X55	
	8	W18X35	W24X55	W24X55	

Table 3.3 Type I archetypical building gravity framing column sizes

Column Size				
No. of stories	Story	Frame Line A	Frame Line C	
		Lines 1, 6	Lines 2, 5	Lines 3, 4
1	1	W14x43	W14x90	W14x61
2	1	W14x43	W14x90	W14x61
	2	W14x43	W14x90	W14x61
4	1	W14x43	W14x90	W14x61
	2	W14x43	W14x90	W14x61
	3	W14x30	W14x90	W14x61
	4	W14x30	W14x90	W14x61
8	1	W14x61	W14x120	W14x74
	2	W14x61	W14x120	W14x74
	3	W14x43	W14x90	W14x68
	4	W14x43	W14x90	W14x68
	5	W14x34	W14x90	W14x68
	6	W14x34	W14x90	W14x68
	7	W14x30	W14x90	W14x68
	8	W14x30	W14x90	W14x68

Table 3.4 Type I archetypical building gravity framing beam sizes

Beam Size			
	Frame Line A	Frame Line C	
	Bays 1, 5	Bays 1, 5	Bays 2, 3, 4
All stories	W24x68	W24x68	W16x31

The Type I ductile moment frame archetypes employed a ductile moment frame designed for moderate seismic demands. The ductile special steel moment frames (SMF) with reduced beam sections (RBS) were designed for the FEMA P-695 Seismic Design Category (SDC) D_{min}, and previously developed in the ATC-76 project (NIST 2010a). SMF designed for SDC D_{max} are also used for purposes of comparison. The details of the design and member sizes are available in Appendix D of the ATC project report. The ATC-76 project did not consider wind loads. The gravity framing was identical to that used in the Type I non-ductile buildings.

3.2.2 Type II Archetype Buildings

The second type ("Type II") was an archetypical long period (4-story) office building that employed a non-ductile moment frame with fully-restrained flange welded connections. This building was selected from the AISC (2013) *Design Examples* to illustrate the behavior of a typical mid-rise steel building in the central United States where the building design is controlled by moderate wind loads and has low seismic loads.

The building configuration and overall plan layout is shown in Figure 3.10. The building is a 4-story steel-frame structure comprised of seven 30-ft bays in the longitudinal (East-West) direction and one 30-ft and four 22.5-ft bays in the transverse (North-South) direction. The story height is 13.5 ft., except the fourth story height is 14 ft.

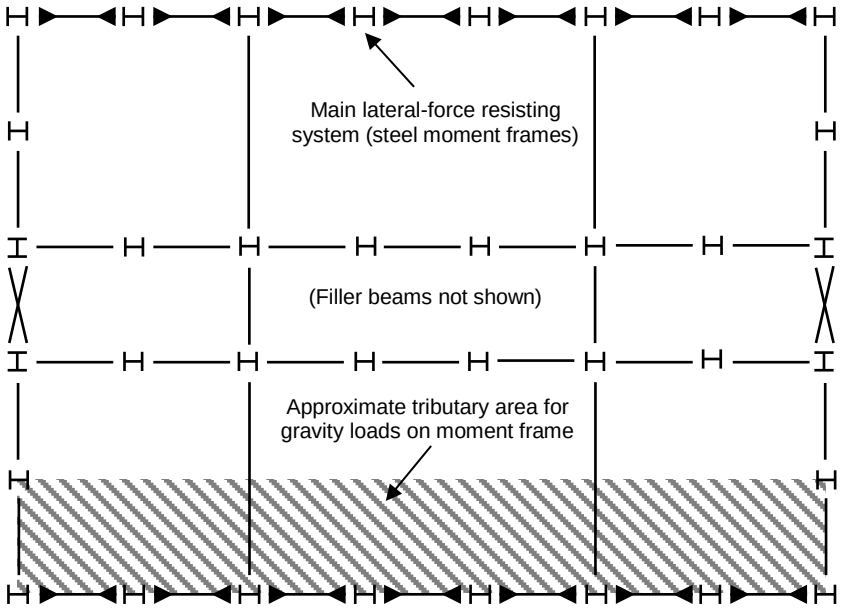

Figure 3.10 Type II non-ductile moment frame 4-story building plan

The building uses steel moment frames along the perimeter for lateral resistance in the longitudinal direction, and braced frames in the transverse direction. Columns in the gravity frame are spliced 4 feet above the 3rd story floor level. Each floor consisted of a composite 6-inch concrete slab on 3-inch steel deck system. The roof consisted of a steel deck and steel joist system.

The building was designed for wind loads based on a basic wind speed of 115 mph, and for seismic loads based on S_s = 0.121 g, S_1 = 0.060 g, and soil site class D (Seismic Design Category B). The design was controlled by wind (where the seismic C_s is equal to 0.043). A detailed description of the building, its loads, and the selection and design of the gravity and lateral systems is provided in the *Design Examples* (AISC 2013), except that in this research fully-restrained flange welded connections were used instead of bolted connections.

3.2.3 Type III Archetype Buildings

The third type ("Type III") was an archetypical long period (10-story) office building that employed a non-ductile moment frame with fully-restrained flange welded connections. Figure 3.11 shows the structural plan and elevation of the building. Moment frames consist of fully rigid, wide-flange girder welded to a wide-flange column with single plate bolted shear connection. Only the longitudinal (moment frame) direction was modeled.

The building was designed for a generic location in the United States where wind loads control strength (basic wind speed of 115 mph and ASCE 7-10 terrain exposure category C) and seismic detailing is not required. In the moment-frame direction, the wind base-shear force, V equal to 494 k. Based on an estimated building weight, W equal to 10,920 k, this corresponds to a wind base shear coefficient, C_{wind} (V/W) equal to 0.045.

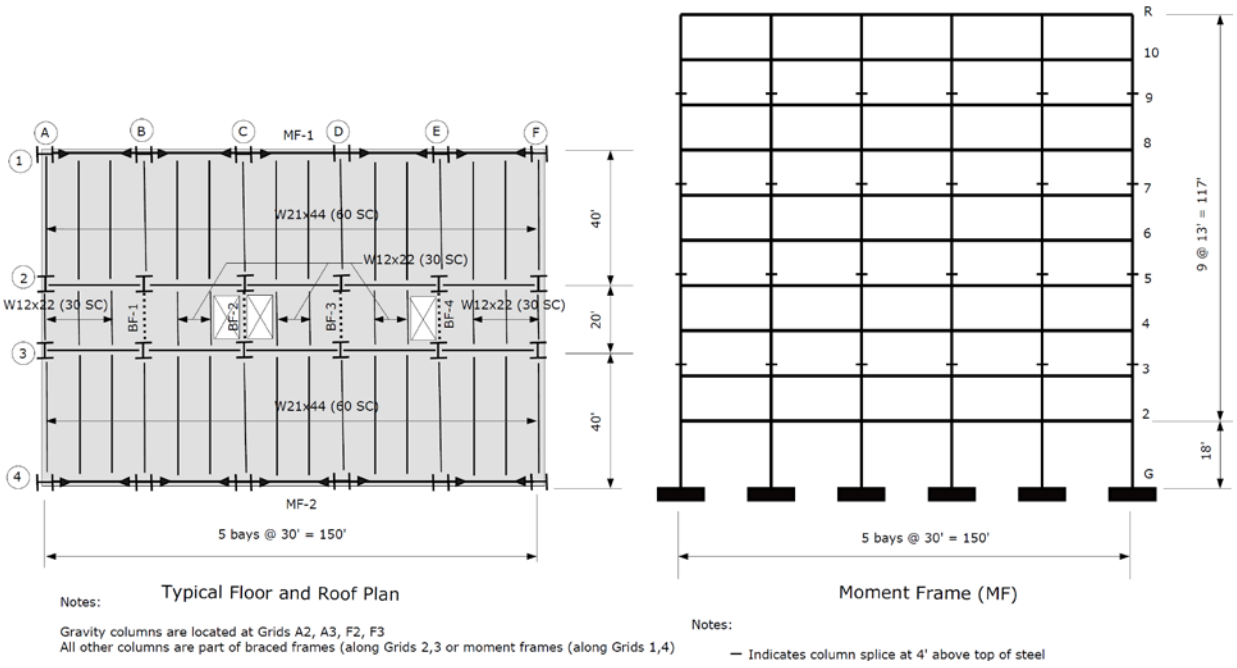

Figure 3.11 Type III non-ductile moment frame 10-story building framing plan and elevation (Plan and elevation drawing by Larry Griffis)

3.2.4 Collapse Prevention Systems

Reserve lateral strength in the shear tab connections was considered for both Type I and Type II archetypical buildings. In the Type III archetypical building, the gravity columns are oriented in the weak-axis (with respect to the moment frames), so reserve lateral strength was not considered. Enhanced shear tab connections were considered only in Type II archetypical buildings. The enhanced connections used a 0.5-in thick by 3.5-inch wide yield region. The reduced region length was 6 inches for W16x31 beams, and 8.25 inches for W24x68 beams. The length of the reduced region was based on limiting the strain demand to 0.085 in./in.

Additionally, in Type I archetypical buildings, slack-cable and loose-linkage mechanisms were deployed in bays 1–5 along frame A, and in bays 2–4 along frame C. Full-bay slack-cable X bracing was not included in this study. Telescoping brace mechanisms were used in bays 2 and 4 along frame A. Using the capacity based design described in the next section, the structural cables ranged from 21-mm diameter and 79 k breaking force, to 45-mm diameter and 434 k breaking force, with properties based on Ronstan Galfan full-locked structural cables (www.ronstan.com). The links consisted of A992 steel bars with an effective net area, A_e that ranged from 1.0 in.^{2} to 8.4 in.^{2}. The telescoping brace (9x9x1/4 HSS A1085) area was 8.03 in.^{2}. The expected yield strength was used, but no material overstrength was included.

A nonlinear static (pushover) analysis was used to determine the target drift at which collapse inhibiting mechanisms become engaged, typically between 2% to 4%. When utilized, energy dissipating devices (small viscous fluid dampers or viscoelastic solid high-damping rubber) were sized to provide 10% equivalent system damping (see Charney and McNamara 2008), based on a free-vibration analysis.

3.3 Analytical Modeling

Archetypical buildings were idealized using two-dimensional half-building models and *OpenSees* (PEER 2012) finite element software. Figure 3.12 shows a perspective view of the Type I analytical (half-building) models.

Structural framing members were modeled using a phenomenological (concentrated plasticity) approach (Figure 3.13). Beams and columns were represented using an assembly of rotational springs (zero-length elements) and elastic beam-column elements in series to simulate the potential for plastic behavior to be developed near the end of each member. The formation of a plastic hinge in the column or beam at the location of a collapse inhibiting component (cable or link) connection was precluded by employing a capacity-based design approach (limiting the component capacity based on member limit states).

In the beam or column assembly was defined using a method proposed by Ibarra and Krawinkler (2005), where the rotational spring stiffness, K_s was defined relative to elastic beam-column rotational stiffness, K_{bc} in order to permit the secondary stiffness (strain hardening) to be expressed as a function of the initial elastic stiffness.

$$K_s = nK_{bc} \tag{3.1}$$

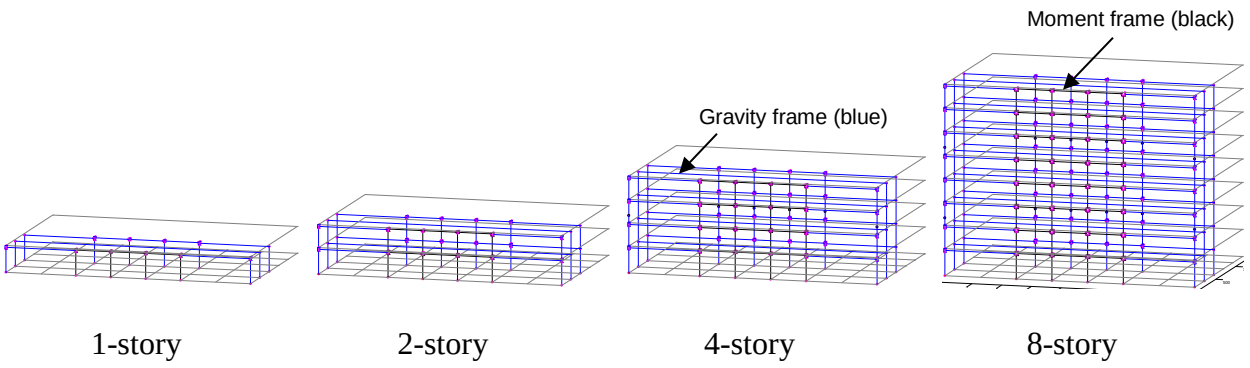

Figure 3.12 Perspective view of Type I analytical (half-building) models

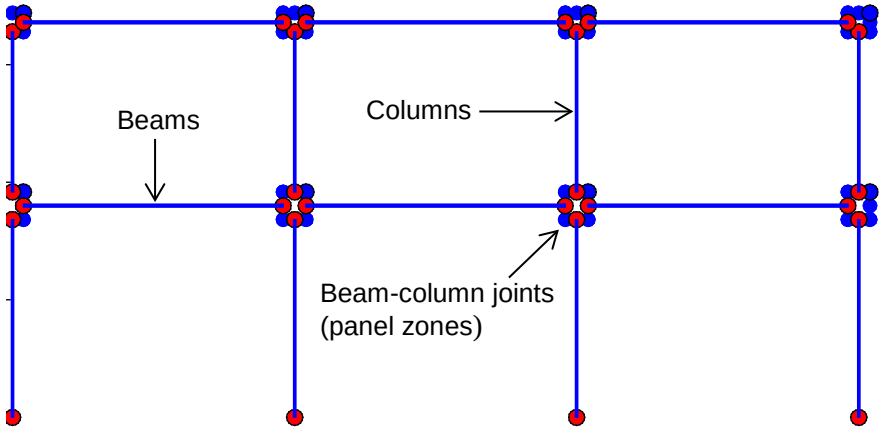

Figure 3.13 Phenomenological (concentrated plasticity) analytical modeling approach: moment frame shown for Type I non-ductile moment frame 2-story building

The rotational stiffness of the beam or column assembly K_{mem}, was then calculated as

$$K_{mem} = \left(\frac{1}{K_s} + \frac{1}{K_{bc}}\right)^{-1} \quad (3.2)$$

For fully-restrained (moment) connections and plastic column hinges, the ratio of spring to elastic beam-column stiffness, n was taken as 10. This value of the ratio was selected in order to avoid numerical instability when the ratio is large (Ibarra and Krawinkler 2005).

The rotational stiffness of the assembly K_{mem}, was based on a conjugate-beam analysis. For members subjected single-curvature bending (i.e. columns pinned at the base, or columns that are spliced) the assembly stiffness was calculated using Equation 3.3.

$$K_{mem} = \frac{3EI}{L} \quad (3.3)$$

For members subjected to double-curvature bending (i.e. beams, fixed-based columns) the assembly stiffness was calculated using Equation 3.4.

$$K_{mem} = \frac{6EI}{L} \quad (3.4)$$

In this method for beam or column assembly, one of two conditions of curvature in bending (the moment gradient) was assumed *a priori* and was assumed to remain constant through the analysis. Thus, a column splice could only be modeled as a fully-rigid joint (no splice) or true hinge column splice (no rotational capacity). Similarly, a plastic hinge in the beam or column at the location of the collapse prevention system component connection could not be employed because it requires a change in the moment gradient. This limitation is discussed later in this chapter (see also Figure 3.22).

3.3.1 Location of Beam Plastic Hinge

In this research, the assumed location of the plastic hinge depended on the type of beam-to-column connection. In previous research, the assumed location of the plastic hinge varied depending on the researcher (e.g. Rojas 2003, Lee 2003, and others). Interestingly, regardless of the actual distribution of plasticity and the assumed location of the plastic hinge, previous studies (e.g. Ibarra and Krawinknler 2005) have shown that the global response of the building frame was relatively insensitive to the precise location of the plastic beam hinge (column plastic hinges controlled global collapse).

For modeling purposes, for beam-to-column connections without flange reduction or reinforcement, the plastic hinge was assumed to occur at the face of the column (PEER/ATC 2010). In actuality, first yielding of the beam occurs at the face of the column. The center of rotation eventually migrates into the beam span with a "final" center of rotation located at approximately half the beam depth from the column. This includes both ductile and non-ductile (pre-Northridge) connections. For reduced beam section ("RBS") beam-to-column connections, the plastic hinge occurs at the centerline of the radius-cut reduced section.

For ductile beam-column connections with flange reinforcement (e.g. haunches or cover plates) the plastic hinge occurs away from the column face a distance depending on the particular type of connection. This distance may be determined using procedures given in AISC 358-10 (AISC 2011b). In this research, the NEES structural component databases (Lignos and Krawinkler 2012) were used to determine moment-rotation deterioration parameters of the connections, but it is noted that ductile reinforced beam-to-column connections were excluded from the regression analysis used to determine connection parameters (Lignos and Krawinkler 2011). For simple shear (gravity) connections including composite action, the hinge was assumed to occur at the column face.

3.3.2 Column Fixity, Splices and Plastic Hinge

In this research, the assumed location of the plastic hinge was at the top or bottom of the column. Columns participating in the moment frame were idealized as fixed at the base (except the 1-story frames); all other columns (gravity frame columns) were idealized as pinned. Column splices (at story 3 and story 5) were modeled as a pinned connection. In this study, column splices were assumed to have no rotational capacity, and column bases were assumed to be either fixed (rigid) or hinged (fully flexible). Partial fixity was not modeled. The analytical model could be refined to represent the base as a partial restraint (e.g. Hamburger et al. 2009), but this was beyond the scope of this study. The sensitivity of the seismic collapse assessment to the inclusion of gravity column splices is discussed in Chapter 6. Interaction between axial and flexure (P-M interaction) is described in the next section.

3.3.3 Fully-Restrained (Moment Frame) Beam-to-Column Connections

Ductile connections

The moment-rotation behavior of ductile beam-to-column connections (Figure 3.14) was represented using the `Bilin` uniaxial material with parameters based on regression analysis of test data (Lignos and Krawinkler 2011).

The modified Ibarra-Medina-Krawinkler moment-rotation model (PEER/ATC 2010; Lignos and Krawinkler 2011) was used in this study. In this model, cyclic degradation is considered directly in the hysteresis behavior. The moment-rotation behavior follows the monotonic response and is reduced or degrades as a typical cyclic analysis progresses. The hysteresis behavior is rule-based (Judd 2005). The primary parameters for the moment-rotation model are shown in Figure 3.15. (For non-symmetric behavior, these parameters are defined for both positive and negative directions.)

The model also requires Λ = reference cumulative rotation capacity, c = empirical parameter taken as 1.0, and D = decrease rate of cyclic deterioration. Parameter values depend on the ductility of the connection or plastic hinge. For steel beams, different values of Λ (for different modes of cyclic deterioration) do not significantly improve the model (Lignos and Krawinkler 2011), so one value was used in this study.

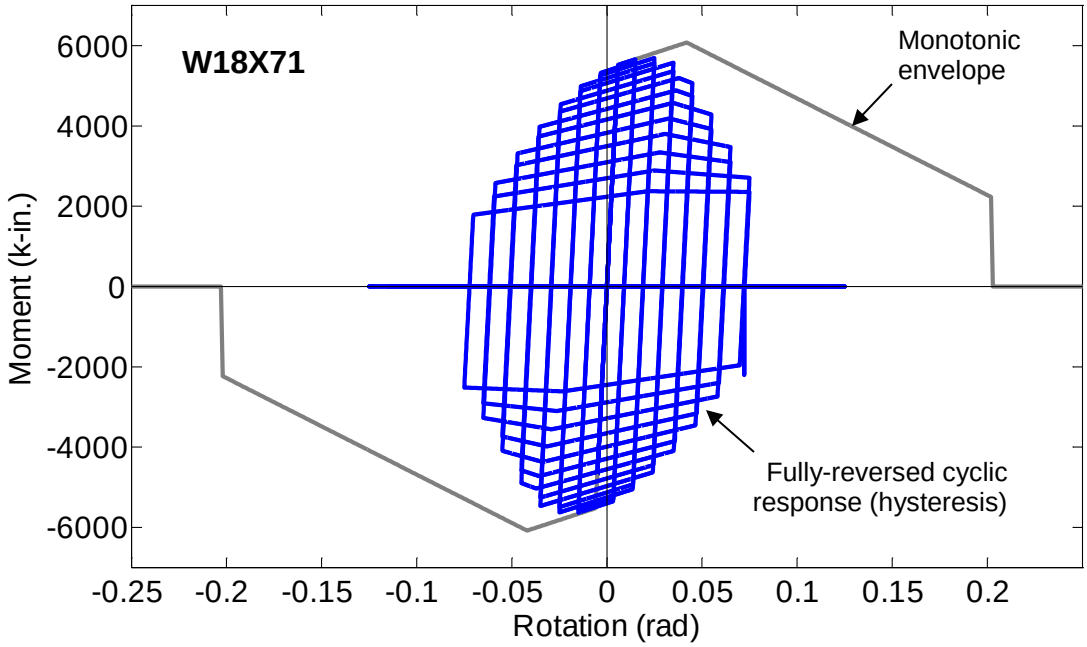

Figure 3.14 Typical idealized behavior for a ductile fully-restrained beam-to-column connection: W18x71 beam in Type I ductile moment frame 4-story building

The plastic moment, M_p was based on the expected yield strength, $F_y R_y$ (where R_y = 1.1) and the plastic section modulus, Z. For RBS beams, Z was based on the centerline of the RBS cut using AISC 358-10 Equation 5.8-4 (AISC 2011b). For non-RBS beams, Z was as given in the AISC *Steel Construction Manual* (AISC 2011a).

Isotropic hardening was included in the model in an approximate way by increasing the plastic moment to an "effective" yield strength, M_y = 1.1 M_p (see Lignos and Krawinkler 2011). This strength represented an "average" strain hardening (Lignos 2008) but did not account for cyclic hardening.

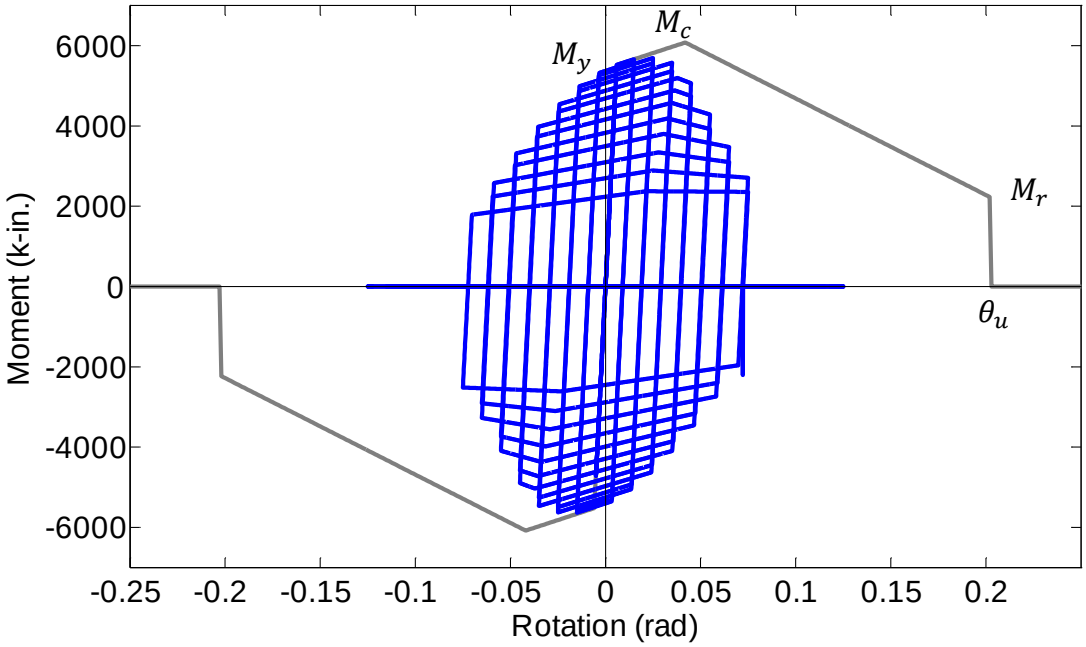

a) Modified Ibarra-Medina-Krawinkler moment-rotation model

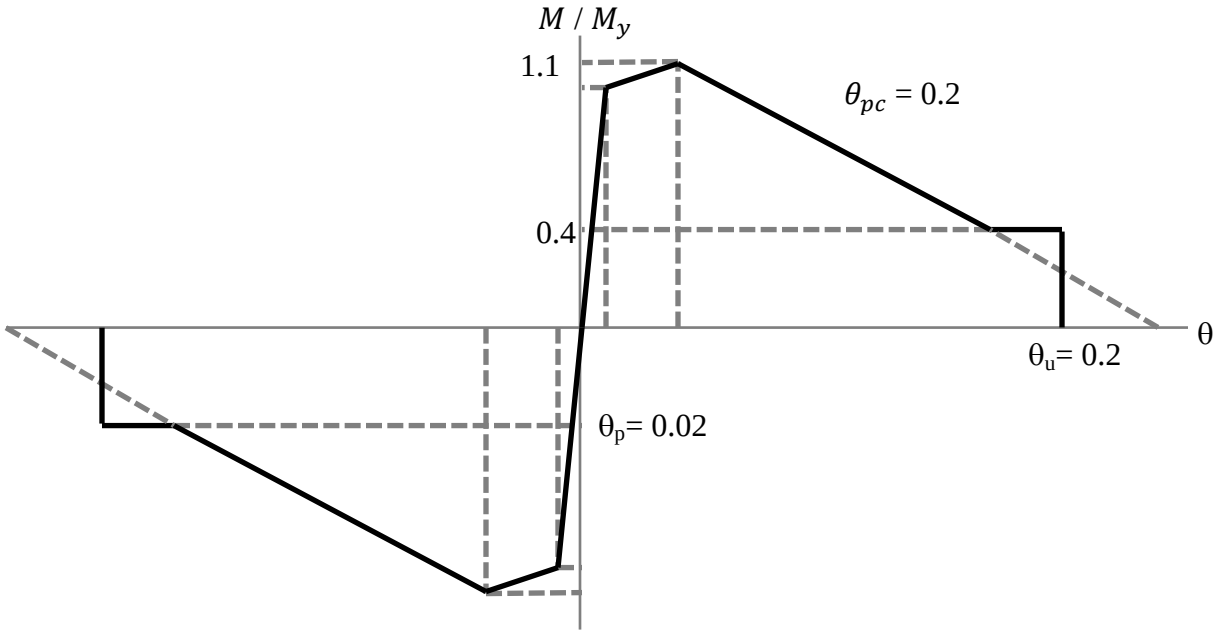

b) Typical parameter values

Figure 3.15 Modified Ibarra-Medina-Krawinkler moment-rotation model

The post-yield strength ratio (M_c/M_y) was calculated as the ratio of the capping strength to the effective yield strength. This is similar to the strain hardening ratio, as expressed by the C_{pr} factor. This factor accounts for the peak strength (see AISC 358-10 page 9.2-6). Therefore, the C_{pr} factor is similar to M_c/M_y ratio, except M_y incorporates average strain hardening.

In this study, the parameters for the modified Ibarra-Medina-Krawinkler moment-rotation model (Table 3.5) were based on statistical analysis of a database of experimental testing (Lignos and Krawinkler 2011). In that statistical analysis, beam-to-column connections were classified as RBS or non-RBS (which includes a variety of connection types). The statistical analysis indicated that pre-capping plastic rotation θ_p is small (about 0.02 rad), but post-capping deformation θ_{pc} is large. As a result, loss in strength is predicted to be slow after the peak strength (PEER/ATC 2010).

Yield and capping moment parameters represent mean values. Average values (used in ATC-76) are about 1.10 for both normalized yield and capping moments. The normalized residual moment was an approximate value suggested by Lignos and Krawinkler (2011).

Table 3.5 Moment-rotation model parameters for ductile beam-to-column connections

	Normalized strength			Deformation			Hysteresis	
Connection	M_y / M_p	M_c / M_y	M_r / M_y	θ_p (rad)	θ_{pc} (rad)	θ_u (rad)	Λ (rad)	D
RBS rad	1.06	1.09	0.4	Eqn.[a] (~0.02)	Eqn.[a] (~0.20)	(0.06 to 0.07)[b]	Eqn.[a] (~1.0)	1.0
Non-RBS	1.17	1.11				(0.05 to 0.06)[b]		
ATC-76	1.10	1.10				0.2		

(a) Regression equation in Lignos and Krawinkler (2011).
(b) Depends on loading history. Range shown is for symmetric cyclic loading protocols.

In this study, the ultimate rotation capacity θ_u was taken as 0.2, but it was recognized that the actual ultimate rotation capacity depends on the loading protocol. For monotonic loading the value may be three times larger than the value for symmetric cyclic loading, and larger values may be expected for near-fault loading or for ratchet loading in one direction, such as occurs in side-sway dynamic instability (Lignos and Krawinkler 2011). For example, ultimate rotation capacity was observed to be 0.37 rad for shake table testing of scale model steel frames (Lignos 2008). Thus, in ATC-76 (NIST 2010a) an assumed value of 0.20 rad was used.

In this research, M_c/M_y =1.1. In the ATC-76 project, M_c/M_y =1.1 (see NIST 2010a, page D-8). The average of the mean values from the statistical analysis of the database of testing were M_c/M_y = 1.09 for RBS, and M_c/M_y = 1.11 for non-RBS connections (see Lignos and Krawinkler 2011, Table 3). In AISC 358-10, Equation 2.4.3-2 is used to calculate C_{pr}. Based on AISC 2010 Manual Table 2-4, F_y = 50 ksi and F_u = 65 ksi. Therefore, C_{pr} = 1.15. (There are three factors used in the ATC-76 report that all equal 1.10.) The M_c/M_y ratio was used instead of C_{pr}.

Non-Ductile Connections

The moment-rotation behavior of the non-ductile beam-to-column connections (Figure 3.16) was represented using a tri-linear loading and unloading rule-based hysteresis model (Lowes et al. 2004) that includes degradation of stiffness and strength. The model was incorporated in the analysis using the `Pinching4` and `MinMax` uniaxial materials in *OpenSees*, with load-deformation and hysteresis parameters based on FEMA P-440A (FEMA 2009b), ASCE 41 (ASCE 2006, 2014), and FEMA 355D (FEMA 2000b).

Beam-column connections in steel moment frames not detailed for seismic resistance ("R=3" systems) were assumed to exhibit non-ductile behavior, and the moment-rotation

parameters were based on the performance of fully-restrained flange welded connections designed prior to the 1994 Northridge earthquake (so-called “pre-Northridge” connections).

Stojadinovic et al. (2000) performed experimental tests of pre-Northridge connections. Shi (1997) developed a connection model for non-ductile connections, and Shi and Foutch (1997) implemented the model in DRAIN-2DX (Prakash et al. 1993). Foutch and Yun (2002) used this model to predict the performance of steel moment frames with non-ductile and ductile connections, as well as simple shear connections (Yun et al. 2002). Lee (2000) and Lee and Foutch (2002) also used the model to predict performance of pre-Northridge type buildings.

Parameters for the model are given in Table 3.6. Typical values are shown in Figure 3.17. It is noted that the empirical equations in ASCE 41-13 (ASCE 2014) and previous versions of the standard, as well as the pre-standard, for non-ductile (pre-Northridge or WUF) connections were based the analysis used in FEMA 355D (2000b).

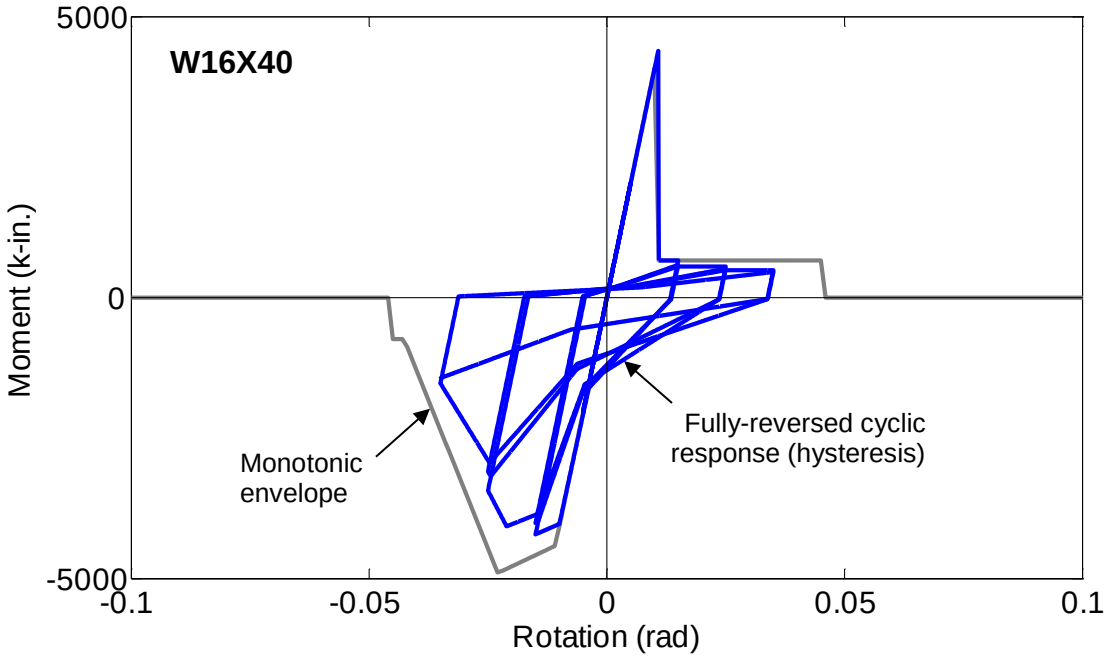

Figure 3.16 Typical idealized behavior for a non-ductile fully-restrained beam-to-column connection: W16x31 beam in Type I non-ductile moment frame 4-story building

The non-ductile connections lose strength immediately after yielding in positive moments (simulating fracture of the bottom flange) and more gradually in negative moments. The connections exhibit cyclic degradation of both stiffness and strength, within a 15% residual strength boundary until approximately 4% drift, after which the rotational stiffness and flexural strength of the connection is zero.

Table 3.6 Moment-rotation model parameters for non-ductile beam-to-column connections

Connection (Moment)	Normalized strength			Deformation			Hysteresis parameters
	M_y / M_p	M_c / M_y	M_r / M_y	θ_p (rad)	θ_{pc} (rad)	θ_u (rad)	
Pre-Northridge WUF M^+ M^-	1.10[(a)] 1.10[(a)]	1.00[(b)] 1.10[(a)]	0.15[(b)]	0.001 0.011	0.001 Eqn.[(c)]	Eqn.[(c)] – θ_p	[(d)]

(a) Approximate value based on average of ductile connections in Lignos and Krawinkler (2011).
(b) Residual moment based on FEMA P440A Page 3-15 (FEMA 2009b).
(c) Equation 2-12a in FEMA 355D (FEMA 2000b). See also ASCE 41-13 (ASCE 2014).
(d) Parameters from FEMA P440A (FEMA 2009b): displacement ratio = 0.2, reloading force ratio = 0.4, unloading force ratio = 0.05, cyclic strength degradation parameters = 0.0, except gF2 = 0.7, gF4 = 0.5, and gFLim = 0.8, and maximum cyclic to monotonic energy displacement ratio = 10.

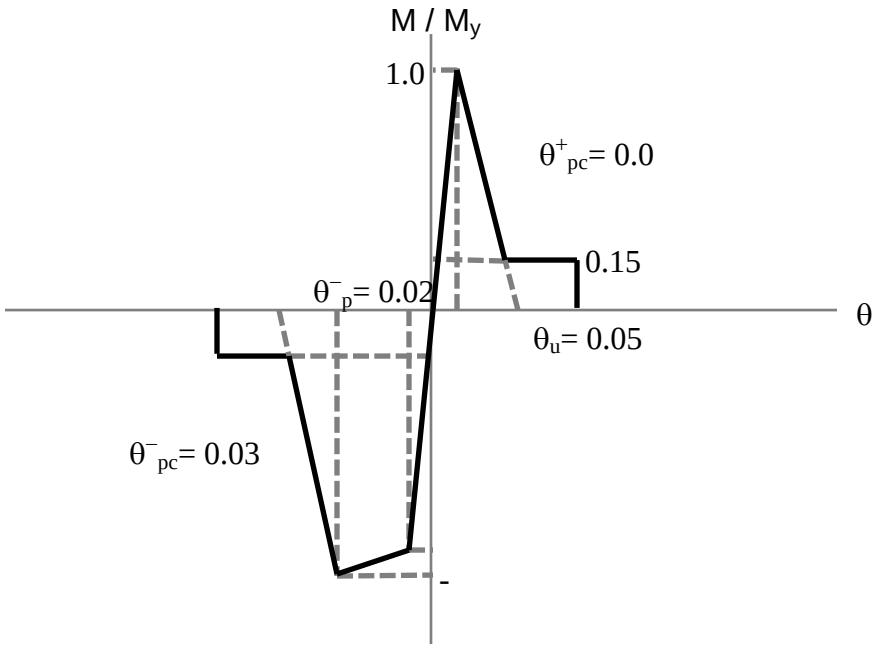

Figure 3.17 Typical parameter values for non-ductile behavioral model

Fully-Restrained Beams with Composite Action

The stiffness and moment-rotation of beams mechanically fastened to a concrete slab on a steel deck ("composite beams") can be significant due to composite action. For example, Lignos et al. (2011) performed an experimental shake-table test and an analytical study of a 4-story building with a steel moment using composite beams and showed that composite action significantly affected side-sway collapse capacity.

Experimental tests of composite beams with fully-restrained RBS beam-to-column connections (Tremblay et al. 1997; Engelhardt et al. 2000; Ricles et al. 2004) exhibit asymmetric moment-rotation behavior, whereas similar tests of bare steel beams for ductile beam-column connections (Uang et al. 2000) exhibit symmetric moment rotation behavior.

Although the effect of composite action between the beam and the concrete slab has been shown to generally enhance the seismic behavior of ductile (RBS) connections (Elkady and Lignos 2013, 2014) the influence on non-ductile connections has not yet been determined. As a result, composite action was not included in this study.

For purposes of comparison, in Table 3.7 the moment-rotation parameters for ductile connections were modified to account for composite action based on analysis by Lignos (2008) and Lignos et al. (2011). Tabulated parameters with a dash instead of a value were not modified by composite action. The flexure strength of composite beams is predicted to be 25% to 30% higher than the strength of the bare steel beams. Furthermore, the composite beam pre-capping plastic positive and negative rotations θ_p are modified by a factor 2 and 0.9, respectively, and θ_{pc} is increased by a factor of 1.5, compared to bare steel beams. The reduction in positive rotation is due to lateral torsion of the bottom flange (Lignos et al. 2011).

The stiffness of composite beams may be estimated in various ways. One method is to use the lower-bound elastic moment of inertia, which only includes the portion of the concrete slab used to balance the shear force transferred by the shear stud anchors (AISC 2011a, page 3-13). Thus, the quantity of shear stud anchors (or the degree of composite action) must be assumed or specified.

Table 3.7 Moment-rotation parameters for ductile connections with composite action

Sub-assembly (Moment)	Normalized strength relative to bare steel			Deformation relative to bare steel			Hysteresis relative to bare steel	
	M_y	M_c	M_r	θ_p (rad)	θ_{pc} (rad)	θ_u (rad)	Λ (rad)	D
Exterior								
M^+	1.20	1.25	--	2.0	1.5	--	1.0	1.0
M^-	1.10	1.10		0.9	1.0			1.0
Interior								
M^+	1.25	1.30	--	2.0	1.5	--	1.0	0.85
M^-	1.15	1.10		0.9	1.0			1.0
Slab / column face gap								
M^+	1.0	1.20	--	2.0	1.5	--	1.0	1.0
M^-	1.0	1.05		1.0	1.0			1.0

3.3.4 Partially-Restrained (Shear Tab) Beam-to-Column Connections

Literature related to the analytical modeling of partially-restrained gravity framing connections is limited compared to fully-restrained connections. One modeling approach has been to simply assume the flexural strength of the connection is a percentage of the beam plastic strength (Hines et al. 2009; Flores et al. 2012). Another approach has been to "lump" the gravity framing (individual beam-to-column connections are not explicitly modeled) (Lee and Foutch 2002; NIST 2010b; Eatherton and Hajjar 2011). Explicit modeling has been centered on rule-based

hysteresis (Barber 2011; Zhang 2012; Wen et al. 2013) and complex models (Rassati et al. 2004) using commercial finite element software [i.e. *Abaqus* (Dassault Systèmes)].

In this research, the moment-rotation behavior of the shear tab connections (Figure 3.18) was represented using the tri-linear loading and unloading rule-based hysteresis model (Lowes et al. 2004), implemented using the `Pinching4` and `MinMax` uniaxial materials in *OpenSees*, with load-deformation and hysteresis parameters based on test data of shear tab connections (Liu and Astaneh-Asl 2000), corresponding analytical models (Liu Astaneh-Asl 2004; Wen et al. 2013), and FEMA P-440A. The shear tab connection behavior is asymmetric due to the effect of composite action with the concrete slab. The connections exhibit cyclic degradation of both stiffness and strength, until approximately 10% to 12% drift, after which the rotational stiffness and flexural strength of the connection is zero. The negative-moment capacity boundary (monotonic envelope) was based on the behavior of the bare steel beam.

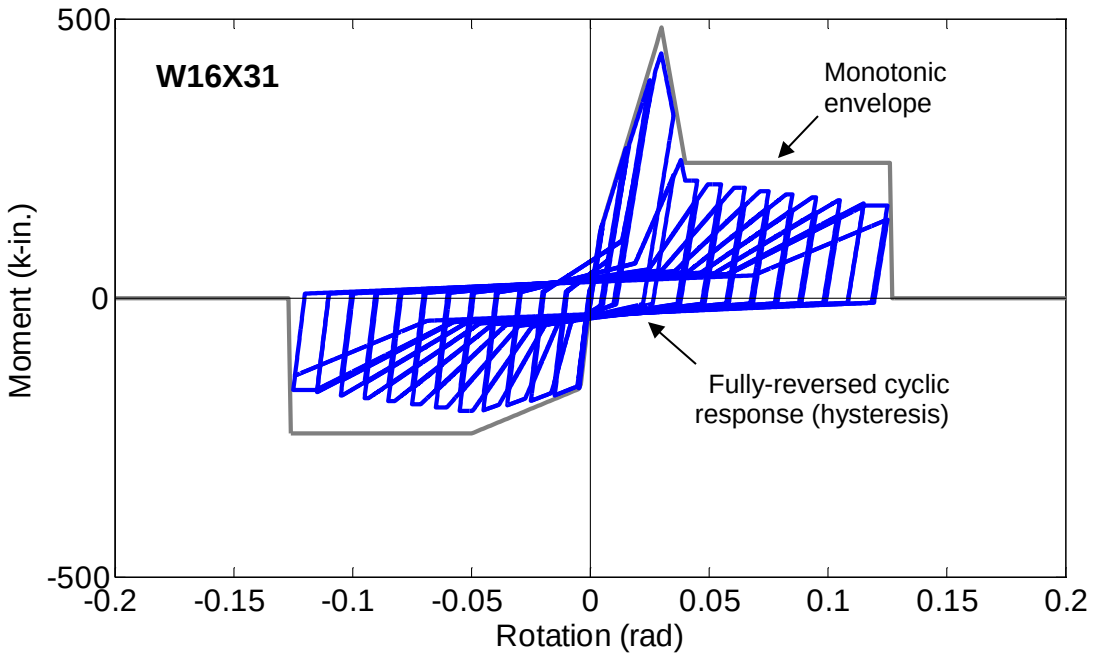

Figure 3.18 Typical idealized behavior for a shear-tab beam-to-column connection: W16x31 beam in Type I non-ductile moment frame 4-story building

Experimental data and finite element analyses (Wen et al. 2013) have shown that a linear-elastic stress distribution is developed at the negative yield moment (Equation 3.5), and a uniform plastic stress distribution is developed at the negative ultimate moment (Equation 3.6), based on the geometry of the shear tab connection, where d_{st} is the height of shear tab (taken as d_{beam} – 6 inches), t_{st} is shear tab thickness (taken as 3/8 inches), R_y = 1.1, and F_y = 50 ksi.

$$M_y^- = \frac{1}{6} {d_{st}}^2 t_{st} R_y F_y \quad (3.5)$$

$$M_u^- = \frac{1}{4} {d_{st}}^2 t_{st} R_y F_y \quad (3.6)$$

The positive-moment capacity boundary was based on observations of experimental data (Liu and Astaneh-Asl 2004) that indicate maximum strength for positive moment (Equation 3.7) is twice that for negative moment, and positive-moment yield strength (Equation 3.8) is a quarter of maximum strength.

$$M_y^+ = 0.25\, M_u^+ \quad (3.7)$$

$$M_u^+ = 2\, M_u^- \quad (3.8)$$

The total (ultimate) rotational capacity (Equation 3.9) for positive and negative moment was based on the gap, g between the beam flange and the column, and distance from the mid-height of the shear tab to the beam flange, $d_{beam}/2$ (Liu and Astaneh-Asl 2004).

$$\theta_{Total} = \frac{g}{d/2} \quad (3.9)$$

As was assumed in FEMA P-440A, the displacement ratio was 0.5, reloading force ratio was 0.25, unloading force ratio was 0.05, cyclic strength degradation parameters $gK = gD$ = [0.0 0.1 0.0 0.0 0.2], gF = [0.0 0.4 0.0 0.4 0.9], and maximum cyclic to monotonic energy displacement ratio = 10.

3.3.5 Columns and Column Panel Zones

Column Plastic Hinge

Column behavior was idealized similarly to beam behavior, except column plastic hinging moment-rotation behavior (Figure 3.19) was represented using the `Bilin` uniaxial material with parameters based on regression analysis of test data (Lignos and Krawinkler 2011), and with an approximate reduction to account for axial load interaction. The reduction was based on AISC 360-10 Equations H1-1a and H1-1b (AISC 2010a) using a constant axial load resulting from the gravity load plus half the lateral load calculated in a nonlinear static (pushover) analysis under wind or seismic loads. This was the same method used in the ATC-76 project (NIST 2010a). A fiber model was not used in order to make incremental dynamic analyses feasible.

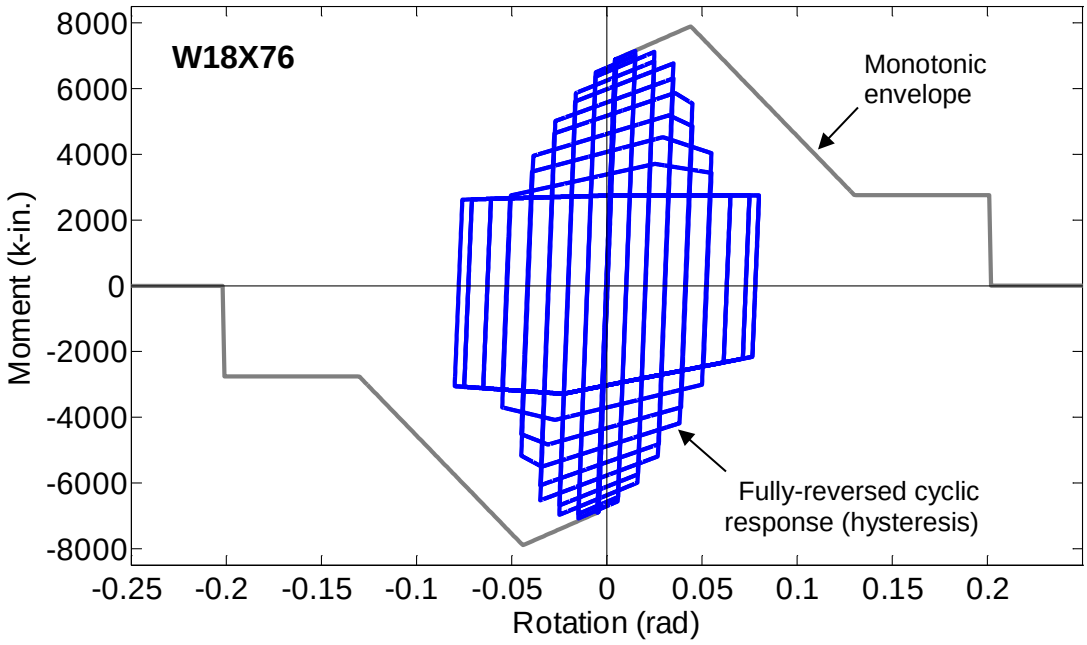

Figure 3.19 Typical idealized behavior for a column plastic hinge: W18x76 column in Type I non-ductile moment frame 4-story building

This is the same approximate approach used in other collapse assessments (e.g. NIST 2010a,b; Deierlein et al. 2010), and was necessary not only because the finite element model representation could not capture axial and flexure interaction directly, but was also necessary because both the moment-rotation models and the experimental data used to define the column hinge moment rotation behavior do not account for variation in axial load (see section 6.5.4 of NIST 2010a).

Column Panel Zones

Beam-to-column joints to the weak-axis connections (no panel zone) were represented using a centerline joint model. Column panel zones (beam connections to the strong axis of the column) were explicitly represented using the Krawinkler joint model (Krawinkler 1978; Charney and Marshall 2006). Figure 3.20 shows the finite element model corresponding to the Krawinkler joint model. The Krawinkler model consisted of 8 rigid beam elements connected by hinges and one spring. The spring represented the combined contributions of the panel zone (column web plus doubler plate, where added) and the column flanges.

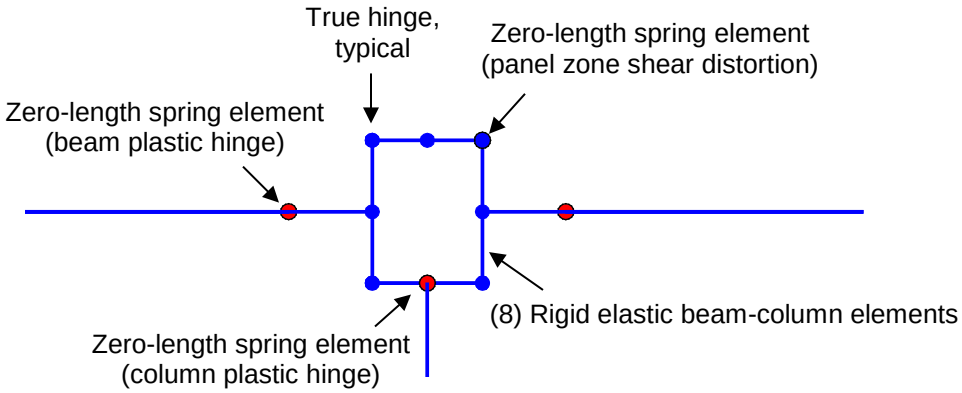

Figure 3.20 Explicit (Krawinkler) column panel zone model (reduced beam section shown)

The shear-distortion behavior of column panel zones (Figure 3.21) was represented using the `Hysteretic` uniaxial material option, with a tri-linear envelope curve and bilinear hysteresis behavior (Gupta and Krawinkler 1999) based on the column depth d_c, the panel zone thickness (column web thickness plus doubler plate thickness, if specified) t_{pz}, the shear modulus G, the column flange width b_{fc}, column flange thickness t_{fc}, and beam depth d_b:

$$V_y = 0.55\,(R_y F_y)\,d_c t_{pz}$$

$$K_e = 0.95\,G\,d_c t_{pz}$$

$$K_p = \left[0.95\,G\,b_{fc} {t_{fc}}^2\right]\,/d_b$$

Degradation of the joint model was neglected because experimental research has indicated that it is unlikely to occur, unless there is shear buckling (PEER/ATC 2010). The intent was to preclude shear buckling by designing the panel zone using AISC 360-10.

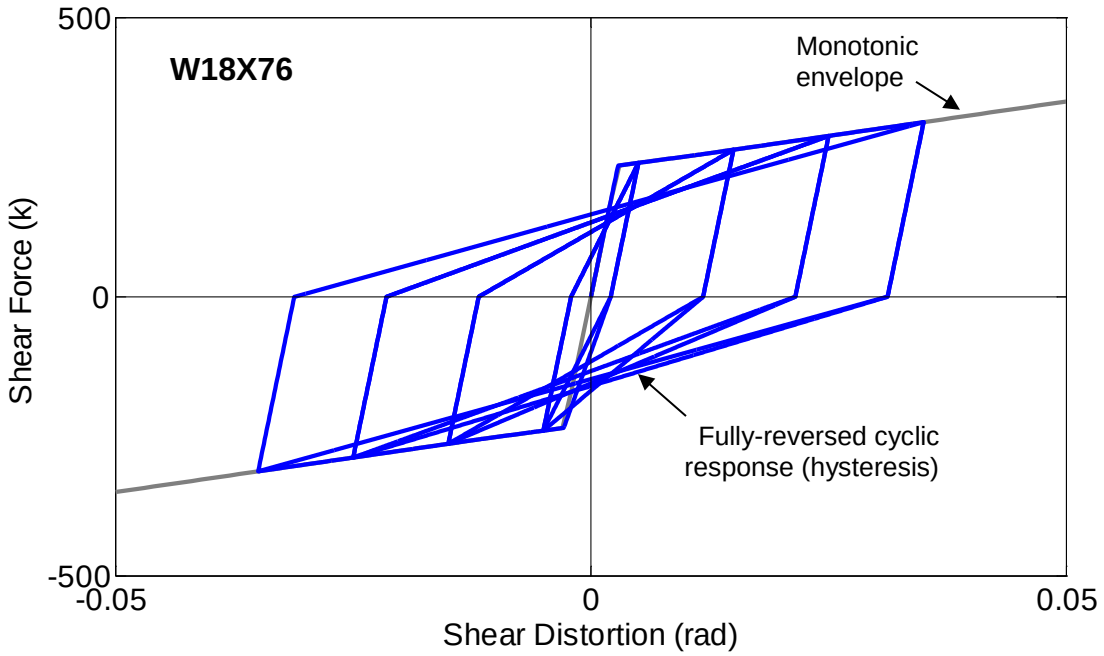

Figure 3.21 Typical idealized behavior for a column panel zone distortion: W18x76 column in Type I non-ductile moment frame 4-story building

3.3.6 Collapse-Inhibiting Mechanisms

Slack-cable collapse inhibiting mechanisms were represented using truss elements with a multi-linear elastic material behavior (to simulate initial slackness) until fracture at the cable breaking load. The loose-linkage collapse inhibiting mechanism was represented using corotational truss elements that are elastic until fracture, approximated as the tensile yield limit state of the links. Energy dissipating devices (small viscous fluid dampers or viscoelastic solid high-damping rubber) were idealized using viscous corotational truss elements.

The model representation for beams and columns did not admit a change in the moment gradient, as previously discussed. Therefore, the formation of a plastic hinge in the column or beam at the location of the cable or link connection was precluded by limiting the axial capacity of the collapse prevention system component (cable or link). The limiting capacity was based on two limit states: (1) interaction of axial load and moment at the location of the brace-to-column or brace-to-beam connection, as described in AISC 360-10 section H1.1; and (2) shear yielding of the column or beam web, as described in AISC 360-10 section G2.1. The size of the collapse prevention system component was based on the lower value obtained according to the two limit states for either the beam or column.

The nominal axial strength, P_n was determined according to AISC 360-10 section E3. The column effective flexural strength, M_n was calculated by increasing the expected plastic moment, M_p (Equation 3.10) to account for isotropic hardening by the ratio M_y/M_p and average strain hardening by the ratio M_c/M_y in Equation 3.11, based on information extracted from a database of experimental testing of steel components (Lignos and Krawinkler 2011).

$$M_p = R_y F_y Z \tag{3.10}$$

$$M_n = \left(\frac{M_c}{M_y}\right)\left(\frac{M_y}{M_p}\right)M_p \quad (3.11)$$

The nominal flexural strength at each end of the column was reduced to account for flexure and axial load, P interaction, as previously discussed. The nominal flexural strength at the connection location, M_a was determined according to AISC 360-10 section F2 and adjusted according to the moment gradient using the lateral-torsional buckling modification factor, C_b:

C_b = 1.60 for double curvature

= 1.36 for single curvature

The interaction of axial load and moment at the location of the brace-to-column or brace-to-beam connection was determined using AISC 360-10 section H1.1 (Equation 3.12) based on the axial and moment force diagram shown in Figure 3.22.

$$1 = \alpha\frac{(P - F_y)}{P_n} + \beta\frac{(M_a + M_x)}{M_n} \quad (3.12)$$

where

$$\alpha = \begin{cases} 0.5 & if\ (P - F_y)/P_n < 0.2 \\ 1.0 & otherwise \end{cases} \quad (3.13)$$

$$\beta = \begin{cases} 1.0 & if\ (P - F_y)/P_n < 0.2 \\ 8/9 & otherwise \end{cases} \quad (3.14)$$

The maximum capacity of the collapse prevention system component, for interaction of axial and moment forces, was then back-calculated using (Equation 3.15):

$$F_{max1} = \frac{P_n M_n - \alpha M_n P - \beta P_n Q M_y}{\left[\frac{\beta P_n a(L-a)}{L\sqrt{2}}\right] - \frac{\alpha M_n}{\sqrt{2}}} \quad (3.15)$$

where

$$Q = \begin{cases} (L-2a)/L & double\ curvature \\ (L-a)/L & single\ curvature \end{cases} \quad (3.16)$$

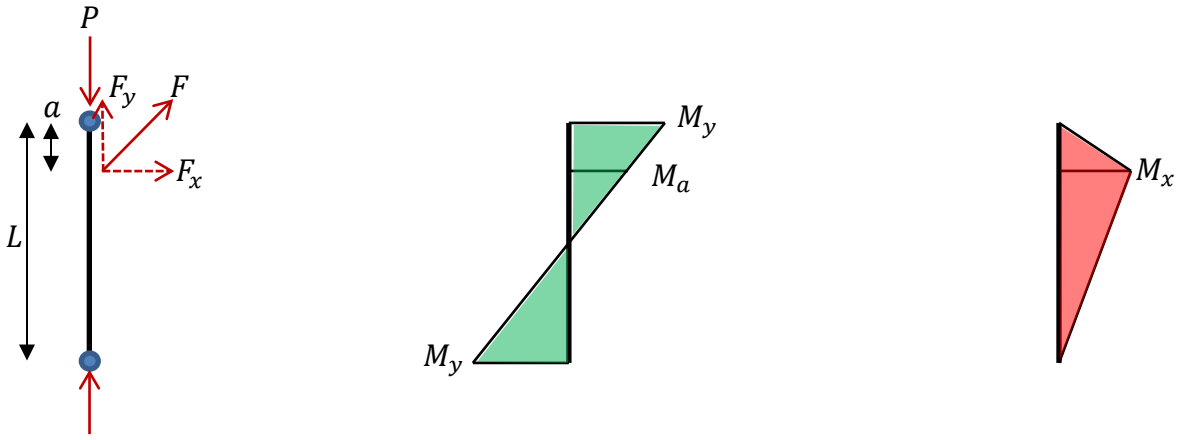

a) Structural member b) Moments due to double curvature c) Moments due to device

Figure 3.22 Axial and moment forces in column with collapse prevention system

Shear yielding of the column or beam web was determined using AISC 360-10 section G2.1, $V_n = 0.6(F_y R_y)A_w$, where A_w is the area of the web (web thickness times the section depth). Ultimately, the lowest value of the two limit states (minimum of $V_n\sqrt{2}$, F_{max1}) was used to size the collapse-prevention system component.

3.3.7 Partially-Restrained (Enhanced Shear Tab) Beam-to-Column Connections

The moment-rotation behavior of the enhanced shear-tab connections (Figure 3.23) was represented using the `Pinching4` and `MinMax` uniaxial materials in *OpenSees*, with load-deformation and hysteresis parameters based on test data of T-stub type flange connections (Pryor and Murray 2013) and FEMA P-440A. The connections exhibit cyclic degradation of both stiffness and strength, until 9% drift, after which the rotational stiffness and flexural strength of the connection is zero (based on monotonic tests results).

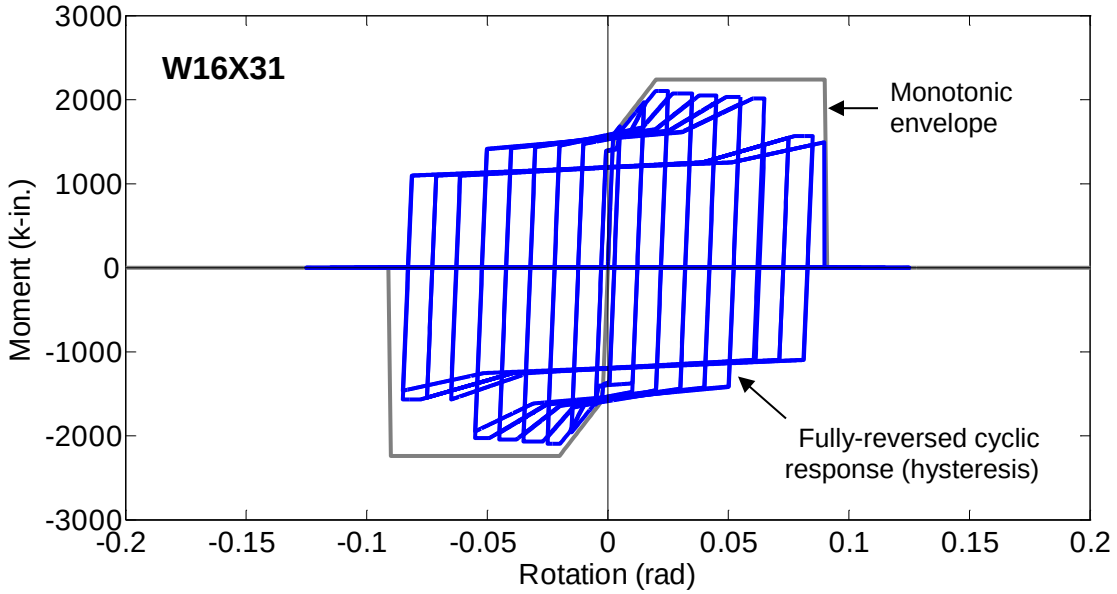

Figure 3.23 Typical idealized behavior for an enhanced shear tab beam-to-column connection: W16x31 beam in Type I non-ductile moment frame 4-story building

The axial strength of the T-stub stem was calculated based on the reduced region.

$$P_y = A_y(R_y F_y) \tag{3.17}$$

$$P_u = A_y(R_t F_u) \tag{3.18}$$

The moment strength of the connection was calculated based on the axial force couple, where d is the beam depth and t is the stem plate thickness.

$$M_y = P_y(d + t) \tag{3.19}$$

$$M_u = P_u(d + t) \tag{3.20}$$

The yield rotation of the connection θ_y was calculated based on the effective rotational stiffness of the connection K_{eff} (ICC-ES 2013).

$$\theta_y = \frac{2P_y}{K_{eff}(d + t)} \tag{3.21}$$

The ultimate and failure rotations were estimated to be 0.02 rad and 0.05 rad, respectively, based on test data.

Two limit states were considered for the design of the T-stub stem: yielding of the reduced region of the stem, and high-mode buckling of the reduced region of the stem. The stem was proportioned so that inelasticity was limited primarily to the reduced region. The yield length was determined based on a target strain demand. The theoretical lateral out-of-plane thrust forces exerted on the restraint plate and beam flange during high-mode buckling of the weak-axis of the reduced region of the link stem were calculated. Similarly, the theoretical lateral in-plane thrust forces exerted on the spacer plates during high-mode buckling of the strong-axis was calculated. The out-of-plane thrust force was used to determine the required thickness of the restraint plate.

The thrust forces were predicted based on constrained buckling theory (Bleich 1952; Chai 1998; Chai 2001; Chai 2002; Genna and Bregoli 2014). A lower and upper bound on the thrust force was based on classical inelastic column theory (Shanley 1947; Chen and Lui 1987; Gere and Timoshenko 1990). A detailed description of the design procedure for the enhanced shear tab connections is available in a separate report (Judd and Charney 2015b).

3.4 Nonlinear Analysis Approach

Archetypical structural systems were analyzed in *OpenSees* (PEER 2012). This section describes the general procedures used to include second-order effects, damping, and the solution strategy used to solve the non-linear equations of motion. Specific analysis procedures for seismic loads are described in Chapter 4, and specific analysis procedures for wind loads are described in Chapter 5.

3.4.1 Second-Order Effects

Second-order (P-Δ) effects were included using the "corotational" approach, where the local element frame continuously rotates with the element to capture large displacements, and small-strain constitutive relationships are applied. Instead of a "leaning column," the gravity framing was explicitly represented. The effect of the approach used to include second-order effects is examined in Chapter 6.

3.4.2 Damping

When a building vibrates, energy is dissipated by various mechanisms (Chopra 2012; PEER/ATC 2010; Deierlein et al. 2010). This energy dissipation is commonly referred to as damping. Inherent damping (damping not explicitly modeled through component hysteresis in the finite element model) is caused by a variety of structural and non-structural mechanisms, such as loading and reloading of components, internal friction of deformed components, friction between structural components, foundation-soil interaction, and so on. In contrast to inherent damping, active, semi-active, or passive energy dissipation devices can provide added damping

to the building. Such added supplemental energy dissipation devices (e.g. linear viscous dampers) were not considered "inherent damping."

Mathematical Model for Damping

This study used a viscous model for damping. This model is mathematically convenient since the damping matrix in the equation of motion can be assembled as a linear combination of the mass and stiffness matrices ("Rayleigh" damping). For example, Figure 3.24 shows the damping curve for the Type I non-ductile moment frame 1-story building.

The viscous model is also convenient in the sense that damping may be expressed as a fraction of critical damping. Also, reconnaissance and field studies often report building damping using a percent of critical viscous damping.

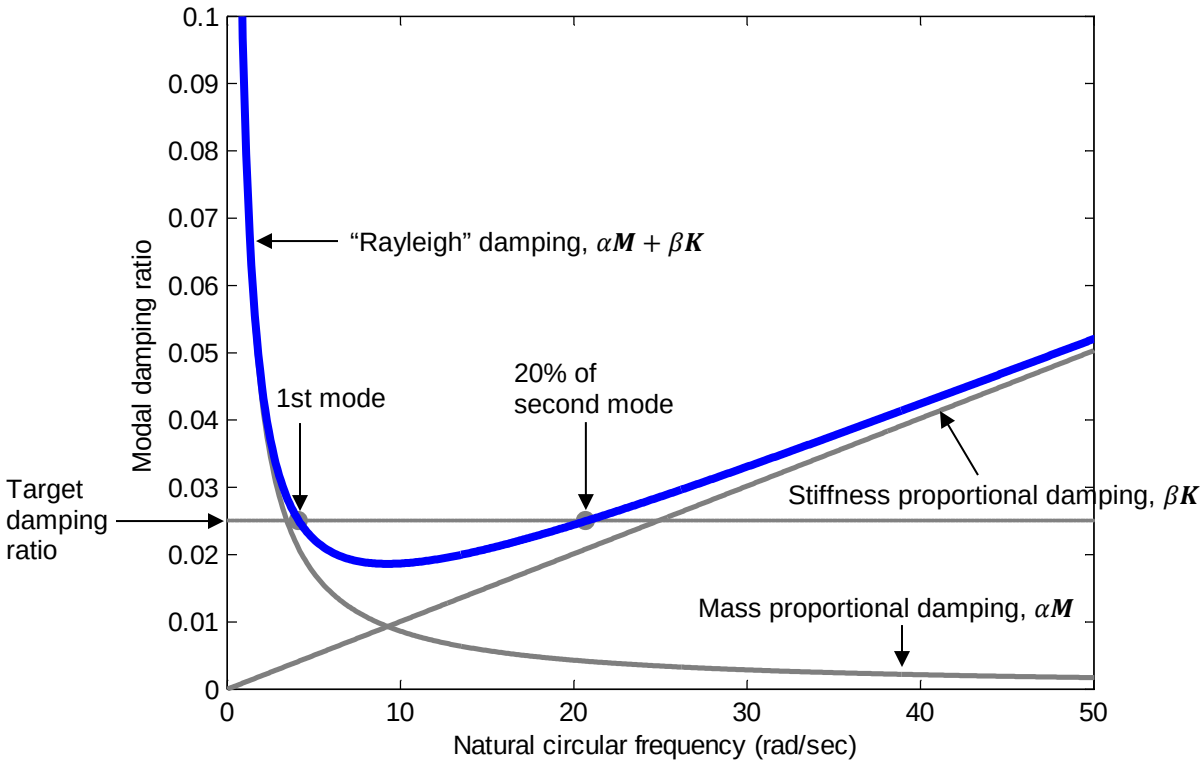

Figure 3.24 Proportional damping curve for Type I non-ductile moment frame 1-story building

It was recognized that invoking viscous damping to capture damping that is not explicitly incorporated in the model is problematic, at best, and may be inaccurate. Many researchers (Bernal 1994; Medina and Krawinkler 2003; Hall 2006; Priestly and Grant 2007; Powell 2008; Charney 2008; Bowland and Charney 2010; Zareian and Medina 2010; Jehel et al. 2011; Puthanpurayil et al. 2011; Hardyneic 2014) have demonstrated the complications with using viscous damping in inelastic models. Namely, viscous damping tends to over-estimate internal forces (e.g. unrealistic damping forces) and under-estimate deformations under inelastic behavior. A primary cause of these errors is the deterioration of component force-deformation relationships. The explicitly modeled hysteresis damping degrades and no longer contributes toward dissipating energy.

Commonly proposed solutions to these concerns maintain viscous damping, but with a varying degree of stiffness-proportional damping. For example, Petrini et al. (2008) verified the use of viscous damping in elastic analysis using experimental data from concrete piers. Among other approaches, for example, Charney (2008) recommends using tangent stiffness-based viscous damping with solution procedures, such as a small time step, to ensure equilibrium. Using initial stiffness may lead to over-damping (e.g. Priestly et al. 2007) and, on the other hand, using tangent stiffness is computationally expensive and may lead to numerical instability. Thus, Zareian and Medina (2010) proposed using a modified initial stiffness by excluding structural elements that may behave inelastically. Similarly, Deierlein et al. (2010) suggest excluding or minimizing the effect of components with degradation or artificial stiffness (such as “rigid” beams or links). In addition to excluding degrading components (i.e. plastic hinges), Ibarra and Krawinkler (2005) increase the stiffness-proportional damping of the internally modified elastic

beam-column elements. Some researchers (e.g. Lignos et al. 2013) advocate using only mass-proportional damping (no stiffness-proportional damping).

Other researchers have altered or completely discarded the assumption of viscous damping. Bowland and Charney (2010) proposed two methods: in the first method, damping was modeled through a rigid-link "ghost element" with rotational dampers, attached to the structure; in the second method, damping was based on internal stresses, a so-called instantaneous viscous damping. Puthanpurayil et al. (2011) showed that a non-viscous model may be more appropriate. Using a relaxation function, a mathematical expression was used that varied from viscous to non-viscous, depending on the dissipation constant (e.g. large value was viscous, small value was non-viscous). The difficulty with this model was that an appropriately tuned value for seismic analysis was undetermined.

For the above reasons, in this research, Rayleigh damping was only applied to linear elastic components of the finite element model.

Critical Damping Ratio

This research assumed 2.5% critical damping ratio, except that in a wind strength design analysis 1% damping was assumed (ASCE 2010), and 1% damping was used in a wind collapse analysis (see Chapter 5). Mass and stiffness proportional ("Rayleigh") damping was defined using the fundamental building period and a period corresponding to 20% of the second mode period of the building (see Figure 3.24). It is noted that this definition of proportional damping (NIST 2010a) differs from the recommendation by Smyrou et al. (2011) for nonlinear dynamic analyses to use the first mode and the n-th mode, where n = number of stories of the building. A free vibration analysis was used to verify the model damping.

It was recognized that the appropriate amount of proportional damping depends on the structure and hazard intensity considered. Traditionally, 2% to 5% total damping has been used for seismic analysis of buildings. However, this overestimates the damping for nonlinear analysis because some of the damping is already explicitly modeled via component hysteresis. The assumed damping in this research falls in the range between 1% and 5%, but not greater than 3% for tall buildings, where the damping effect of foundations and nonstructural cladding is small relative to the structural characteristics, recommended by FEMA P-58 (FEMA 2012a,b).

3.4.3 Analysis Solution Procedures

For nonlinear static analysis, the finite element system of equations was solved using static load control for gravity analysis, and displacement control (Batoz and Dhatt 1979; Ramm 1981) for seismic or wind pushover analysis. For nonlinear response history analysis, the system of equations was solved using the implicit integration method proposed by Newmark (1959) with the special case of average acceleration (Tedesco et al. 1999), where the corresponding integration parameters are $\gamma = 1/2$ and $\beta = 1/4$. The integration method is unconditionally stable for linear analysis (Bathe 1996), however stability for nonlinear analysis has not been proven (Belytschko et al. 2014, pages 356 to 357). Explicit integration was not used for two reasons. The first reason is that the stable time increment (Equation 3.22) required for an explicit integration scheme was very small and may lead to impractical run-time.

$$\Delta t \quad \leq \quad \frac{2}{\omega_{max}} + \left(\sqrt{1 + \xi_{max}{}^2} - \xi_{max} \right) \tag{3.22}$$

In Equation 3.22, ξ_{max} is the critical damping ratio in the mode with the highest frequency. The consequence is that damping in the analysis actually reduces the stable time

increment (Dassault Systèmes 2011b). Nevertheless, previous experience suggests that much larger time steps can still be used for an implicit scheme, compared to an explicit scheme (Belytschko et al. 2014).

The second reason is that the explicit integration necessitates the inclusion of mass at each degree of freedom in the finite element model (Carr 2004), but the model used in this study employed a lumped mass approach. The primary disadvantage of an implicit integration scheme is the high-computational cost and insufficient robustness for rough response.

Thus, a self-adaptive solution strategy (Appendix C) was required to solve the non-linear equations. The Newton-Raphson method was the initial default solution algorithm. The default convergence tolerance (based on absolute energy balance) was between 10^{-4} and 10^{-5} depending on the analysis type (static gravity, pushover, or dynamic) and the solution algorithm.

- In the first step of the strategy, the Newton-Raphson method was used. This method was computationally expensive in that it required the tangent stiffness matrix to be reformulated, but the method was robust.

- In the second step of the strategy, if required, the analysis time step was reduced.

- In the third step, the solution strategy tried the following solution algorithms (in this order). A Newton-Raphson with Line Search was used to improve slow convergence with the Newton-Raphson algorithm. An initial interpolated line search was used with tolerance = 0.8, max number of iterations = 10, minimum root to the solution function, η_{min} = 0.1, and maximum root to the solution function, η_{max} = 10.0. A Newton-Raphson

with Krylov subspace accelerator (a low-rank least-squares analysis) was used to improve slow convergence by identifying where the largest changes in structural state occurred and then correcting for smaller changes at the remaining degrees of freedom (Scott and Fenves 2010) using an initial tangent stiffness matrix. As an alternative to the Newton-Raphson methods for dynamic analyses (Bathe and Cimento 1980), a secant approximation of the stiffness matrix was employed using the Broyden–Fletcher–Goldfarb–Shanno (BFGS) matrix-updating (quasi-Newton) method. Successive rank-one updates of the tangent stiffness matrix were used based on the first iteration of the current time step using the Broyden method. The Newton-Raphson algorithm was modified (the stiffness matrix was not reformulated) using initial stiffness solution iterations. In the fourth step of the strategy, the TRBDF2 integrator (Bathe 2007) was temporarily applied. Finally, the convergence tolerance was temporarily loosened.

As an example, Figure 3.25 compares the solution information for nonlinear static "pushover" analysis and nonlinear dynamic response history analysis of the Type I non-ductile 2-story building with enhanced shear tab connections. The colors indicate the final algorithm that was used to achieve a solution. The number of iterations shown in the lower plots refers only to the final algorithm, and does not include the number of algorithms tried and the number of iterations attempted for those analyses.

In the static analysis, at approximately 3% roof drift the solution algorithm switch from the default (Newton-Raphson) to include a line search. At approximately 7% the Krylov subspace accelerator was used. Finally, at approximately 8% the solution returned to using default algorithm. The static analysis required up to 63 iterations to achieve a solution.

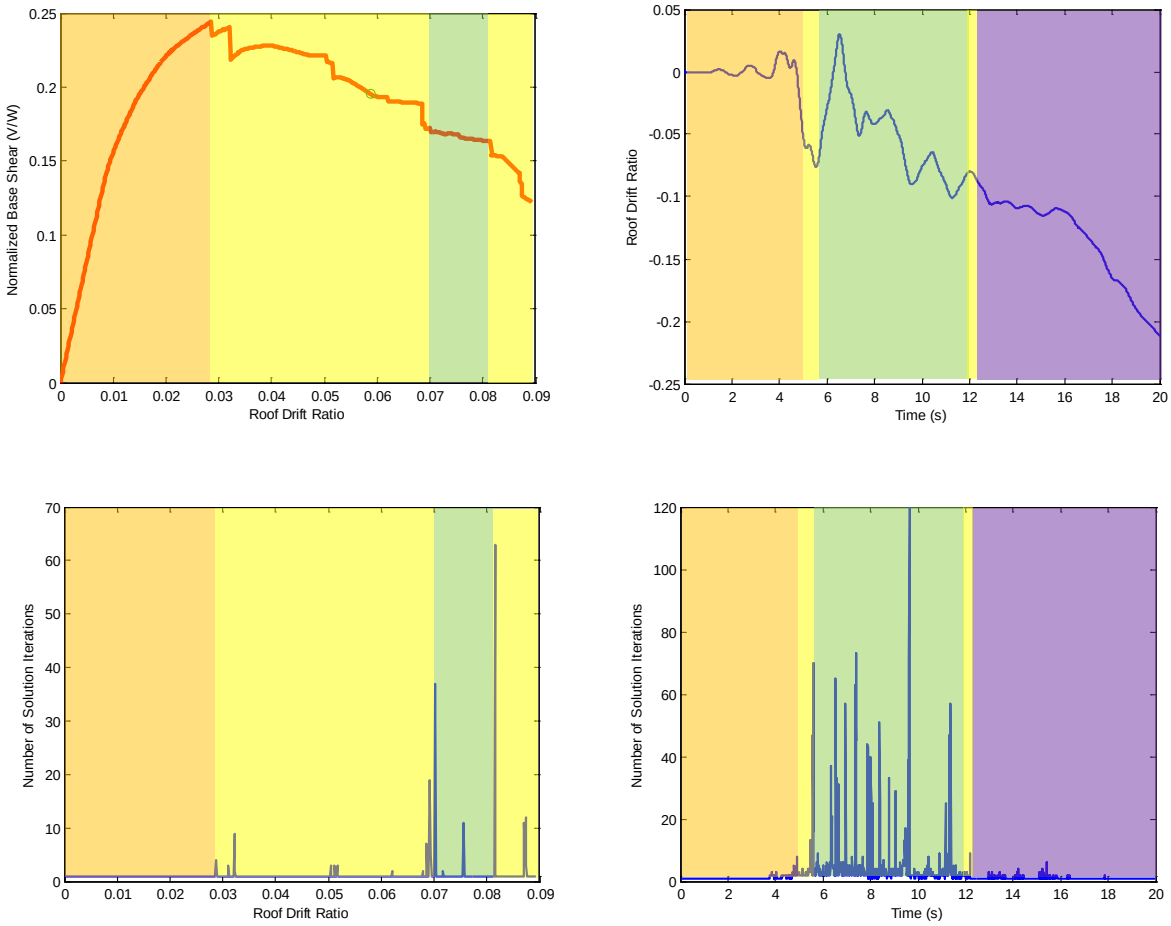

a) Nonlinear static pushover analysis b) Nonlinear response history analysis

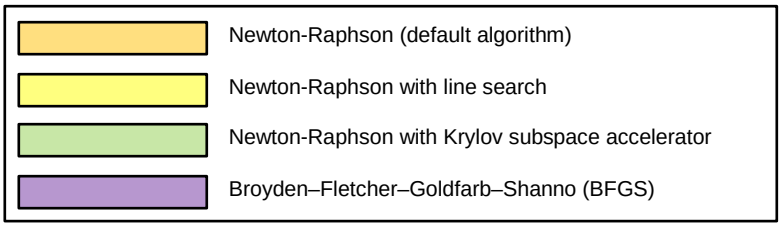

Figure 3.25 Solution algorithm and maximum number of iterations: seismic analysis of Type I non-ductile 2-story building with enhanced shear tab connections for LOS000 ground motion scaled to collapse intensity

In the dynamic analysis, a similar pattern of algorithm switching was observed but more iterations (up to 120) were typically required.

Thus, the appropriate algorithm and number of steps depended on the nonlinear equations that were solved. Depending on the structure, these equations varied considerably, and it was not apparent which solution algorithm was most appropriate. In fact, previous research of nonlinear analysis of framed structures (Vamvatsikos and Cornell 2004; Bathe 1996; Vamvatsikos 2011; Hardyniec 2014; Hardyneic and Charney 2015) have employed similar ad-hoc self-adaptive solution strategies.

Chapter 4

SEISMIC COLLAPSE ASSESSMENT

This chapter assesses the seismic collapse safety of the archetype structural systems with and without collapse prevention systems. The collapse vulnerability (collapse fragility) was determined using a sequence of gravity, frequency, nonlinear static "pushover" analyses, followed by nonlinear dynamic response history analyses incrementally scaled, with respect to a target spectrum, until side-sway collapse. The risk of seismic collapse was determined by integrating collapse fragility and hazard, accounting for directional effects and site response. Results of selected archetype systems are discussed. Finally, a comparison with the seismic collapse assessment of traditional structural systems is included.

4.1 Seismic Collapse Vulnerability Procedures

The probability of building seismic collapse given the MCE was assessed following the FEMA P-695 methodology (FEMA 2009a) with two adaptations appropriate for the collapse prevention systems approach and for the central and eastern United States.

- First, the computed (model) fundamental period of vibration was used for both referencing spectral accelerations and for estimating the inherent damping (taken as 2.5%) in the building that was not explicitly modeled through component hysteresis.

- Second, incremental dynamic analyses were run until all ground motions caused collapse and the measured record-to-record dispersion was used when incorporating uncertainty.

The collapse assessment consisted of several analysis procedures. A gravity load analysis was first conducted. An eigenvalue analysis was then used to determine the period of vibration used as a reference for ground motion scaling and used as a reference for damping. Nonlinear static seismic (pushover) analyses were conducted to determine the axial loads used in the column plastic hinge approximation and to determine period-based ductility. Finally, nonlinear dynamic response history analyses were completed. Appendix C contains excerpts of the *OpenSees* (PEER 2012) scripts and selected seismic modeling results for the Type I non-ductile moment frame 4-story building with enhanced shear tab connections.

4.1.1 Gravity Load Analysis

Vertical gravity roof and floor dead (D) and floor live (L) loads were calculated using the load combination given in Equation 4.1. The gravity loads are defined in Appendix B.

$$\text{Total load} = 1.05D + 0.25L \tag{4.1}$$

The load combination was intended to represent the expected gravity loads present in the building during an earthquake [see ASCE 7-10 Table C4-2 (ASCE 2010); FEMA (2009a)]. Second-order effects were included in the gravity load analysis.

4.1.2 Frequency (Building Period of Vibration) Analysis

After the gravity pre-load analysis, an eigenvalue frequency analysis was used to determine the periods of vibration of the building and associated mode shapes. For example, Figure 4.1 shows the first four modes of vibration for the Type I non-ductile moment frame 8-story building.

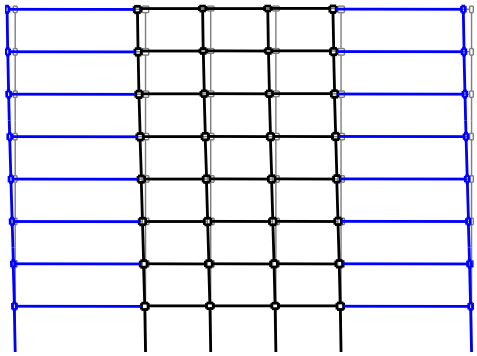

a) Mode 1 (T_1 = 2.85 seconds/cycle)

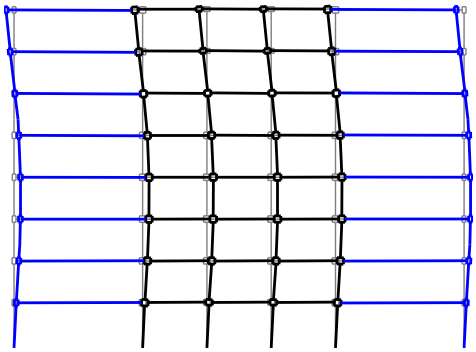

b) Mode 2 (T_2 = 1.00 seconds/cycle)

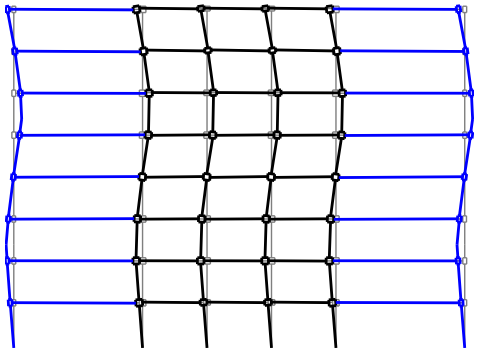

c) Mode 3 (T_3 = 0.55 seconds/cycle)

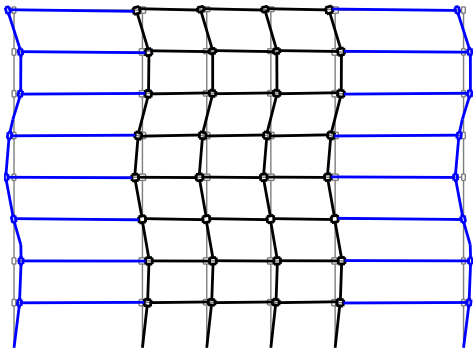

d) Mode 4 (T_4 = 0.33 seconds/cycle)

Figure 4.1 Mode shapes and periods of vibration: Type I non-ductile moment framing 8-story building

4.1.3 Nonlinear Static Seismic ("Pushover") Analysis

In the nonlinear static seismic "pushover" response analysis, the building model was subjected to a static lateral force at each story. Pushover analysis serves three purposes: it provides information regarding dynamic response (see below), the post-peak negative slope is a predictor of P-D instability (Humar et al. 2000), and it provides a method to verify that the analytical modeling (i.e. story collapse mechanisms are reasonable).

In this research, the distribution of lateral forces was proportioned to match the mode shape corresponding to the fundamental period of vibration of the building (previously discussed). The lateral forces were applied using a displacement-control solution strategy until the roof displacement of the building exceeded at least the displacement corresponding to a 20% loss in lateral strength of the building. For example, Figure 4.2 shows the seismic pushover response for the Type I ductile moment frame 4-story building.

The seismic pushover analysis was used to determine the static overstrength, Ω and the period-based ductility, μ_T. The static overstrength was calculated as the ratio of the maximum base shear resistance to the design base shear force (Equation 4.2).

$$\Omega = \frac{V_{max}}{V_{design}} \tag{4.2}$$

The period based ductility was calculated based on the ratio of ultimate roof displacement to effective yield roof displacement (Equation 4.3), where a single-degree-of-freedom (SDOF) displacement is correlated to the building roof displacement, using C_0 as calculated in ASCE 41-13 (ASCE 2014).

$$\mu_T = \frac{\delta_u}{\delta_{y,eff}} = \frac{\delta_u}{\left\{C_0 \frac{V_{max}}{V_{design}} \left(\frac{g}{4\pi^2}\right) [max(C_u T_a, T_1)]^2\right\}} \quad (4.3)$$

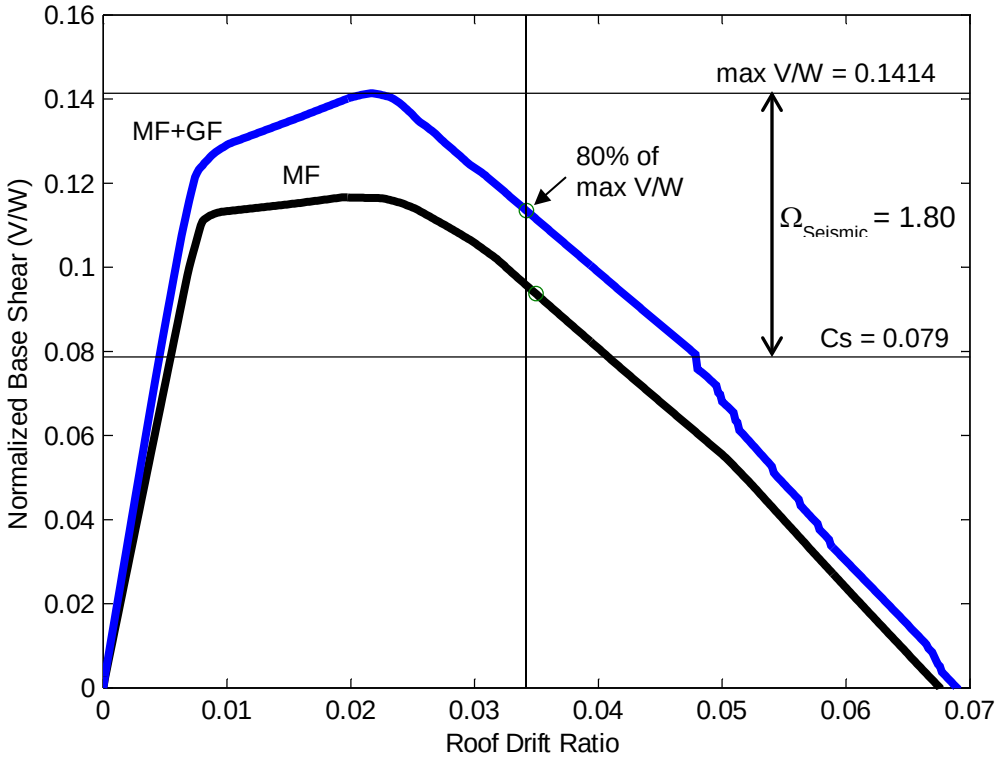

Figure 4.2 Seismic pushover response of Type I ductile moment frame 4-story building

4.1.4 Ground Motion Set for Nonlinear Response History Analysis

Response history analysis of a structure requires the use of an input ground motion, and these input ground motions can be legitimately derived from a variety of sources (see discussion in Chapter 6). In this study, the FEMA P-695 "Far-Field" ground motion set (Table 4.1) was used.

It is recognized that this choice is imperfect. It has been shown in this study that ground motions in the central and eastern United States have different characteristics—namely

frequency content—compared to ground motions in the western United States or from other tectonic boundary regions. [See Baker et al. (2011) for example ground motion set for tectonic boundary regions.] Moreover, due to the scarcity of large-magnitude earthquakes and the lack of strong motion instrumentation, we know less about earthquakes outside the western United States.

Table 4.1 Ground motion set (FEMA P-695 Far-Field set) used for dynamic analysis

FEMA P-695 ID	Record Name	Earthquake	Magnitude
1	Beverly Hills - Mulhol	1994 Northridge	6.7
2	Canyon Country-WLC USC	1994 Northridge	6.7
3	Bolu ERD	1999 Duzce, Turkey	7.1
4	Hector SCSN	1999 Hector Mine	7.1
5	Delta UNAMUCSD	1979 Imperial Valley	6.5
6	El Centro Array	1979 Imperial Valley	6.5
7	Nishi-Akashi CUE	1995 Kobe, Japan	6.9
8	Shin-Osaka CUE	1995 Kobe, Japan	6.9
9	Duzce ERD	1999 Kocaeli, Turkey	7.5
10	Arcelik KOERI	1999 Kocaeli, Turkey	7.5
11	Yermo Fire Station CDMG	1992 Landers	7.3
12	Coolwater SCE	1992 Landers	7.3
13	Capitola CDMG	1989 Loma Prieta	6.9
14	Gilroy Array #3	1989 Loma Prieta	6.9
15	Abbar BHRC	1990 Manjil, Iran	7.4
16	El Centro Imp.	1987 Superstition Hills	6.5
17	Poe Road (temp)	1987 Superstition Hills	6.5
18	Rio Dell Overpass	1992 Cape Mendocino	7
19	CHY101 CWB	1999 Chi-Chi, Taiwan	7.6
20	TCU045 CWB	1999 Chi-Chi, Taiwan	7.6
21	LA - Hollywood	1971 San Fernando	6.6
22	Tolmezzo --	1976 Friuli, Italy	6.5

In this research, two overriding considerations in choosing ground motions for analysis were (1) that the ground motions match (more or less) the spectral shape expected for the location, and (2) a wide-range of motion based on the spectral shape should be used to account

for the lack of known constraints on the motion. The selected ground motion set was considered to be a reasonable choice since the primary interest was in the comparison between structural systems, as opposed to an attempt to accurately predict collapse for an actual site location.

4.1.5 Target Spectrum

In this study, the ASCE 7-10 design spectrum was used as the target spectrum. This approach follows the approach used in the prevailing seismic collapse assessment method (FEMA P-695).

It is recognized that in the western United States a conditional mean spectrum is theoretically an appropriate target, whereas in the central and eastern United States, the uniform hazard spectrum is theoretically more appropriate. This is the case because outside the western United States the uniform hazard and conditional mean spectrums do not differ much. This lack of dissimilarity is due to the fact that the same earthquake event is the dominant contributor to hazard across the range of spectral periods (Baker 2011). However, the objective is to compare structural systems, so the design spectrum was used in this research.

As an example, Figure 4.3 shows the response spectrum for the Type I non-ductile 2-story building. The analytical model included reserve lateral strength in the gravity framing.

4.1.6 Intensity Measure for Seismic Hazard

In this study, the spectral acceleration at the fundamental period of vibration was selected as the seismic hazard intensity measure. The sensitivity of the collapse assessment to the conditioning period used for the intensity measure is discussed in Chapter 6.

Various intensity measures can be used in a seismic collapse assessment, including single parameter measures, such as peak ground acceleration (PGA), peak ground velocity (PGV), and

peak ground displacement (PGD), and multiple parameter measures, or so-called vector intensity measures (e.g. Baker and Cornell 2005). A vector intensity measure using spectral acceleration and epsilon (difference between observed and expected lognormal spectral accelerations in terms of standard deviations) has been shown to be an effective intensity measure for predicting seismic damage in ductile steel frame buildings, whereas a vector intensity measure using peak ground displacement and peak ground velocity (PGD, PGV) has been shown to be more suited for seismic collapse predictions of ductile steel frame buildings (Olsen et al. 2014; Buyco 2014). Interestingly, a related study indicated that applying a low-pass Butterworth filter to the peak ground acceleration with a cutoff period larger than the fundamental building period (termed a "peak filtered acceleration"), in order to isolate the long-period component of the ground motion, is another effective intensity measure for seismic collapse of ductile steel frame buildings (Song 2014; Buyco 2014). Notwithstanding, perhaps the most commonly used single-parameter seismic intensity measure for structural engineering is spectral acceleration at the fundamental period of vibration [i.e. FEMA P-695 (FEMA 2009a); FEMA P-58 (FEMA 2012a,b)].

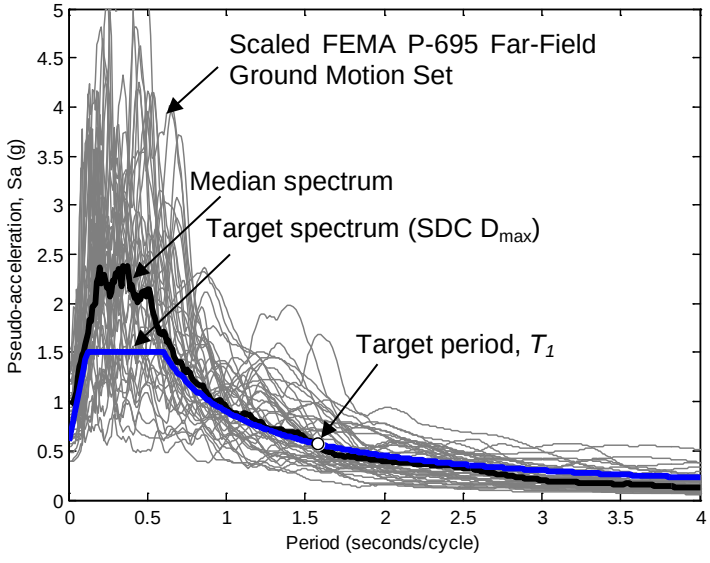

Figure 4.3 Response spectrum for Type I non-ductile 2-story building

4.1.7 Nonlinear Dynamic Response History Analysis

In the nonlinear dynamic response history analysis, the FEMA P-695 "Far-Field" ground motion set (shown in Table 4.1) was collectively scaled so that the median response spectrum matched the target spectrum (SDC D_{max}) at the reference period. Each building model was subjected to the ground motion set in successive incrementally increasing levels of intensity (as measured by the spectral acceleration at the fundamental period) until all ground motions caused side-sway collapse, assumed to occur when the maximum interstory drift ratio is at least 0.2.

This procedure of conducting nonlinear dynamic response history analyses with increasing hazard intensities is commonly called an incremental dynamic analysis (IDA). Although the concept of incremental dynamic analyses is not new (e.g. Nassar and Krawinkler 1991; Elnashai and Di Sarno 2008), it was impractical for the computational resources of the time and was not commonly done until Vamvatsikos and Cornell (2004). It was recognized that the linear scaling approach used in the IDA leads to a loss in accuracy for large ground motions (Baker 2013), but at the same time the IDA approach was the most viable approach when collapse is to be assessed in numerous locations with variations in the underlying seismic hazard, as is considered in this study.

In an IDA, the ground motion scaling is relative to a reference magnitude. The scaling procedure was a multi-step scaling process. The ground motion record was first scaled (in FEMA P-695) by a factor to normalize the velocity of the ground motion set. Next the record was scaled so that the median of the record set matches the target design spectrum. Finally, the record is incrementally scaled relative to the normalization factor times the anchor factor. The following scheme was used to determine the anchor factor. (An alternate scheme was used for seismic performance assessment in Chapter 7.)

Each ground motion record was scaled relative to the original record intensity. (For example, the record was multiplied by 2, 3, 4, and so on.) The advantage of this method is that the scaling was independent of a target spectrum (which target depends on several factors, including the building location, seismic design category (SDC), and period of vibration). Additionally, this scaling method allowed the IDA results to be independent of the sub-set of motions selected from the full set (since the normalization factor is a function of the set of motions considered). Another advantage was that this scaling method allowed the seismic collapse fragility curve to exhibit non-vertical data points (since ground motions are not being run at the same spectral acceleration intensity for a given period).

Moreover, the intensity factor correlates to how much the magnitude of original ground motion has been altered, whereas the intensity factor for anchored scaling (used for performance assessment in Chapter 7) does not show the normalization and anchoring factors. A disadvantage of this scaling scheme is that the individual response for a given ground motion is not necessarily calculated at exactly the DBE, MCE, or some other hazard intensity level.

The anchor record reference scheme was used for response history analyses when used as part of a collapse assessment using the FEMA P-695 procedure, for the reasons previously outlined. However, the anchor reference scheme is used for performance assessment using the FEMA P-58 framework, since this scheme calculates response at exactly the hazard level of interest, as previously noted.

The nonlinear dynamic analyses were advanced in the IDA scaling procedure using parallel processing with a bisection approach (Vamvatsikos 2011; Hardyniec and Charney 2015). Each ground motion was assigned to one processor and incremental analyses were run until completion of the IDA for that ground motion.

4.1.8 Collapse Fragility

The seismic vulnerability of the building to side-sway collapse (seismic collapse fragility) was determined by fitting individual collapse points (spectral acceleration at the reference period and corresponding probability of collapse for a one scaled ground motion record) with a curve, assuming a lognormal cumulative distribution function. The lognormal cumulative distribution function was defined by two parameters: the median collapse spectral acceleration with reference to the ground motion set $S_a(T_1)$, and the standard deviation of the natural logarithm β (dispersion due to variability and uncertainty). Prior analytical studies suggest that the lognormal distribution is appropriate for seismic collapse fragility (Ibarra and Krawinkler 2005; Bradley and Dhakal 2008; Ghafory-Ashtiany et al. 2011; Eads et al. 2013).

The median collapse spectral acceleration was adjusted (increased) to account for spectral shape, estimated using period-based ductility, μ_T and the total dispersion, β_{Total} in collapse capacity was calculated using Equation 4.4.

$$\beta_{Total} = \sqrt{{\beta_{RTR}}^2 + {\beta_{DR}}^2 + {\beta_{TD}}^2 + {\beta_{MDL}}^2} \quad (4.4)$$

In Equation 4.4, β_{RTR} was the measured (record-to-record) dispersion in the nonlinear seismic response history analyses. Epistemic uncertainty was incorporated by assigning dispersion due to design β_{DR}, test data β_{TD}, and modeling uncertainty β_{MDL}. The qualitative ratings (using FEMA P-695 rubric) given in Table 4.2 were used in this study.

Table 4.2 Qualitative rating used to quantify uncertainties in seismic collapse assessment

	Non-ductile moment frame	Ductile moment frame
Design requirements	B (β=0.20)	A (β=0.10)
Test data	C (β=0.35)	B (β=0.20)
Analytical model	C (β=0.35)	B (β=0.20)

For non-ductile moment frame buildings, β_{DR} = 0.2 ("Good"), and β_{TD} = β_{MDL} = 0.35 ("Fair"). For ductile moment frame buildings, β_{DR} = 0.1 ("Superior"), and β_{TD} = β_{MDL} = 0.2 ("Good").

The ASCE 7-10 (ASCE 2010) target is that the average conditional collapse probability for a group of similar archetypical structures does not exceed 10%, and the FEMA P-695 (2009a) target is that the conditional collapse probability for any individual building does not exceed 20%.

4.2 Seismic Collapse Risk Procedures

Seismic collapse risk (probability of collapse considering the likelihood of seismicity) was calculated by integrating the seismic collapse fragility and seismic hazard and by accounting for directional effects and site response. The ASCE 7-10 (ASCE 2010) target risk is 1% in 50 years.

4.2.1 Directional Effects

Ground motion is a three-dimensional phenomenon that can be described in terms of three components: one component in the vertical direction and two orthogonal horizontal components. Relative to a structure, the direction of ground motion and spectral acceleration may be based on the geometric mean ("geomean") of two horizontal components. The USGS ground motions use the geomean due to the ground motion attenuation models used. See FEMA P-750 (FEMA 2009c) and Abrahamson and Shedlock (1997). Alternatively, the direction may be based on the square root of the sum of the squares (SRSS) of the two horizontal components, or on the "maximum-direction" of the two components. Maximum-direction spectral acceleration is determined by calculating the maximum spectral acceleration based on both horizontal

components for an entire orbit (orientations from 0° to 360°). The maximum direction is the orientation with the maximum spectral demand (identified by the point on the orbit farthest from the origin) (Huang et al. 2008; Huang et al. 2010a).

To illustrate, Figure 4.4 compares the geomean, SRSS, and maximum-direction spectra for the 1999 Kocaeli, Turkey earthquake ground motion recorded at the Duzce station (FEMA P-695 Far-Field ground motion ID No. 9). The maximum-direction spectrum envelopes the component and geomean spectra, but is less than the SRSS spectrum.

As would be expected, the direction of ground motion affects structural response. Three-dimensional analyses of buildings, subjected to two orthogonal components of ground motion simultaneously, systematically show that structural collapse is predominately in the direction of the stronger component. See FEMA P-750 (FEMA 2009c). As a consequence, the overall structural failure rate is higher for three-dimensional analyses compared to two-dimensional analyses, all other factors being equal.

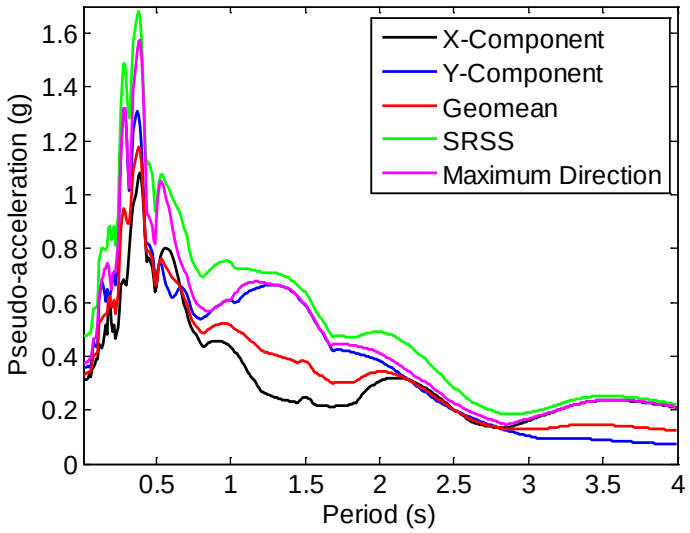

Figure 4.4 Spectral acceleration for the 1999 Kocaeli, Turkey earthquake ground motion recorded at the Duzce station (FEMA P-695 Far-Field ground motion ID No. 9)

To remove this non-conservative bias in collapse capacity, the ASCE 7-10 ground motion design data has been adjusted (increased) from the USGS geomean uniform-hazard spectral accelerations to approximate maximum-direction demand. See FEMA P-751 (FEMA 2012e). The ASCE 7-10 (NEHRP) approximation is based on the ratio of maximum-direction to geomean spectral demand for near-field ground motions in the western United States (Huang et al. 2008).

Table 4.3 gives the ratio of maximum-direction to geomean spectral demand for sets of ground motions used in FEMA P-695 and in the development of ASCE 7-10. The ratios reflect the fact that the maximum-direction spectral acceleration depends on the ground motions. The ratios for far-field ground motion sets and for ground motion sets intended for the central and eastern United States can be quite different from each other. For far-field ground motions in the western United States, the median ratio is 1.20 and 1.27, for 0.2-second and 1.0-second spectral accelerations, respectively. In the central and eastern United States, the 0.2-second ratio is equal to 1.28 and the 1.0-second ratio is equal to 1.35.

Table 4.3 Ratio of maximum-direction to geomean spectral acceleration

	P-695			Huang et al. (2010)			
		Near-Field		Western US		Central and	
T (s)	Far-Field	Pulse	No Pulse	Far-Field	Near-Field	Eastern US	NEHRP
0	1.2	1.21	1.25	1.18	1.21	1.23	1.1
0.2	1.29	1.24	1.31	1.2	1.22	1.28	1.1
0.5	1.32	1.26	1.31	1.23	1.29	1.32	1.2
1	1.3	1.27	1.37	1.27	1.31	1.35	1.3
2	1.39	1.41	1.4	1.27	1.31	1.39	1.3
3	1.34	1.33	1.31	1.27	1.31	1.35	1.35
4	1.27	1.48	1.35	1.31	1.37	1.4	1.5

Figure 4.5 and Figure 4.6 compare the ratio of maximum direction to geomean spectral acceleration for the three FEMA P-695 ground motion sets with the NEHRP approximation. Note that the ratios using the FEMA P-695 method will differ for these periods compared to the NEHRP approximation.

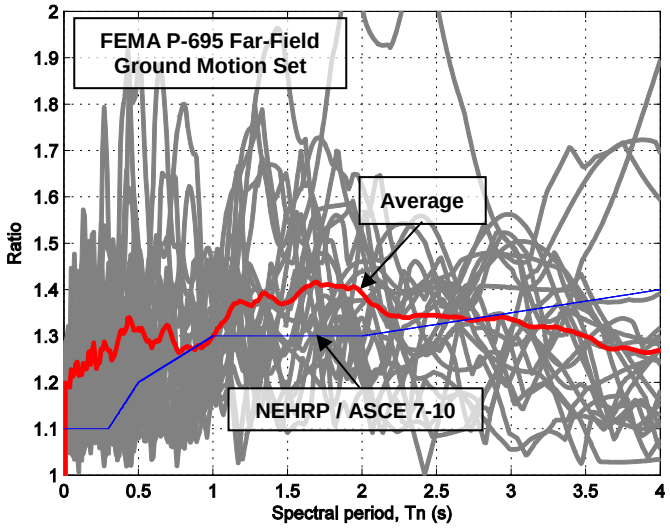

Figure 4.5 Ratio of maximum-direction to geomean S_a for FEMA P-695 far-field ground motion set (individual record ratio is indicated by gray lines)

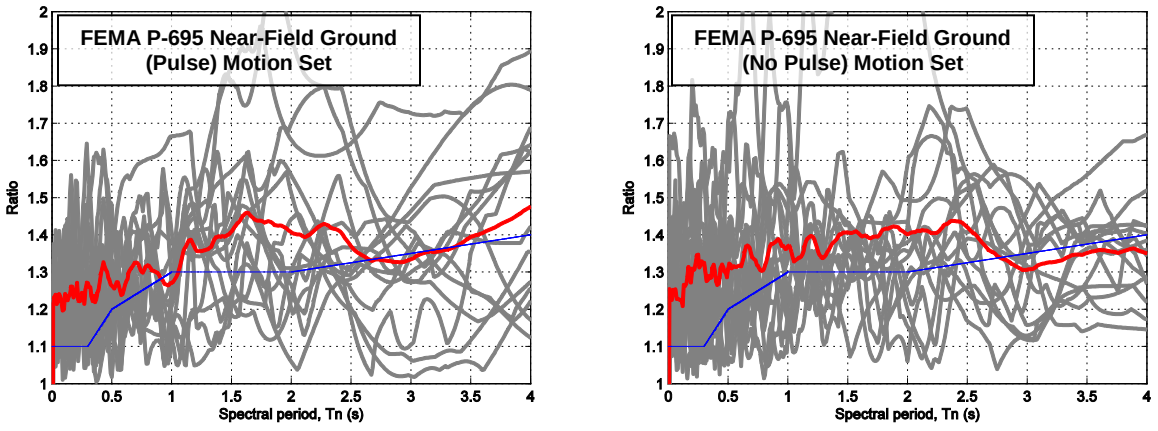

a) Near-field ground pulse b) Near field no pulse

Figure 4.6 Ratio of maximum-direction to geomean S_a for FEMA P-695 near-field ground pulse

Based on data from Huang et al. (2010a), maximum-direction to geomean spectral acceleration ratios of 1.2 and 1.3 are appropriate in the western United States, whereas ratios of 1.3 and 1.4 may be more appropriate in the central and eastern United States, for 0.2-second and 1.0-second spectral accelerations, respectively.

4.2.2 Site Response

A coarse estimate of ground motion amplification can be correlated using geological data (Kottke et al. 2012), topographic data as a proxy for V_{s30} (Wald and Allen 2007; Allen and Wald 2009), or a combination thereof (Magistrale et al. 2012). Such an estimate is especially useful in situations where it is not feasible to know site conditions with certainty (such as when generating a ground motion map for code adoption). In fact, ground motion maps along these lines are proposed for Italy (Crowley et al. 2009).

Figure 4.7 shows a map of V_{s30} for the conterminous United States based on topographic data. An important consideration using the topographic proxy method is that the effect of sediment thickness is not included (among other effects), and that the proxy method tends to under-predict V_{s30} for hard rock sites (Kottke et al. 2012).

In the ASCE 7-10 approach to risk, site amplification of ground motion is not considered until after calculation of the risk-targeted motions. Site amplification is dependent on the spectral acceleration, however, due to soil non-linearity, and so the amplification varies for different intensities of seismic hazard. For example, Figure 4.8 shows the effect of soil amplification on both the seismic hazard curve and the ground motion spectrum for a location in San Francisco.

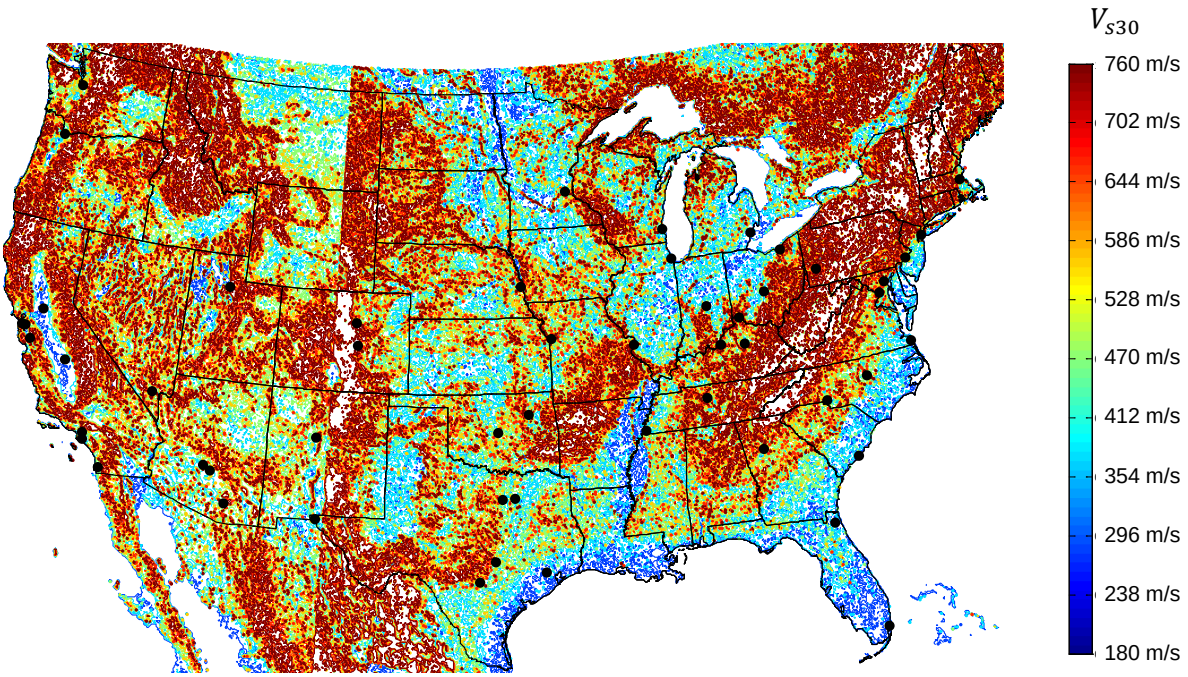

Figure 4.7 Average shear wave velocity (V_{s30}) based on topographic data

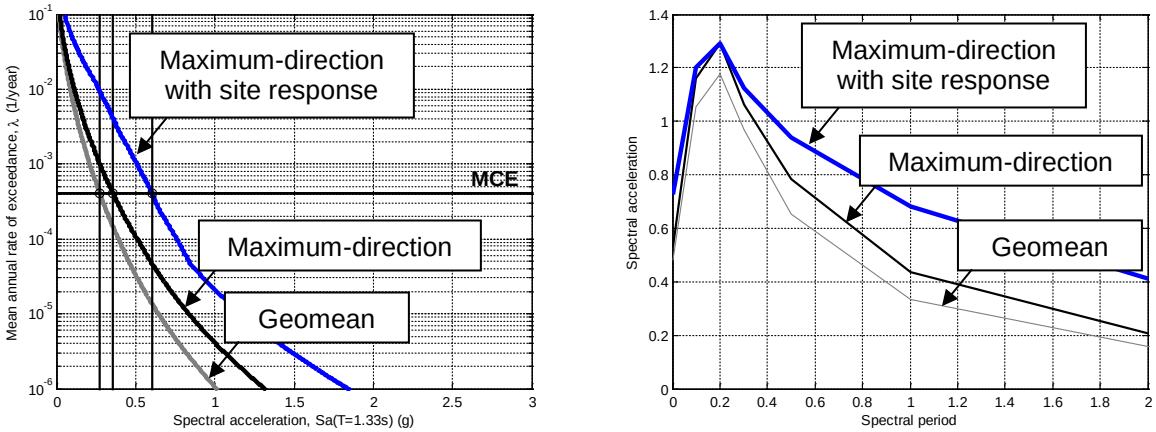

a) Seismic hazard curves b) uniform hazard spectra

Figure 4.8 Seismic hazard data for location in San Francisco (38.0º latitude, -121.7º longitude) with soil site class D (average V_{s30} = 180 m/sec)

Clearly, a more accurate seismic risk analysis requires a geotechnical investigation (where possible), or an estimate of site response using proxy data, to obtain the soil-amplified hazard curve before integrating hazard and vulnerability.

4.2.3 Integration of Seismic Hazard and Seismic Collapse Vulnerability

Seismic hazard (the occurrence of earthquakes) is commonly described as a Poisson' process (FEMA 2012a), that assumes events (e.g. earthquakes) occur randomly and independent of other events (earthquakes). Although the Poisson process is an inaccurate description for characteristic earthquake sources, where other descriptions may be more accurate (Matthews et al. 2002), the description is generally useful (Cornell and Winterstein 1988) and was employed in this research. For a Poisson process, the probability of occurrence of an event, N in t years is

$$P(N \geq 1) \quad = \quad 1 - e^{(-\lambda_a t)} \tag{4.5}$$

where λ_a is the mean hazard exceedence frequency corresponding to an intensity measure (i.e. spectral acceleration), the probability that the intensity of an earthquake, *A* will exceed some level, *a* in a given year.

$$\lambda_a \quad = \quad P(A > a \mid t = 1yr) \tag{4.6}$$

For low annual hazard rates, Equation 4.5 is numerically equivalent to the hazard curve (inverse of MRI) expressed by Equation 4.6.

$$P(N \geq 1) \quad = \quad \lambda_a t$$

$$= \quad \lambda_a$$

As noted earlier, the collapse fragility curve is simply the probability of collapse or failure, *F* conditioned on the occurrence of a spectral acceleration value: $P(F|A < a) = \int_{-\infty}^{a} f(t)dt$, where *f(t)* is the probability density function of collapse.

Calculation of collapse risk requires the integration of seismic hazard curves and structural collapse vulnerability (fragility) curves. Integrating hazard and fragility depends on the overall approach. For example, in a "deterministic" analysis, each fragility ordinate is multiplied by the corresponding hazard probability (Wang 2011). In probabilistic seismic hazard analysis (PSHA), there are three analytically equivalent methods to integrate hazard and fragility. These methods are discussed in Chapter 6. Each method leads to some approximation, and an alternate form of the risk integral that does not require differentiating the hazard curve is attractive. This alternate method was used by the USGS to create risk-targeted ground motion maps (Luco 2006). The alternate form may be derived as follows. Given the risk integral:

$$\lambda_F = -\int_0^{+\infty} P(F|a)\left(\frac{d\lambda_a}{da}\right) da$$

Let

$$u = P(F|a)$$

$$du = \frac{dP(F|a)}{da}$$

where the latter is the same as

$$du = f(a)\, da$$

and let

$$dv = \left(\frac{d\lambda_a}{da}\right) da$$

$$v = \lambda_a$$

Invoking definite integration by parts:

$$\lambda_F = -\int_0^{+\infty} udv$$

$$= -\left[uv|_0^{+\infty} - \int_0^{+\infty} vdu\right]$$

$$= \quad -[P(F|a)\,\lambda_a]_0^{+\infty} + \int_0^{+\infty} \lambda_a\, f(a)\, da$$

$$= \quad -[(1)(0) - (0)(1)] \quad + \int_0^{+\infty} \lambda_a\, f(a)\, da$$

$$= \quad \int_0^{+\infty} \lambda_a\, f(a)\, da \tag{4.7}$$

Note that this form of the risk integral (Equation 4.7) requires the derivative of the fragility curve—the CDF, which yields the probability density function (PDF). This was a more stable approach than taking the derivative of the hazard curve. It is important to note that there is not a closed form solution to the risk integral regardless of the method used, and in practice the integral is performed numerically. The cumulative risk (P_F) to seismic collapse during the building lifetime (t in years) was calculated using Equation 4.8.

$$P_F \quad = \quad 1 - \, e^{(-\lambda_F t)} \tag{4.8}$$

The seismic risk analysis procedures are illustrated in Figure 4.9 for two locations. The first location is in Saint Louis, Missouri and the second location is in Charleston, South Carolina. The hazard curves in the top plots correspond to the spectral acceleration for the building without considering the gravity framing (black) and with the gravity framing (blue).

The hazard curve was based on the USGS 2008 United States National Seismic Hazard Maps, adjusted for the maximum-direction spectrum of the FEMA P-695 Far-Field Set and adjusted for soil amplification using the NGA correlation between shear wave velocity, V_{s30} and bedrock motion (Huang et al. 2010b), assuming soil site class D and V_{s30} = 180 m/s.

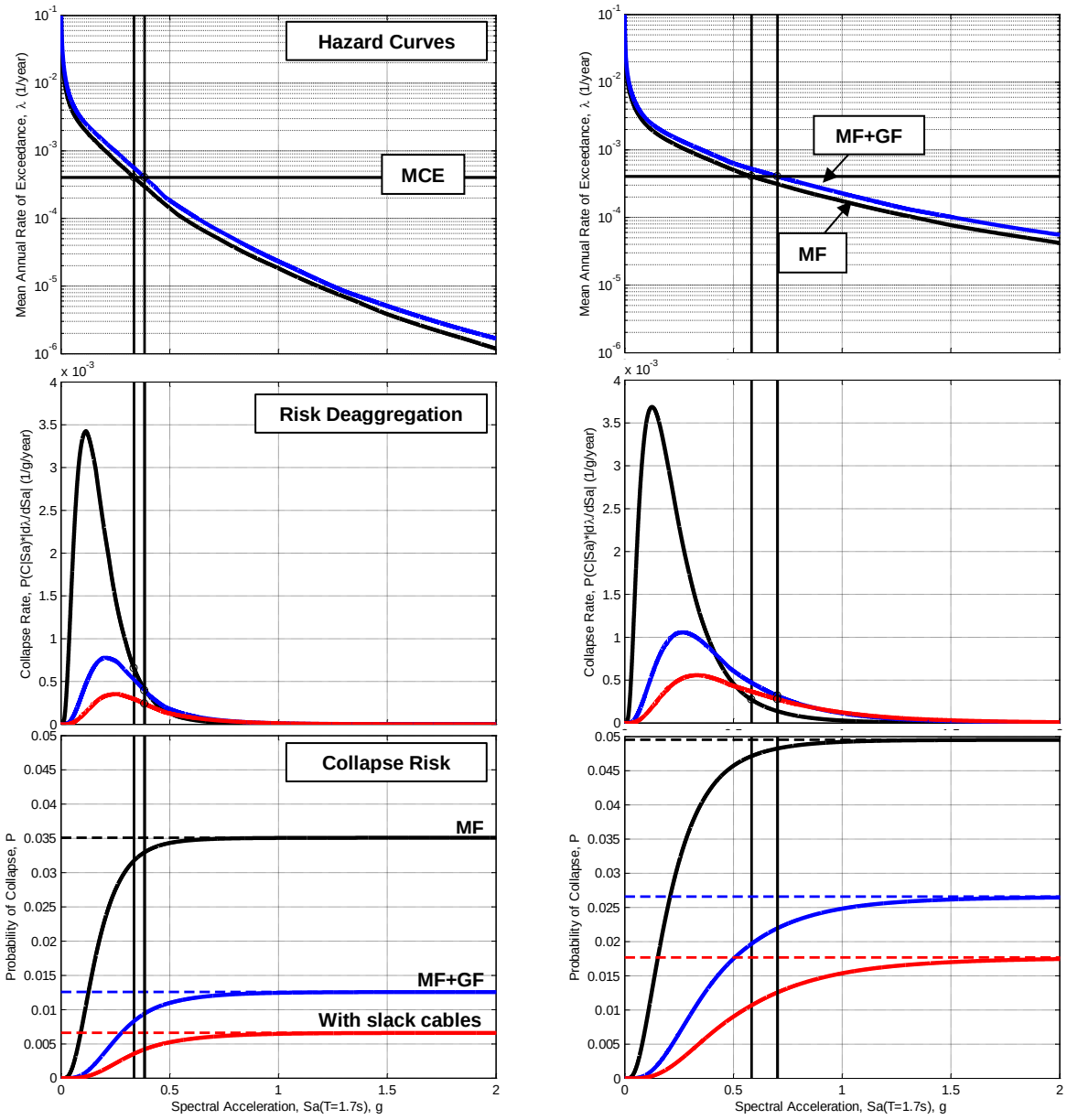

a) Saint Louis, Missouri b) Charleston, South Carolina

Figure 4.9 Seismic collapse risk analysis for Type I non-ductile moment frame 4-story building

4.3 Results

4.3.1 Type I Non-ductile and Ductile Moment Frame Buildings

The collapse assessment results are summarized in Table 4.4 for non-ductile and Table 4.5 for ductile moment frames. Table 4.6 provides comparative results for ductile frames designed for SDC D_{max}. It is noted that the fundamental period values determined in the eigenvalue analysis, T_1 are high compared to empirical estimates of actual buildings. Nevertheless, the periods are similar to those reported in the ATC-76 report (NIST 2010a).

The static pushover results are described in terms of the seismic base shear coefficient C_s and static "overstrength" Ω for SDC D_{max}, and period-based ductility, μ_T described in FEMA P-695. The dynamic IDA results are shown relative to SDC D_{max} and include the intensity measure (the spectral acceleration corresponding to the MCE ground motion S_{aMCE}), collapse margin ratio (*CMR*), Spectral Shape Factor (*SSF*), adjusted *CMR* (*ACMR*), record-to-record dispersion, β_{RTR} total dispersion, β_{Total} and the probability of collapse conditioned on the MCE level ground motion ($P_c|S_a{}^{MCE}$). Results relative to SDC D_{min} are not shown.

Figure 4.10a shows the contribution of the moment frame (MF), gravity frame (GF), and slack cable (SC) mechanism to the pushover response of the 4-story ductile-frame building. The slack-cables engage at approximately 2% drift, and the cables fail at approximately 6% drift. The pattern of collapse prevention component failure depends on the loading and archetype building.

For example, the sequence of mechanism failures is described in Figure 4.10b for the loose-linkage (LL) mechanism. At 4% drift, the initial linkage failure occurs in story 1 of the gravity frame. At 6% drift, five additional linkage failures occur in both the moment and gravity

framing. Just prior to 7% drift, 14 linkages pairs have failed, and a building collapse mechanism forms at story 2. The story-2 collapse mechanism was formed in this building model regardless of the inclusion of gravity frame reserve lateral strength or collapse inhibiting mechanism deployed.

Table 4.4 Seismic collapse assessment (for SDC D_{max}) for Type I non-ductile moment-frame building (designed for wind, SDC B_{min})

		Static Pushover			Dynamic IDA						
Archetype	T1 (s)	Cs	Ω	μT	SaMCE (g)	CMR	SSF	ACMR	βRTR	βTotal	Pc | MCE
1-Story											
MF	1.52	0.33	0.41	1.16	0.59	0.81	1.10	0.90	0.38	0.65	57%
MF+SST	1.14	0.33	0.66	2.69	0.79	1.11	1.25	1.39	0.38	0.65	31%
MF+GF	1.14	0.33	0.66	2.72	0.79	1.11	1.25	1.39	0.38	0.65	31%
+SC	1.13	0.33	0.75	3.13	0.80	1.30	1.28	1.66	0.37	0.65	22%
+LL	1.14	0.33	0.75	2.42	0.79	1.25	1.23	1.54	0.34	0.64	25%
2-Story											
MF	1.87	0.33	0.28	1.89	0.48	0.59	1.22	0.72	0.38	0.66	69%
MF+SST	1.33	0.33	0.73	4.11	0.68	1.65	1.37	2.26	0.33	0.63	10%
MF+GF	1.58	0.33	0.39	1.45	0.57	0.95	1.16	1.10	0.36	0.64	44%
+SC	1.58	0.33	0.39	3.26	0.57	1.42	1.34	1.91	0.34	0.63	15%
+LL	1.58	0.33	0.44	3.30	0.57	1.24	1.35	1.67	0.33	0.63	21%
4-Story											
MF	2.38	0.21	0.33	2.90	0.38	0.74	1.32	0.98	0.37	0.65	51%
MF+SST	1.67	0.21	0.60	5.26	0.54	1.22	1.47	1.80	0.32	0.62	17%
MF+GF	2.01	0.21	0.41	3.94	0.45	0.93	1.39	1.30	0.37	0.65	34%
+SC	2.01	0.21	0.42	6.00	0.45	1.28	1.51	1.93	0.35	0.64	15%
+LL	2.01	0.21	0.41	4.01	0.45	1.00	1.40	1.39	0.36	0.64	30%
8-Story											
MF	3.16	0.12	0.43	3.26	0.28	0.65	1.34	0.87	0.44	0.69	58%
MF+SST	2.47	0.12	0.73	3.01	0.36	0.91	1.33	1.21	0.49	0.72	40%
MF+GF	2.85	0.12	0.55	2.35	0.32	0.87	1.27	1.10	0.34	0.63	44%
+SC	2.86	0.12	0.56	1.99	0.32	1.03	1.23	1.27	0.36	0.64	36%
+LL	2.85	0.12	0.55	3.10	0.32	0.78	1.33	1.04	0.33	0.63	48%

Table 4.5 Seismic collapse assessment (for SDC D_{max}) for Type I ductile moment-frame building (designed for SDC D_{min})

Archetype	T1 (s)	Static Pushover			Dynamic IDA						
		Cs	Ω	μT	SaMCE (g)	CMR	SSF	ACMR	βRTR	βTotal	Pc | MCE
1-Story											
MF	1.46	0.13	1.38	2.97	0.62	1.53	1.32	2.01	0.44	0.53	9%
MF+SST	0.92	0.13	3.44	5.15	0.98	2.12	1.34	2.84	0.34	0.45	1%
MF+GF	1.11	0.13	2.16	3.43	0.81	1.64	1.29	2.12	0.43	0.52	7%
+SC	1.11	0.13	2.53	2.88	0.81	1.74	1.26	2.19	0.40	0.50	6%
+LL	1.11	0.13	2.16	3.43	0.81	1.71	1.29	2.21	0.42	0.51	7%
2-Story											
MF	1.55	0.13	1.28	3.66	0.58	1.33	1.37	1.82	0.47	0.56	14%
MF+SST	1.20	0.13	2.29	4.16	0.75	1.99	1.35	2.68	0.39	0.49	2%
MF+GF	1.36	0.13	1.73	3.98	0.66	1.71	0.43	2.34	0.43	0.53	5%
+SC	1.36	0.13	1.83	4.85	0.66	1.85	1.42	2.63	0.37	0.48	2%
+LL	1.36	0.13	1.73	3.98	0.66	1.78	1.37	2.44	0.40	0.50	4%
4-Story											
MF	1.75	0.08	1.48	5.06	0.51	1.17	1.46	1.71	0.34	0.46	12%
MF+SST	1.42	0.08	2.24	4.05	0.63	1.64	1.38	2.27	0.36	0.47	4%
MF+GF	1.60	0.08	1.80	4.92	0.56	1.45	1.45	2.11	0.32	0.44	5%
+SC	1.60	0.08	1.80	6.19	0.56	1.63	1.52	2.48	0.36	0.47	3%
+LL	1.60	0.08	1.79	5.19	0.56	1.48	1.47	2.17	0.34	0.45	4%
8-Story											
MF	3.18	0.05	1.15	3.04	0.28	0.66	1.33	0.88	0.37	0.48	61%
MF+SST	2.50	0.05	1.76	3.49	0.36	0.95	1.36	1.29	0.40	0.50	30%
MF+GF	2.88	0.05	1.31	3.44	0.31	0.87	1.36	1.18	0.34	0.46	36%
+SC	2.88	0.05	1.34	3.99	0.31	1.03	1.39	1.43	0.34	0.46	22%
+LL	2.88	0.05	1.31	3.52	0.31	0.96	1.36	1.31	0.34	0.45	27%

Table 4.6 Seismic collapse assessment (for SDC D_{max}) for Type I ductile moment-frame building (designed for SDC D_{max})

Archetype	T1 (s)	Static Pushover			Dynamic IDA						
		Cs	Ω	μT	SaMCE (g)	CMR	SSF	ACMR	βRTR	βTotal	Pc | MCE
4-Story											
MF+GF	1.36	0.08	2.26	5.63	0.66	1.93	1.46	2.82	0.35	0.46	1%

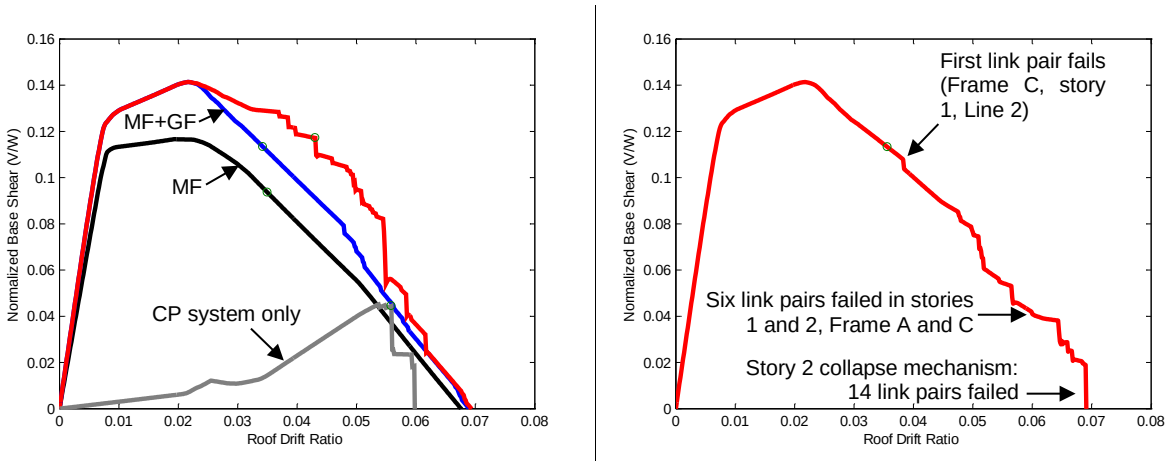

a) Effect of GF and slack cables

b) Effect of loose links

Figure 4.10 Effect of CP system on pushover response of ductile 4-story building

The basic process of assessing collapse is illustrated in Figure 4.11 through Figure 4.13 for the 4-story building with non-ductile moment frames. Figure 4.11a shows the scaled response spectra for the moment-frame and gravity-frame (MF+GF) archetype model.

Figure 4.11b shows the interstory drift response at each story of the moment-frame (MF) model at the collapse intensity for the 1994 Northridge earthquake Canyon Country Component 1 (LOS000) record.

Figure 4.11c compares the response history of the MF and MF+GF models and shows that the reserve lateral strength in the shear-tab connections prevents collapse at S_a = 0.36 g. Figure 4.11d compares the MF+GF response to the same building model incorporating loose-linkages (+LL). For this ground motion record, the collapse prevention system prevents collapse at S_a = 0.39 g. Figure 4.12 shows the response of the 4-story building with non-ductile moment frames at S_a = 0.36 g. Figure 4.12a compares the deformed (and-undeformed) configurations of the MF, MF+GF, and +LL models. At this shaking intensity, the reserve strength in the shear tab connections is sufficient to prevent collapse.

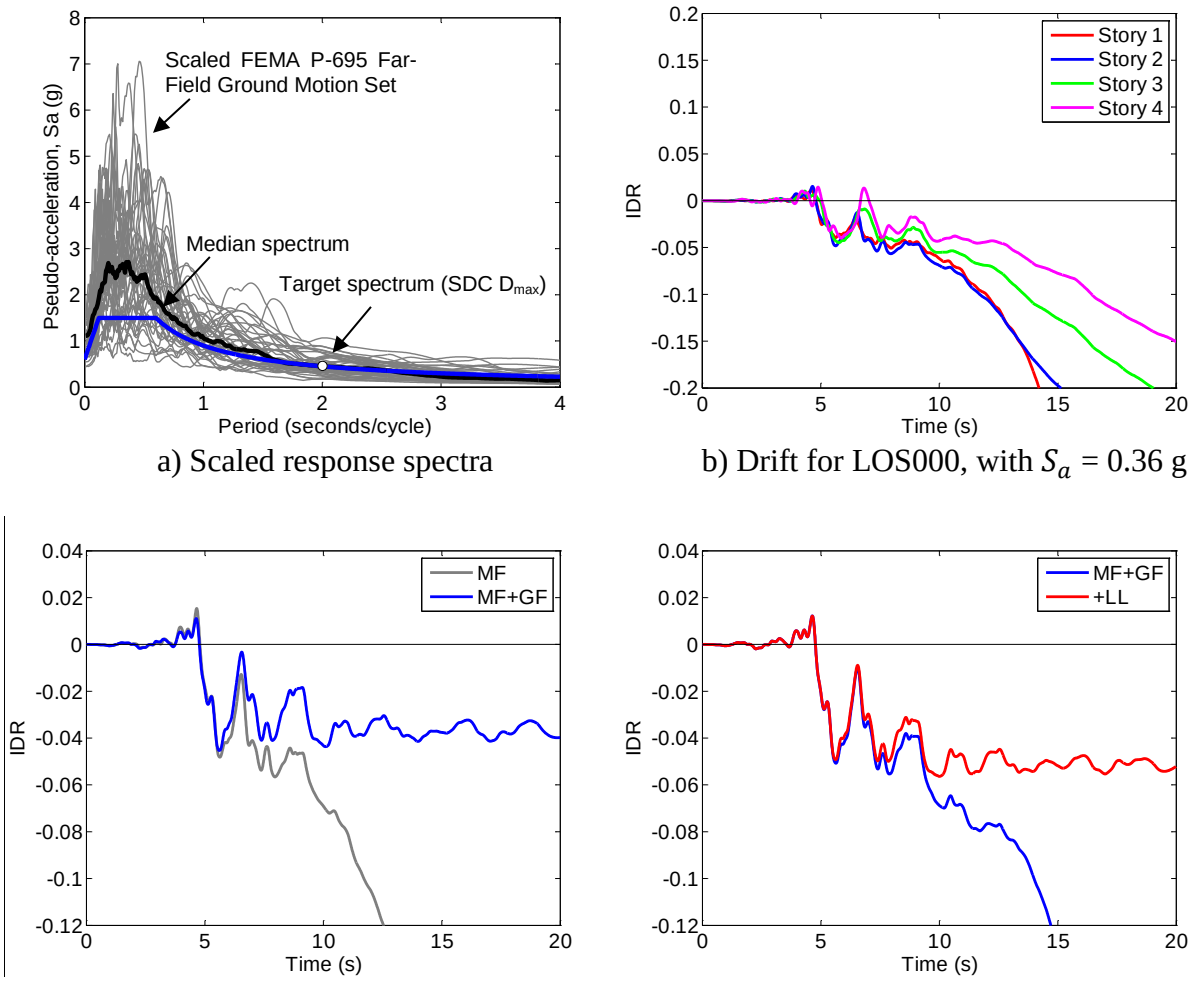

a) Scaled response spectra

b) Drift for LOS000, with S_a = 0.36 g

c) Story 2 drift for LOS000, S_a = 0.36 g

d) Story 2 drift for LOS000, S_a = 0.39 g

Figure 4.11 Representative response of 4-story building with non-ductile moment frames

The addition of the back-up mechanism (loose-linkages) prevents failure of the non-ductile beam-to-column connection (Figure 4.12b) in the first story. The behavior of a typical shear tab connection (Figure 4.12c) and a typical column panel zone (Figure 4.12d) is shown for the three models. The +LL model reduces building side-sway and utilizes less ductility in the shear-tab connection, which leads to increased panel zone deformations.

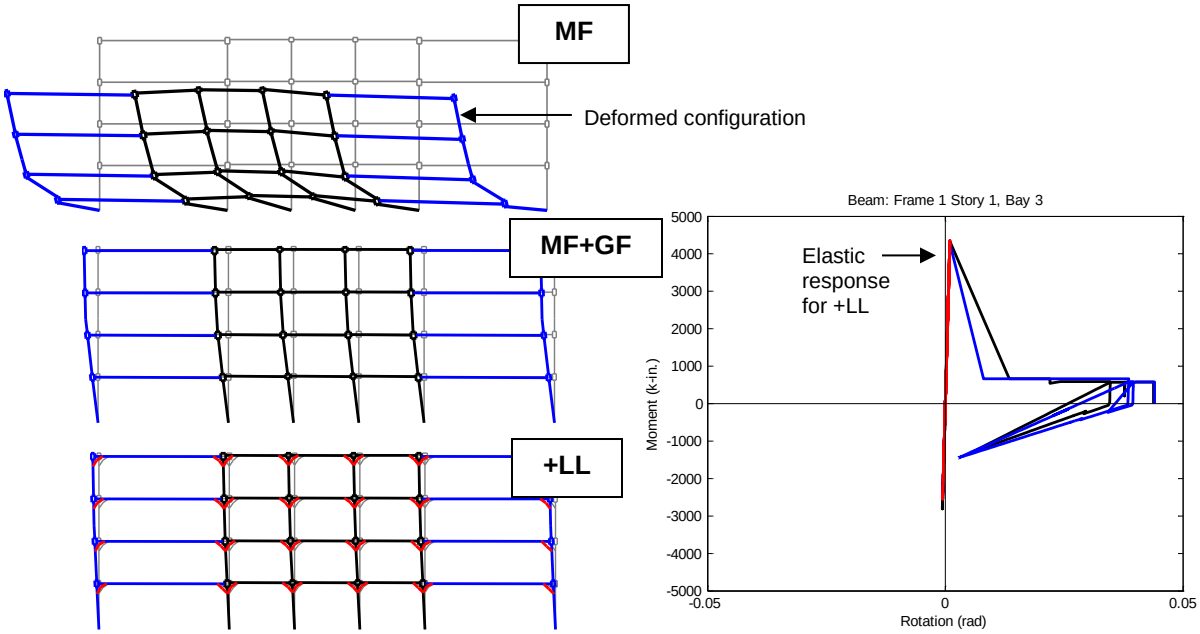

a) Perimeter frame configuration

b) Non-ductile connection

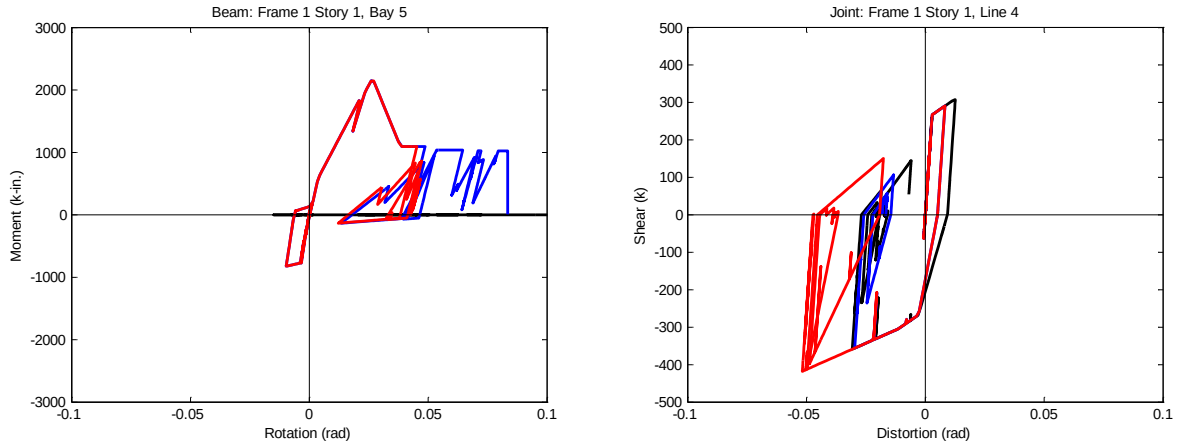

c) Shear-tab connection

d) Column panel zone

Figure 4.12 Response of 4-story building with non-ductile moment frames for LOS000, with S_a = 0.36 g

Figure 4.13a shows individual incremental dynamic analysis (IDA) curves representing the response of different building models to the same ground motion record. The spectral acceleration (for the MF+GF building) corresponding to SDC D_{max} and D_{min} is shown for reference. (Note that in an IDA plot, the spectral acceleration refers to the median of the ground motion set, which generally is not the same as the spectral acceleration of each individual ground motion.) In contrast, Figure 4.13b shows the IDA curves for the entire ground motion set for one (MF+GF) building model. The median spectral acceleration at collapse (red line) is shown relative to the SDC D_{max} spectral acceleration (black horizontal line).

Figure 4.14a compares the collapse fragility curves for the MF, MF+GF, and the same building model incorporating slack-cables (+SC). The median collapse spectral acceleration was adjusted (increased) to account for spectral shape, estimated using period-based ductility, μ_T and the total dispersion, β_{Total} in collapse capacity was calculated as previously described. The adjusted seismic collapse fragility curves are shown in Figure 4.14b.

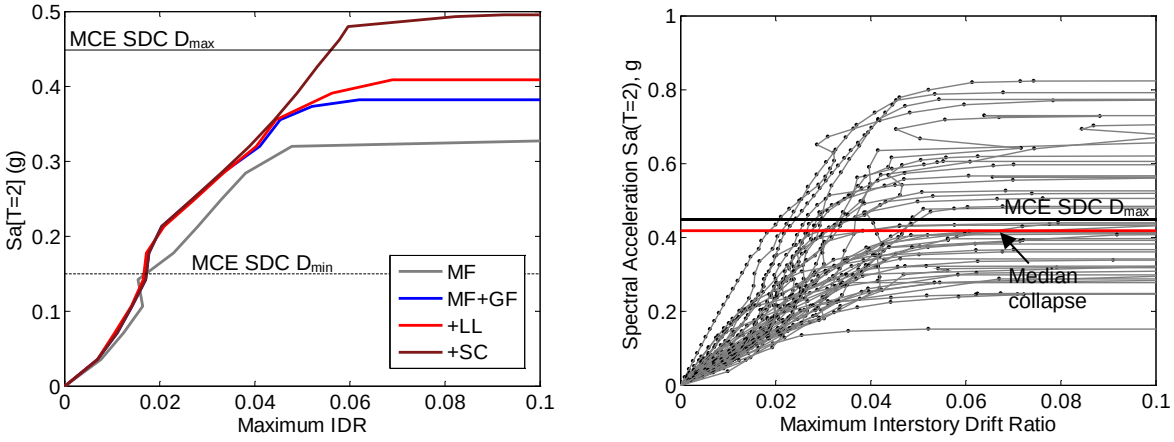

a) LOS000 IDA curves b) IDA curves for MF+GF archetype

Figure 4.13 Representative response of 4-story building with non-ductile moment frames

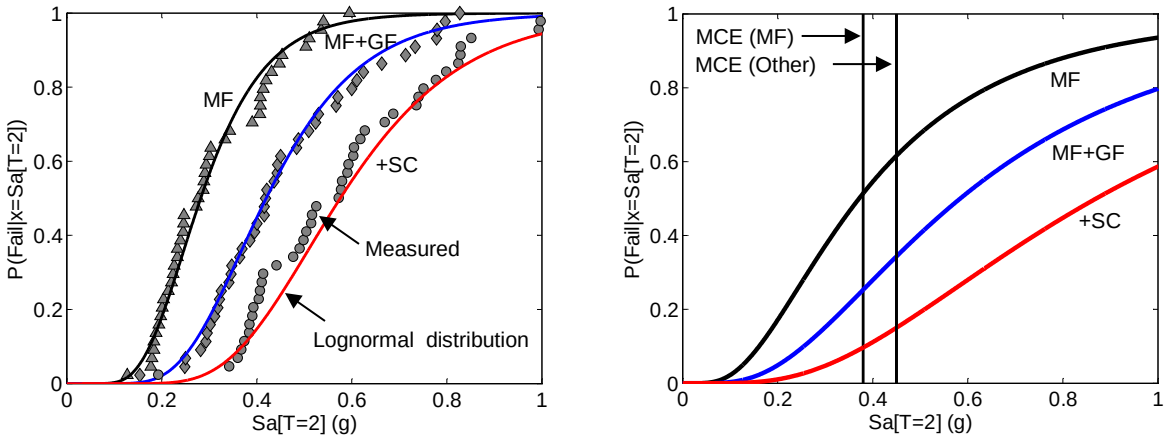

a) Collapse fragility curves b) Collapse fragility curves with β_{Total}

Figure 4.14 Seismic collapse results for 4-story building with non-ductile moment frames

The reserve lateral strength in the shear-tab connections reduced the collapse probability considerably compared to moment frames alone. Employing collapse prevention mechanisms improved the collapse safety, but the amount of improvement depended on the number of stories and the collapse inhibiting mechanism. Collapse prevention systems with a non-ductile moment-frame passed the FEMA P-695 acceptance criteria for SDC D_{min}. For collapse prevention systems with ductile moment-frames, the short-period (1-story, 2-story) performance group and the 4-story buildings passed the acceptance criteria for SDC D_{max}.

A risk analysis was used to illustrate areas where collapse prevention systems are applicable for the Type I archetype building. Collapse risk was calculated by integrating collapse fragility (from Table 4.4 and Table 4.5) and seismic hazard—based on 2008 USGS data, and adjusted for site amplification based on a correlation between shear wave velocity, V_{s30} and bedrock motion using Next Generation Attenuation (NGA) relationships (Huang et al. 2010b). This risk analysis was repeated for every 0.5-degree latitude and longitude to generate a map of risk values in the conterminous United States. Soil site class D (V_{s30} = 180 m/s) is assumed.

Figure 4.15 shows regions (shaded contours) where the seismic collapse risk exceeds 1% in 50 years for the non-ductile moment frame building. Blue and red shaded areas in the central and eastern United States indicate (for this particular building archetype) where the collapse prevention system is needed, compared to the moment frame alone. Yellow shaded areas indicate where the collapse prevention system using slack cables is not sufficient. Major metropolitan areas (dots) are shown based on 2011 population estimate using 2010 census data.

The maps show that the slack cable collapse prevention system with non-ductile moment frames is adequate for many regions in the central and eastern United States. Although buildings with non-ductile frames were not suitable for the maximum intensity possible in SDC D, the collapse prevention systems were viable for the major portion of the SDC D regions.

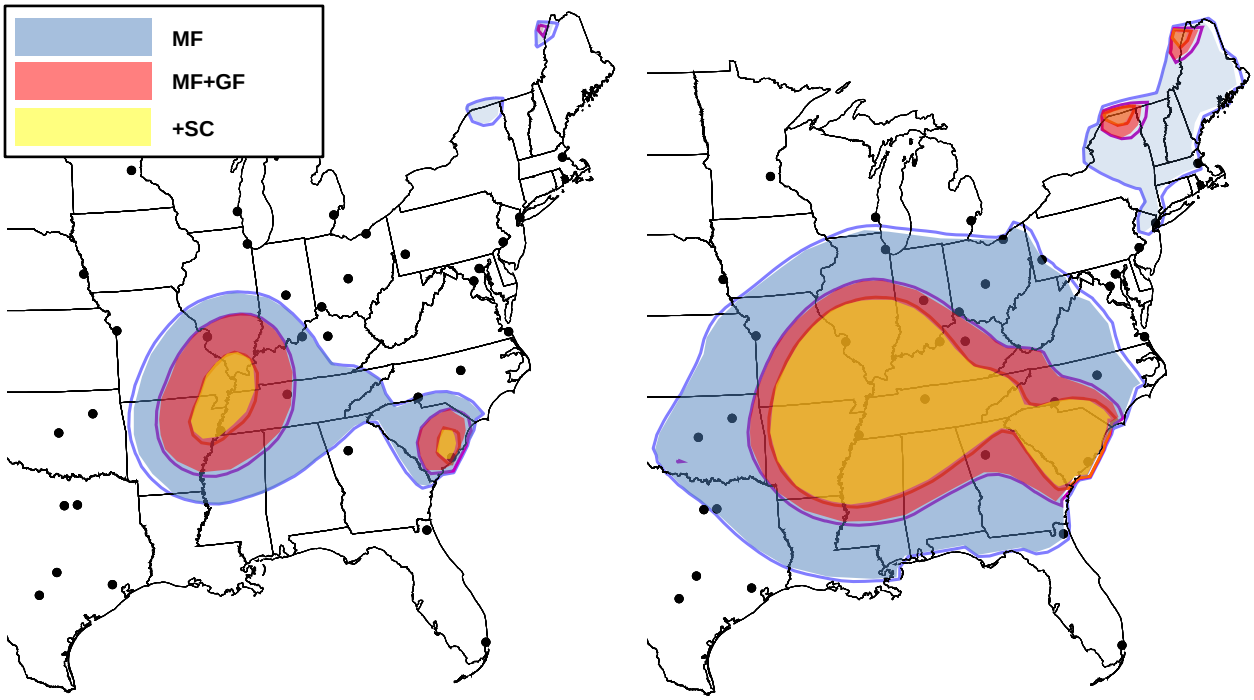

a) 2-story b) 8-story

Figure 4.15 Regions where seismic collapse risk exceeds 1% in 50 years: Type I non-ductile

For example, consider the non-ductile moment frame 4-story building. Figure 4.16 shows contour lines where the probability of collapse given the MCE exceeds 10% (gray contours correspond to SDC boundaries). Memphis, Tennessee and Charleston, South Carolina are the only major cities in the central and eastern United States not reached by the slack cable collapse prevention system (orange contour lines).

Figure 4.17 to Figure 4.20 show the applicability of using enhanced shear tab connections (SST) as a collapse prevention system in non-ductile moment frame buildings. (Blue shaded areas indicate where the collapse prevention system is needed; red shaded areas indicate where the enhanced shear tab connection collapse prevention system is not sufficient.)

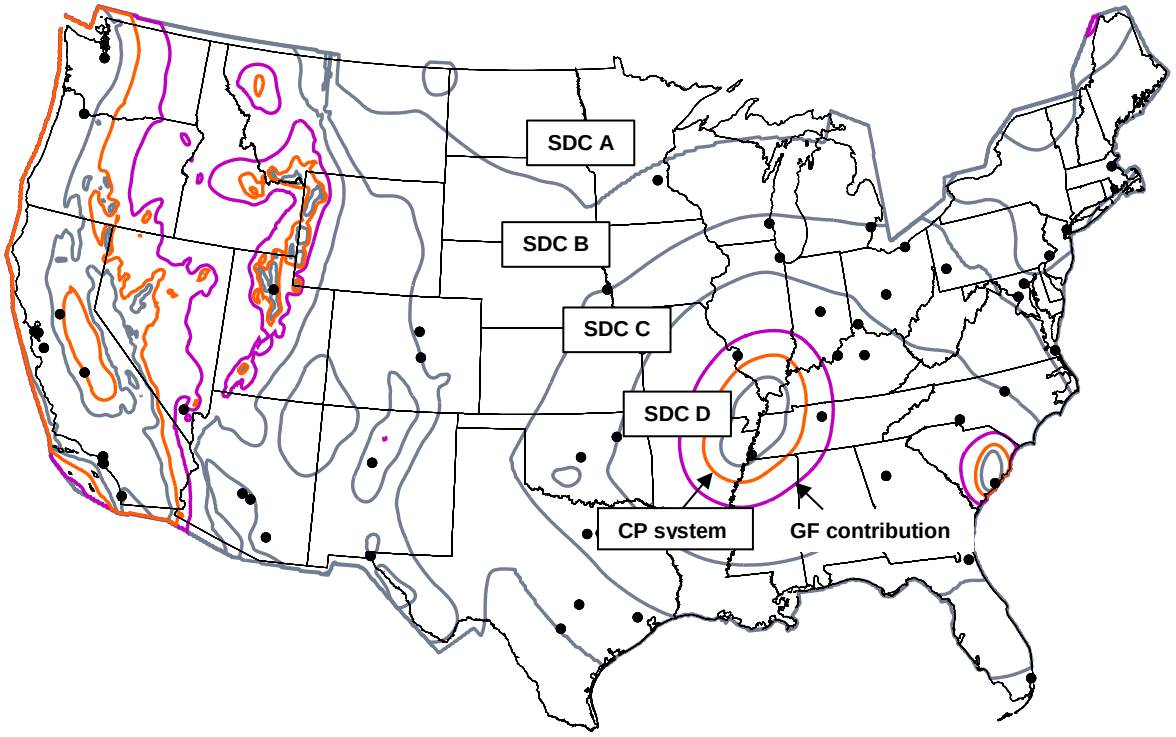

Figure 4.16 Regions where the probability of seismic collapse (given the MCE) exceeds 10%: Type I non-ductile moment frame 4-story building with slack cable collapse prevention system

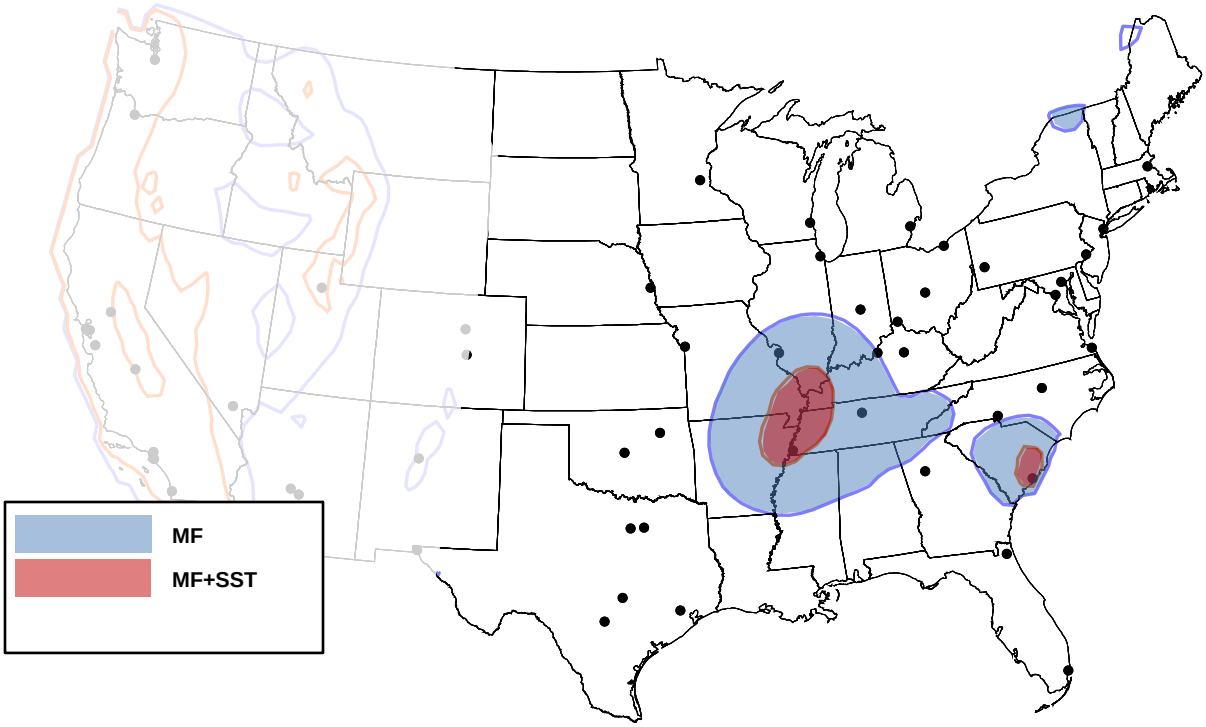

Figure 4.17 Regions where seismic collapse risk exceeds 1% in 50 years: non-ductile 1-story

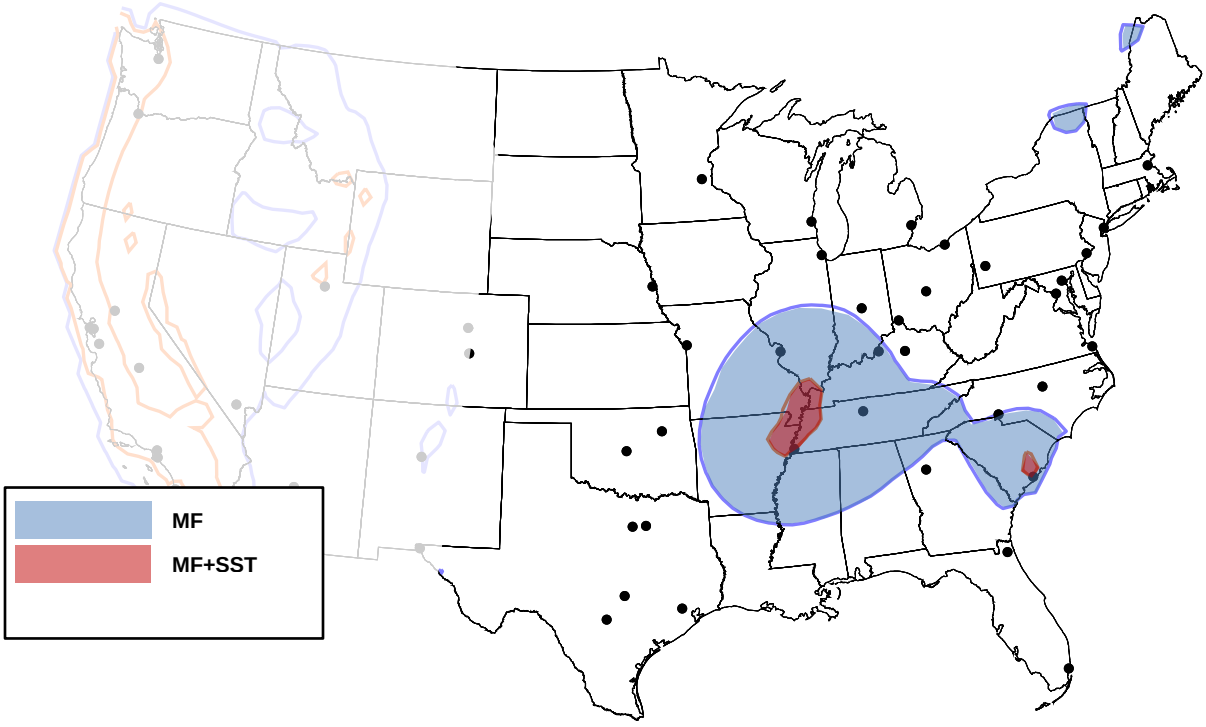

Figure 4.18 Regions where seismic collapse risk exceeds 1% in 50 years: non-ductile 2-story

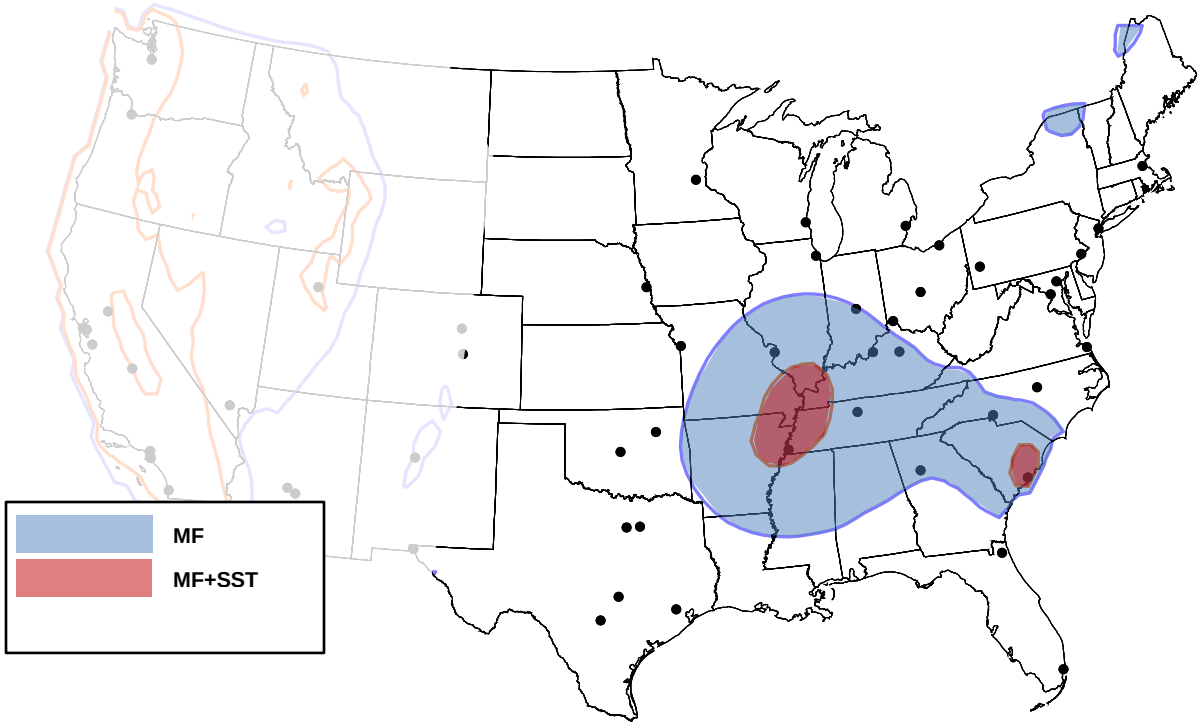

Figure 4.19 Regions where seismic collapse risk exceeds 1% in 50 years: non-ductile 4-story

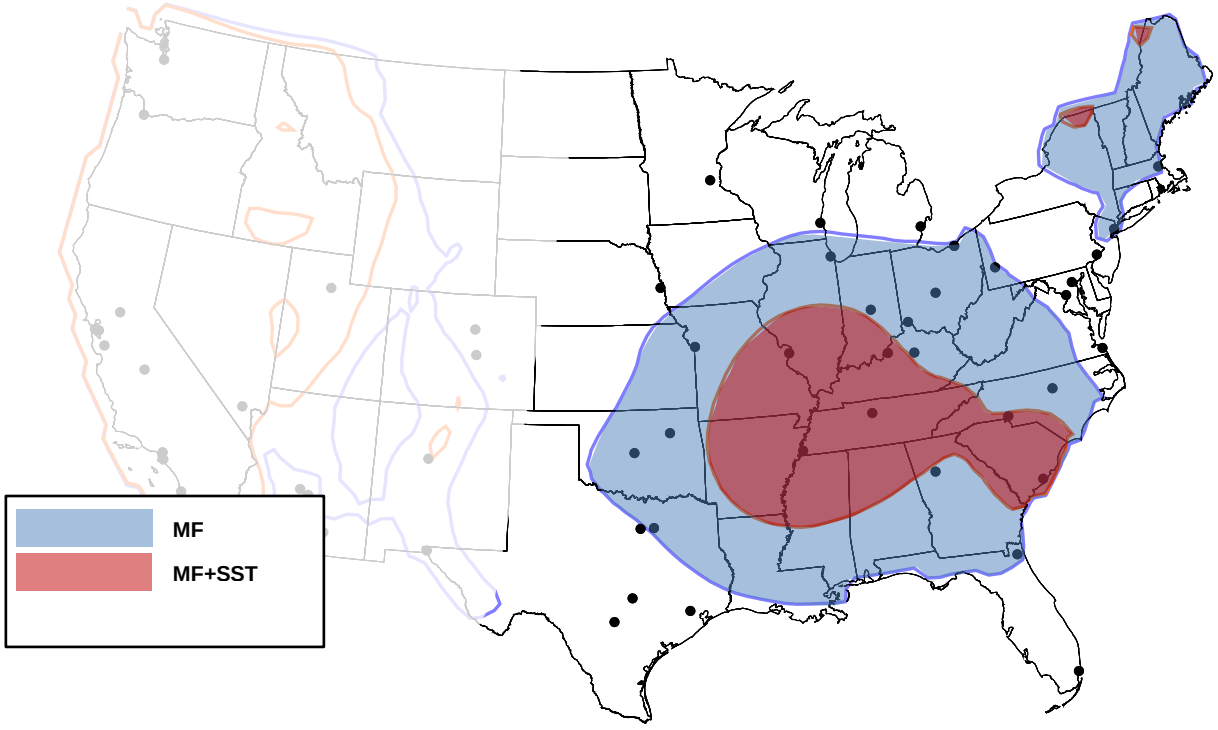

Figure 4.20 Regions where seismic collapse risk exceeds 1% in 50 years: non-ductile 8-story

The maps show that collapse prevention systems are adequate for many regions in the central and eastern United States, but the applicability depends on both the ductility of the primary moment frame, the building height (building stories) and the type of collapse prevention mechanism employed. The collapse prevention system concept was predicted to be viable for a major portion of the SDC D regions.

4.3.2 Type II Non-ductile Moment Frame Buildings

The Type II non-ductile moment frame buildings with and without considering the lateral strength in the gravity framing were subjected to the FEMA P-695 "Far-Field" ground motion set (Figure 4.21a), and the set was incrementally scaled (relative to the median response spectrum and target spectrum SDC D_{max}) until collapse (Figure 4.21b). The collapse points (spectral acceleration at the reference period and corresponding probability of collapse) were fit with a curve assuming a lognormal cumulative distribution function (Figure 4.22a), and the median collapse spectral acceleration is adjusted to account for spectral shape. Spectral shape effects are estimated using period-based ductility (μ_T). The total uncertainty (β_{Total}) in collapse capacity (Figure 4.22b) was calculated by dispersion in the response history analysis (record-to-record dispersion β_{RTR}) together with a "rated" dispersion due to design, test data, and modeling uncertainty. Design requirements were rated '(B)'; test data and model quality were each rated '(C)'.

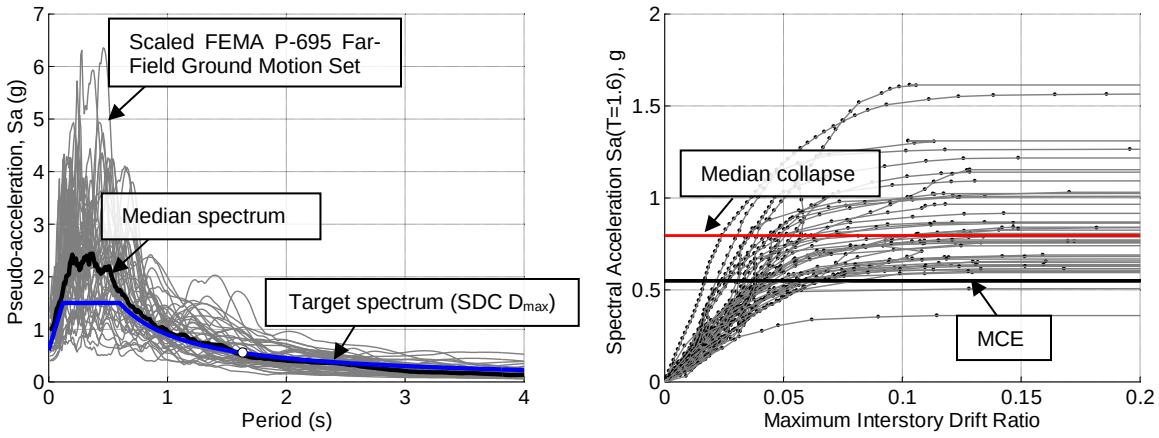

a) Scaled response spectrum b) Incremental dynamic analyses

Figure 4.21 Nonlinear dynamic analyses for the Type II non-ductile moment frame buildings

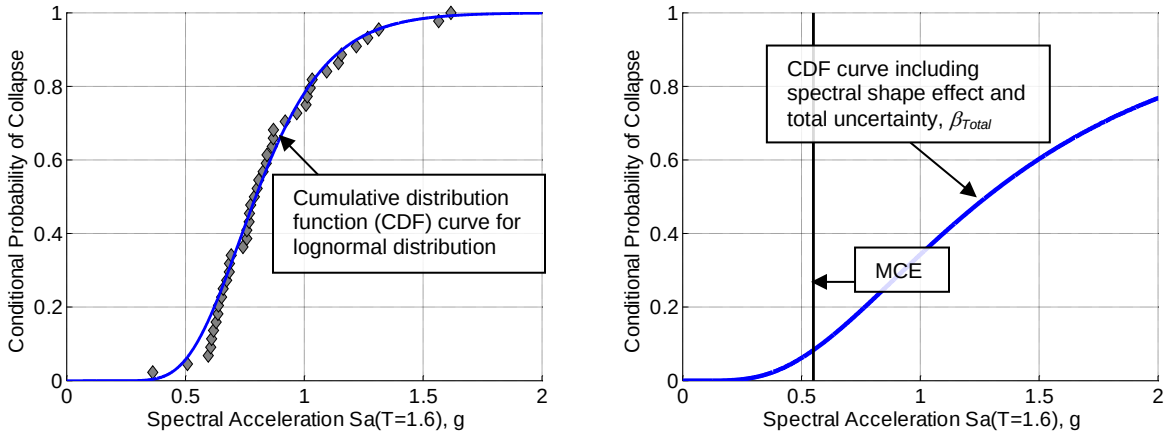

a) Measured / fitted collapse fragility b) Total fitted collapse fragility

Figure 4.22 Seismic collapse analyses for the Type II non-ductile moment frame buildings

The collapse assessment results for the east-west direction (moment frames) are summarized in Table 4.7. The computed fundamental period of the analytical model, T_1 is 1.64 seconds. This is reasonable, but larger than both the empirically determined period for wind analysis (T_w = 1.11 seconds) and the empirically determined period for seismic analysis ($C_u T_a$), which ranges from 0.97 seconds (SDC D_{max}) to 1.18 seconds (SDC B_{min}). The values of Ω shown are relative to C_s for SDC D_{max}. Relative to C_s equal to 0.043 used to design the building (see *Design Examples*, page III-51) the overstrength, Ω is equal to 2.64. Seismic pushover analysis showed that the period-based ductility, μ_T values are dominated by the panel zones. Reserve strength in the gravity framing increased overstrength and reduced the conditional probability of collapse by 3%, which was enough to "pass" the 10% conditional collapse criterion set by FEMA P-695.

Table 4.7 Seismic collapse assessment (for SDC D_{max}) for Type II non-ductile moment-frame building (designed for SDC B, design controlled by wind)

		Static Pushover			Dynamic IDA					
					Sa[T₁] (g)					
Model	T_1 (s)	C_s	Ω	μ_T	MCE	Collapse	*SSF*	*ACMR*	β_{Total}	P_c|*MCE*
MF	1.77	0.21	0.46	8.71	0.51	0.65	1.61	2.05	0.61	12%
MF+GF	1.64	0.21	0.54	8.26	0.55	0.80	1.61	2.33	0.61	8%

A risk analysis is used to display areas where the Type II non-ductile moment frame 4-story building would provide a 1% or less risk of seismic collapse in 50 years. The probability of collapse, P_c was computed in both directions and the total probability (risk of collapse) was computed using Equation 4.9.

$$P_{c-Total} = P_{c-EW} + P_{c-NS} - (P_{c-EW})(P_{c-NS}) \quad (4.9)$$

This is repeated for every 0.5-degree latitude and longitude to generate the map shown in Figure 4.23. The shaded areas in the figure show regions where seismic collapse risk exceeds 1% in 50 years.

The prototype building provides adequate seismic life-safety for many regions in the central and eastern United States, except the Mid-America and Charleston high-seismic areas. Note that the Type II non-ductile moment frame 4-story building was designed for moderate wind, and buildings designed for higher wind pressures along the hurricane-prone gulf and eastern coasts have an even lower risk of seismic collapse.

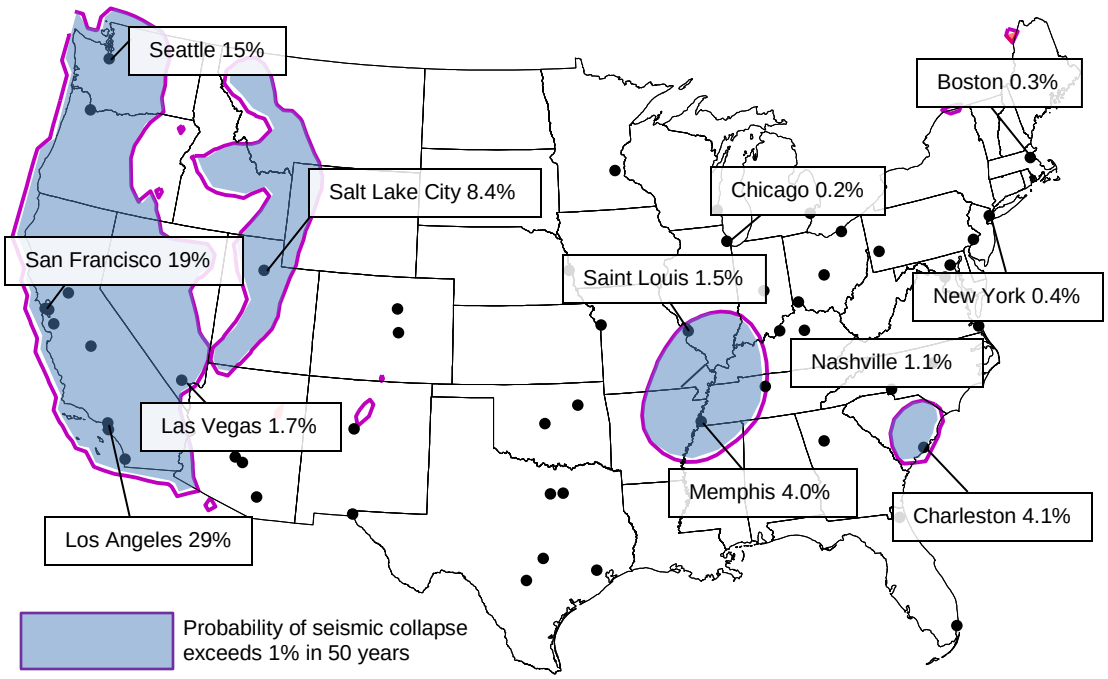

Figure 4.23 Regions where seismic collapse risk exceeds 1% in 50 years: Type II non-ductile moment frame 4-story building

4.3.3 Type III Non-ductile Moment Frame 10-story Building

The Type III non-ductile moment frame 10-story building was subjected to the FEMA P-695 "Far-Field" ground motion set (Figure 4.24a). The median spectrum of the ground motion set was incrementally scaled relative to four target spectrums, SDC B_{min}, SDC C_{min}, SDC D_{min}, and, as in previous analyses, SDC D_{max}, until collapse (Figure 4.24).

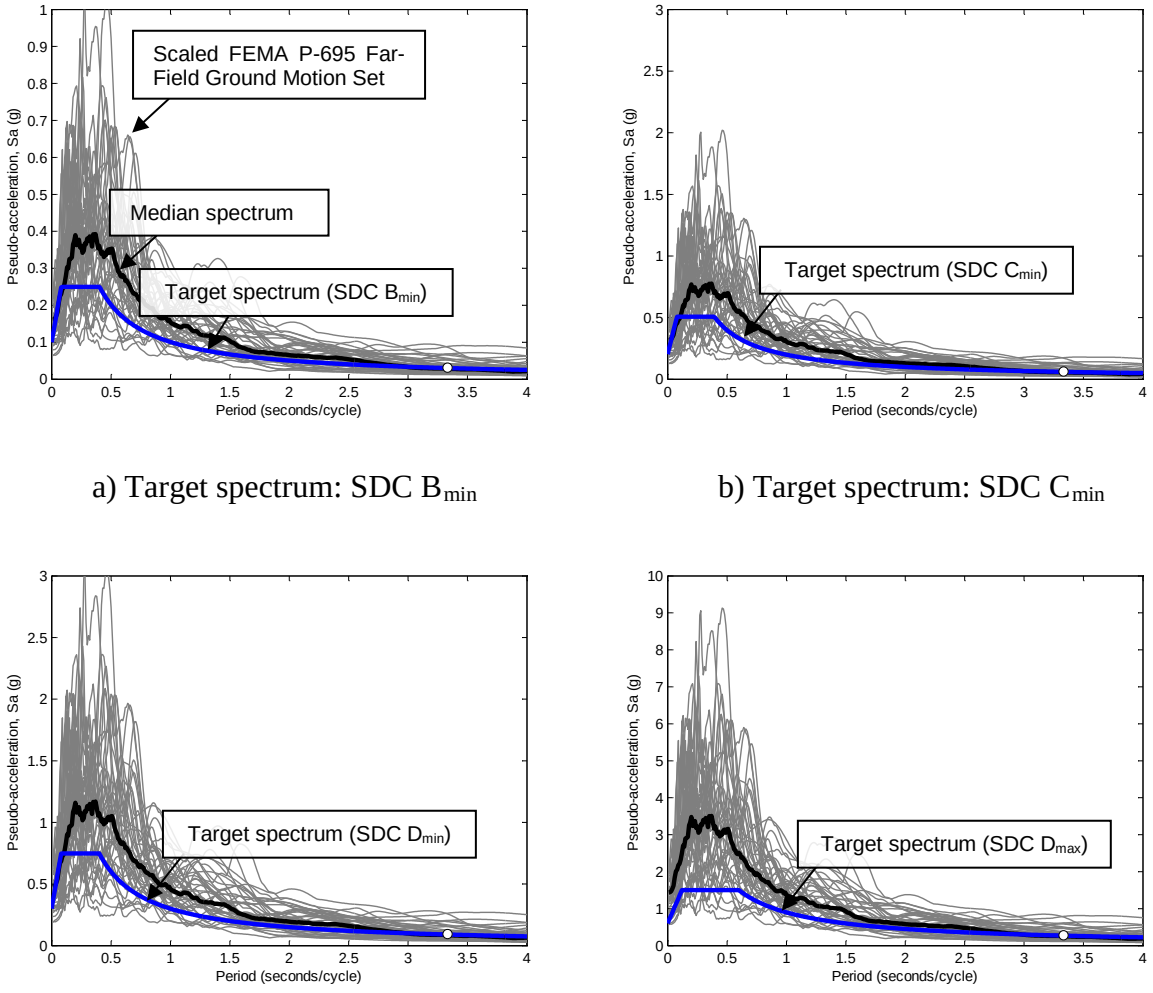

a) Target spectrum: SDC B_{min}

b) Target spectrum: SDC C_{min}

c) Target spectrum: SDC D_{min}

d) Target spectrum: SDC D_{max}

Figure 4.24 Scaled response spectra: Type III non-ductile moment frame 10-story building

The collapse points were fit with a curve assuming a lognormal cumulative distribution function (Figure 4.25a) and adjusted to account for spectral shape and total uncertainty β_{Total} in collapse capacity (Figure 4.25b). The collapse assessment results are summarized in Table 4.8 relative to the four target applications (SDC B_{min}, SDC C_{min}, SDC D_{min}, and SDC D_{max}). The building was viable for SDC B and most of SDC C, but was inadequate (as would be expected) for higher seismic regions.

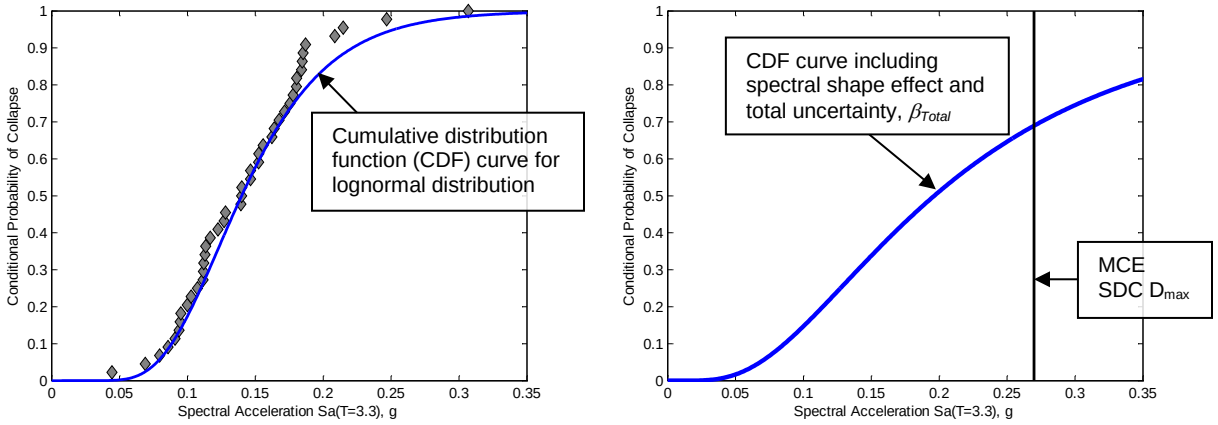

a) Measured / fitted collapse fragility b) Total fitted collapse fragility

Figure 4.25 Seismic collapse analyses for the Type III non-ductile 10-story building

Table 4.8 Seismic collapse assessment for Type III non-ductile 10-story building (designed for wind and evaluated at SDC B_{min}, C_{min}, D_{min}, and D_{max})

SDC	T_1 (s)	T_w (s)	T_e (s)	Static Pushover			Dynamic IDA					
							$Sa[T_1]$ (g)					
				C_s	Ω	μ_T	MCE	Collapse	SSF	ACMR	β_{Total}	$P_c\|MCE$
B_{min}	3.34	2.28	2.41	0.01	7.45	4.12	0.03	0.52	1.40	0.73	0.64	0.2%
C_{min}			2.32	0.02	3.63		0.06					3%
D_{min}			2.13	0.03	2.21		0.09					11%
D_{max}			1.98	0.10	0.69		0.27					69%

4.4 Comparison with Traditional Structural Systems

The collapse assessment for seismic hazards of traditional lateral-force resisting structural systems for new buildings in the United States is examined in the context of comparing FEMA P-695 evaluations reported to-date in the literature. Although the focus of this research is steel moment-frame structures, also included in the comparison are steel moment frame and braced-frame, reinforced concrete moment-frame and shear wall, reinforced masonry shear wall, and light-frame wood shear wall structures.

In a FEMA P-695 evaluation, a structure is deemed to "pass" if (1) the average conditional collapse probability for a group of similar archetypical structures does not exceed 10%, and if (2) the conditional collapse probability for any individual structure does not exceed 20%. As discussed previously, FEMA P-695 includes the effect of modeling and design uncertainties in the evaluation, and it incorporates an estimate of the effect of spectral shape on collapse capacity. In the tables shown, for each Performance Group (PG) the dispersion, overstrength, Ω, Adjusted Collapse Margin Ratio (*ACMR*) accounting for the effect of spectral shape, and the acceptable *ACMR* corresponding to 10% probability of collapse are given.

4.4.1 Steel Moment Frame

The vulnerability of steel moment frame structures is summarized in Table 4.9. Three types of steel moment structures are examined: special steel moment frames (SMF) (NIST 2010a), partially-restrained composite connection (PR-CC) steel moment frames (Bozorgmehr 2012; Bozorgmehr and Leon 2012), and cold-formed steel bolted moment frames (Sato and Uang 2013). All steel SMF systems are adequate except one performance group: the steel SMF long-period SDC D_{max} performance group does not pass (but is not far off from passing the criteria).

Table 4.9 Steel moment-frame seismic collapse assessment results

Lateral Force Resisting System (LFRS)	β	PG No.	Ω	ACMR	Accept. 10%
Steel special moment frame (R=8, Ω=3)	0.5	1	4.16	2.97	1.9
	0.45	2	3.67	1.94	1.75
	0.475	3	2.55	2.53	1.81
	0.45	4	4.27	3.13	1.77
		Ave	**4.27**	**2.64**	
	0.5	1	4.7	2.91	1.9
	0.475	2	2.61	1.76	1.81
	0.45	3	2.84	2.72	1.78
	0.475	4	2.93	3.28	1.84
		Ave	**4.7**	**2.67**	
Steel PR-CC frame (R=6, Ω=3)	0.6	1	1.39	2.19	2.16
		2	1.57	2.89	
		3	1.58	3.99	
		4	1.59	3.96	
		5	1.78	4.74	
		6	1.63	4.25	
		Ave	**1.78**	**3.67**	
Cold-form steel Special bolted MF (R=3.5, Ω=3)	0.5	1	1.9	2.2	1.9
		2	2.09	2.16	
		3	3.14	3.66	
		4	5.59	4.98	
		Ave	**5.59**	**3.25**	

4.4.2 Steel Braced Frames

The vulnerability of steel braced-frame structures is summarized in Table 4.10. Two types of steel braced-frames are considered (NIST 2010a): steel special concentrically braced frames (CBF), and buckling restrained braced (BRB) frames. For further consideration of BRB frames, see also Ariyaratana and Fahnestock (2011).

All steel braced-frame structures satisfy the FEMA P-695 requirements, except one performance group: the CBF short-period SDC D_{max} performance group did not pass. However, a recent study of special CBF buildings (Hsiao et al. 2013) indicates that 3-story and 20-story buildings also do not pass. In fact, short-period systems often do not pass the FEMA P-695 criterion, regardless of the type of structure (Charney et al. 2012; NIST 2012b).

Table 4.10 Steel braced-frame seismic collapse assessment results

Lateral Force Resisting System (LFRS)	β	PG No.	Ω	ACMR	Accept. 10%
Steel Special CBF (R=6, Ω=2)	0.525	1	1.42	1.63	1.96
		2	1.67	3.37	
		3	1.9	2.93	
		4	1.87	4.73	
		Ave	**1.9**	**3.17**	
Steel BRB (R=8, Ω=2.5)	0.525	1	1.4	3.13	1.96
		2	1.21	4.12	
		3	1.77	2.86	
		4	1.29	4.19	
		Ave	**1.77**	**3.58**	

4.4.3 Reinforced Concrete Moment Frames

The vulnerability of reinforced concrete moment frame structures is summarized in Table 4.11. Two types of moment-frames are included: special (SMF) and ordinary (OMF) based on the FEMA P-695 supporting study (FEMA 2009a).

Most concrete frame structures pass FEMA P-695 requirements. However, SMF frames taller than 4 stories (the long-period perimeter frame performance groups) do not. The long-period performance group for OMF frames also fails to pass. Accordingly, the study suggested that a height limit is needed for SMF frames and that OMF frames should not be allowed.

The reinforced concrete moment frame results and recommendations underscore a weakness of the assumption for the current uniform risk-targeted maps: structures designed using ASCE 7-10 do not necessarily have less than a 10% probability of collapse given the MCE.

Table 4.11 Reinforced concrete moment-frame seismic collapse assessment results

Lateral Force Resisting System (LFRS)	β	PG No.	Ω	ACMR	Accept. 10%
Reinforced concrete SMF (R=8, Ω=3)	0.5	1	1.7	1.9	1.9
		2	1.9	1.84	
		3	3.5	2.66	
		4	2.8	2.36	
		Ave	**3.5**	**2.19**	
Reinforced concrete OMF (R=3, Ω=3)	0.575	1	2.2	3.86	2.09
		2	6	4.58	
		3	1.6	2.2	
		4	3.2	2.44	
		Ave	**6**	**3.27**	
		1	1.6	2.2	
		2	3.2	2.44	
		3	1.5	1.48	
		4	2.4	2.12	
		Ave	**3.2**	**2.06**	

4.4.4 Reinforced Concrete Shear Walls

The vulnerability of reinforced concrete shear wall structures is summarized in Table 4.12. Two types of shear walls are considered: special and ordinary (NIST 2010a). The results indicate that long-period performance groups pass, but short-period performance groups do not. One and two story structures collapsed due to shear failures at low drift levels (about 1.5%). The study notes that in past earthquakes, collapse of low-rise concrete shear wall buildings has only been observed in precast parking type structures where the diaphragm failed, yet "insufficient information exists to establish more liberal failure criteria."

Table 4.12 Reinforced concrete shear-wall seismic collapse assessment results

Lateral Force Resisting System (LFRS)	β	PG No.	Ω	ACMR	Accept. 10%
Reinforced concrete Special SW (R=5, Ω=2.5)	0.525	1	1.98	1.5	1.96
		2	1.54	3.18	
		3	2.41	1.5	
		4	3.88	5.71	
		5	2.08	1.75	
		6	1.7	3.2	
		7	2.41	1.5	
		8	3.52	4.65	
		Ave	**3.88**	**3.05**	
Reinforced concrete Ordinary SW (R=4, Ω=2.5)	0.525	1	2.85	1.77	1.96
		2	3.43	5.8	
		3	3.25	2.28	
		4	5.2	8.23	
		5	2.85	1.77	
		6	2.37	6.42	
		7	3.25	2.28	
		8	3.37	9.38	
		Ave	**5.2**	**5.06**	

4.4.5 Reinforced Masonry Shear Walls

The vulnerability of reinforced masonry shear wall structures is summarized in Table 4.13. Again, two types of shear walls are considered: special and ordinary (NIST 2010a). The results indicate that many reinforced masonry structures do not pass the FEMA P-695 criteria. 1-story, 2-story, and 4-story OMF shear wall buildings with low gravity loads pass, but high gravity loads do not. Part of the poor performance is attributed to the low ductility capacity of short shear walls. Regardless of the reason for performance, the results again demonstrate that structures designed using ASCE 7-10 do not necessarily meet the 10% probability of collapse assumption.

Table 4.13 Reinforced masonry shear-wall seismic collapse assessment results

Lateral Force Resisting System (LFRS)	β	PG No.	Ω	ACMR	Accept. 10%
Reinforced masonry Special SW (R=5, Ω=2.5)	0.525	1	2	1.41	1.96
		2	1.75	2.3	
		3	2.12	1.69	
		4	1.75	2.25	
		5	1.8	1.71	
		6	1.53	2.33	
		7	1.71	1.95	
		8	1.5	2.28	
		Ave	**2.12**	**1.99**	
Reinforced masonry Ordinary SW (R=2, Ω=2.5)	0.525	1	1.89	1.51	2.23
		2	2.08	1.54	2.38
		3	1.41	1.46	2.16
		4	1.99	1.96	2.38
		5	1.91	1.98	2.23
		6	1.67	2.69	2.38
		7	1.37	1.94	2.16
		8	1.64	3.19	2.38
		Ave	**1.99**	**2.20**	

4.4.6 Wood (Light-Framed) Shear Walls

The vulnerability of light-frame wood shear wall structures (i.e. residential and small commercial buildings) is summarized in Table 4.14. The table is based on the results from the P-695 supporting study (FEMA 2009a). All performance groups pass, except the short-period low-aspect-ratio performance group. However, a recent study shows that the collapse margins of wood buildings in the western United States are significantly lower than those in the central and eastern United States due to regional construction practices (Li et al. 2010). In this manner, it is possible that wood structures may not necessarily have the performance implied by conformance with ASCE 7-10.

Table 4.14 Wood (light-framed) shear-wall seismic collapse assessment results

Lateral Force Resisting System (LFRS)	β	PG No.	Ω	ACMR	Accept. 10%
Wood light-frame wood panels (R=2, Ω=2.5)	0.5	1	2.2	1.89	1.9
	0.675	2	3.4	2.48	2.38
	0.675	3	4.1	2.91	2.38
	0.675	4	3.6	3.18	2.38
		Ave	**4.1**	**2.62**	

4.5 Discussion

The seismic collapse safety was assessed for archetypical buildings with and without collapse prevention systems. The results indicated that collapse prevention systems could (1) effectively reduce the probability of collapse during MCE-level ground motion, and (2) lower the seismic collapse risk of a building with moment frames not specifically detailed for seismic resistance.

Reserve lateral strength in the gravity framing, specifically in the shear tab connections, was a significant factor in the success of the collapse prevention system. In most buildings, simply utilizing the reserve strength in the shear tab connections significantly reduced the probability of collapse. The pattern of collapse prevention component failure depended on the loading and archetype building. Generally speaking, the collapse prevention devices did not change the story failure mechanism, compared to the moment frame alone, but the opposite was observed for the shear tab connections. Reserve lateral strength in the gravity framing or enhanced shear tab connections sometimes changed the story failure mechanism for the building.

Collapse prevention systems using non-ductile moment frames were adequate for many regions in the central and eastern United States, but a conventional lateral resisting system, or a collapse prevention system with a ductile moment frame designed for moderate seismic demands, was required for several regions of higher seismicity (namely, New Madrid and Charleston areas). The region of the United States where the results suggest that collapse prevention systems are applicable was wide, and covers up to a quarter of the United States population for some building archetypes.

Seismic collapse assessments reported in the literature, according to the available P-695 evaluations, indicate that on average, the assumed ASCE 7-10 fragility curve was conservative in terms of the variability in structural vulnerability (seismic collapse fragility), at least for

structures that have been detailed for seismic resistance. Nevertheless, in some cases the conditional probability of collapse during MCE-level ground motion may exceed 10%, even for structures detailed for seismic resistance using ASCE 7-10. It is important to note that the seismic collapse assessments surveyed did not calculate collapse risk.

Chapter 5

WIND COLLAPSE ASSESSMENT

This chapter assesses the wind collapse safety of the archetype structural systems with and without collapse prevention systems. The wind collapse vulnerability (collapse fragility) was determined using a sequence of gravity, frequency, and nonlinear static "pushover" analyses, followed by nonlinear dynamic response history analyses incrementally scaled, with respect to a reference wind speed, until side-sway collapse.

5.1 Wind Collapse Vulnerability Procedures

The probability of wind collapse was determined using an approach (Judd and Charney 2015a) similar to the prevailing method utilized for seismic loads (FEMA P-695) adapted in Chapter 4. A gravity load analysis was first conducted. Equivalent single-degree-of-freedom models were used to represent the hysteretic behavior, including in-cycle degradation, of typical main wind-force resisting systems (MWFRS). Single-degree-of-freedom modeling has been used by a several researchers in wind engineering (e.g. Tsujita et al. 1997; Chen and Davenport 2000; Hong 2004; Gani and Légeron 2011). Multiple-degree-of-freedom modeling in the literature is more limited (Muthukumar et al. 2012). The single-degree-of-freedom models reflected the overall response characteristics of structural subassemblies expected to be present in

corresponding real buildings, although these simplified and idealized models obviously are not a detailed representation of the structure. Notwithstanding these limitations, similar simplified equivalent single-degree-of-freedom models have been shown to demonstrate salient features of dynamic behavior for earthquake ground motion (FEMA 2009b).

Figure 5.1 shows the monotonic envelope and fully-reversed cyclic behavior assumed for the characteristic main wind-force resisting systems and gravity framing system (shear tab connections). Force-deformation behavior parameters used in this study, including in-cycle degradation, matched those used in FEMA P-440A (FEMA 2009b).

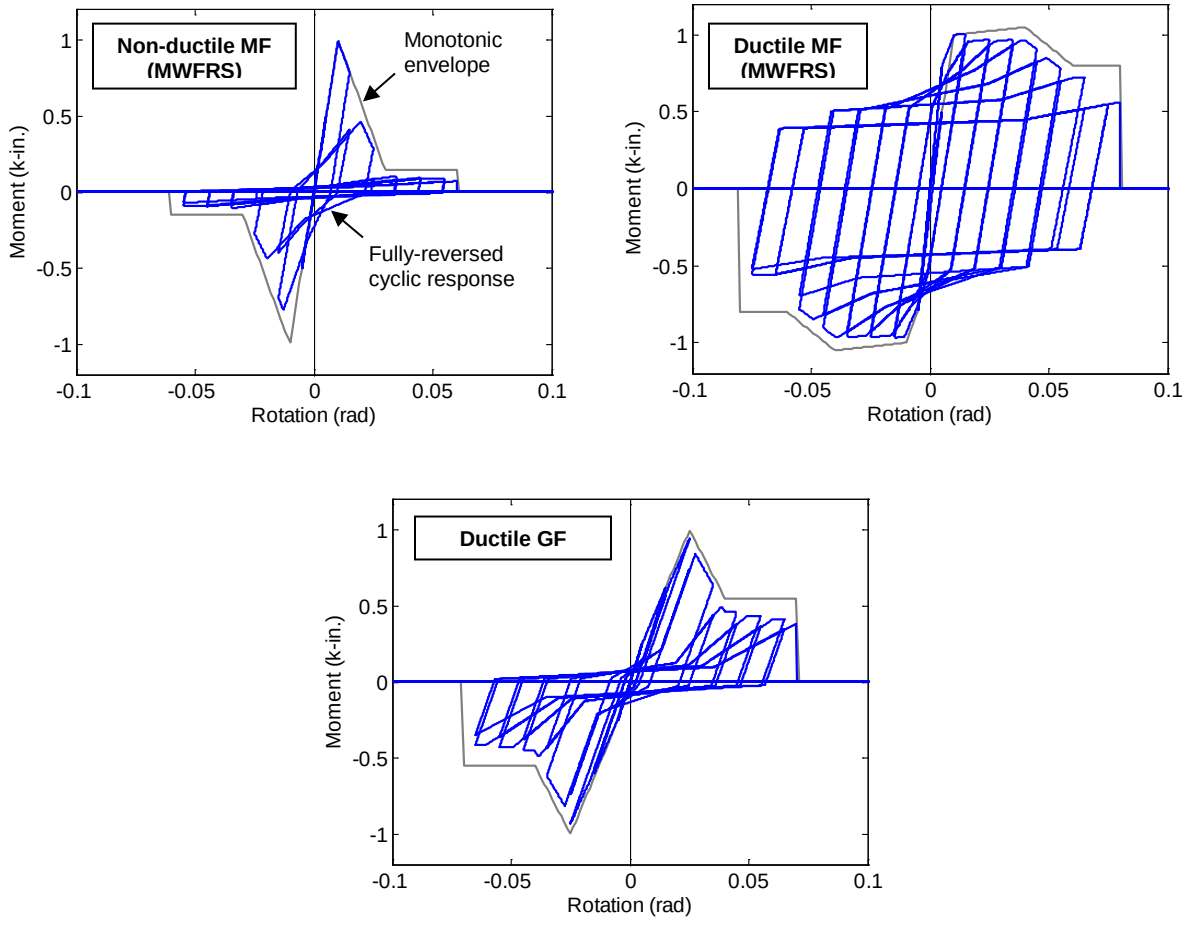

Figure 5.1 Equivalent single-degree-of-system force-deformation models

An eigenvalue analysis was used to determine the fundamental period of vibration associated with the equivalent single-degree-of-freedom model. Nonlinear static wind "pushover" analysis was used to determine the strength of the equivalent single-degree-of-freedom model.

Nonlinear dynamic response history analysis of the equivalent single-degree-of-freedom model was completed using an ensemble of wind load records from boundary-layer wind tunnel tests applied to capture both along-wind and cross-wind effects on buildings. Wind loads were then scaled (intensified corresponding to increasing hazard levels) using an incremental dynamic analysis (IDA) approach until lateral instability and collapse occurs. The risk of collapse was quantified by incorporating epistemic uncertainty and integrating collapse fragility with ASCE 7-10 (ASCE 2010) wind speed data. Appendix C contains excerpts of the *OpenSees* (PEER 2012) scripts for a Type I non-ductile moment frame 4-story building.

5.1.1 Gravity Loading

Vertical gravity roof and floor dead (D) and floor live (L) loads were calculated using the same load combination used in seismic collapse assessment (Equation 4.1). The load combination was intended to represent the expected gravity loads present in the building during a wind event. Second-order effects were included in the gravity load analysis.

5.1.2 Frequency (Period) Determination

After the gravity pre-load analysis, an eigenvalue frequency analysis was used to determine the periods of vibration of the building and associated mode shapes. This was the same procedure used for seismic collapse assessment.

For example, Figure 5.2 shows the fundamental period and mode of vibration as determined by computer analysis for the Type III non-ductile moment frame 10-story building. As expected, the fundamental period estimated using ASCE 7-10 (ASCE 2010) Equation 26.9-2, is shorter (2.28 seconds). Note that, in contrast to seismic analysis, however, the longer period from the computer analysis is the more conservative value for wind analysis.

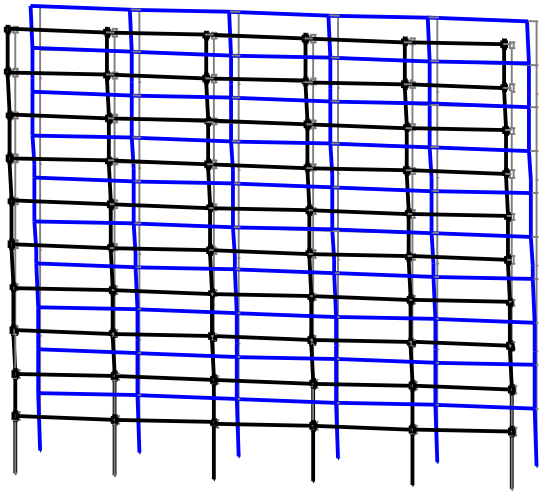

Figure 5.2 First mode (T_1 = 3.34 s) of Type III non-ductile moment frame 10-story building

5.1.3 Nonlinear Static Wind ("Pushover") Analysis

In the nonlinear static wind "pushover" response analysis, the building model was subjected to a static lateral force at each story. The distribution of lateral forces was proportioned to match the wind-exposure C atmospheric boundary layer wind (synoptic wind) profile, based on the ASCE 7-10 directional procedure. This method for wind pushover analysis differed from the distribution used in seismic pushover analysis, which was proportioned to match the first mode shape of the building. The lateral forces were applied using a displacement-control solution strategy until the roof displacement of the building exceeded at least the displacement corresponding to a 20% loss in lateral strength of the building.

The wind pushover analysis was used to determine the wind static overstrength. The static overstrength was calculated as the ratio of the maximum base shear resistance to the design base shear force (Equation 5.1).

$$\Omega_{Wind} = \frac{V_{max}}{V_{design}} \tag{5.1}$$

For example, Figure 5.3 shows the pushover response of the Type III non-ductile moment frame 10-story building. Figure 5.3b shows the deformed "pushover" shape of the building frame. The frame yielding was distributed over several stories. The loss in strength was due to a combination of beam, column, and panel zone yielding. The maximum wind pushover capacity normalized by the building weight, (V_{max}/W) equal to 0.10. Based on the wind base shear coefficient, the static wind overstrength, Ω_{Wind} is equal to 2.22.

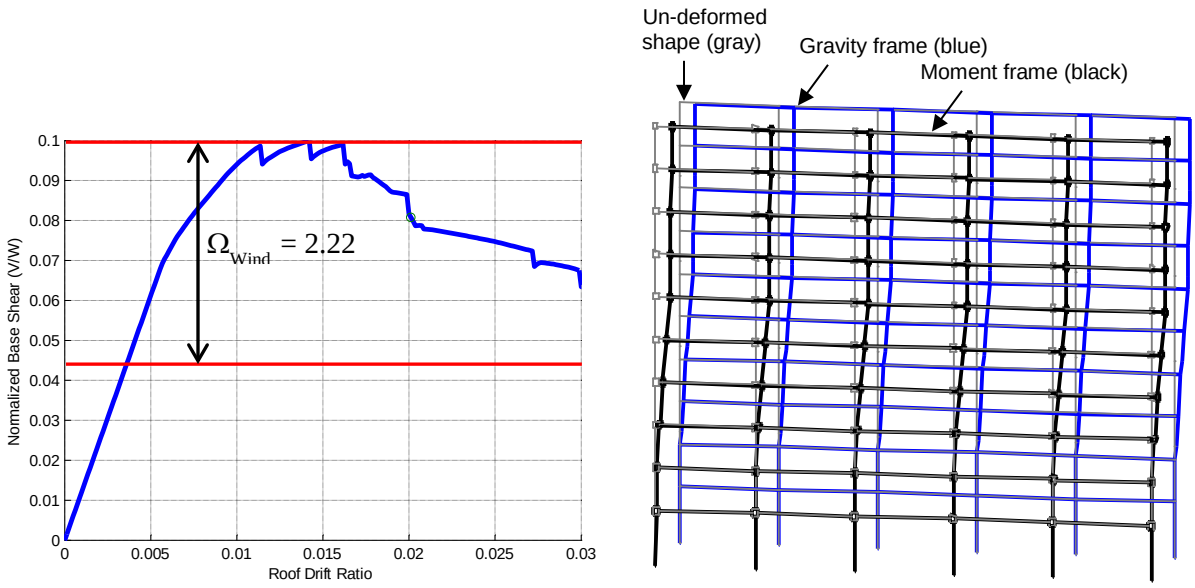

(a) Wind pushover curve (b) Wind pushover deformation

Figure 5.3 Wind pushover response of Type III non-ductile moment frame 10-story building

5.1.4 Wind Load Ensemble for Nonlinear Response History Analysis

An ensemble of wind loads was created using records generated from boundary-layer wind tunnel testing of small-scale building models. A representative wind tunnel building model is shown in Figure 5.4. This study used a database of wind tunnel data from Tokyo Polytechnic University (http://www.wind.arch.t-kougei.ac.jp). The database has previously been used to study wind effects of buildings (e.g. Tamura et al. 1999; Huang and Chen 2007). The database contains time series data of point wind pressure coefficients on the surface of small-scale aeroelastic (nominally rigid) building models. Force (base) balance building models were not used.

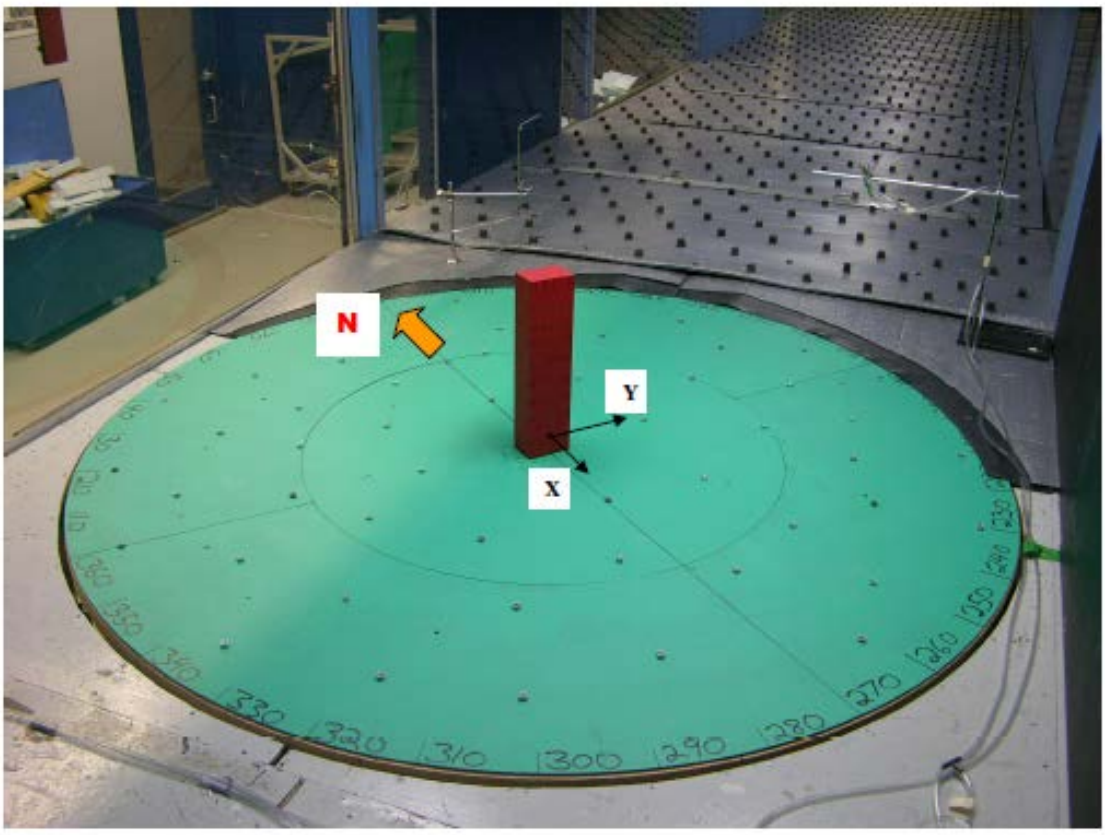

Figure 5.4 Wind tunnel test of a small-scale model of a 46-story building

(Photograph provided by RWDI Inc., Guelph, Ontario.)

For the Type I and Type II moment frame buildings, the data corresponded to the "low-rise" model database. The low-rise model contained 144 to 288 wind pressure taps (depending on the model size) uniformly distributed over the surfaces of the models. Each wall had 2 to 8 layers of pressure taps (depending on the model size), with 5 pressure taps per layer.

For example, Figure 5.5 shows the location of pressure taps for the Type I archetype building wind tunnel model. The simulated terrain corresponded to ASCE 7-10 terrain category B and C (terrain exponent, α = 1/4), and the wind tunnel length scale was 1/400. In order to capture along-wind and cross-wind effects, the wind direction for each test ranged from 0° (cross-wind) to 90° (along-wind) in 15° increments. Wind pressures were sampled every 0.0667 seconds for a total of 9,000 data points (10 minutes).

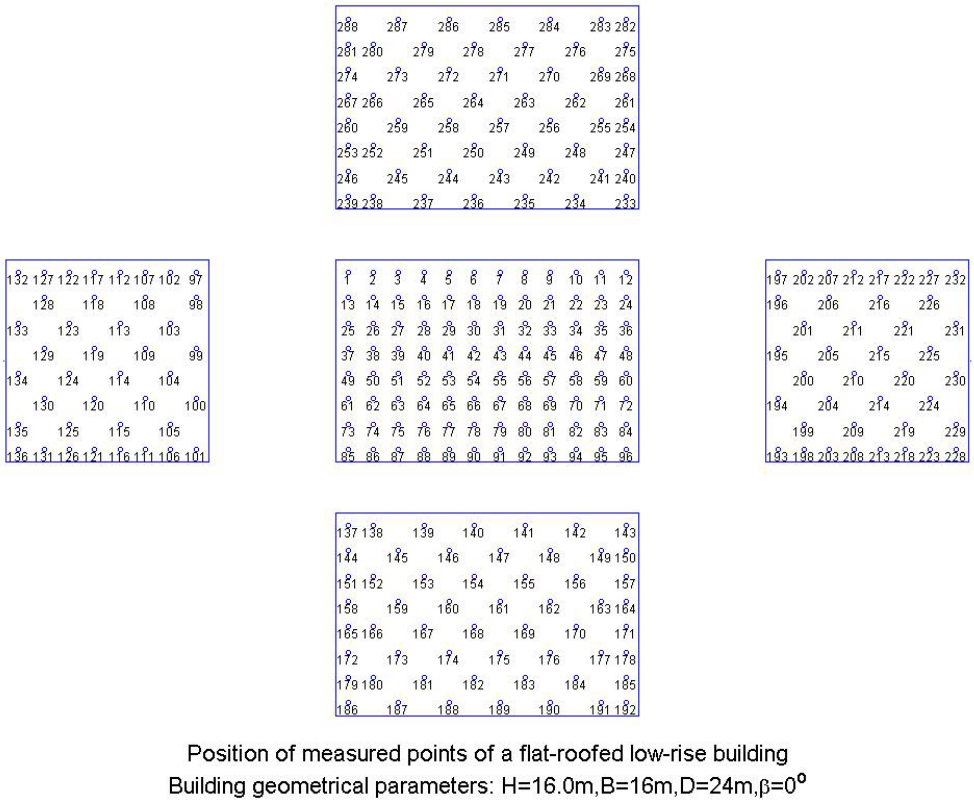

Figure 5.5 Location of pressure taps for Type I archetype building wind tunnel model

(Figure from http://www.wind.arch.t-kougei.ac.jp)

For the Type II moment frame building, the data corresponded to the "high-rise" model database. The high-rise model contained 240 wind pressure taps uniformly distributed over the vertical surfaces of the models. Each wall had 8 layers of pressure taps, with 10 pressure taps per layer. The simulated terrain corresponded to ASCE 7-10 terrain category B and C (terrain exponent, α = 1/4), and the wind tunnel length scale was 1/400. The wind direction for each test ranged from 0° (cross-wind) to 90° (along-wind) in 5° increments. Wind pressures were sampled every 0.00128 seconds for a total of 32,768 data points (about 42 minutes).

The wind pressure data depends primarily on the shape and aspect ratios of the building. This has been observed to be the case for actual buildings, where for a given synoptic or non-synoptic wind event actual wind loads are essentially independent of the spatial location of the building (with the exception that real-world locations have predominate wind directions). Such location independence is a contrast to ensembles of seismic loads that are used for nonlinear analysis, such as the FEMA P-695 Far-Field ground motion set (FEMA 2009a), that depend on the spatial location (intra-plate versus plate boundary, for example) but do not depend on the shape or aspect ratio of the building.

5.1.5 Intensity Measure for Wind Hazard

In this study, the basic wind speed in miles per hour (V_{mph}) was selected as the wind hazard intensity measure. Although this study is the first of its kind (i.e. a wind IDA), and there is no precedent for the wind intensity measure, the basic wind speed has been commonly used in other studies as an intensity measure (e.g. ASCE 2010; Yeo et al. 2014).

5.1.6 Nonlinear Dynamic Response History Analysis

The wind pressure exerted on the surface of the building was calculated using Bernoulli's equation, $p = 0.5\rho V_{mph}{}^2$ for the density of the air, ρ at standard temperature (59° F), and barometric pressure (29.92 in. Hg). The wind load history was then calculated using the wind-tunnel test pressure coefficient history data, scaled from the model to the building size and hazard intensity of interest. As a result, the wind speed record is not the same for different hazard levels. For example, if the wind speed is doubled, the equivalent data sample rate is also doubled, and the record length is only half as long.

In order to maintain the same duration of loading during an incremental dynamic analysis, the wind load record was replayed. For the response history analysis, the wind load was linearly ramped for the initial record segment of the loading. Finally, for the purposes of the single-degree-of-freedom model, windward and leeward forces at each story in the building were aggregated into a single equivalent (generalized) lateral load.

Structural analysis of the equivalent single-degree-of-freedom model was performed using *OpenSees* finite element software (PEER 2012). As previously discussed, the single-degree-of-freedom model was subjected to full-scale wind load records that were scaled (intensified) corresponding to increasing hazard levels (higher wind speeds), and the wind speed was used as the intensity measure. For example, Figure 5.6 shows the response just prior to collapse and at collapse for the Type I ductile moment frame 8-story building with the enhanced shear tab connection collapse prevention system with a reference wind speed of 20 mph. A single IDA curve (wind speed versus drift for one wind record) is also shown for 0° (cross-wind).

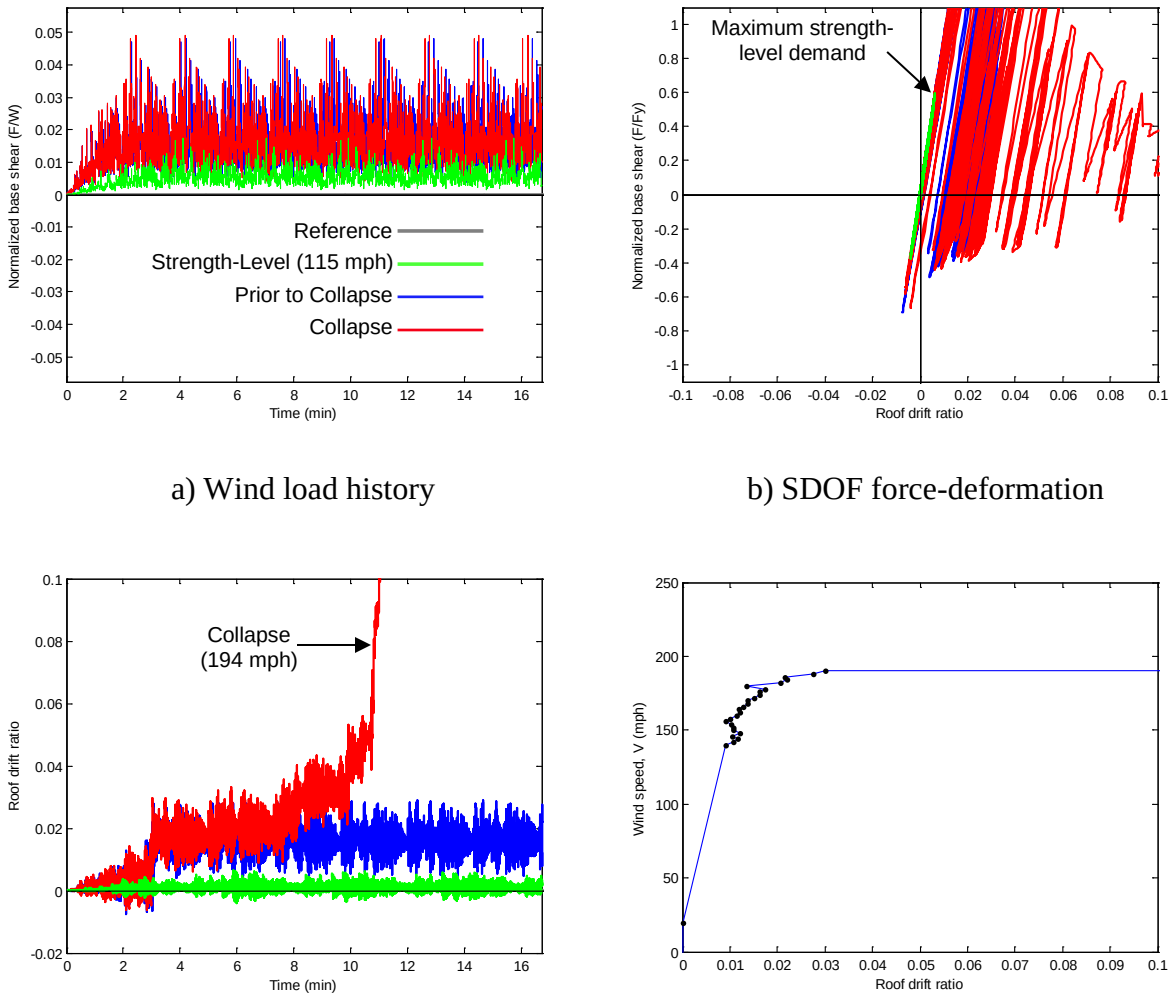

a) Wind load history

b) SDOF force-deformation

c) Roof drift ratio

d) Single IDA

Figure 5.6 Response of Type I ductile moment frame 8-story building with enhanced shear tab collapse prevention system for 0° (cross-wind) (reference wind speed 20 mph)

The incremental dynamic analyses were continued until lateral instability and presumed collapse, when the drift ratio exceeds 0.2. The equivalent single-degree-of-freedom drift was converted to a multi-degree-of-freedom roof drift using Equation 5.2 based on ASCE 41-13 (ASCE 2014). See also FEMA P-695 Equation 6-8 and Appendix B (2009a), where m is the mass, and φ is the mode shape of the building (an array the size of the number of stories).

$$\Delta_{Roof} = C_0 \Delta_{Roof}$$

$$= \left[\varphi_{1,roof} \frac{\sum_1^{N=number\ of\ stories} m_{story} \varphi_{1,story}}{\sum_1^{\varphi_{1,roof}} m_{story} \left(\varphi_{1,story}\right)^2} \right] \Delta_{Roof} \quad (5.2)$$

For simplicity, it was assumed that the building envelope remained intact, although it is recognized that at higher hazard levels, wind-borne debris and missile impact would likely compromise the cladding and fenestration integrity.

The appropriate ratio of critical damping for conventional structures for inelastic wind analysis was estimated to be 2.5%, half that used for linear seismic analysis (5%). Damping was incorporated in the analysis in two parts. First, energy dissipation was explicitly modeled through the nonlinear hysteretic behavior, which is a function of the wind intensity. Second, stiffness and mass proportional ("Rayleigh") equivalent viscous damping was conservatively set at 1% to account for the non-explicitly modeled part of the damping. The effect of damping is considered in Chapter 6.

As previously discussed, if the wind speed increases, the time-interval (sample rate) decreases, and the record duration is inversely reduced. Thus, unlike in a seismic IDA, the duration must be defined in a wind IDA. In this study, a constant loading duration was maintained by adjusting the record length relative to an initial reference intensity wind speed. For the baseline condition, the reference wind speed and duration was 100 mph and 28 min.

5.1.7 Collapse Fragility

The wind vulnerability of the building to side-sway collapse (wind collapse fragility) was determined by fitting individual collapse points (wind speed in miles per hour and corresponding probability of collapse for a one scaled wind load record) with a curve assuming a lognormal

cumulative distribution function. A Kolmogorov-Smirnov "goodness-of-fit" test (Massey 1951) at the 1% confidence level was used to verify that the fragility curve could be assumed to have a lognormal distribution. The lognormal cumulative distribution function was defined by two parameters: the median collapse wind speed, and the standard deviation of the natural logarithm β (dispersion due to variability and uncertainty).

For example, Figure 5.7 shows the incremental dynamic analyses and wind collapse fragility curves for the Type I ductile moment frame 8-story building with enhanced shear tab connection collapse prevention system with reference wind speed of 20 mph.

Since wind loads are a random vibration, variability in the response was generated by wind directionality (angle of attack). Such variation provided a practical way to incorporate epistemic uncertainties in the incremental dynamic analysis. This "directional" variation differs from the variation used in seismic load ensembles, which were generated using actual records from a range of earthquake magnitude-distance pairs for (mostly) independent events.

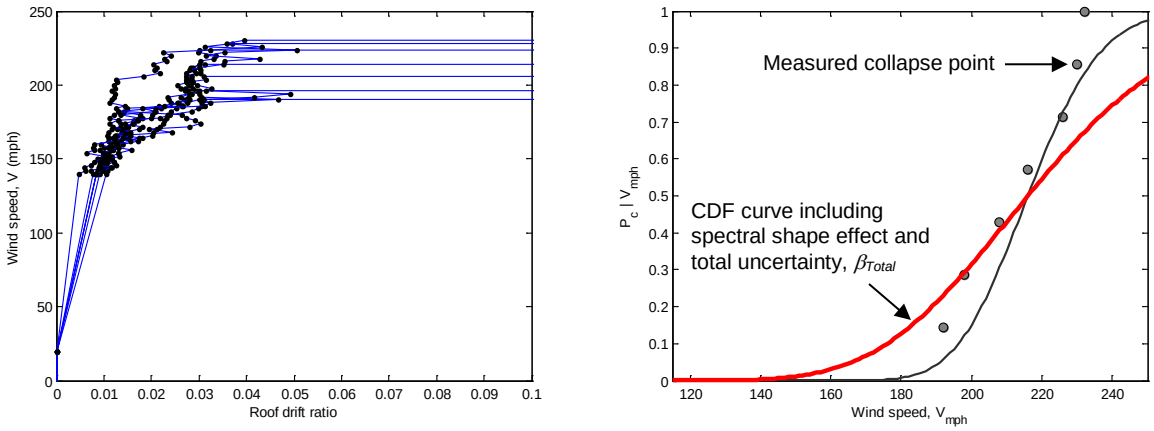

a) Incremental dynamic analyses b) Wind collapse fragility curve

Figure 5.7 Response of Type I ductile moment frame 8-story building with enhanced shear tab connection collapse prevention system (reference wind speed 20 mph)

The total dispersion, β_{Total} in collapse capacity was calculated using Equation 5.3, following the method adopted in FEMA P-58 (FEMA 2012a,b):

$$\beta_{Total} = \sqrt{\beta_{RTR}{}^2 + \beta_C{}^2 + \beta_Q{}^2} \quad (5.3)$$

In Equation 5.3, β_{RTR} was the measured (record-to-record) dispersion in the nonlinear wind response history analyses. Epistemic uncertainty was incorporated by assigning dispersion due to construction uncertainty β_{DR}, and analytical model quality uncertainty β_Q. The qualitative ratings (using FEMA P-58 rubric) given in Table 5.1 were used in this study. The dispersion values in the table correspond to new buildings constructed with rigorous quality assurance and a sufficiently accurate analytical model.

Table 5.1 Qualitative rating used to quantify uncertainties in wind collapse assessment

	Non-ductile moment frame	Ductile moment frame
Construction	β=0.10	β=0.10
Analytical model	β=0.10	β=0.10

5.2 Wind Collapse Risk Procedures

Wind collapse risk (probability of collapse considering the likelihood of wind speed) was calculated by integrating the wind collapse fragility and wind hazard. A target risk of 0.15% in 50 years for ordinary occupancy was based on ASCE 7-10 Table C.1.3.1a (ASCE 2010).

Wind hazard (the occurrence of windstorms) may be described as a Bernoulli sequence or process, that assumes events (e.g. windstorms) occur randomly, independently, and the probability of occurrence is constant. For "well behaved climates away from the hurricane coast" the probability of occurrence may be describe using an extreme value type I distribution

(Boggs and Peterka 1992). Assuming a geometric distribution, the probability of occurrence of an event, N in t years is

$$P(N \geq 1) \quad = \quad 1 - (1 - \lambda_a)^t \tag{5.4}$$

where λ_a is the mean hazard exceedence frequency corresponding to an intensity measure (i.e. wind speed in miles per hour), the probability that the intensity of windstorm, A will exceed some level, a in a given year: $\lambda_a = P(A > a \mid t = 1yr)$. As in the seismic collapse assessment, for low annual hazard rates, Equation 5.4 is numerically equivalent to the hazard curve (inverse of MRI), so that $P(N \geq 1) = \lambda_a$.

Integration of the wind hazard (wind speed) curve and the structural collapse vulnerability (wind collapse fragility) curve followed the process used for seismic analysis. The vulnerability of the structure to the wind hazard (conditional probability of failure), in terms of an annual failure rate, was calculated using the Equation 5.5.

$$\lambda_F \quad = \quad \int_0^{+\infty} \lambda_a \, f(a) \, da \tag{5.5}$$

As before, this form of the risk integral requires the derivative of the fragility curve—the CDF, which yields the probability density function (PDF). This was a more stable approach than taking the derivative of the hazard curve. And, as before, the integral was performed numerically. In contrast to seismic risk analysis in Chapter 4, directional effects and site response were not included in the wind risk analysis. The cumulative risk (P_F) to wind collapse during the building lifetime (t in years) was calculated using Equation 5.6.

$$P_F \quad = \quad 1 - (1 - \lambda_F)^N \tag{5.6}$$

Equation 5.6 is different than the equation used to calculate cumulative seismic risk (Equation 4.8), but produces similar values for low annual failure rates and typical exposure times.

The wind collapse risk analysis procedures are illustrated in Figure 5.8 for Type I ductile moment frame 8-story building with enhanced shear tab connection collapse prevention system, with a reference wind speed 20 mph. Wind hazard (Figure 5.8a,b) was based on the ASCE 7-10 wind speed data (ATC 2011) for the interior of the conterminous United States (see Chapter 2). Extreme hazard, where the mean recurrence interval (MRI) exceeds 1,700 years, was based on extrapolation.

The ASCE 7-10 data does not include downdrafts and tornadoes. Tornado hazard was estimated by using the number of tornado events that have been cataloged for 2°-latitude×2°-longitude regions and correlating the tornado scale factor with a wind speed (Ramsdell and Rishel 2007). The wind hazard curves shown in Figure 5.8 are only for the extrapolated data, and do not include tornado data.

Where the hazard curve incorporated tornado effects, it is important to note that this integration reflected the building vulnerability (collapse fragility) to straight-line wind forces of long duration, not to a tornado-like wind force vortex of short duration. Experimental studies of high-rise buildings (Yang et al. 2011) and low-rise buildings (Haan et al. 2010) subjected to a tornado vortex suggest that the wind pressure coefficients is on the order of 1.5 times larger compared to the straight-line effects.

A deaggregation of wind collapse risk (Figure 5.8c) indicates the wind speeds that contribute the most to the annual risk rate. The cumulative risk to wind collapse (Figure 5.8d) during the building lifetime was calculated using Equation 5.6.

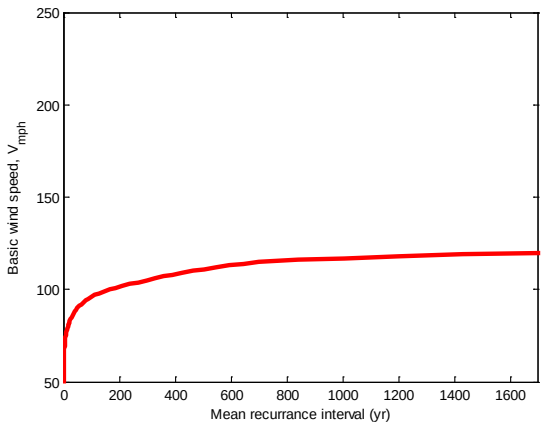

a) Wind hazard (wind speed versus MRI)

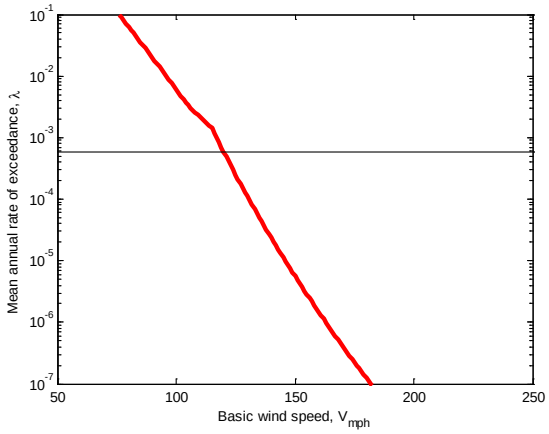

b) Wind hazard (λ versus wind speed)

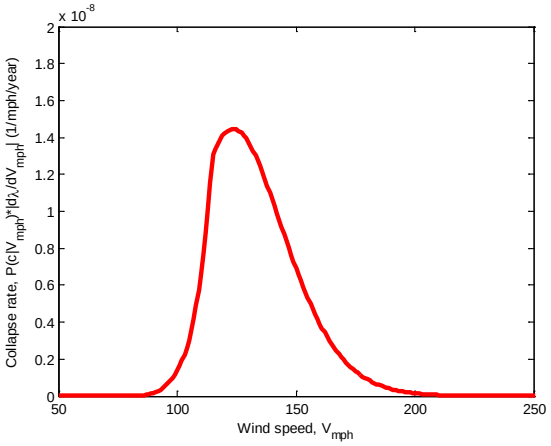

c) Deaggregation of wind collapse risk

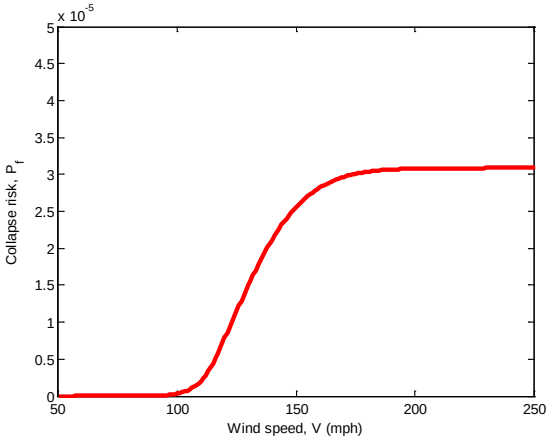

d) Cumulative wind collapse risk

Figure 5.8 Response of Type I ductile moment frame 8-story building with enhanced shear tab collapse prevention system (reference wind speed 20 mph)

5.3 Results

5.3.1 Type I Non-ductile and Ductile Moment Frame Buildings

The collapse assessment results, relative to risk category II (115 mph basic wind speed), are summarized in Table 5.2 for non-ductile and Table 5.3 for ductile moment frames. The empirical period, T_w and calculated period, T_1 from an eigenvalue analysis are given. As in the seismic evaluation, the fundamental period values determined in the eigenvalue analysis, T_1 are high compared to empirical estimates of actual buildings, even for wind evaluation. The static pushover results are described in terms of the wind base shear coefficient C_{s-Wind} and static "overstrength" Ω. The dynamic IDA results include the collapse margin ratio (*CMR*), record-to-record dispersion β_{RTR}, total dispersion β_{Total}, and the risk of wind collapse (unconditional) based on a location in the interior of the United States.

The reserve lateral strength in the shear-tab connections reduced the risk of collapse noticeably compared to moment frames alone.

Table 5.2 Wind collapse assessment of Type II non-ductile moment frame buildings (relative to Risk Category II)

Archetype	T_w (s)	T_1 (s)	Static Pushover		Dynamic IDA			
			Cs,wind	Ω	CMR	βRTR	βTotal	Pf,50
4-Story								
MF	1.10	2.38	0.03	2.99	1.43	0.104	0.176	0.57%
MF+GF		2.01		3.02	1.46	0.105	0.176	0.42%
MF+SST		1.67		5.22	1.69	0.107	0.178	0.05%
8-Story								
MF	1.88	3.16	0.03	2.10	1.44	0.046	0.149	0.20%
MF+GF		2.85		2.45	1.37	0.057	0.153	0.48%
MF+SST		2.47		2.96	1.48	0.036	0.146	0.12%

Table 5.3 Wind collapse assessment of Type II ductile moment frame buildings (relative to Risk Category II)

Archetype	T_W (s)	T_1 (s)	Static Pushover		Dynamic IDA			
			$C_{s,wind}$	Ω	CMR	β_{RTR}	β_{Total}	$P_{f,50}$
4-Story								
MF+GF	1.10	1.60	0.03	3.34	2.30	0.060	0.154	0.00%
MF+SST	1.10	1.60	0.03	7.35	2.56	0.109	0.179	0.00%
8-Story								
MF+GF	1.88	2.88	0.03	2.45	1.62	0.080	0.162	0.05%
MF+SST	1.88	2.50	0.03	2.71	1.88	0.075	0.160	0.00%

Employing enhanced shear tab connection collapse prevention systems decreased the risk dramatically. Without collapse prevention systems, only the ductile buildings passed the target risk (0.15%). With collapse prevention systems, all buildings easily passed the target risk.

Maps are used to illustrate areas where collapse prevention systems are applicable for the Type I archetype non-ductile building. Wind collapse risk was calculated by integrating collapse fragility (from Table 5.2 and Table 5.3) and wind hazard based on extrapolated ASCE 7-10 wind speed data. The wind risk analysis was repeated for every 0.5-degree latitude and longitude to generate a map of risk values in the conterminous United States. Major metropolitan areas (dots) are shown based on 2011 population estimate using 2010 census data.

Regions where the wind collapse risk exceeds 0.15% in 50 years (shaded contours) are shown in Figure 5.9 for the 4-story non-ductile building, and in Figure 5.10 for the 8-story non-ductile building. The maps show that the enhanced shear tab connection (SST) collapse prevention system with non-ductile moment frames is necessary for all of United States, except the west coast, for the 4-story building. For both the 4-story and 8-story buildings, the collapse prevention system was not suitable for use in high wind regions along the hurricane coastline and extending up along the eastern seaboard to New York and Boston.

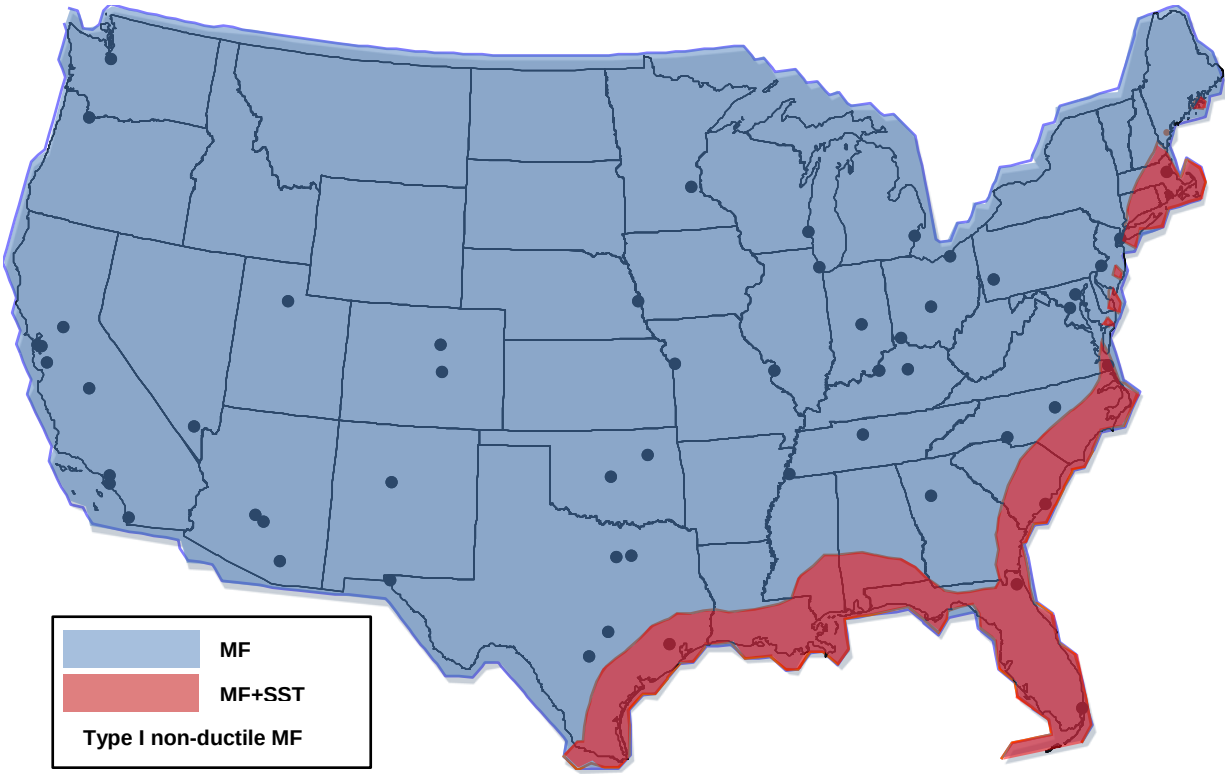

Figure 5.9 Regions where wind collapse risk exceeds 0.15% in 50 years (4-story building)

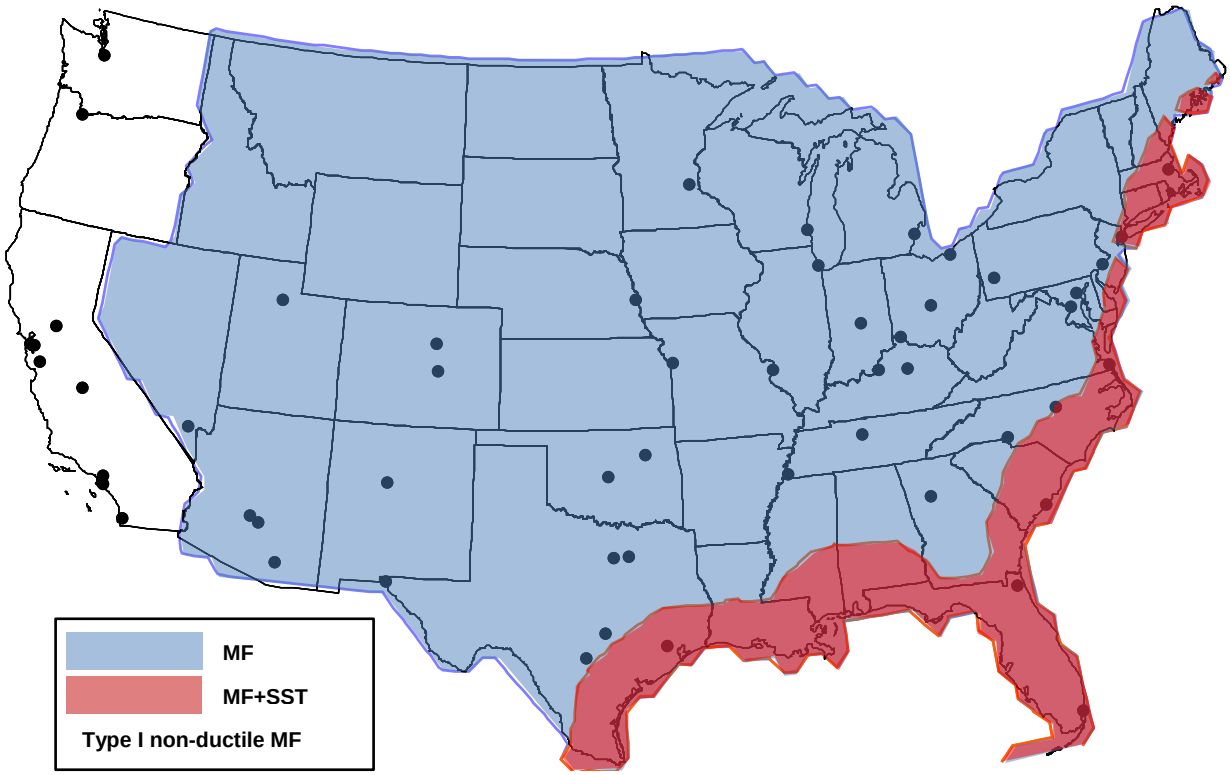

Figure 5.10 Regions where wind collapse risk exceeds 0.15% in 50 years (8-story building)

5.3.2 Type II Non-ductile Moment Frame 4-story Building

The wind collapse assessment results are summarized in Table 5.4 for the non-ductile 4-story building, relative to Risk Category II. As before, the reserve lateral strength in the shear-tab connections reduced the risk of collapse significantly. The building easily passed the target risk of 0.15%. Figure 5.11 shows regions where the wind collapse risk exceeds 0.15% in 50 years (shaded contours). The wind collapse risk exceeds 0.15% only in areas of high hurricane hazard.

Table 5.4 Wind collapse assessment of Type II non-ductile moment frame building

			Static Pushover		Dynamic IDA			
Archetype	T_W (s)	T_1 (s)	Cs,wind	Ω	CMR	β_{RTR}	β_{Total}	$P_{f,50}$
MF+GF	1.11	1.64	0.02	6.27	1.84	0.086	0.165	0.0%

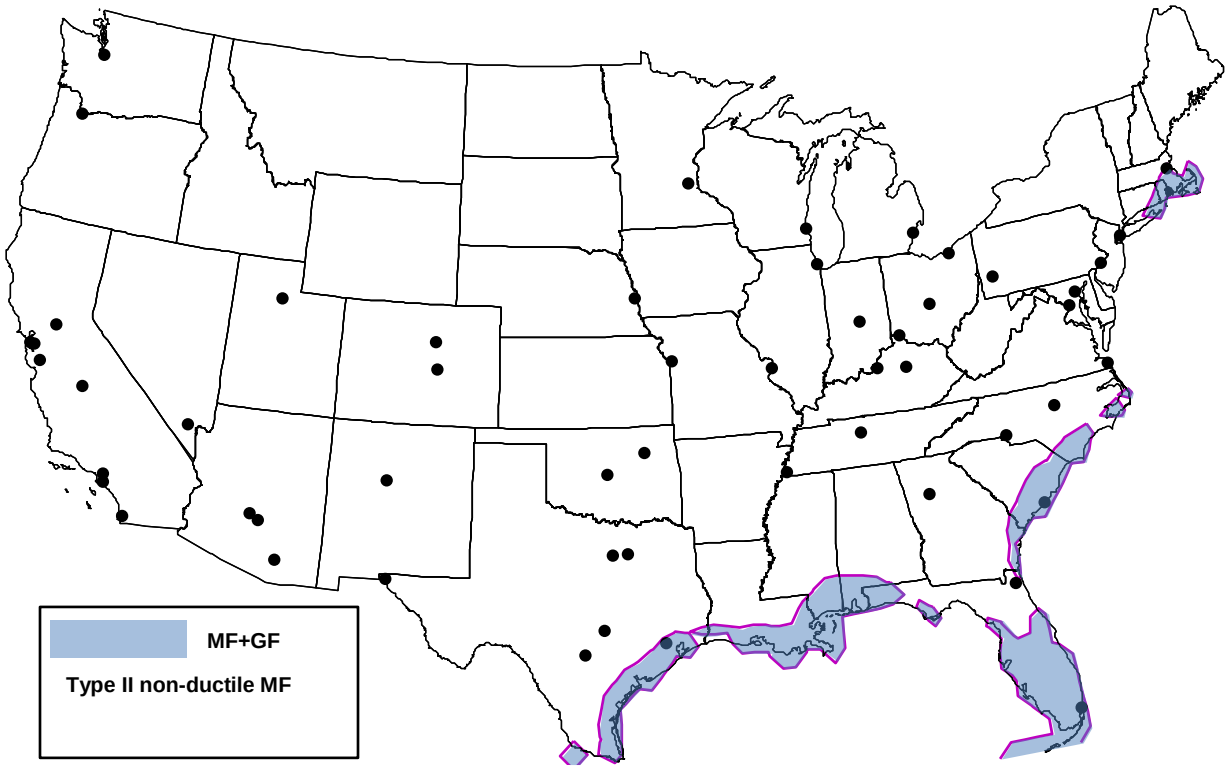

Figure 5.11 Regions where wind collapse risk exceeds 0.15% in 50 years (4-story building)

5.3.3 Type III Non-ductile Moment Frame 10-story Building

The wind collapse assessment results are summarized in Table 5.5 for the Type III non-ductile 10-story building. This building structural plan was configured such that there were no shear tab connections with columns oriented in the strong direction, thus no reserve strength comparison was made. The results indicate that the building does not pass the target risk (0.15%) by a large margin.

Figure 5.12 illustrates the process of calculating the wind collapse risk. Wind hazard (Figure 5.12a) was based on the ASCE 7-10 wind speed data (ATC 2011) for the interior of the conterminous United States. Extreme hazard, where the mean recurrence interval (MRI) exceeds 1,700 years, was based on extrapolation. Hazard curves for the west coast of the United States and for Jacksonville, Florida (on the hurricane-prone east coast) are also shown. The effect of tornado hazard is shown for Jacksonville and Oklahoma City. The plot indicates that tornado hazards dominate extreme events for the interior of the United States, whereas hurricanes pose a greater hazard along the eastern seaboard.

Building vulnerability, or the collapse fragility (Figure 5.12b), was integrated with the wind hazard using the derivative of the fragility curve.

The contribution of hazards to the annual rate of collapse risk (λ_{Fail}), or so-called deaggregation, displayed in Figure 5.12c shows that the effect of extrapolating wind speed data was negligible for the non-ductile moment frame building for most locations in the interior of the United States. Even in Oklahoma City and Jacksonville, where tornadoes or the effect of wind speed data extrapolation are significant, non-extreme wind events (wind events with less than a 1,700-year MRI) still contribute the most to the annual risk rate for wind collapse.

Table 5.5 Wind collapse assessment of Type III non-ductile moment frame 10-story building (relative to Risk Category II)

Archetype	T_W (s)	T_1 (s)	Static Pushover		Dynamic IDA			
			Cs,wind	Ω	CMR	β_{RTR}	β_{Total}	$Pf_{,50}$
MF	2.28	3.34	0.05	2.21	1.20	0.069	0.158	3.3%

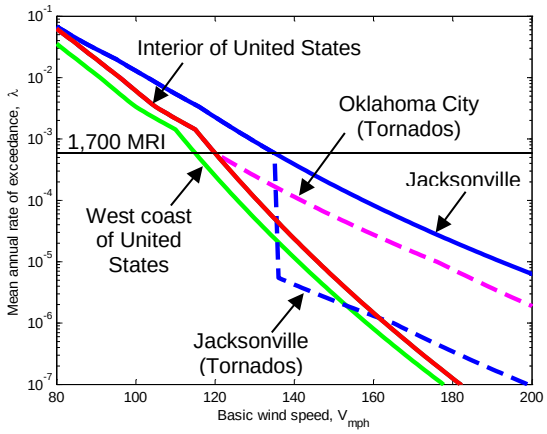

a) Wind hazard

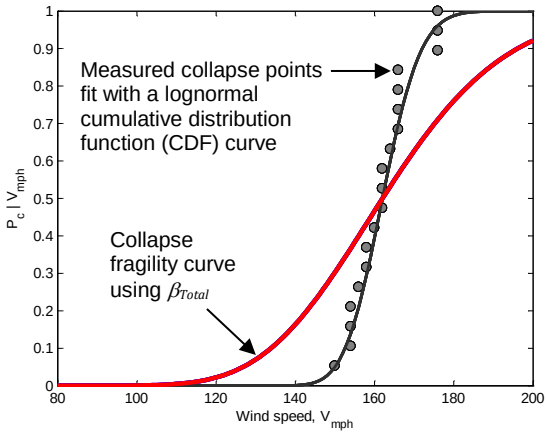

b) Wind collapse fragility

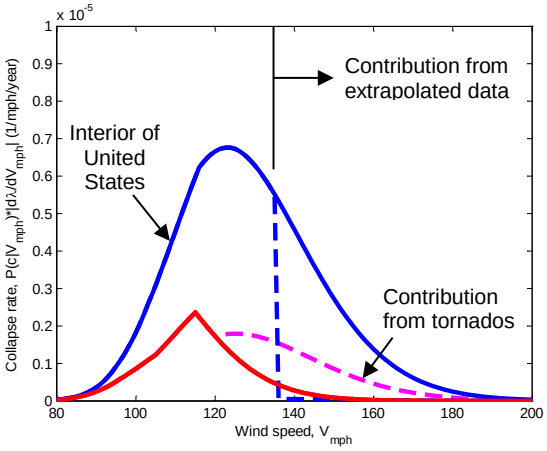

c) Wind collapse risk deaggregation

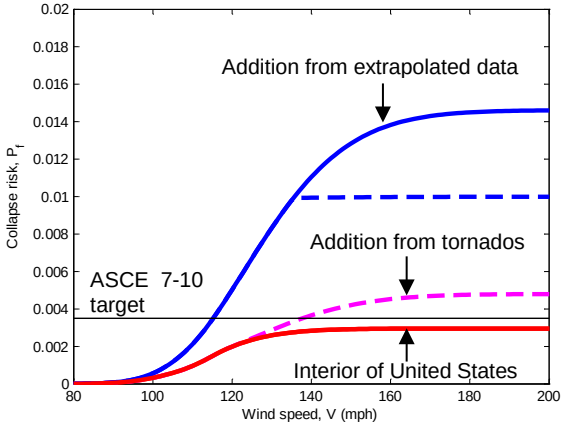

d) Cumulative risk of wind collapse

Figure 5.12 Collapse risk analysis for Type I non-ductile moment frame building

5.4 Discussion

Wind collapse assessments indicated that the probability of collapse was acceptably low for most archetypical structural systems in the interior (and west coast) of the United States. Taller buildings, however, had a higher risk, and one archetype (the Type III non-ductile moment frame 10-story building) did not pass the suggested 0.15% target risk. Collapse prevention systems are needed and viable in the interior of the United States, but along the hurricane-prone coastline the risk of collapse often exceeded the target risk, depending on the location and type of archetype structural system.

In seismic analysis, the conditional probability of collapse is often used to determine structural safety: the building collapse probability should not exceed 10% given the Maximum Considered Earthquake (MCE) ground motions. The conditional probability may be appropriate for seismic engineering for the reason that the seismic risk reflects the underlying seismic hazard, and thus the seismic risk changes dramatically from one site to another site, even in the same general location. In other words, calculation of seismic risk may not enable a uniform comparison of structural response to earthquakes.

In wind analysis, on the other hand, there is no equivalent "Maximum Considered Wind" speed event. The closest such event is the design wind speed. In ASCE 7-10, for risk category II structures the design wind speed (115 mph in the interior of the United States) is associated with a 700-year MRI. For risk category III and IV structures the design wind speed (120 mph in the interior of the United States) is associated with a 1,700-year MRI. This suggests that a "Maximum Considered Wind" could take on various wind speeds.

Moreover, a target for the conditional probability of wind collapse given such an event has not been established. The results in this chapter suggest that such a target would need to be much less than 10% (used for seismic), perhaps on the order of 1% to 2%.

Chapter 6

SENSITIVITY OF COLLAPSE ASSESSMENT

This chapter discusses the sensitivity of seismic and wind collapse assessments to parametric changes in hazard or structural vulnerability via analytical modeling. The seismic hazard parameters included ground motions, site response, regional risk, and intensity measures. The seismic modeling parameters included column panel zone representation, the method used to account for second-order (P-Δ) effects, column splices, and the risk integration method. The wind hazard parameters included duration of wind. The wind modeling parameters included type of lateral system, static overstrength, fundamental building period, and structural system degradation of stiffness and strength.

6.1 Seismic Collapse Sensitivity

In the analytical modeling approach (Chapter 3) used in this study, beams and columns were represented using an assembly of rotational springs and elastic beam-column elements in order to simulate the potential for inelastic behavior at or near the end of the member. Aside from component behavior, key aspects of analytical modeling are the beam-column joint (panel zone) representation, the method used to take into account second-order (P-Δ) effects, modeling of

column splices, spectral matching between the ground motion record and the target response spectrum, risk integration method, regional risk, and site response.

This section discusses the sensitivity of the seismic collapse assessment to these parameters for the Type I archetype structural systems. Three types of moment-frame designs were considered: a non-ductile moment frame designed for FEMA P-695 Seismic Design Category (SDC) B_{min}, and a ductile moment frame using a reduced-beam section designed for SDC D_{min} or SDC D_{max}. Although the scope of the sensitivity study was limited to these specific structures, related sensitivity studies of second-order effects and damping have shown similar effects for a braced-frame and an 8-story moment-frame building (Hardyniec 2014).

6.1.1 Panel Zone Representation

Background

Shear distortion in the panel zone of a beam-to-column connection has been shown to be an important factor in the seismic analysis of steel moment-frame buildings (Charney and Horvilleur 1995; Charney and Johnson 1986; FEMA 2000a; Charney and Pathak 2007). The panel zone may be represented analytically in a variety of ways. In the simplest representation, the steel frame is modeled using centerline dimensions and rigid joints. In this "centerline" model the shear distortion in the panel zone behavior is not explicitly considered, but is approximated (the underestimated shear and overestimated bending moment within the joint region tend to cancel out as "compensating errors"). More importantly, the centerline model does not account for inelastic deformation. Another representation is the "scissors" model, where the panel zone is modeled using a beam and a column, with rigid links at each end, connected by a hinge with a spring. In this model, the spring rotation is equal to the shear

distortion of the panel zone. A more correct representation was proposed by Krawinkler (1978). In the "Krawinkler" model, the panel zone is modeled using rigid beam elements connected by hinges and springs that form a parallelogram. It should be noted that the kinematic behavior differs for scissors and Krawinkler models, and the properties for springs are not the same (Charney and Marshall 2006). Although it is clear that the kinematic behavior of the Krawinkler model is closer to the true connection behavior (Charney and Marshall 2006), the scissors and centerline models require fewer degrees of freedom. The number of degrees of freedom has a significant impact on the computational demand for seismic collapse analyses, which, as previously discussed, involve multiple ground motions run at increasing intensity levels until collapse.

Results

The sensitivity of the seismic collapse assessment to the panel zone representation is summarized in Table 6.1 for the Type I non-ductile moment frame 4-story building, and in Table 6.2 for the Type II ductile moment-frame 4-story building designed for SDC D_{max}. The results are shown relative to the Krawinkler model (the "baseline" or reference model). The fundamental period, T_1 was based on the eigenvalue analysis. The static response is described in terms of the seismic base shear coefficient C_s, the "overstrength", Ω, and the period-based ductility, μ_T. The dynamic response is described in terms of the seismic intensity measure (spectral acceleration at the fundamental period corresponding to the MCE-level ground motion, S_{aMCE}), the collapse margin ratio (*CMR*), the measured record-to-record dispersion (β_{RTR}), the total dispersion (β_{Total}) dispersion including epistemic uncertainties), and the conditional probability of seismic collapse (failure conditioned on occurrence of the MCE-level ground motion intensity).

Table 6.1 Sensitivity of collapse assessment (for SDC D_{max}) for Type I non-ductile moment-frame building (designed for wind, SDC B_{min}) to the panel zone representation

Model Aspect	T1 (s)	Static Pushover			Dynamic IDA						
		Cs	Ω	μT	SaMCE (g)	CMR	SSF	ACMR	βRTR	βTotal	Pc | MCE
Baseline (Reference) Model											
Krawinkler	2.01	0.21	0.41	3.94	0.45	0.93	1.39	1.30	0.37	0.65	34.0%
Alternate Panel Zone Model											
Centerline	1.44	0.21	0.43	3.65	0.62	1.04	1.36	1.41	0.30	0.61	28.8%
Scissors	1.99	0.21	0.40	4.33	0.45	0.93	1.42	1.32	0.36	0.64	33.4%

Table 6.2 Sensitivity of collapse assessment (for SDC D_{max}) for Type I ductile moment-frame building (designed for SDC D_{max}) to the panel zone representation

Model Aspect	T1 (s)	Static Pushover			Dynamic IDA						
		Cs	Ω	μT	SaMCE (g)	CMR	SSF	ACMR	βRTR	βTotal	Pc | MCE
Baseline (Reference) Model											
Krawinkler	1.36	0.08	2.26	5.63	0.66	1.89	1.46	2.75	0.33	0.45	1.2%
Alternate Panel Zone Model											
Centerline	1.01	0.08	2.03	11.66	0.89	1.89	1.46	2.76	0.36	0.47	1.5%
Scissors	1.35	0.08	2.24	5.88	0.67	1.87	1.47	2.74	0.33	0.45	1.2%

A comparison of *CMR* values from each model indicates that the non-ductile moment frame building assessment was more sensitive than the ductile frame building to the change in the panel zone model representation. The total dispersion of the collapse results, represented by β_{Total}, was similar for both panel zone models, and the conditional probability of collapse was similar. Overall, the *CMR*, static overstrength, and period-based ductility values were greater for the ductile frames, while the conditional probability and dispersion were greater for the non-ductile frames, which were expected based on the design considerations for the two frames.

A comparison of the incremental dynamic analyses for the non-ductile moment frame buildings (Figure 6.1) and ductile moment frame buildings (Figure 6.2) augments the results from the previous tables. The *CMR* values, calculated from the spectral acceleration associated with the median collapse and the spectral acceleration at the MCE level, represented by the red and black lines, respectively, were generally near 1.0 for the non-ductile frames and near 2.0 for the ductile frames. The greater ductility of the ductile moment frames was also apparent in the higher interstory drift ratios that the models reached before collapse.

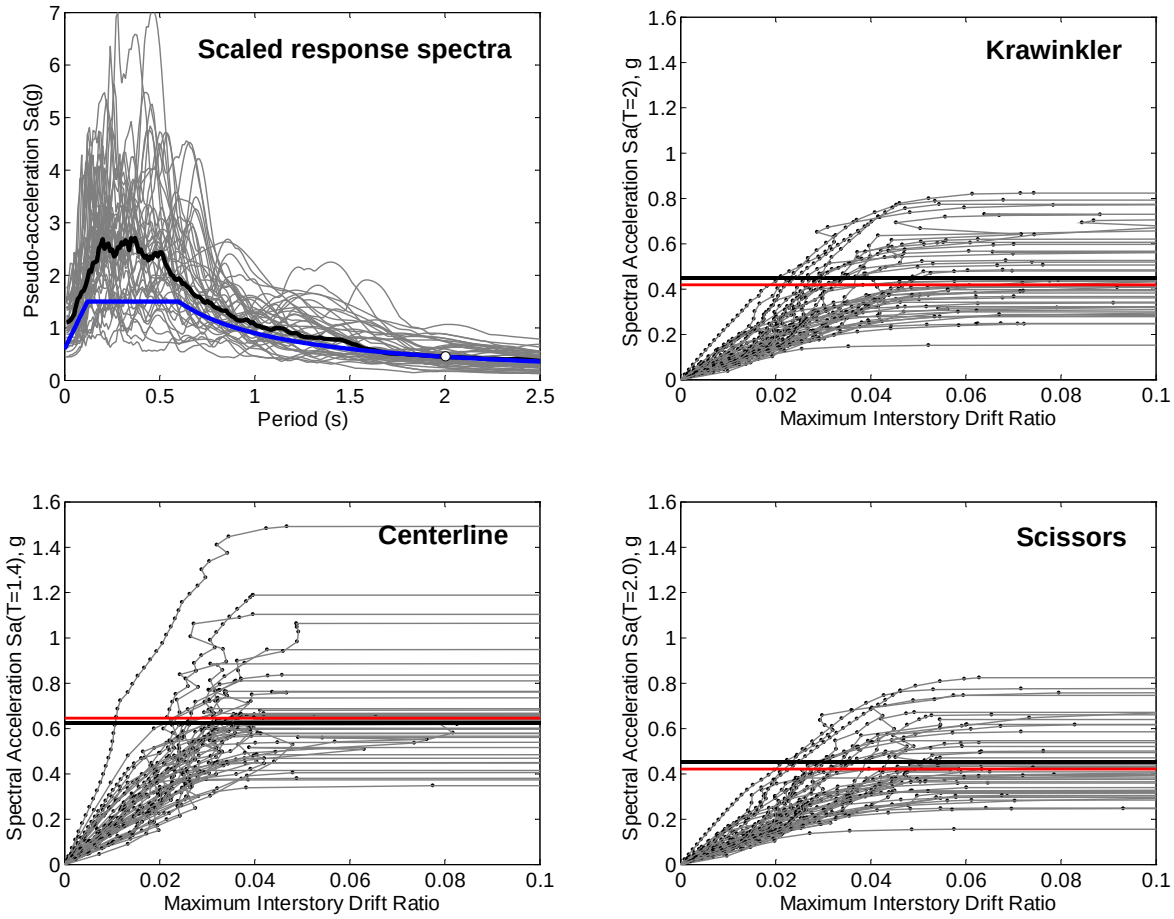

Figure 6.1 Incremental dynamic analyses: Type I non-ductile moment frame 4-story building

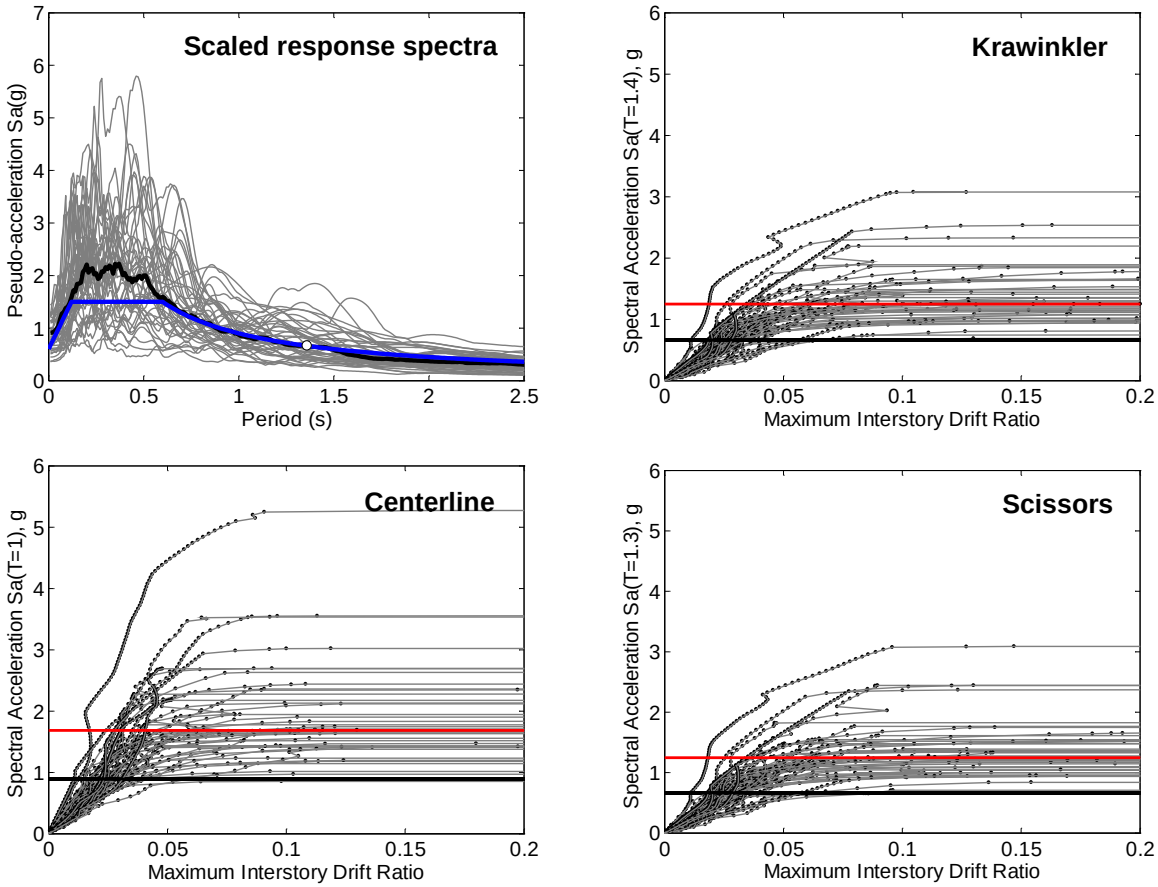

Figure 6.2 Incremental dynamic analyses: Type I ductile moment frame 4-story building

6.1.2 Second-Order Effects

Background

Second-order effects are also known to be an important factor in the analysis of flexible structures like steel moment frames, especially for seismic collapse analysis (Gupta and Krawinkler 2000; Christoph et al. 2004). In a first-order analysis, the displaced configuration of a structure is not considered, and equilibrium is calculated based on the undeformed configuration. However, the undeformed configuration cannot be used to satisfy equilibrium as displacements increase. The effects of these equilibrium unbalances are commonly referred to as second-order effects. To reduce the equilibrium unbalances induced by large displacements, geometric nonlinearity approaches are incorporated.

For small displacements, second-order effects can be reasonably estimated using a P-Δ approximation, where lateral (transverse) member displacements are considered, but axial (longitudinal) member displacements are ignored (referred to as the Euler-beam theory "large-displacement" assumption). The "corotational" method is one way to account for large displacements.

In the corotational method, the local element coordinate system continuously rotates with the element (Balling and Lyon 2011). In its usual form, the corotational method assumes small-strain relationships. The small-strain assumption is valid for collapse analysis of steel moment-frame buildings, where the ultimate plastic rotation of the beam-to-column connection does not exceed 0.15 radians (Lignos and Krawinkler 2011).

Results

The sensitivity of the collapse assessment to the second-order method is summarized in Table 6.3 for the Type I non-ductile moment frame 4-story building, and in Table 6.4 for the Type I ductile moment-frame 4-story building. A comparison of *CMR* values from each model indicates that the seismic collapse assessment of both types of moment frame buildings were very sensitive to a change from a first-order (linear) to a second-order modeling approach.

Table 6.3 Sensitivity of collapse assessment (for SDC D_{max}) for Type I non-ductile moment-frame building (designed for wind, SDC B_{min}) to the method used for second-order effects

		Static Pushover			Dynamic IDA						
Model Aspect	T1 (s)	Cs	Ω	μT	SaMCE (g)	CMR	SSF	ACMR	βRTR	βTotal	Pc | MCE
Baseline (Reference) Model											
Corotational	2.01	0.21	0.41	3.94	0.45	0.93	1.39	1.30	0.37	0.65	34.0%
Alternate Second-Order Method											
Linear (first-order)	1.91	0.21	0.51	2.32	0.47	2.22	1.27	2.81	0.43	0.69	6.6%
P-Δ approximation	2.00	0.21	0.41	3.81	0.45	0.95	1.38	1.31	0.38	0.65	34.1%

Table 6.4 Sensitivity of collapse assessment (for SDC D_{max}) for Type I ductile moment-frame building (designed for SDC D_{max}) to the method used for second-order effects

		Static Pushover			Dynamic IDA						
Model Aspect	T1 (s)	Cs	Ω	μT	SaMCE (g)	CMR	SSF	ACMR	βRTR	βTotal	Pc | MCE
Baseline (Reference) Model											
Corotational	1.36	0.08	2.26	5.63	0.66	1.89	1.46	2.75	0.33	0.45	1.2%
Alternate Second-Order Method											
Linear (first-order)	1.33	0.08	2.64	7.72	0.68	4.01	1.55	6.20	0.40	0.50	0.0%
P-Δ approximation	1.36	0.08	2.25	5.60	0.66	1.79	1.46	2.60	0.34	0.45	1.8%

As in the previous sensitivity study, the *CMR*, static overstrength, and period-based ductility values were greater for the ductile frames while the conditional probability and dispersion were greater for the non-ductile frames. The predicted conditional probability of collapse was much less using a first-order model.

A comparison of the incremental dynamic analyses for the non-ductile moment frame buildings (Figure 6.3) and ductile moment frame buildings (Figure 6.4) supplements the results from the previous tables. Higher dispersion, related to β_{RTR}, was evident in the incremental dynamic analyses for first-order model.

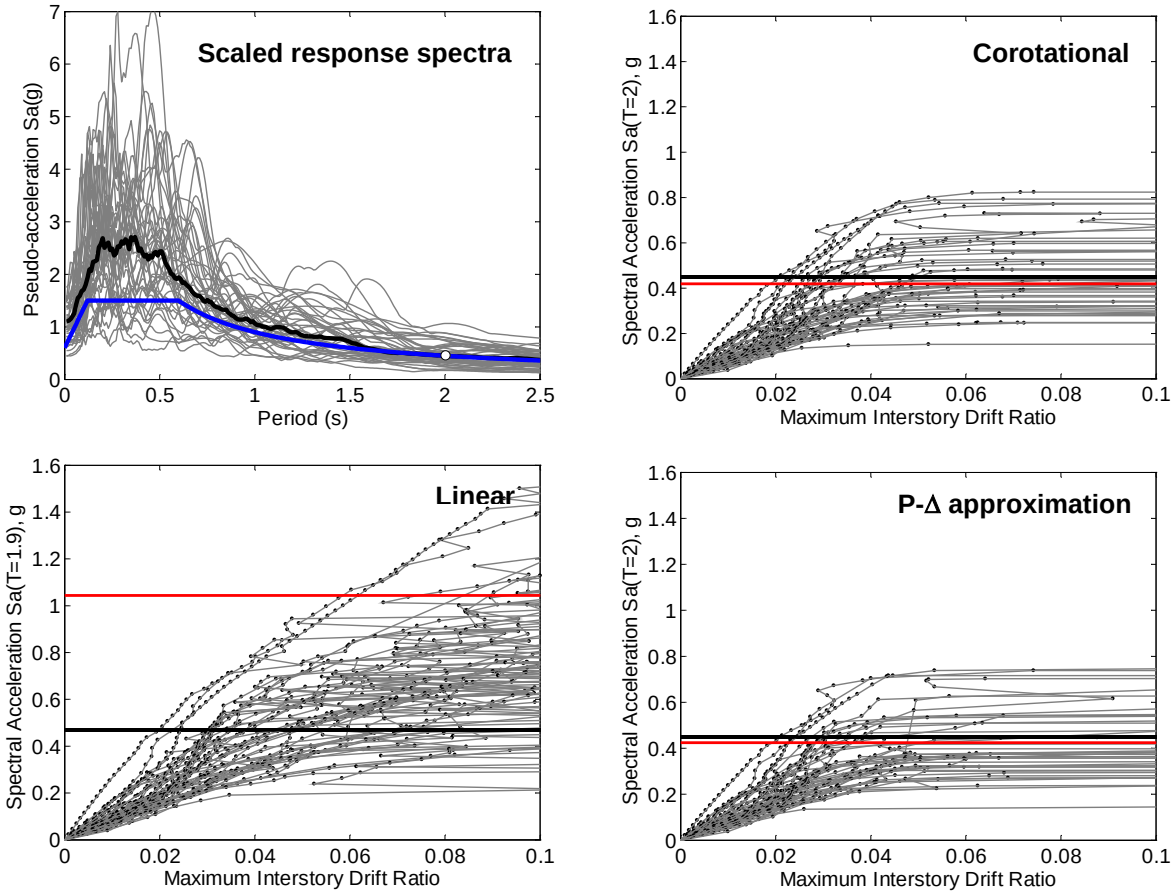

Figure 6.3 Incremental dynamic analyses: Type I non-ductile moment frame 4-story building

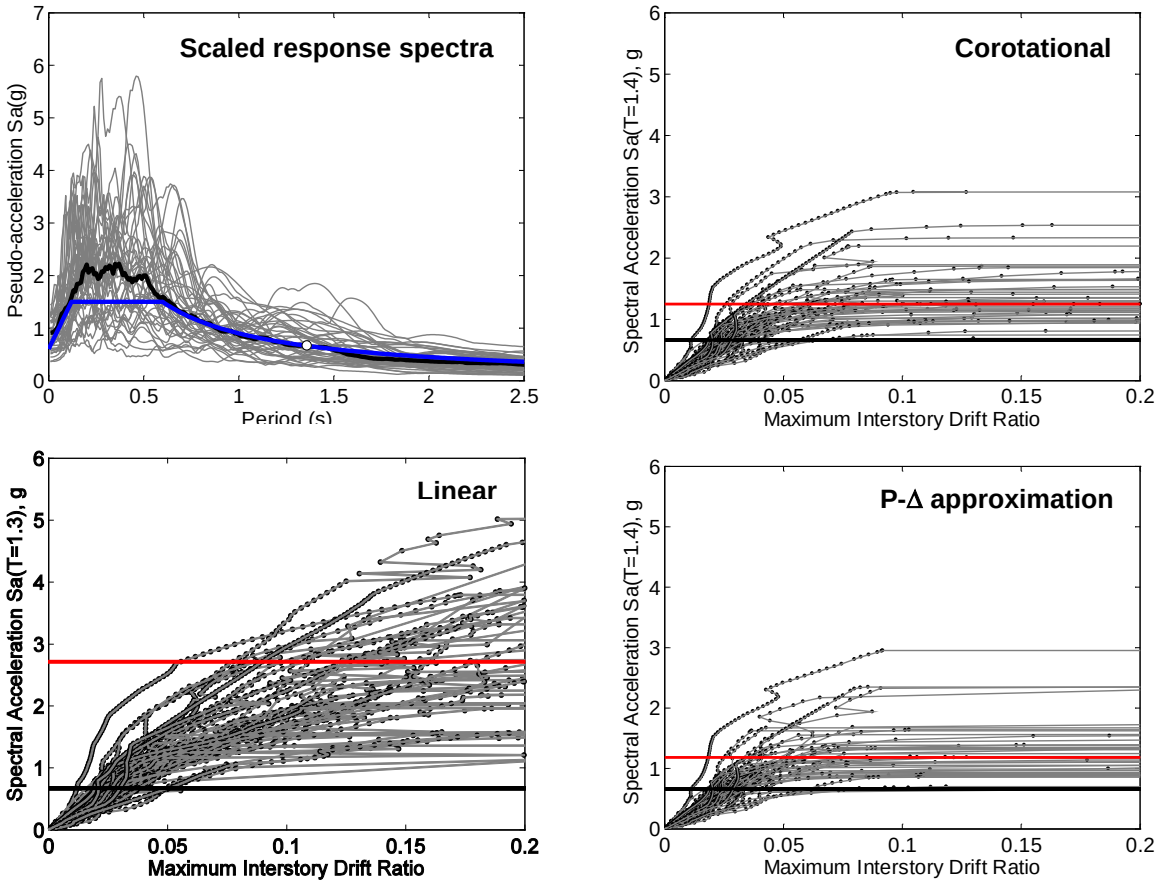

Figure 6.4 Incremental dynamic analyses: Type I ductile moment frame 4-story building

6.1.3 Column Splices

The sensitivity of the seismic collapse assessment of the Type I ductile moment frame 4-story building, designed SDC D_{max}, to the inclusion of splices in the gravity columns is determined in this section. Columns participating in the moment frame were idealized as fixed at the base. Gravity frame columns were idealized as pinned at the base. Column splices were located at story 3. Column splices were assumed to have no rotational capacity (a pinned connection). Partial rotational capacity was not modeled.

The sensitivity study results are summarized in Table 6.5. As a supplement, Figure 6.5 shows the seismic pushover response, story collapse mechanism, and incremental dynamic analyses including column splices (left column of figure) and not including splices (right column of figure). The collapse assessment was sensitive to the inclusion of column splices, both in terms of static overstrength and probability of collapse at the MCE-level ground motion intensity. The inclusion of column splices changed the predicted static collapse story mechanism from story 4 to story 3.

These sensitivity analysis results confirm a previous study of steel moment frame buildings with column splices (Flores 2015) that utilized a lumped column approach.

Table 6.5 Sensitivity of seismic collapse assessment to column splices

(Type I ductile moment frame 4-story building designed SDC D_{max})

Column Splices	T1 (s)	Static Pushover			Dynamic IDA						
		Cs	Ω	μT	SaMCE (g)	CMR	SSF	ACMR	βRTR	βTotal	Pc | MCE
4-Story											
Included	1.60	0.08	1.80	4.92	0.56	1.45	1.45	2.11	0.32	0.44	5%
Non included	1.36	0.08	2.30	6.54	0.66	2.09	1.50	3.15	0.32	0.44	0%

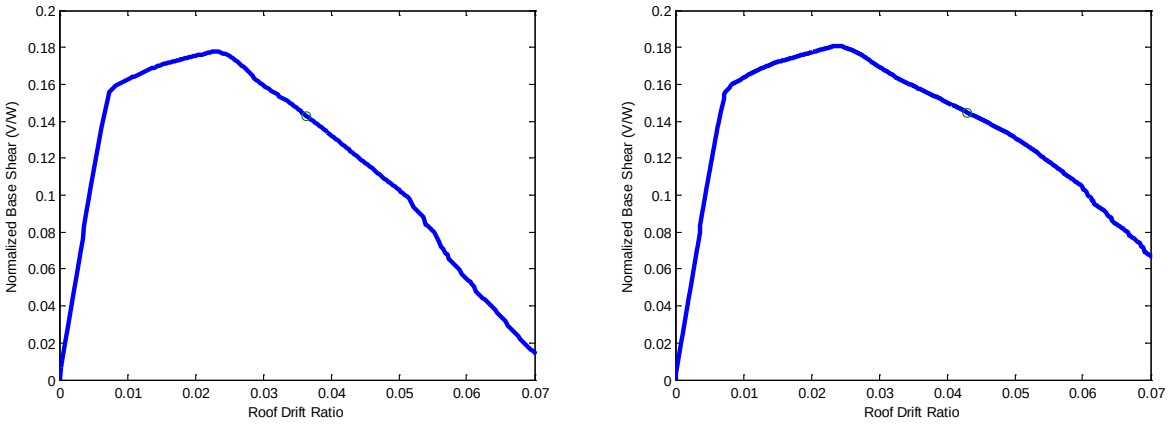

Seismic Pushover Response

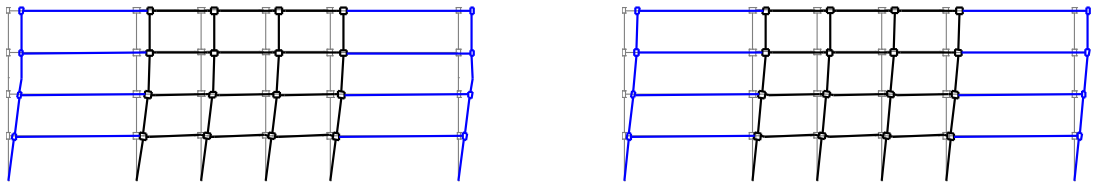

Pushover Story Collapse Mechanisms

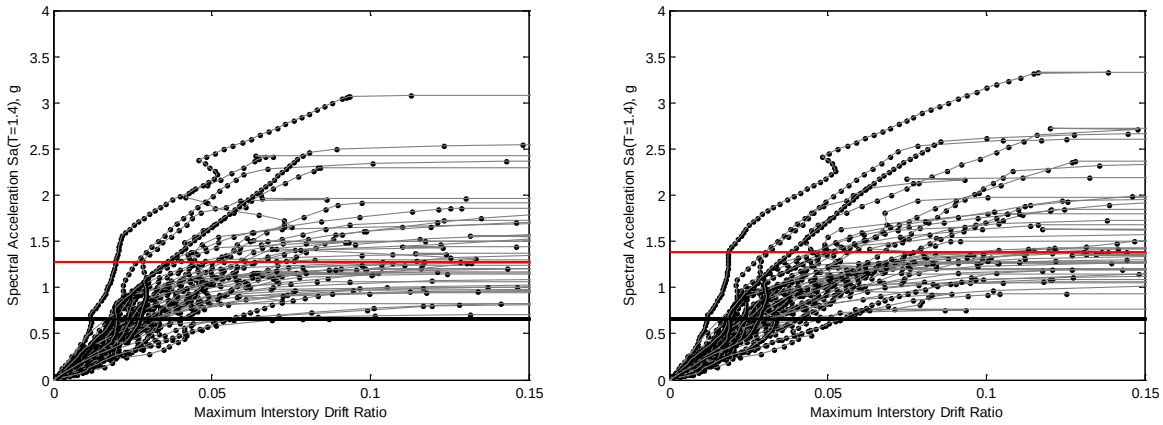

Incremental Dynamic Analyses

a) Column splices b) No column splices

Figure 6.5 Response of Type I ductile 4-story building designed for D_{max}

6.1.4 Ground Motion Spectrum

The sensitivity of the seismic collapse assessment of the Type I non-ductile moment frame 4-story and 8-story building, and the ductile 8-story building, to the ground motion spectrum, of the ground motion set relative to the target spectrum, was determined by comparing the response obtained using spectral matched ground motions to the original (un-matched) response.

Background

Nonlinear response history analysis of a structure requires the use of an input ground motion, and the input ground motion can be derived from a variety of sources:

- real strong-motion ground recordings,
- real recordings that have the amplitude linearly-scaled to match a target spectrum, acceleration or other measure,
- real recordings that have been modified in terms of frequency content, duration, amplitude (and so forth),
- synthetic ground motions based on a "seed" real recording, and
- stochastic ground motions generated using a variety of methods that may or may not be based on physical models.

A set of ground motions (also referred to as an ensemble or suite of ground motions) is then used to capture response variability due to frequency and other attributes of ground motion (Liel et al. 2009). Such variability is termed "record-to-record" (RTR) variability. An alternative approach is to use one ground motion and account for record-to-record variability elsewhere, i.e. in a First Order Second Moment (FOSM) method.

NIST (2011) gives an overview of ground motions, various methods in selecting and scaling ground motions, and the use of ground motions in analysis. Baker et al. (2011) give recommendations for the western United States. Various scaling procedures have been proposed including, for instance, a modal-pushover-based ground-motion scaling procedure (Kalkan and Chopra 2011).

Ground motions in the central and eastern United States, however, differ from ground motions in the western United States due to geological dissimilarities between the two regions, as discussed in Chapter 2. Namely, the central and eastern ground motions have higher frequency content (NIST 2011; GEER Team 2012), owing to various factors: hazard contributions tend to come from smaller-magnitude earthquakes that have less low-frequency content ground motion for a given hazard level; earthquakes have more high-frequency energy; attenuation of motion (especially high-frequencies) is slower due to a high Q factor; and the target uniform hazard spectral shape for a site is shifted towards higher frequencies because the reference ground motion often corresponds to a hard-rock condition, and high-frequency motion is not attenuated as much by near-surface site effects (NIST 2011).

Thus, various ground motion sets have been proposed for structures located in the central and eastern United States. For example, while developing a ground motion prediction model for the central and eastern United States, Somerville et al. (2001) generated a set of ground motions using a physics-based simulation procedure. Fernández (2007), Rix and Fernandez (2006), developed a synthetic ground motion ensemble for the Mississippi embayment area. Celik (2007) used ground motions by Fernández in his analysis of the central and eastern United States in order to capture nonlinear soil behavior (i.e., damping) in site response and resonance in the soil column, and concluded that other ground motions (developed by Wen and Wu 2001)

overestimate the ground motion intensity at low periods and do not capture soil column resonance at higher periods.

Huang et al. (2010a) formed a set of ground motions based on real recordings, mostly from the United States, but augmented with records from Canada and elsewhere in the world where there were large intra-plate earthquakes. Some of the recordings were from the western United States where it was determined that the fault mechanism and high-velocity sedimentary layer were appropriate for the eastern United States.

Hines et al. (2011) propose an ensemble of ground motions for the eastern United States. Their ensemble does not employ amplitude scaling. Instead, the motions were selected from a United States Nuclear Regulatory Commission (NUREG) database (McGuire et al. 2001). In the NUREG database, real recordings (mostly from the western United States) were modified (scaled using theoretical transfer functions) as to be appropriate for the tectonic environment of the central and eastern United States: the modified records exhibit higher spectral accelerations and peak in a higher frequency range compared to the original records.

Since high-frequency ground motions are largely stochastic (Hanks and McGuire 1981; Boore 2003), there is no perceived problem (at least theoretically) with modifying ground motions, although synthetic ground motions may lead to differences in the predicted structural response (e.g. Milburn 2009). Synthetic ground motions were obtainable using deaggregation software at the USGS website (http://earthquake.usgs.gov/research/hazmaps). As of 2015, these USGS simulated ground motions were based on 2002 deggregation data. (Simulations based on 2008 data were not yet available.)

Results

The ground motion set was spectral matched to the FEMA P-695 SDC D_{max} target spectrum by employing an algorithm using wavelets and Broyden updating developed by Adekristi (2013).

Figure 6.6 shows a comparison of the acceleration, velocity, and displacement response histories of the original (un-matched) and spectral matched ground motion for a representative record (FEMA P-695 Far Field ground motion ID No. 1). Figure 6.6 shows that realistic physical behavior (i.e. zero velocity and minimal displacement) was maintained in the matching process for this ground motion. This comparison is in line with recommendations for assessing the adequacy of the spectral-matching process (Grant and Diaferia 2012).

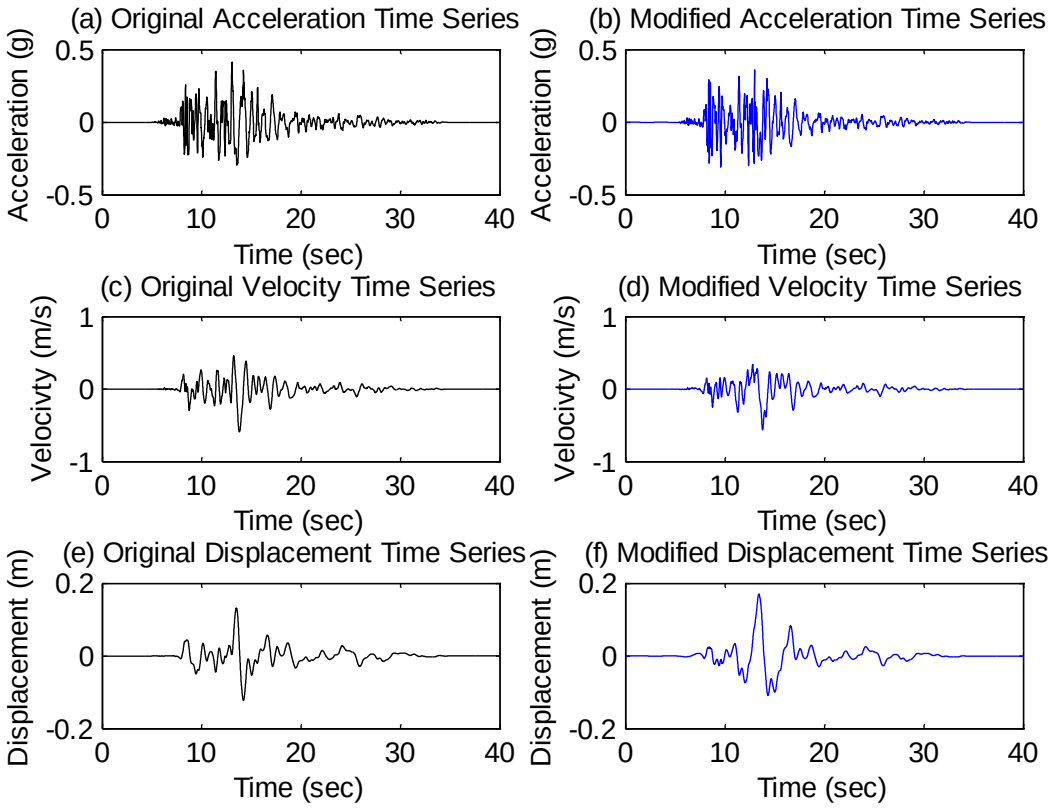

Figure 6.6 Response histories representative ground motion

(FEMA P-695 Far Field ground motion ID No. 1)

For the same ground motion, Figure 6.7 shows a comparison of the response spectrum and normalized arias intensity (acceleration of transient waves) of the original (un-matched) and spectral matched ground motion. The figure shows that the matching process also produced a ground motion that was very similar, in terms of spectral response and ground shaking intensity.

The sensitivity study results are summarized in Table 6.6 for the 4-story and 8-story non-ductile building (with Figure 6.8 and Figure 6.9, respectively), and in Table 6.7 (with Figure 6.10) for the 8-story ductile building. The seismic collapse assessment was sensitive to the ground motion variability (with respect to the target spectrum) and, in general, the matched ground motions led to a higher *CMR* value and consequently a lower probability of collapse. Interestingly, the dispersion in response was much wider for the matched ground motions. A possible cause for the increased dispersion could be attributed to the fact that the high frequency content of ground motions did not match the target spectrum at low periods. To a lesser extent, the low frequency content also did not always match the target spectrum (e.g. Figure 6.8a).

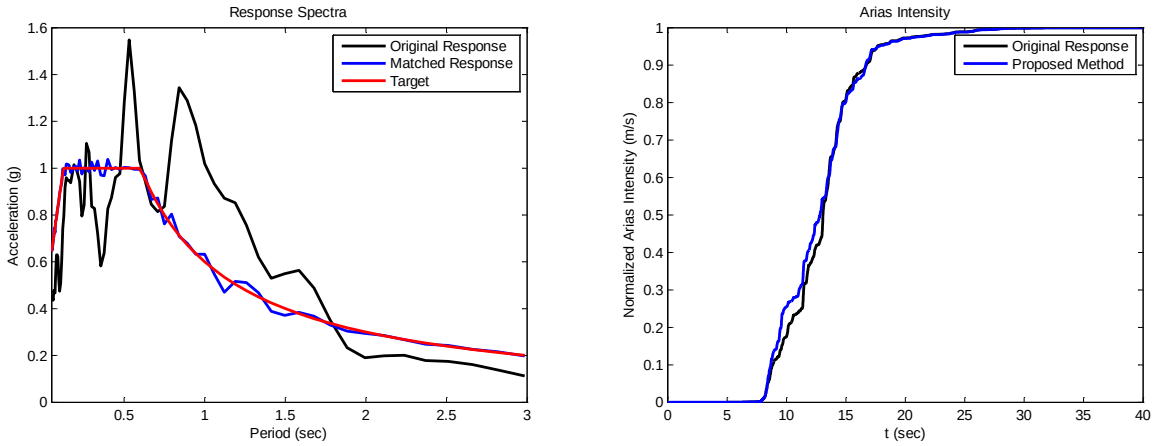

a) Response spectrum b) Normalized arias intensity

Figure 6.7 Response of representative ground motion

(FEMA P-695 Far Field ground motion ID No. 1)

Table 6.6 Sensitivity of seismic collapse assessment to ground motion spectrum

(Type I non-ductile moment frame buildings designed for SDC B_{min} evaluated at SDC D_{max})

Ground Motion Set	T1 (s)	Static Pushover			Dynamic IDA						
		Cs	Ω	μT	SaMCE (g)	CMR	SSF	ACMR	βRTR	βTotal	Pc | MCE
4-Story (MF+GF)											
Original	2.01	0.21	0.41	3.94	0.45	0.93	1.39	1.30	0.37	0.65	34%
Matched						1.08	1.39	1.50	0.34	0.63	26%
8-Story (MF+GF)											
Original	2.85	0.12	0.55	2.35	0.32	0.87	1.27	1.10	0.34	0.63	44%
Matched						1.39	1.36	1.90	0.39	0.66	17%

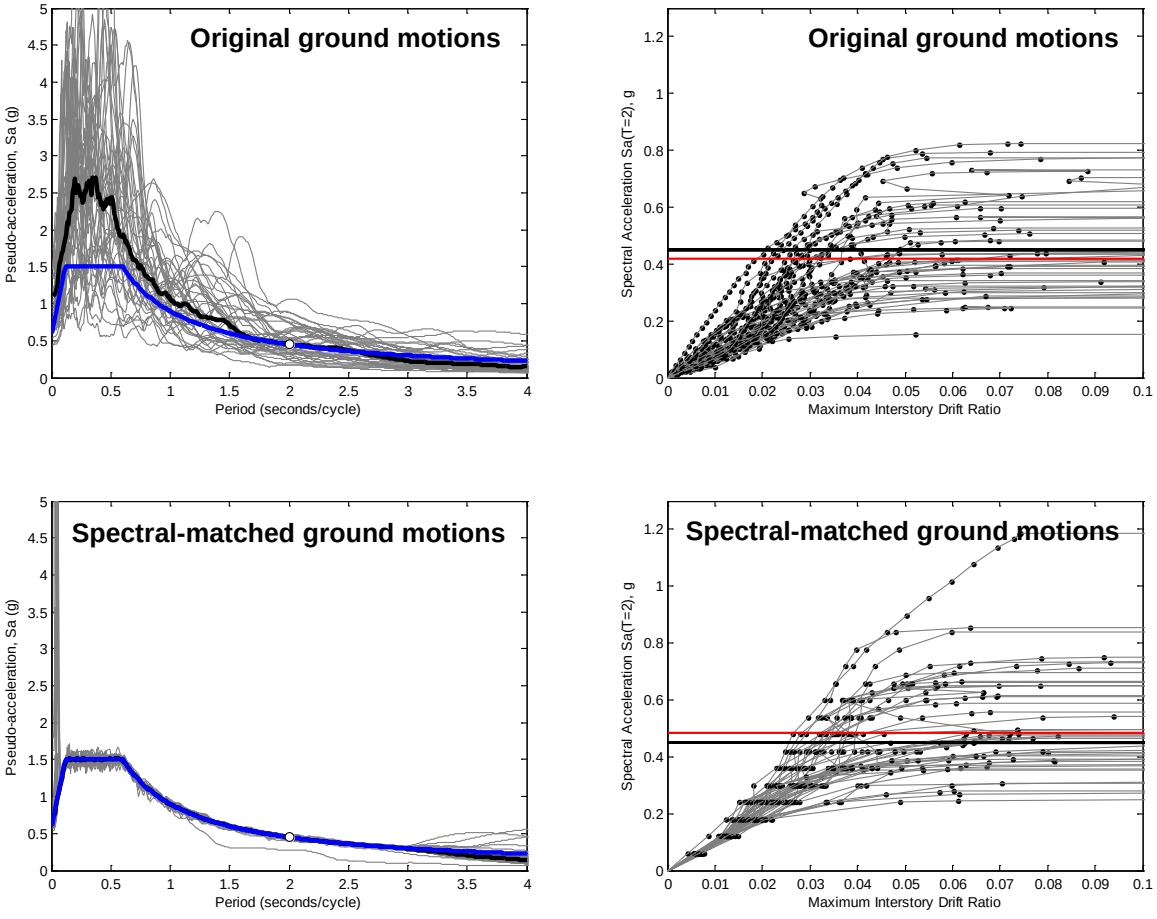

a) Response spectrum b) Incremental dynamic analyses

Figure 6.8 Response of non-ductile 4-story building

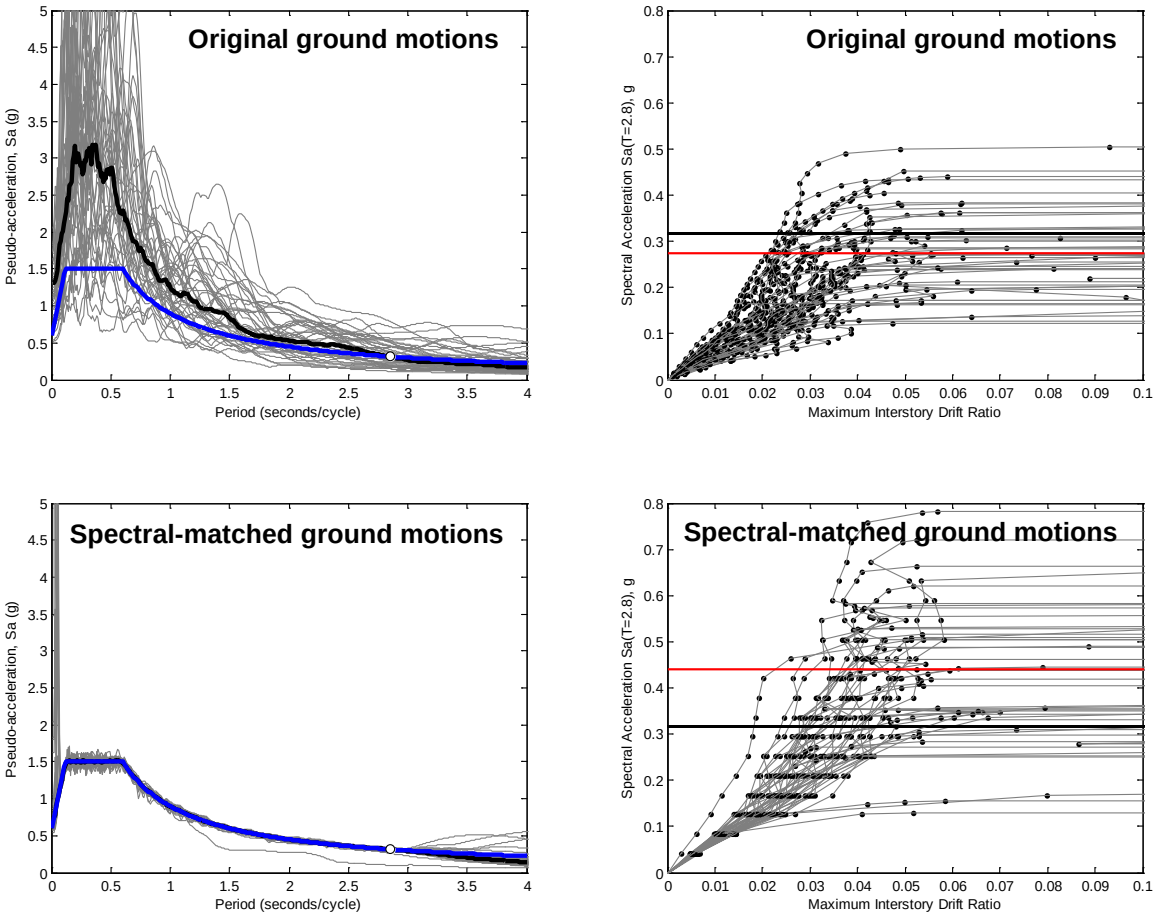

a) Response spectrum b) Incremental dynamic analyses

Figure 6.9 Response of non-ductile 8-story building

Table 6.7 Sensitivity of seismic collapse assessment to ground motion spectrum

(Type I ductile moment frame buildings designed for SDC D_{min} evaluated at SDC D_{max})

Ground Motion Set	T1 (s)	Static Pushover			Dynamic IDA						
		Cs	Ω	μT	SaMCE (g)	CMR	SSF	ACMR	βRTR	βTotal	Pc | MCE
8-Story											
Original	2.88	0.05	1.31	3.44	0.31	0.87	1.36	1.18	0.34	0.46	36%
Matched						1.12	1.36	1.52	0.37	0.48	19%

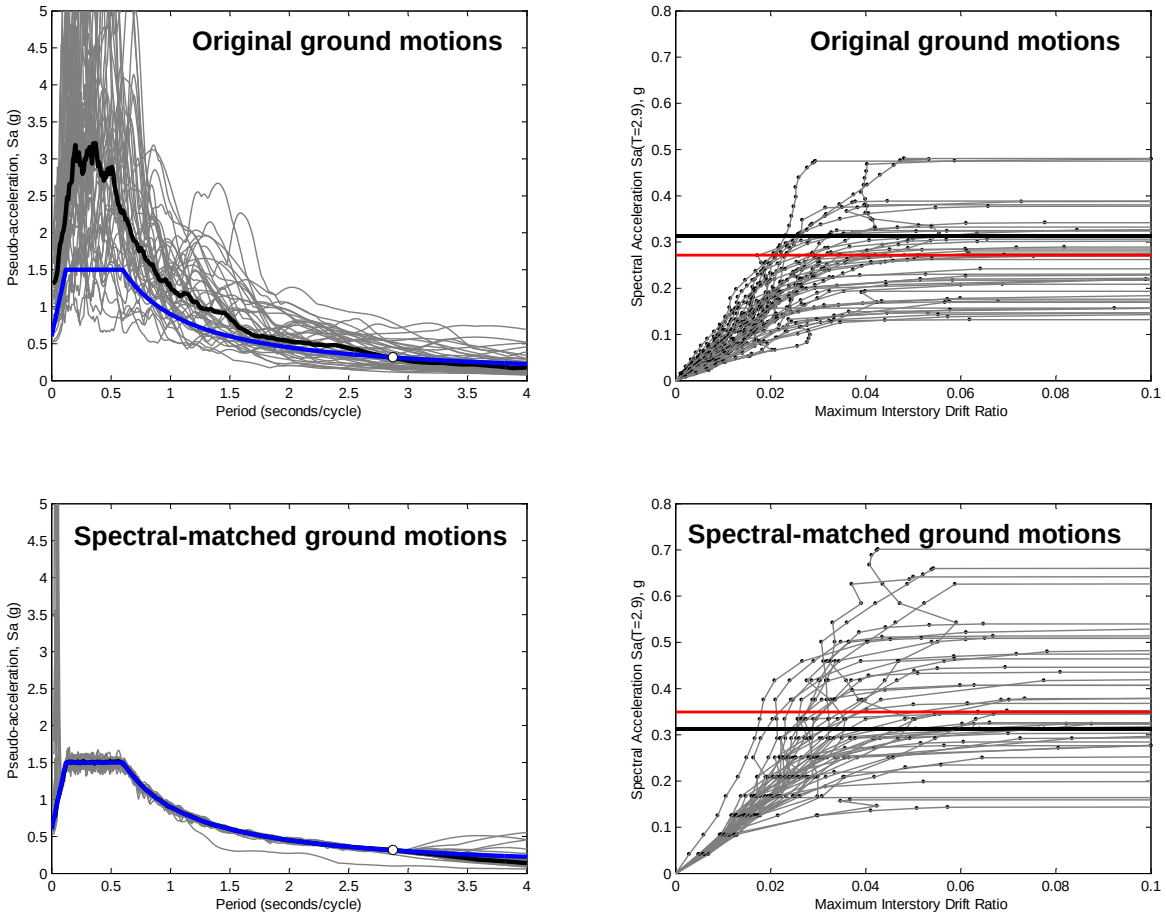

a) Response spectrum b) Incremental dynamic analyses

Figure 6.10 Response of ductile 8-story building

6.1.5 Intensity Measure Conditioning Period

The sensitivity of the seismic collapse assessment of the Type I ductile moment frame 4-story building to the conditioning period used to define the seismic hazard intensity measure (spectral acceleration) was determined.

The sensitivity study results are summarized in Table 6.8. Three definitions of spectral acceleration were considered, based on fundamental building period (1) calculated from an eigenvalue analysis T_1, and determined empirically for (2) wind analysis T_w using ASCE 7-10, or (3) for seismic analysis $T_e = C_u T_a$ using ASCE 7-10.

The results indicate that using a longer period to define the spectral acceleration intensity measure slightly increased the collapse margin ratio and decreased the conditional probability of collapse. The difference in response could be attributed to the nature of the response spectrum for typical ground motions (and as a corollary, ground motion sets) that exhibit higher accelerations for lower periods. Thus, all other factors being equal, a lower value for the conditioning period would be expected to suggest a higher vulnerability to seismic collapse.

Table 6.8 Sensitivity of seismic collapse assessment to ground motion spectrum

(Type I ductile moment frame 4-story building designed for SDC D_{min} evaluated at SDC D_{max})

Seismic Intensity Measure (IM)	T (s)	Static Pushover			Dynamic IDA						
		Cs	Ω	μT	SaMCE (g)	CMR	SSF	ACMR	βRTR	βTotal	Pc | MCE
4-Story											
Sa(T1)	1.36	0.08	2.26	5.63	0.66	1.89	1.46	2.75	0.33	0.45	1.2%
Sa(Tw)	1.10	0.08	2.26	5.63	0.82	1.89	1.40	2.64	0.34	0.45	1.6%
Sa(Te)	0.95	0.08	2.26	5.63	0.94	1.87	1.37	2.56	0.34	0.45	1.9%

6.1.6 Risk Integration Method

This section uses the collapse risk of a 4-story ductile moment frame building as an example to determine the sensitivity of seismic collapse assessment to the method used to integrate hazard and risk. [See also Judd and Charney (2014c).]

For purposes of comparison (i.e. with Eads et al. 2013), the ground motion hazard was determined using the 2002 USGS hazard data for a location in Los Angeles. The fundamental building period, T_1 = 1.33 seconds, and seismic collapse fragility were based on Eads et al. (2013).

Background

In probabilistic seismic hazard analysis, there are three analytically equivalent methods to integrate hazard and fragility.

Method 1: Numerical Derivative of Hazard Curve

The integration of hazard and fragility is shown in the following equation and is the so-called "risk integral" which calculates an annual rate of failure, λ_F:

$$\lambda_F = -\int_0^{+\infty} P(F|a)\left(\frac{d\lambda_a}{da}\right)da \tag{6.1}$$

The failure rate usually refers to the collapse rate, λ_c which can also be used to calculate the risk of collapse in an exposure time (such as calculating the probability of collapse in 50 years). The minus sign accounts for the negative slope of the hazard curve (in PSHA the hazard curve is the probability of exceeding a value so it decreases as the demand parameter increases). An equivalent version of the risk integral could use an absolute value instead of a minus sign.

The risk integral equation represents the concept that the probability of failure is the probability of the ground motion times the probability of building failure given that level, integrated over all possible levels of hazard (Kennedy 2011). The equation assumes ergodicity, meaning hazard and fragility (conditional failure) are independent and "the structure does not deteriorate" and is "instantaneously restored to its original state after each damaging earthquake." This approximation is only accurate as long as the failure rate is small. For probabilities of failure greater than 1%, the approximation overestimates risk (Der Kiureghian 2005).

The hazard curve is not commonly represented using a continuous function, but instead a discrete data set is used, so in practice the derivative is approximated numerically. See, for example, FEMA P-58 (FEMA 2012a).

Method 2: Derivative of Fitted Hazard Curve

An alternative approach to using the discrete set of hazard data points is to fit the hazard curve with a function (usually a polynomial) and then take the derivative of that function when calculating Equation 6.1 (see Eads et al. 2013).

Method 3: Derivative of Fragility Curve

As shown before

$$\lambda_F \quad = \quad \int_0^{+\infty} \lambda_a \, f(a) \, da \tag{6.2}$$

Note that this form of the risk integral (Equation 6.2) requires the derivative of the fragility curve—the CDF, which yields the probability density function (PDF). This is a more stable approach than taking the derivative of the hazard curve.

Results

A comparison between risk calculated using numerical derivative (Method 1) and curve fitting (Method 2) is shown in Figure 6.11. For Method 2, various degree polynomials were fit to the hazard curve. The effect of the methods to determine the slope of the hazard curve is shown in Figure 6.11a. For the hazard curve, the black line was linearly interpolated in log-log space. For the risk deaggregation curves (Figure 6.11b) the gray line was based on the incremental slope, and colors represent a 3-degree (cyan), 4-degree (blue), 5-degree (magenta), and 6-degree (green) polynomial curve fit for the hazard curve.

A 4-degree or more polynomial curve fit converges to the same cumulative risk (Figure 6.11c). For very small spectral accelerations (spectral acceleration less than 0.1g), a 5-degree polynomial is a very bad fit (this effect is not visible in Figure 6.11a). Using the derivative of the fitted polynomial hazard curve gives the collapse rate (number of predicted collapses per year) λ_c = 3.51×10^{-4} and the seismic collapse risk of 1.74% in 50 years (green line) for the Los Angeles location considered. Using the incremental derivative of hazard curve gives λ_c = 3.97×10^{-4} and the seismic collapse risk of 1.97% in 50 years.

Figure 6.12 shows a comparison between Method 1, Method 2 using a 4-degree polynomial fit, and Method 3 (integration by parts and the derivative of the fragility curve). Using Method 3 gives λ_c = 3.97×10^{-4} and the seismic collapse risk of 1.97% in 50 years (red line). For reference, the seismic collapse assessment by Eads et al. (2013) using a 4-degree polynomial curve fit determined that the collapse rate was λ_c = 3.51×10^{-4}.

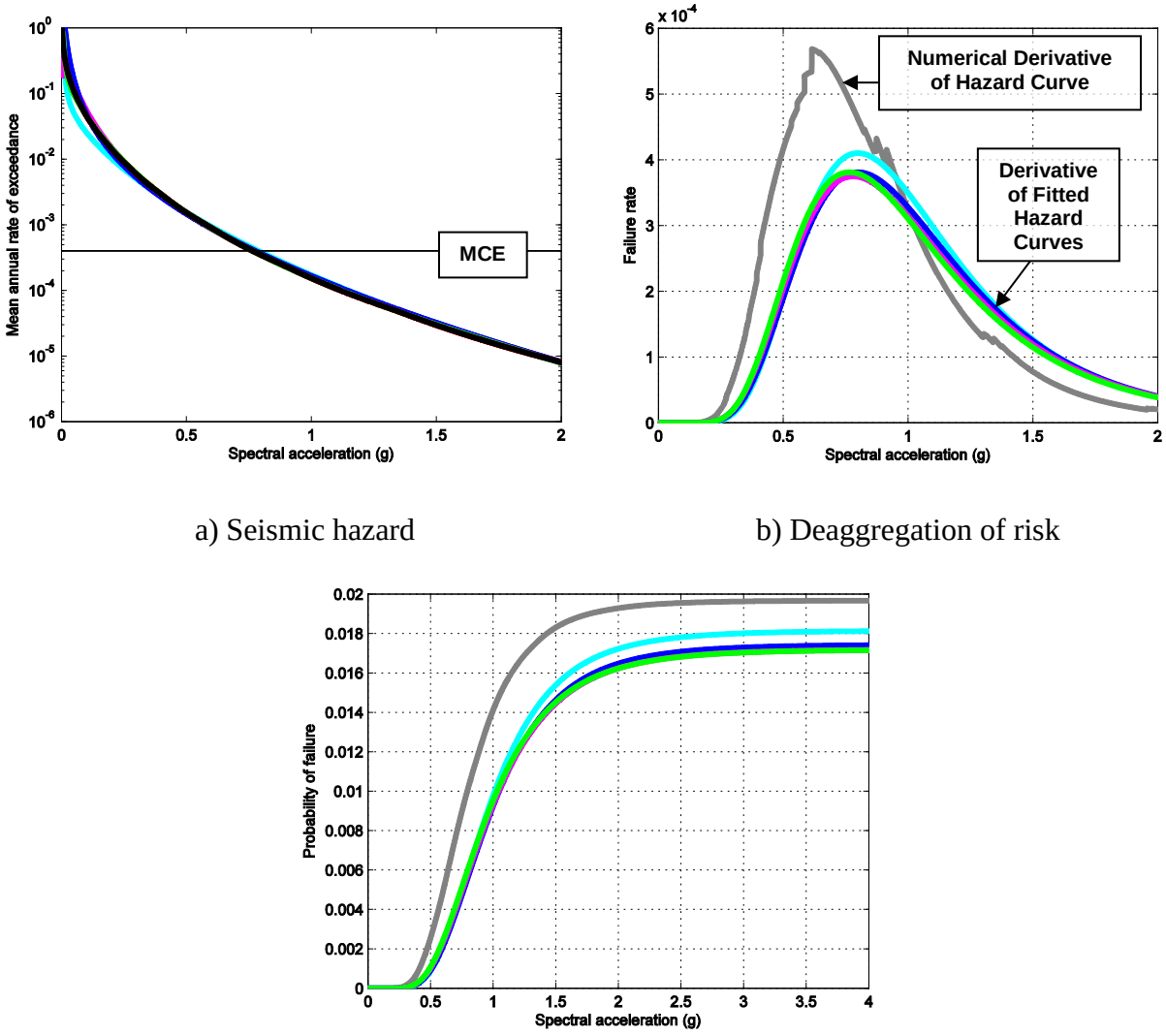

a) Seismic hazard

b) Deaggregation of risk

c) Cumulative collapse risk over exposure time (50 years)

Figure 6.11 Seismic hazard, deaggregation of collapse risk, and cumulative risk (example 4-story ductile moment frame building)

The method used to calculate risk may significantly affect the collapse assessment. Both the contribution of different hazards to this risk (the deaggregation shown in the Figure 6.12a) and the cumulative value of risk calculated (Figure 6.12b) varied. The derivative of the fragility curve (Method 3) was a more stable approach compared to using the other methods, because the

derivative of the hazard curve was avoided. Besides, using a curve-fit (Method 2) was not necessarily more accurate, because the derivative of the curve was unstable.

The deaggregation of the risk was also different in each method because the numerical integration of incremental hazard (da) differed for each method. Thus, Method 1 and Method 3 produced the same value of risk, but differed in terms of hazard contributions, which is easily visualized using deaggregation. Deaggregation of collapse risk was analogous to using deaggregation of ground motion to ascertain magnitude and distance pairs that are primary contributors to hazard (Chapman 1995).

Using Method 2, risk may be over- or under-estimated, depending on the shape of the hazard curve relative to the fragility curve. Hazard curve points are derived from interpolated data, so the validity of using a fitted curve is questionable. Furthermore, fitted curves were sensitive at low values of spectral accelerations. This may be an additional concern for ascertaining multi-hazard performance at lower intensity levels (i.e. serviceability and immediate occupancy levels).

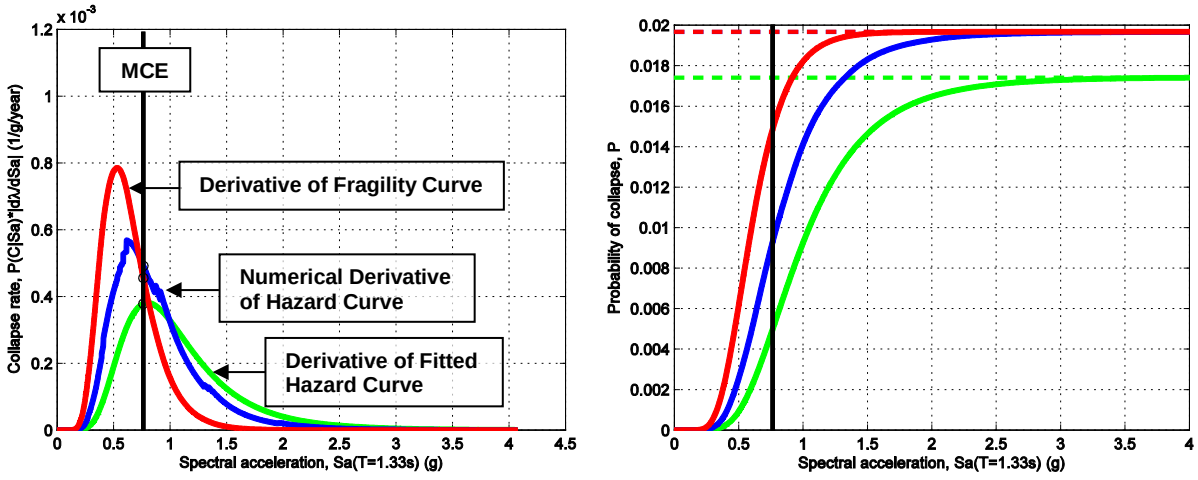

a) Deaggregation of risk b) cumulative risk (50 years)

Figure 6.12 Hazard, deaggregation of risk, and cumulative risk for example structure

6.1.7 Regional Risk

The sensitivity of the seismic collapse assessment to regional risk was explored by contrasting two locations: a location with frequent seismicity, in the San Francisco bay area (38.0° latitude, -121.7° longitude), and a location with infrequent seismicity, in the Memphis metropolitan area (35.2° latitude, -89.9° longitude).

The deaggregation of seismic hazard (spectral acceleration) corresponding to a long-period structure (T = 1.0 seconds) is shown in Figure 6.13 and Figure 6.14 for both locations. For San Francisco (Figure 6.13) the dominant contribution to hazard was along one fault line producing magnitude 5.0 to 7.0 earthquakes. For Memphis (Figure 6.14) the dominant hazard was one fault (New Madrid) about 60 km away. Compared to San Francisco, however, in Memphis there are large uncertainties with respect to source and size of potential earthquakes.

Structural vulnerability results for partially-restrained composite-connection (PR-CC) moment frame buildings (summarized earlier in Chapter 4 Table 4.9) indicate the lateral system static overstrength is somewhat less than anticipated, keeping in mind that the overstrength factor Ω in ASCE 7-10 is a conservative upper bound intended to protect vulnerable components. The primary collapse mechanism of the buildings is generally column hinging of the lower story columns (see Chapter 4). The low collapse margin ratios adjusted for spectral shape and period elongation (as reflected in the *ACMR*) for the 4 story buildings (performance groups 1 and 2) suggest that the mid-rise buildings were more sensitive to collapse than higher-rise buildings.

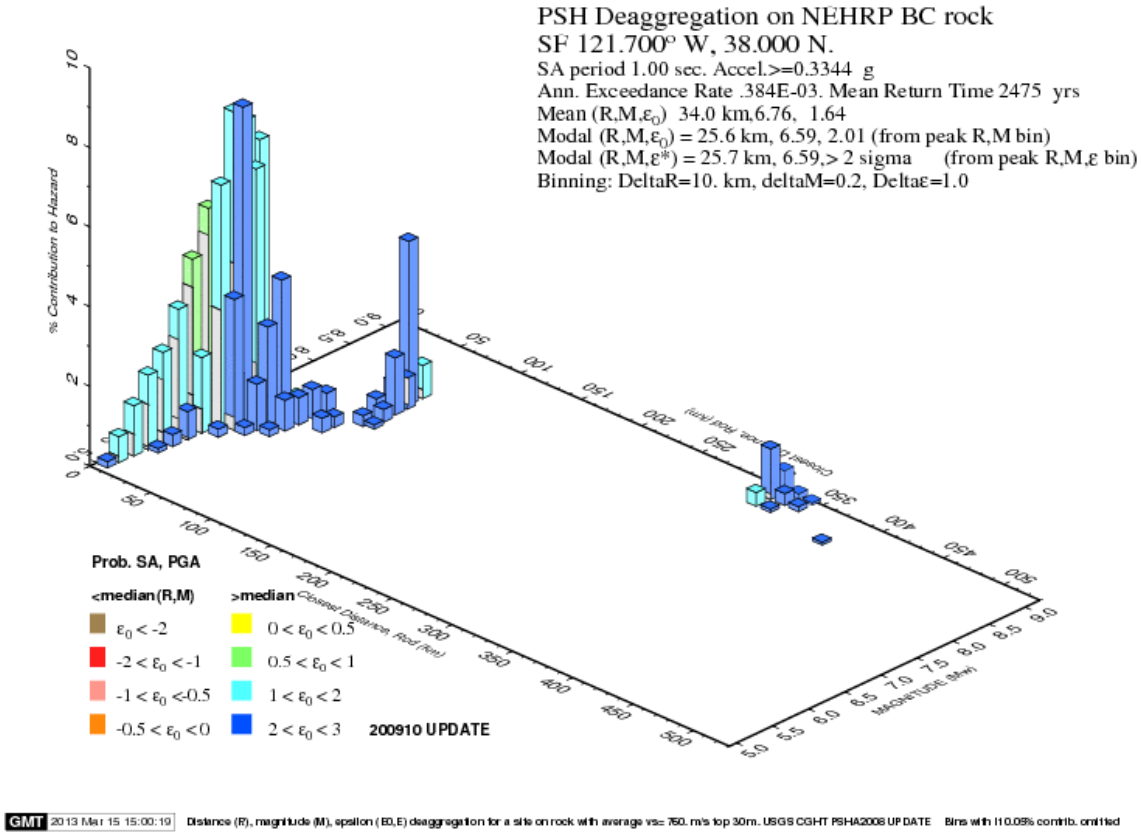

Figure 6.13 Seismic hazards for San Francisco bay area location

(Generated using USGS utility https://geohazards.usgs.gov/deaggint/2008/)

Table 6.3 gives the collapse risk for each building performance group. Site response was included based on the NEHRP relationship and topographic data. Seismic collapse risk was calculated based on achieving the *ACMR* values in Table 4.9. It is noted that this definition of fragility (achieving the *ACMR*) represents the predicted sensitivity of code-conforming PR-CC buildings in general, not the sensitivity of the specific buildings proportioned in the analytical study by Bozorgmehr (2012). For this reason, building fragility was not constant (it increased or decreased geographically) and was for a consistent safety margin.

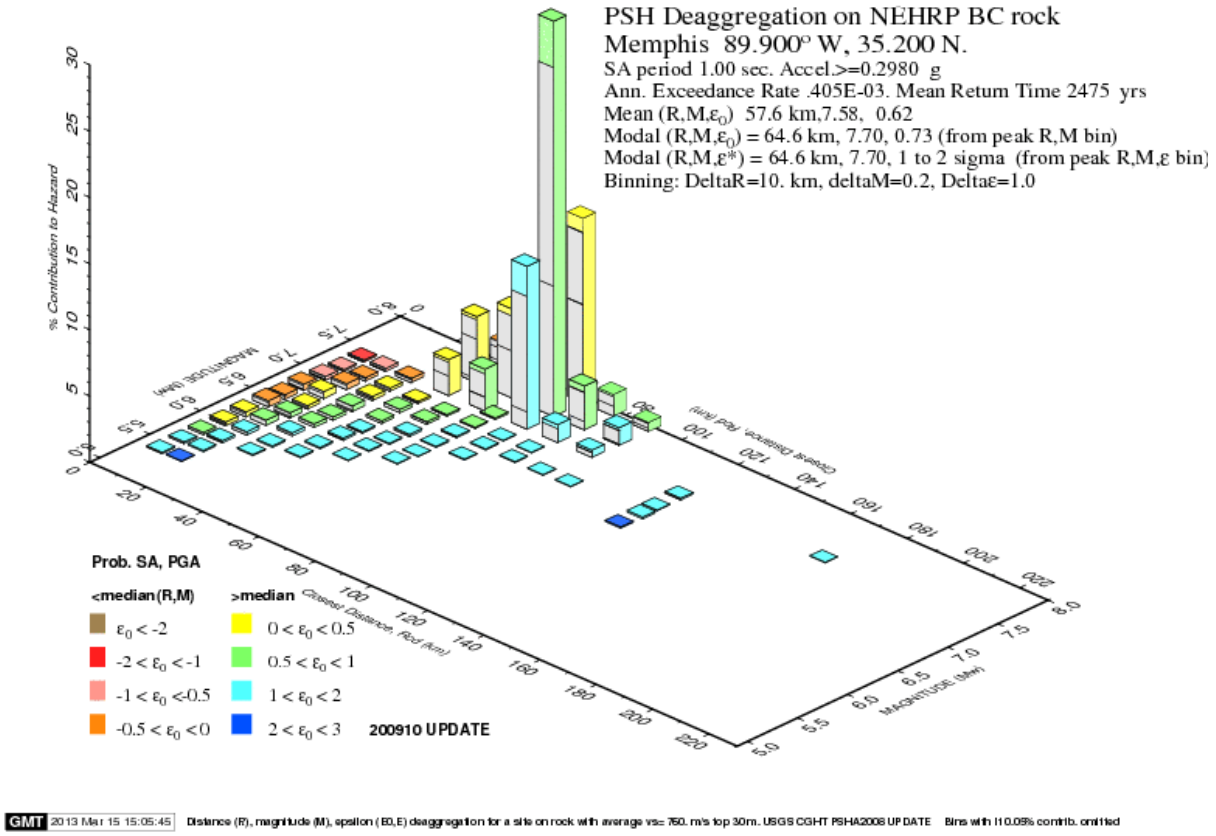

Figure 6.14 Seismic hazards for Memphis metropolitan area location

(Generated using USGS utility https://geohazards.usgs.gov/deaggint/2008/)

The assessment was fairly insensitive to the V_{s30}, but highly sensitive to the method used to calculate the risk (λ_c = 2.57×10^{-4} collapses per year using the derivate of the fragility curve, compared to λ_c = 7.44×10^{-4} collapses per year using the derivative of the fitted hazard curve).

All the PR-CC buildings meet the acceptable risk objective of the building code (seismic collapse risk not greater than 1% in 50 years), except for 4-story buildings with a 12-foot story height in the San Francisco location. Surprisingly, for 6- to 8-story buildings, the risk of collapse in the Memphis location was greater than in the San Francisco location.

Importantly, a deaggregation of the seismic collapse risk (not shown in Table 6.9) reveals that the contribution to risk shifts from likely events (earthquakes with return periods less than 2,475 years) to unlikely events (earthquakes with return periods greater than 2,475 years).

Table 6.9 Collapse risk analysis of PR-CC buildings

Performance Group Summary					Risk analysis (Prob. collapse in 50 years)	
No.	Stories	Hx (ft)	Te (s)	ACMR	SF	Memphis
1	4	12	0.87	2.19	1.30%	0.76%
2	4	14	0.98	2.89	0.45%	0.39%
3	6	12	1.2	3.99	0.12%	0.17%
4	6	14	1.36	3.96	0.12%	0.17%
5	8	12	1.51	4.74	0.05%	0.10%
6	8	14	1.71	4.25	0.08%	0.14%

6.1.8 Site Response

This section explores the effect of site response on the seismic collapse assessment of the Type I 4-story non-ductile moment frame building. The maps were generated by integrating seismic hazard and collapse fragility at every 0.5-degree latitude and longitude.

Figure 6.15 compares the sensitivity of the seismic collapse assessment to the method used to correlate the average shear wave velocity with soil amplification of ground motion, assuming V_{s30} = 180 m/s (D/E boundary). The response not including the lateral reserve strength of the shear tab connections is indicated in blue. The response including the reserve lateral strength from the shear tab connections is indicated in purple. The response including both reserve lateral strength and a slack cable collapse prevention system is indicated in orange.

Figure 6.15a shows contoured regions where the risk of collapse exceeds 1% in 50 years using the NEHRP/ASCE 7-10 (ASCE 2010) soil amplification method. Figure 6.15b shows contoured regions where the collapse risk exceeds 1% in 50 years using the NGA WUS soil amplification method and assuming V_{s30} = 180 m/s (D/E boundary). The predicted difference in seismic collapse risk was significant in the central and eastern United States.

The sensitivity of the assessment to using topographic data as a proxy for average shear wave velocity in the top 100 feet of the soil is shown in Figure 6.16. Again the predicted difference in conditional collapse was significant, but to a lesser extent.

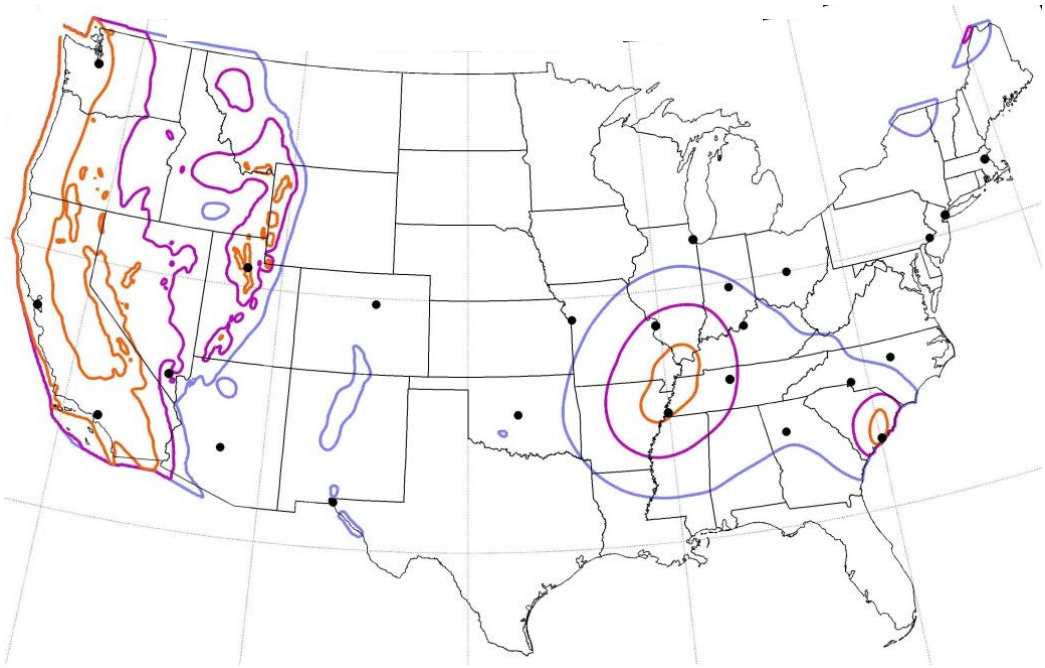

a) NEHRP/ASCE 7-10 soil amplification method

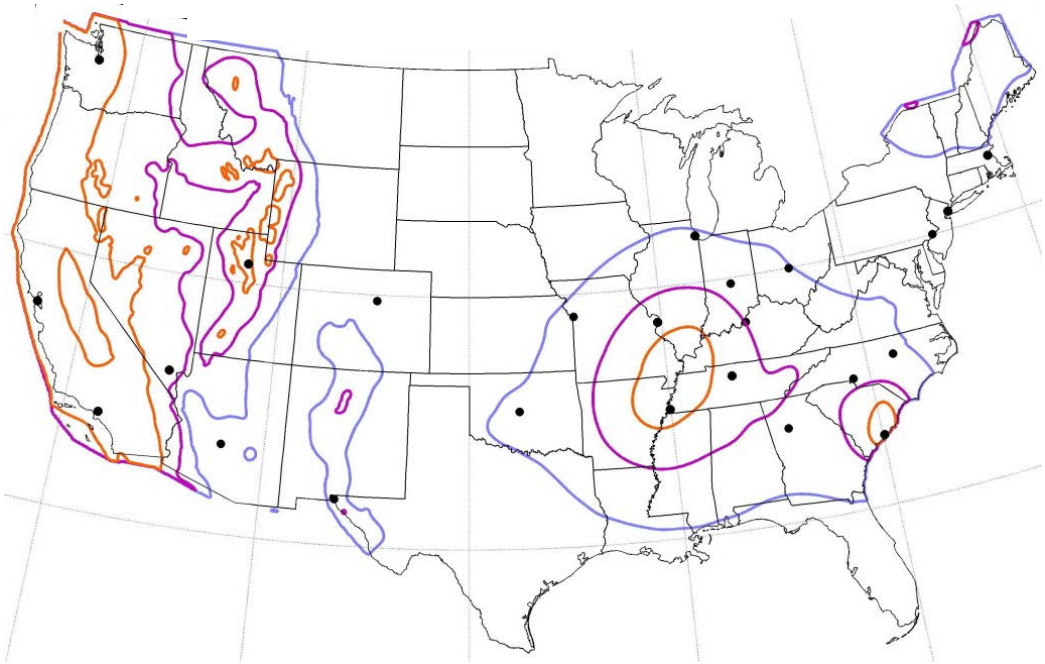

b) NGA WUS soil amplification method

Figure 6.15 Contour regions where the seismic collapse risk exceeds 1% in 50 years

V_{s30} = 180 m/s (D/E boundary), Type I non-ductile moment frame 4-story building

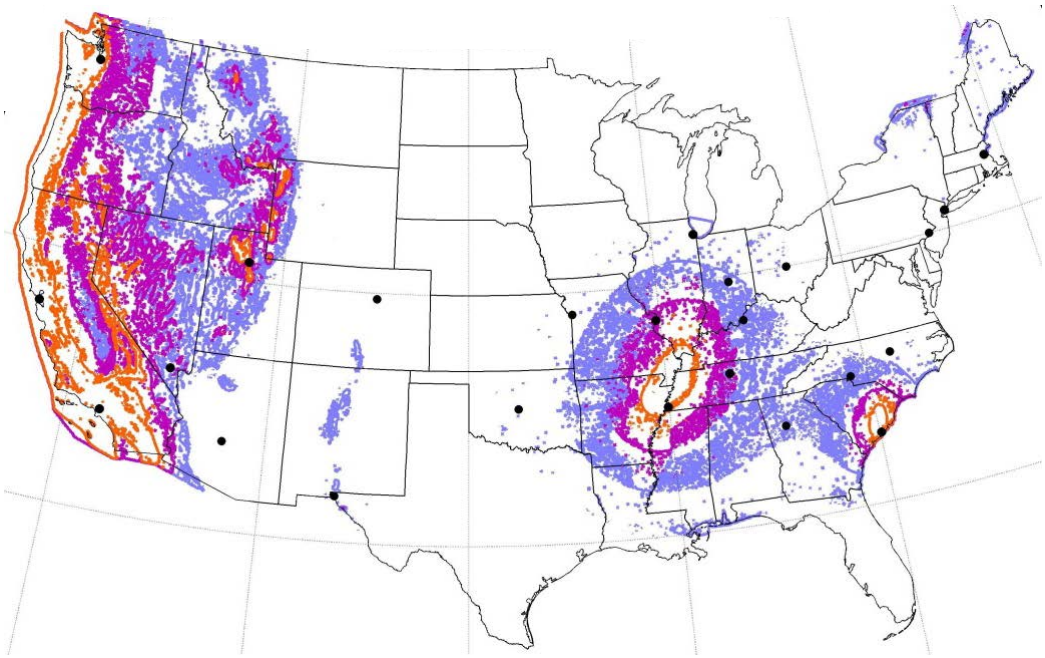

a) NEHRP/ASCE 7-10 soil amplification method

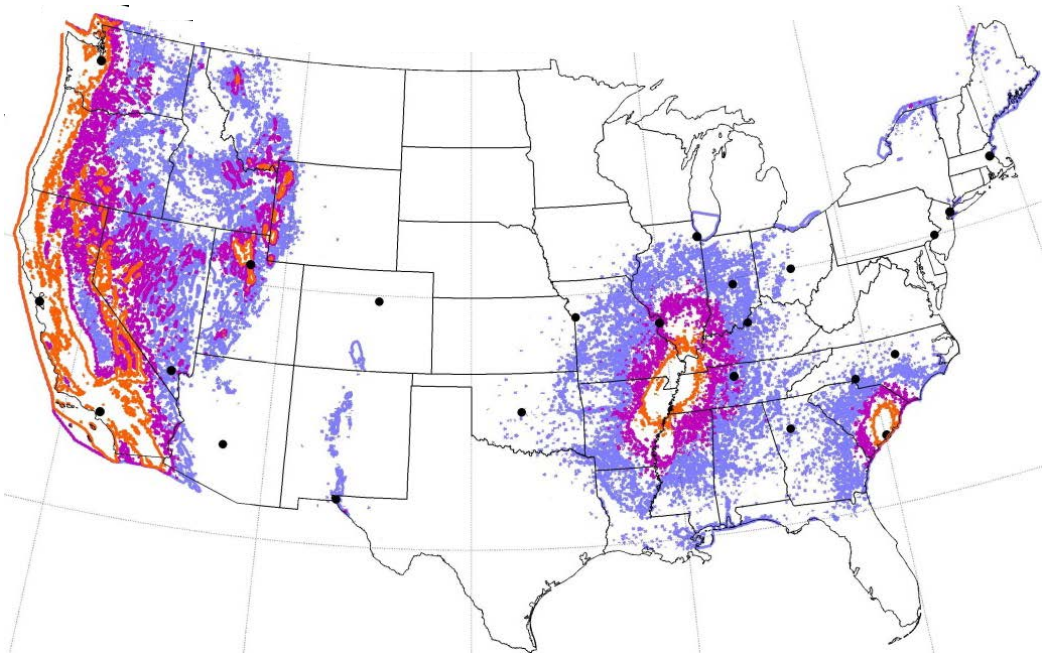

b) NGA WUS soil amplification method

Figure 6.16 Contour regions where the seismic collapse risk exceeds 1% in 50 years V_{s30} based on topographic proxy data, Type I non-ductile moment frame 4-story building

6.2 Wind Collapse Sensitivity

This section discusses the sensitivity of the wind collapse assessment to the characteristic equivalent single-degree-of-freedom model used to represent the main wind-force resisting system (MWFRS) and the gravity framing system, to the static overstrength of the building determined in a wind pushover analysis, to damping, to the fundamental period of vibration of the building, to cyclic degradation of the characteristic system behavior, and to the duration of the wind event.

The Type III non-ductile moment frame 10-story building is considered. As previously discussed (in Chapter 3), the building was a composite steel-frame building designed for a basic wind speed of 115 mph and ASCE 7-10 terrain exposure category C. The equivalent lateral strength of the main wind-force resisting system relative to the building weight, (V_{max}/W) was 0.1, based on a wind pushover analysis of the Type II 10-story building (Chapter 5). Although it is acknowledged that the lateral pushover strength is building-specific, the 0.1 value was used as a baseline for comparison of differing main wind-force resisting systems in the sensitivity study. When considering the effects of gravity framing, the lateral strength contribution from gravity framing was conservatively assumed to be 10% compared to the MWFRS (Judd and Charney 2014b). This value was also recognized to be building-specific and was only used to establish a baseline for comparison in the sensitivity study.

The fundamental period, T_w was approximated by the building height, $H/75$ = 1.8 seconds, based on ASCE 7-10 (ASCE 2010) Equation C26.9-7. This equation is valid for up to 300-ft tall buildings. Building "density" was estimated to be 8 pcf based on the building weight, W equal to 16,200 kips. The wind base-shear force, V_{wind} was equal to 515 kips, and the corresponding wind base shear coefficient, C_{s-wind} was equal to 0.032.

Figure 6.17 shows the monotonic envelope and fully-reversed cyclic behavior of the characteristic main wind-force resisting systems investigated. Three types of steel moment frame (MF) systems (non-ductile, semi-ductile, and ductile) were considered. The non-ductile moment frame was intended to be representative of a fracturing steel moment frame. The semi-ductile moment frame was intended to be similar to the intermediate moment frame ("IMF") system used in structures detailed for seismic resistance. The ductile moment frame was intended to be representative of special moment frame ("SMF") seismic systems, such as steel moment frames with reduced-beam-sections. Stiff non-ductile (braced) frames, and shear wall main wind-force resisting systems were also considered for purposes of comparison.

The potential effect of three types of gravity framing (GF) systems, non-ductile, semi-ductile, and ductile (typical gravity framing with shear-tab connections) was incorporated. Characteristic behavior of the gravity framing systems is shown in Figure 6.18.

Force-deformation behavior parameters used in this study, including in-cycle degradation, matched those parameters used in FEMA P-440A (FEMA 2009b), except for the parameters for the semi-ductile main wind-force resisting system, which were used for comparison purposes in this study. The semi-ductile main wind-force resisting system parameters used in this study were based on the AISC *Seismic Design Manual* (AISC 2012) story drift ratio requirement (0.02) for intermediate moment frames, and a monotonic envelope approximately halfway between the ductile and non-ductile responses.

The results of the sensitivity studies are summarized in Table 6.10 to Table 6.15 (shown in subsequent pages) for the baseline duration (28 minutes) and a reference wind speed of 20 mph.

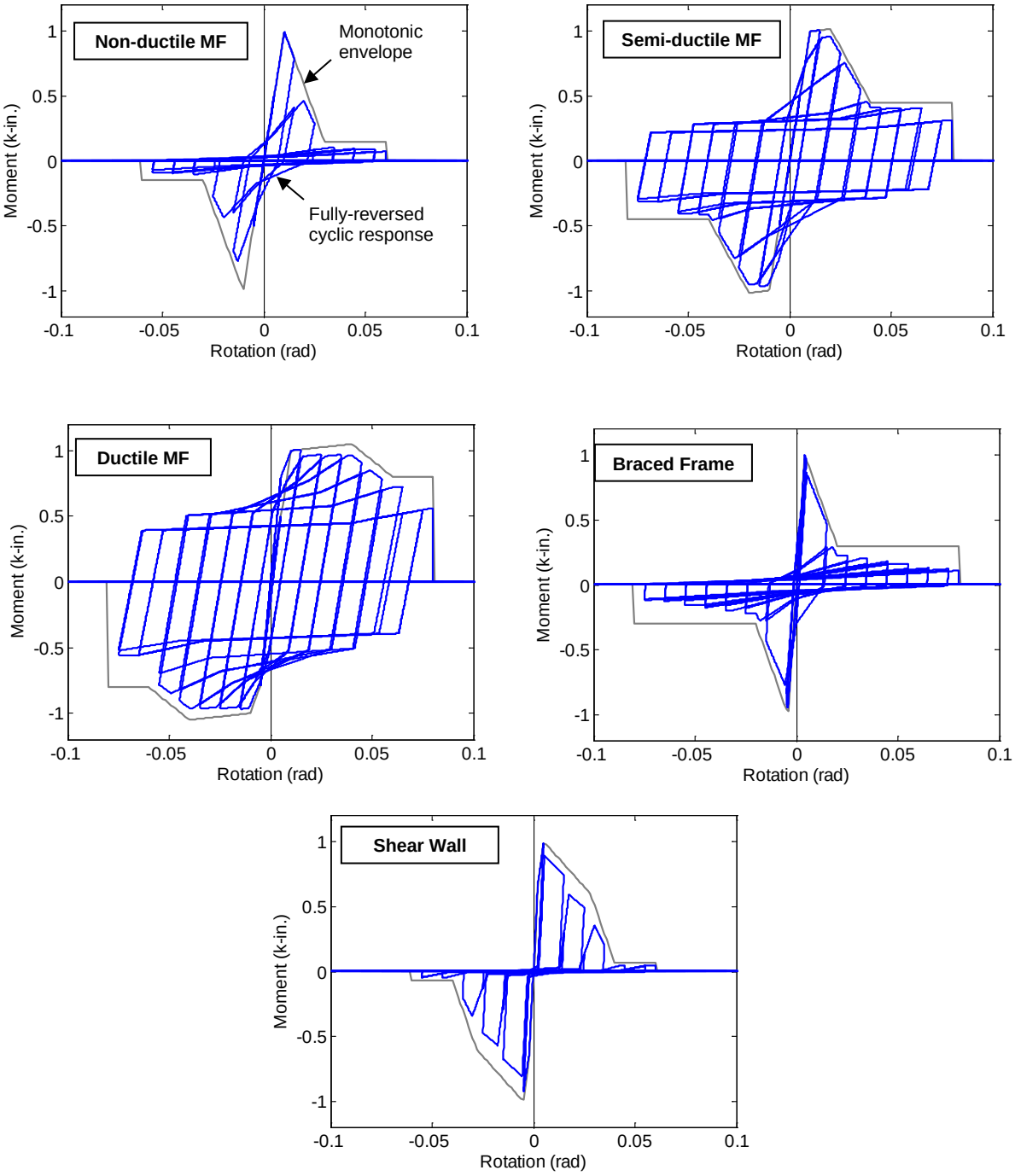

Figure 6.17 Characteristic main wind-force resisting system (MWFRS)

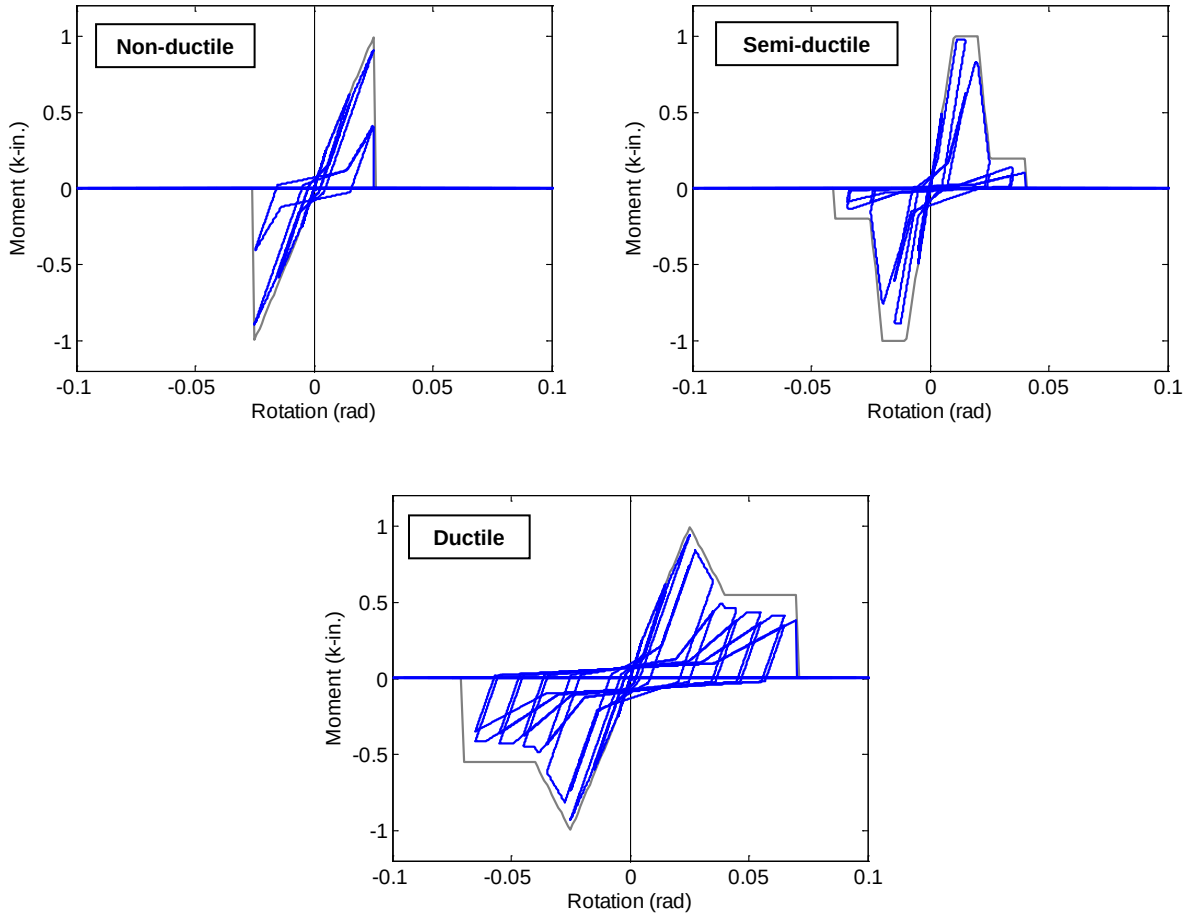

Figure 6.18 Characteristic gravity framing (GF) system

6.2.1 Main Wind-Force Resisting System and Gravity Framing System

The sensitivity of wind collapse assessment to the characteristic main wind-force resisting system was determined. Table 6.10 shows that all the characteristic main wind-force resisting systems passed the target risk (established based on ASCE 7-10, as described in Chapter 5), except for the non-ductile moment frame system. It should be emphasized that the results are intended for comparative purposes only. The results were partly subjective due to the incorporation of epistemic uncertainty. Moreover, the tabulated results were only for the interior

of the United States without consideration of tornado wind hazards. Figure 6.19a shows regions of the United States where the wind collapse risk exceeds 0.35% for the non-ductile moment frame system. Figure 6.19b shows the effect of including tornado hazards. The non-ductile moment frame system has a high wind-collapse risk in much of central United States and along the southern and eastern coastlines.

The results in Table 6.10 suggest that some ductility or moderate degree of reserve capacity was effective at reducing risk, but highly ductile systems may not necessarily reduce the wind collapse risk.

The effect of the type of gravity framing system is given in Table 6.11. The reserve strength of the gravity framing always increased the *CMR* and lowered the collapse risk, compared to the main wind-force resisting system alone (Table 6.10), but the type (ductility) of the gravity frame system was not significant relative to the moment-frame type (ductility).

Table 6.10 Effect of Main Wind-Force Resisting Framing System (MWFRS)

MWFRS	Tw (s)	CMR	β_{RTR}	β_{Total}	$P_{f,50}$
Non-ductile MF	1.80	1.41	0.047	0.149	0.30%
Semi-ductile MF		1.55	0.060	0.154	0.08%
Ductile MF		1.60	0.064	0.155	0.05%
Braced Frame		1.55	0.040	0.147	0.06%
Shear Wall		1.55	0.056	0.152	0.07%

Table 6.11 Effect of gravity framing system

Gravity Frame (GF)	MF/GF	CMR	β_{RTR}	β_{Total}	$P_{f,50}$
Non-ductile Moment Frame (MF)					
Ductile	0.10	1.46	0.042	0.147	0.16%
Semi-ductile		1.48	0.047	0.149	0.14%
Non-ductile		1.48	0.046	0.149	0.14%
Ductile Moment Frame (MF)					
Ductile	0.10	1.63	0.067	0.156	0.03%
Semi-ductile		1.65	0.053	0.151	0.02%
Non-ductile		1.63	0.060	0.154	0.03%

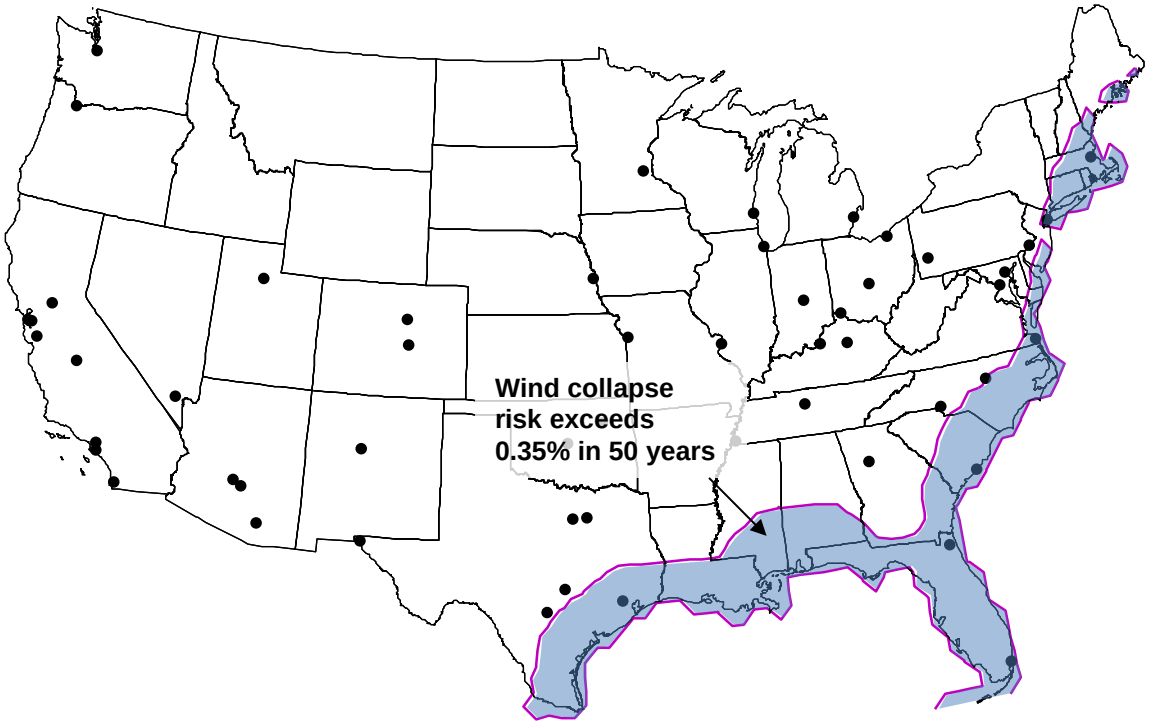

a) Extrapolated ASCE 7-10 wind hazards

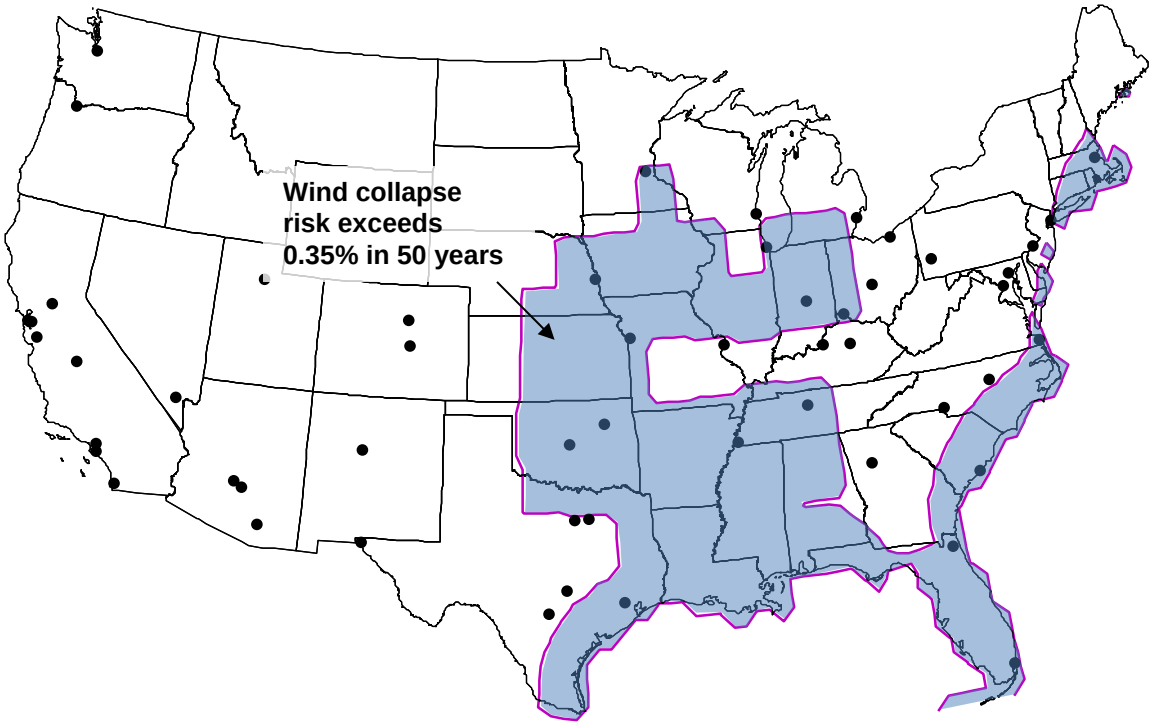

b) Extrapolated based on tornado wind hazards

Figure 6.19 Regions where wind collapse risk exceeds 0.35% in 50 years (non-ductile MF)

6.2.2 Static Overstrength

The effect of strength and ductility for steel moment frame systems is examined in Table 6.12. The assumed lateral strength ratio was varied from the baseline condition, 0.1 up to 0.7 in order to examine if a moderately-ductile system with a reduced relative strength provides the same wind collapse safety as a stronger non-ductile system. (The lateral strength ratio is roughly equivalent to the inverse of an "*R*" value for wind.) The results, based on an equivalent single-degree-of-freedom model and a target wind collapse risk of 0.15% in 50 years, lead to a maximum wind *R* equal to 1.10, for the Type III non-ductile moment frame 10-story building.

Table 6.12 Effect of lateral strength ratio and ductility

MWFRS	F_{max}/W	CMR	β_{RTR}	β_{Total}	$P_{f,50}$
Non-ductile MF	0.100	1.41	0.047	0.149	0.30%
Semi-ductile MF	0.100	1.55	0.060	0.154	0.08%
	0.095	1.53	0.057	0.153	0.09%
	0.090	1.48	0.053	0.151	0.15%
	0.085	1.46	0.063	0.155	0.21%
	0.080	1.43	0.060	0.154	0.29%
	0.075	1.39	0.059	0.153	0.41%
	0.070	1.34	0.058	0.153	0.71%

6.2.3 Damping, Fundamental Period, and Cyclic Degradation

The effect of damping and the fundamental period is shown in Table 6.13, and the effect of cyclic degradation is shown in Table 6.14. For comparison with the baseline model, the fundamental period was calculated using ASCE 7-10 (ASCE 2010) Equation 26.9-2 through Equation 26.9-4. These equations relate to the lower-bound of measured natural frequency data of actual buildings.

The *CMR*, dispersion, and the collapse risk were sensitive to the level of damping assumed in the analysis, as expected, but were less sensitive to the fundamental period estimation. The effect of cyclic degradation in the characteristic system (gravity frame was not included) was significant, doubling the risk of wind collapse.

Table 6.13 Effect of damping and fundamental period on non-ductile moment frame

MWFRS		CMR	β_{RTR}	β_{Total}	$P_{f,50}$
Damping	ζ=1.0%	1.41	0.047	0.149	0.30%
	ζ=2.5%	1.50	0.046	0.149	0.11%
Fundamental Period	T_w=1.80s	1.41	0.047	0.149	0.30%
	T_w=2.28s	1.39	0.042	0.147	0.34%

Table 6.14 Effect of cyclic degradation

Cyclic Degradation	CMR	β_{RTR}	β_{Total}	$P_{f,50}$
Non-ductile Moment Frame (MF)				
Included	1.41	0.047	0.149	0.30%
Not included	1.50	0.065	0.156	0.14%
Ductile Moment Frame (MF)				
Included	1.60	0.064	0.155	0.05%
Not included	1.69	0.067	0.156	0.02%

6.2.4 Wind Duration

The effect of wind load duration is shown in Table 6.15. For illustration, the along-wind (Figure 6.20) and cross-wind (Figure 6.21) responses, respectively, are shown for four intensity levels: reference, strength-level, prior to collapse, and at collapse wind speeds. The left column of each figure shows the responses for the baseline duration (28 minutes). The right columns show the responses for the 138-minute (2.3 hours) duration. The wind load history is shown in the upper plot. Load values are normalized in terms of the building weight. The hysteresis behavior is shown in the middle plot. Load values are normalized relative to the lateral strength of the equivalent single-degree-of-freedom model. The drift ratio history is shown in the lower plot. Ratcheting of the lateral load was especially evident in the along-wind response. For the ductile moment frame model, collapse was imminent for drift ratios between 0.02 and 0.04.

Figure 6.22 shows the incremental dynamic analyses for both durations. The collapse margin ratio (*CMR*) was calculated as the ratio of the median collapse intensity to the strength-level intensity (115 mph for Risk Category II). Duration led to a 6% difference in *CMR*.

Clearly, the duration had a profound effect (evident in Figure 6.20 and Figure 6.22), but the relationship between duration and risk was not predictable. It is postulated that the unpredictable effect of duration may be caused, in part, due to the replayed wind load history records. A more robust study, however, is required to better understand the relationship.

Table 6.15 Effect of duration on ductile moment frame system

MWFRS		CMR	β_{RTR}	β_{Total}	$P_{f,50}$
Duration (min.)	28	1.60	0.064	0.155	0.05%
	55	1.51	0.059	0.153	0.11%
	138	1.50	0.049	0.150	0.12%
	257	1.44	0.036	0.146	0.18%

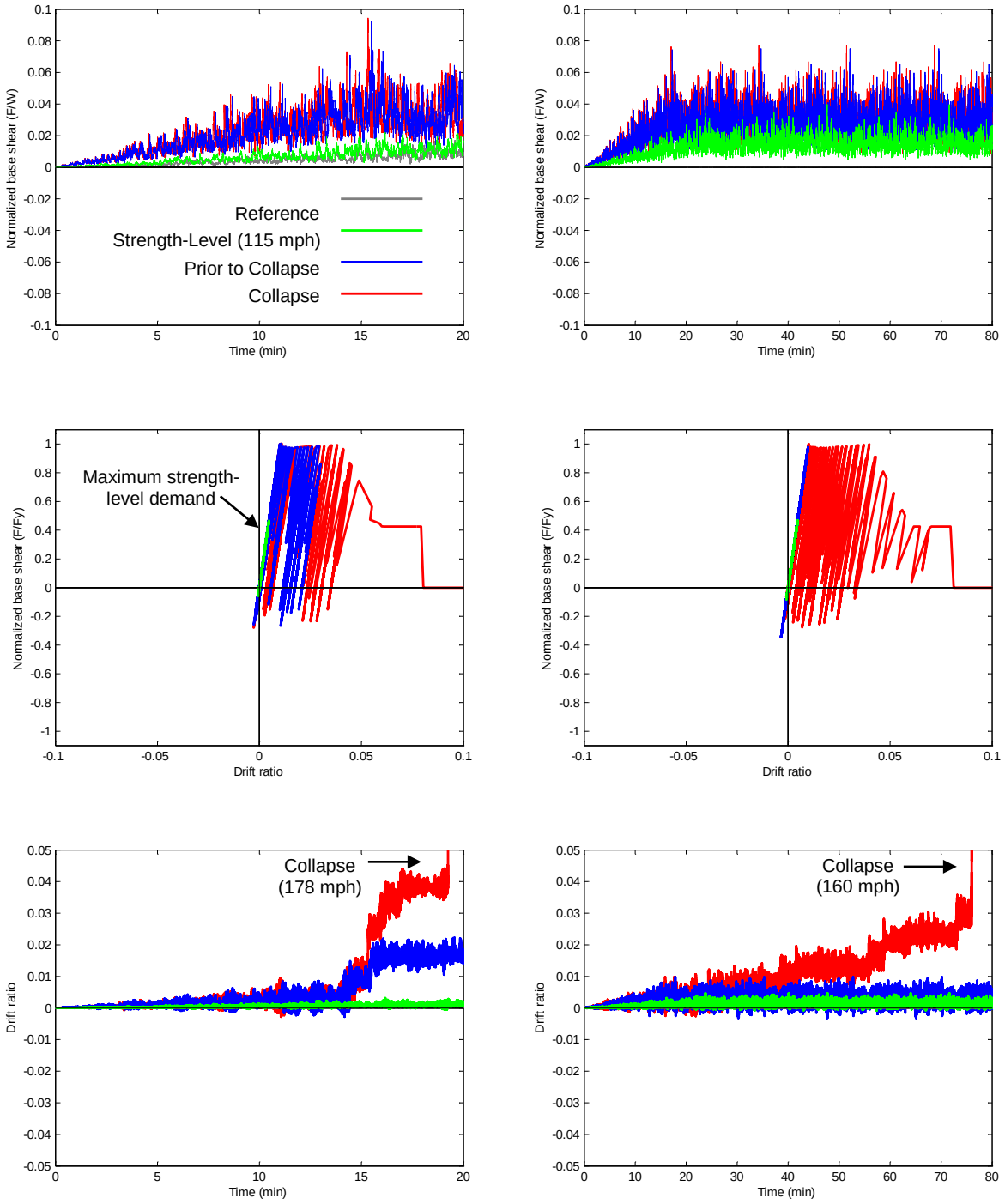

a) 28-minute duration

b) 138-minute duration

Figure 6.20 Along-wind (90°) response history for ductile moment frame system

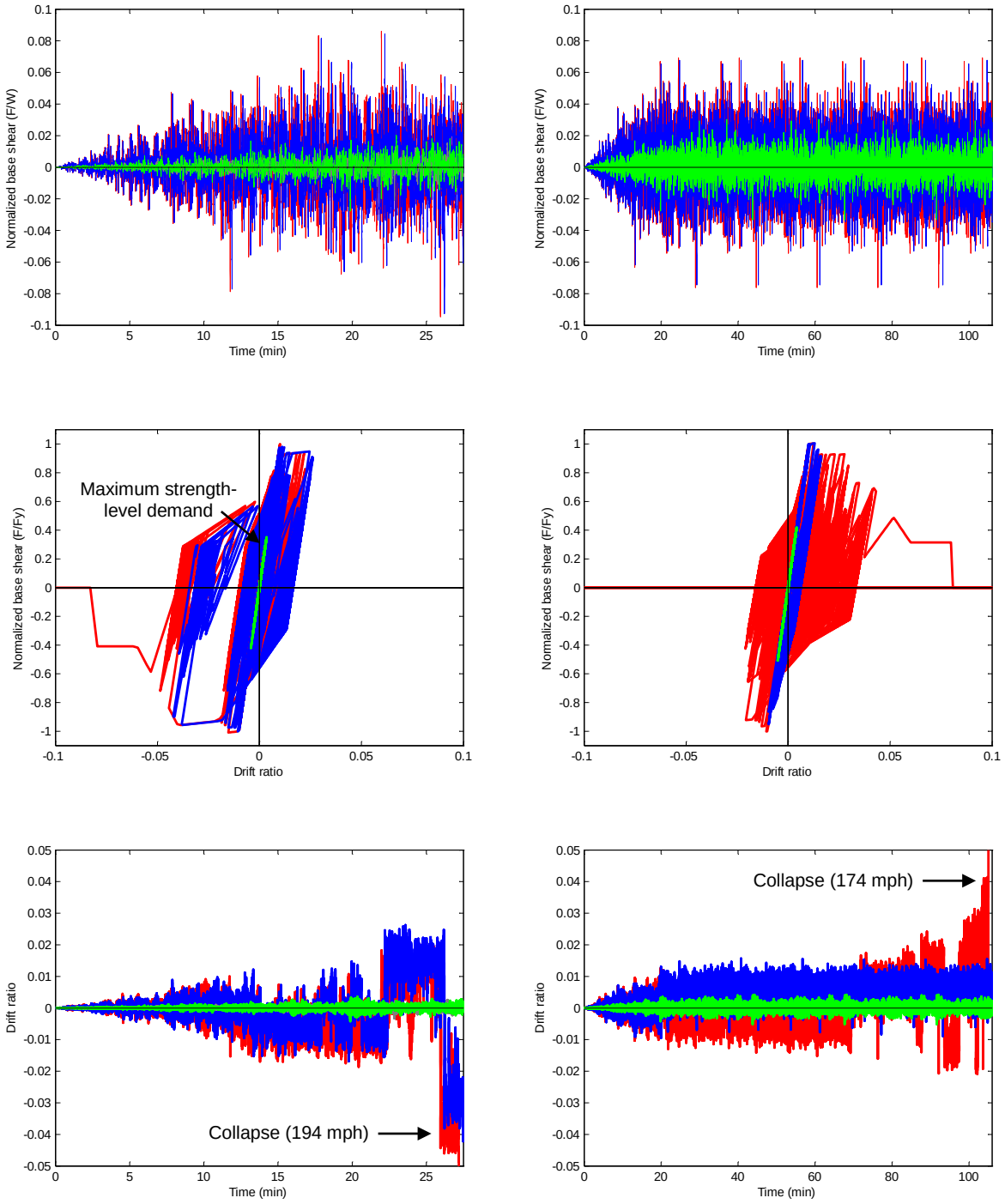

a) 28-minute duration

b) 138-minute duration

Figure 6.21 Cross-wind (0°) response history for ductile moment frame system

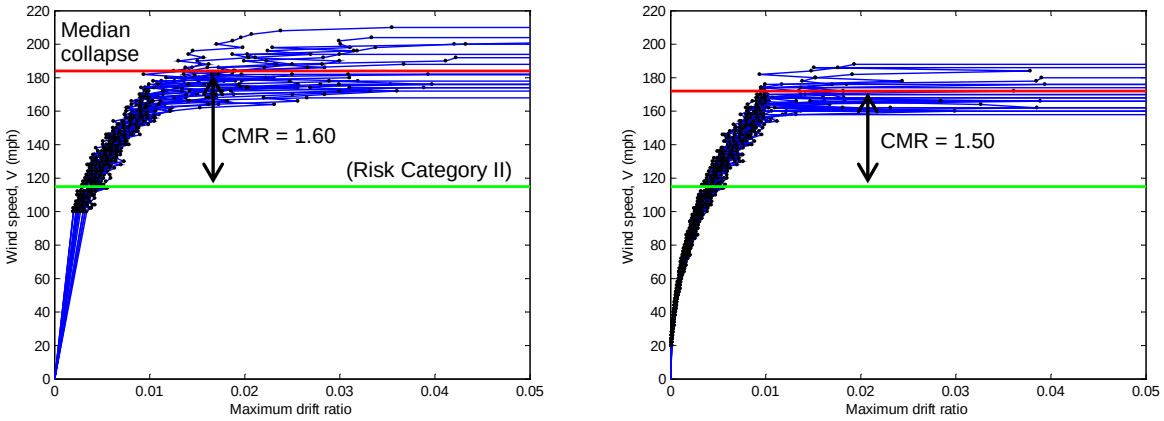

a) 28-minute duration b) 138-minute duration

Figure 6.22 Incremental dynamic analyses curves for ductile moment frame system

6.3 Discussion

Collapse assessments were generally sensitive to parametric changes in hazard or analytical modeling. The seismic collapse assessment was sensitive to the inclusion of column splices and the inclusion of splices changed the predicted static collapse story mechanism. The seismic collapse assessment was sensitive to the ground motion variability. Measured dispersion in incremental dynamic analysis curves was much wider for ground motions spectrally matched to the target spectrum, compared to the original (un-matched) FEMA P-695 Far Field set), a probable reflection of high and low frequency content outside the matching bounds. Spectral acceleration intensity measures defined by longer periods slightly decreased the conditional probability of seismic collapse.

The method used to integrate hazard and collapse fragility significantly affected both the predicted contribution of different hazards to the annual risk rate, and the calculated cumulative value of collapse risk. When applied in seismic analysis, the collapse risk prediction was sensitive to the method used to incorporate site response.

For seismic analysis, the methods used to represent panel zones and to account for second-order effects were most significant. The differences in response from the ductile and non-ductile frames originate in the details for the design of each frame. The non-ductile frame was designed with components that cannot sustain large ductility demands without failure, as opposed to the detailing for the ductile frame. As is observed from comparing the incremental dynamic analysis curves, the ductile frame buildings were capable of sustaining greater interstory drift ratios than the non-ductile frame buildings. Increasing the drift in the stories of the ductile frame increased the ductility demand on the hinges in the beams and columns, which caused collapse at lower ground motion intensity values. Therefore, analytical modeling

approaches that increased interstory drift ratios had a larger effect on the non-ductile frame buildings. In addition, the inability for the connections in the non-ductile frame to sustain large ductility demands increased the sensitivity of the seismic collapse assessment when considering variations in ground motion records. The higher sensitivity was demonstrated by higher β_{Total} values from the non-ductile frame compared to the values from the ductile frame buildings.

Comparing the collapse response of the baseline non-ductile model to the response of the models with the centerline and scissors approaches for the panel zone indicates the effect of stiffening the panel zone joint. The centerline approach stiffened the structure compared to the Krawinkler and scissors approaches, as was indicated by comparing the fundamental periods of vibration. Stiffening the structure increased the spectral acceleration associated with the median collapse value, but the collapse margin ratio was similar to the collapse margin ratio from the models with the Krawinkler and scissors joints because of the increase in spectral acceleration at the MCE-level ground motion.

As anticipated, changing from a second-order analysis to a first-order analysis in the non-ductile frame had a large effect on the collapse response. The first-order approach was incapable of modeling the destabilizing effects of the gravity loads, which effects reduced the interstory drift ratios in the model and increased the collapse resistance. The inability of the non-ductile frame buildings to sustain large, repeated interstory drift ratios prevented the systems from reaching large interstory drift ratios where the differences between the corotational and P-Δ approximation are amplified before the building collapses.

As with the non-ductile frame buildings, the largest differences in response for the ductile frame among changes in modeling approaches occurred for the change from a first-order to second-order approach. However, the ability for the ductile frame to reach higher interstory drift

ratios before collapse amplified the differences in modeling approaches, as demonstrated by the conditional collapse probability values at MCE level ground motion intensity. The larger interstory drift ratios also enabled the building to demonstrate differences in the collapse resistances between employing the corotational and P-Δ approximation. The ability for the corotational approach to model large displacements enabled the ductile frame building model to better distribute ductility demand throughout the structure, increasing the collapse resistance of the building.

Changing from the Krawinkler or scissors panel zone joint model to a centerline model stiffened the ductile frame, as was observed for the non-ductile frame building. The increased collapse resistance from the centerline model also did not have a large effect on the collapse margin ratio because of the larger spectral acceleration associated with the MCE-level ground motion. However, the building with the Krawinkler joint representation had a greater collapse margin ratio than the frame using the scissors approach. The differences in response between the models with the Krawinkler and scissors panel zone were due to the larger deformations in the beam-to-column joints (Charney and Marshall 2006).

Wind analysis was similar to seismic analysis in that the inelastic behavior and subsequent collapse risk was sensitive to the ratio of critical damping assumed, the incorporation of cyclic degradation, and the inclusion of the gravity framing in the model.

For the specific building studied, ductility or reserve capacity was effective at increasing the collapse safety and reducing the risk of collapse. Highly ductile systems did not necessarily lead to matching improvements in response. Adding a limited degree of ductility to the moment frame system, similar to that provided by a so-called intermediate moment frame in seismic design, could justify the use of a wind response modification factor "*R*".

Chapter 7

SEISMIC PERFORMANCE ASSESSMENT

This chapter discusses the seismic performance of archetype structural systems. Performance, in terms of repair costs and downtime, was assessed at serviceability and design hazard levels based on the structural and non-structural component fragility using floor accelerations and inter-story drift from nonlinear response history analyses. Resilience was quantified by calculating the probable loss in functionality during a reference time interval. Resilience contours were used to characterize the tradeoff between construction and repair costs, and the ability to recover rapidly after an earthquake.

7.1 General Procedures

The improved seismic performance of the Type I non-ductile and ductile moment-frame buildings was assessed using the FEMA P-58 framework (FEMA 2012a,b,c) and companion software, *Performance Assessment Calculation Tool (PACT)* (FEMA 2012d). The non-ductile moment framing buildings (designed for wind, SDC B_{min}) were assessed for serviceability considering reserve lateral strength in the gravity framing, and with collapse inhibiting mechanisms augmented with energy dissipation devices. The ductile moment frame buildings

(designed for SDC D_{max}) were assessed for both serviceability and design-level performance (DBE level ground motions), considering reserve lateral strength.

This assessment was accomplished in a two-tier process. First, the structural response for a given hazard intensity level was determined (using the same analytical models used for the collapse assessment). Second, the sensitivity of structural components, non-structural components, and other critical components of the building to ground shaking was determined using *PACT* and the structural response results.

7.1.1 Ground Motion Set for Nonlinear Response History Analysis

A subset (Table 7.1) of the FEMA P-695 "Far-Field" ground motion set was used. The scaling procedure was a multi-step scaling process. The ground motion record was first scaled (in FEMA P-695) by a factor to normalize the velocity of the ground motion set. Next the ground motion record was scaled so that the median of the record set spectral acceleration was equal to the target design spectrum spectral acceleration at the target period. Finally, the record was incrementally scaled relative to the normalization factor times the anchor factor.

Table 7.1 Ground motion set (FEMA P-695 Far-Field set) used for dynamic analysis

FEMA P-695 ID	Record Name	Earthquake	Magnitude
1	Beverly Hills - Mulhol	1994 Northridge	6.7
2	Canyon Country-WLC USC	1994 Northridge	6.7
11	Yermo Fire Station CDMG	1992 Landers	7.3
15	Abbar BHRC	1990 Manjil, Iran	7.4
17	Poe Road (temp)	1987 Superstition Hills	6.5
18	Rio Dell Overpass	1992 Cape Mendocino	7
21	LA - Hollywood	1971 San Fernando	6.6

The ground motion records were scaled relative to an anchor magnitude of intensity. The anchor magnitude of intensity was the scaling value applied to the ground motion record in order for the ground motion record to match a target spectral acceleration for a target period of vibration. This differed from the scaling procedure used in a seismic collapse assessment (Chapter 5).

The advantage of the anchor scaling method used in this Chapter was that the response was determined at exactly the hazard level of interest for the intensity measure. A disadvantage was that the results were not conveniently converted to other anchor spectrums. Also, the fragility curve will show equal-intensity measured collapse points (vertical "dots" in the fragility figure) since ground motions are applied at discrete intensity levels (so failure is shown at discrete intensity levels).

As an example, Figure 7.1 shows the response spectrum for the Type I non-ductile moment frame 2-story building including reserve strength in the gravity framing. The sub set of ground motions was normalized using the FEMA P-695 Toolkit (Hardyneic 2014).

7.1.2 Structural and Non-structural Component Fragility

The component fragilities used in the assessment were determined using the FEMA P-58 *Normative Quantity Estimation Tool*. As an example, Table 7.2 summarizes the component fragilities used in the assessment of the Type I non-ductile moment frame buildings. Structural components consisted of beam-to-column connections, column splices, and base plates. Although components of the collapse-inhibiting mechanism, such as cables, links, and HSS members could not be included (since the fragility test data was not yet available), it is likely that the ease of access and size would mitigate (lower) costs, compared to other components. Non-

structural components included a variety of items, ranging from mechanical, electrical, and plumbing (MEP) to exterior cladding and partition walls. Earthquake ground shaking intensity was correlated to component performance by median demand θ, and dispersion, β parameters.

Structural components used interstory drift ratio (IDR). Non-structural components used floor or roof acceleration. All IDR parameters were directional, meaning that the performance depended on the direction of ground motion relative to the principal directions of the building (longitudinal or transverse), and all accelerations are non-directional.

Quantities of components were estimated using the FEMA P-58 spreadsheet tools (FEMA 2012c) and depended on the number of stories and the component type. For example, buildings with the moment frame columns not fixed at the base (1- and 2-story buildings) did not utilize the base plate fragility.

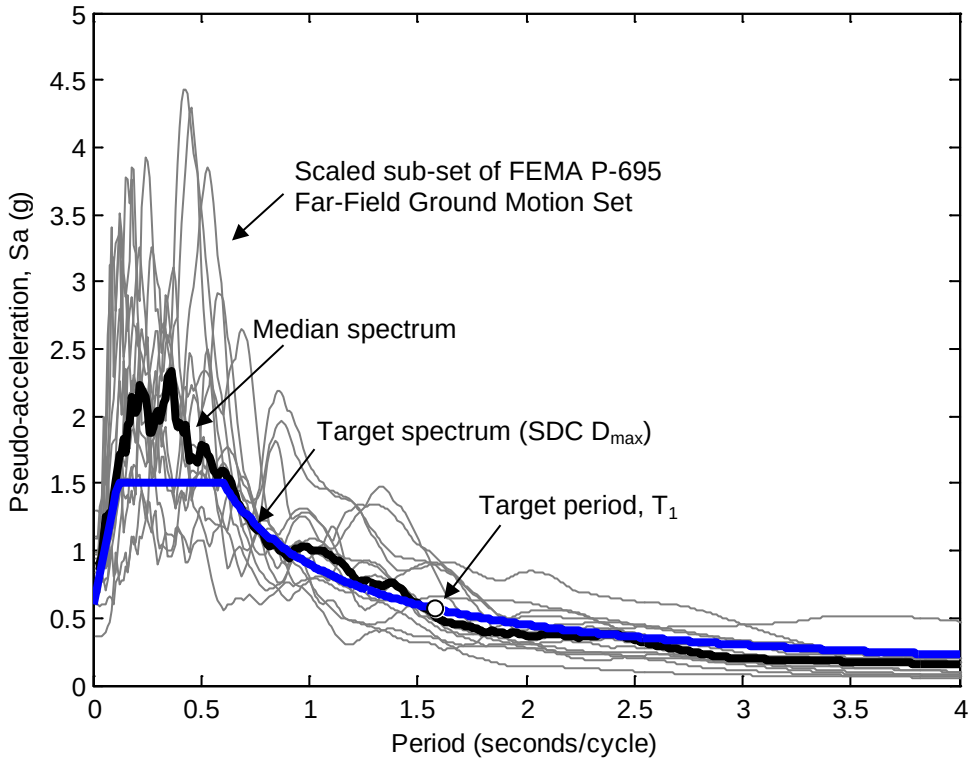

Figure 7.1 Response spectrum for Type I non-ductile 2-story building

Table 7.2 Summary of component fragilities used for Type I non-ductile buildings

Component Description (FEMA P-58 Fragility ID)		Quantity	Demand Parameter
Structural Components			
Beam-to-column connections	Non-ductile, Pre-Northridge WUF-B, single sided (B1035.041)	4	IDR
	Non-ductile, Pre-Northridge WUF-B, double sided (B1035.051)	4	IDR
	Gravity frame, bolted shear tab (B1031.001)	32	IDR
Moment frame columns	Base plates with column W < 150 plf (B1031.011a)	8	IDR
	Column W < 150 plf (B1031.021a)	8	IDR
Non-Structural Components			
All stories	Curtain Walls (B2022.001)	4,200 sf	IDR
	Wall Partition (C1011.001a)	1,400 lf	IDR
	Prefabricated steel stair (C2011.001b)	2 ea	IDR
	Wall Partition (C3011.001a)	106 lf	IDR
	Raised Access Floor (C3027.001)	10,500 sf	Acceleration
	Suspended Ceiling (C3032.001a)	12,600 sf	Acceleration
	Independent Pendant Lighting (C3034.001)	210 ea	Acceleration
	Cold Water Piping (D2021.011a)	210 lf	Acceleration
	HVAC Metal Ducting (D3041.011a)	1,050 lf	Acceleration
	HVAC Metal Ducting (D3041.012a)	280 lf	Acceleration
	HVAC Drops (D3041.031a)	126 ea	Acceleration
	(VAV) box (D3041.041a)	98 ea	Acceleration
	Fire Sprinkler Water Piping (D4011.021a)	2,800 lf	Acceleration
	Fire Sprinkler Drop (D4011.031a)	126 ea	Acceleration
	Low Voltage Switchgear (D5012.021a)	225 ea	Acceleration
1st story	Traction Elevator (D1014.011)	4 ea	Acceleration
Roof	Chiller (D3031.011a)	360 tn/ea	Acceleration
	Cooling Tower (D3031.021a)	360 tn/ea	Acceleration
	Air Handling Unit (D3052.011a)	88,200 cf	Acceleration
	Motor Control Center (D5012.013a)	6 ea	Acceleration

7.2 Predicted Seismic Performance

Comprehensive building seismic performance for Type I buildings and Type II buildings was predicted in *PACT* using 200 Monte Carlo simulations using the results from the structural analysis (interstory drift ratio and floor/roof accelerations) and the median demand values and dispersion for all component fragilities and associated damage consequences.

7.2.1 Type I Non-ductile Moment Frame Buildings

A sub-set of 7 ground motion component pairs was selected from the FEMA P-695 Far-Field Suite. For serviceability-level performance, the ground motions were scaled to 10% of the spectral acceleration corresponding to the MCE ground motion level. As previously discussed in Chapter 2, this intensity level generally corresponds to a 72-year MRI for the central and eastern United States. For design-level (DBE) performance, the ground motions were scaled to 67% of the spectral acceleration corresponding to the MCE ground motion level (with roughly a 475-year MRI). A similar evaluation at other intensity levels was performed in a related study (Jarrett et al. 2015).

Figure 7.2 shows median peak interstory drift ratio (IDR) and accelerations for the 4-story non-ductile moment-frame building. The collapse prevention system using loose-linkages with dampers limited the drift ratio below the threshold limit for visual damage under wind loads (0.003) (Griffis 1993). Accelerations exceed the threshold for human comfort (0.025 g) at high-frequency motion in an office building (Griffis 1993; Murray et al. 2003; Griffis et al. 2012), although this is probably not an issue for the short duration of shaking.

The sensitivity to ground motion for two selected components is shown in Figure 7.3. In FEMA P-58 sensitivity is described in terms of “damage” consequences. There are three

damage states and associated consequences for wall partitions, but only one damage state for chillers. Based on comparing the fragility curves with the median peak interstory drift ratio and acceleration response, the collapse prevention system using loose-linkages with dampers eliminated moderate and significant damage to wall partitions. Damage to shear-tab connections is unlikely to be important at this intensity level, but serious damage to the chiller is possible. For reference, exterior cladding damage fragility (not shown) has a median demand, θ = 0.04 interstory drift ratio and dispersion, β = 0.4. Thus, no damage to glazing is expected.

Table 7.3 to Table 7.5 summarize the seismic performance (relative to SDC D_{max}) in terms of the median repair cost, C_{Repair} and time, t_{Repair}, and the probability of unsafe placards determined in the *PACT* analyses. Design level performance was only assessed for the ductile moment frame buildings. Resilience, *R* was calculated using Equation 7.1 originally proposed by Bruneau and Reinhorn (2007) and used by Cimellaro et al. (2010). In Equation 7.1 the reference time, t_c was taken as 60 days.

$$R = \int_{t_0}^{t_c} [1 - Q(t)]dt = 1 - \frac{1}{2}\left(\frac{C_{Repair} + P_{Placard}C_{Tenant}}{C_{Total}}\right)\left(\frac{t_{Repair}}{t_c}\right) \quad (7.1)$$

The total replacement cost, C_{Total} of a moment-frame building has been suggested in the literature (RSMeans 2013; ENR 2011; Zareian 2012) to be anywhere from 150-350 dollars/sf, where the upper end of cost was representative of construction on the west coast. In this study, the focus was on steel-framed buildings constructed in a low or moderate seismic area in the central and eastern United States, so the total replacement cost for the prototype building was estimated at 230 dollars/sf with 30% attributed to the core and shell (building cost excluding tenant improvements, C_{Tenant}) (Cheever 2013).

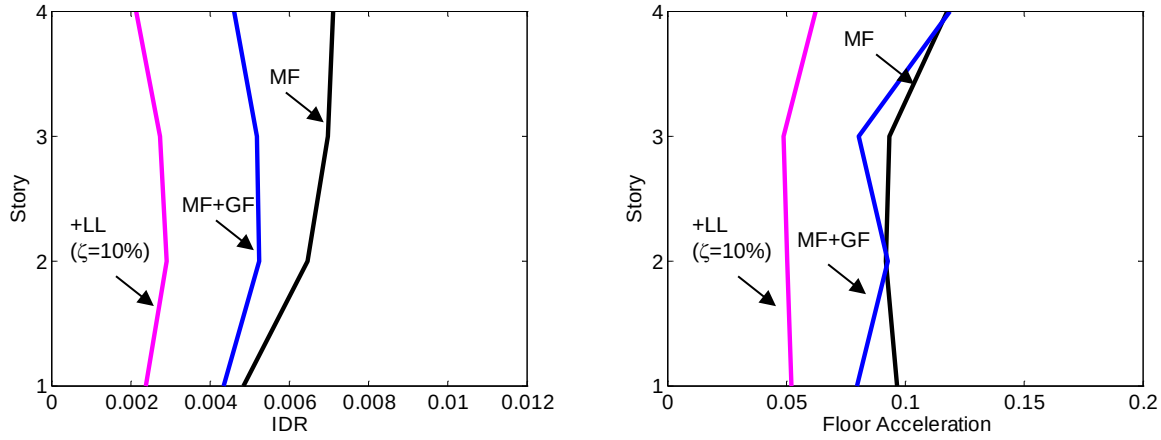

a) Median inter-story drift ratio (IDR) **b)** Median peak floor acceleration (g)

Figure 7.2 Median response for 4-story non-ductile moment-frame building at 10% of MCE.

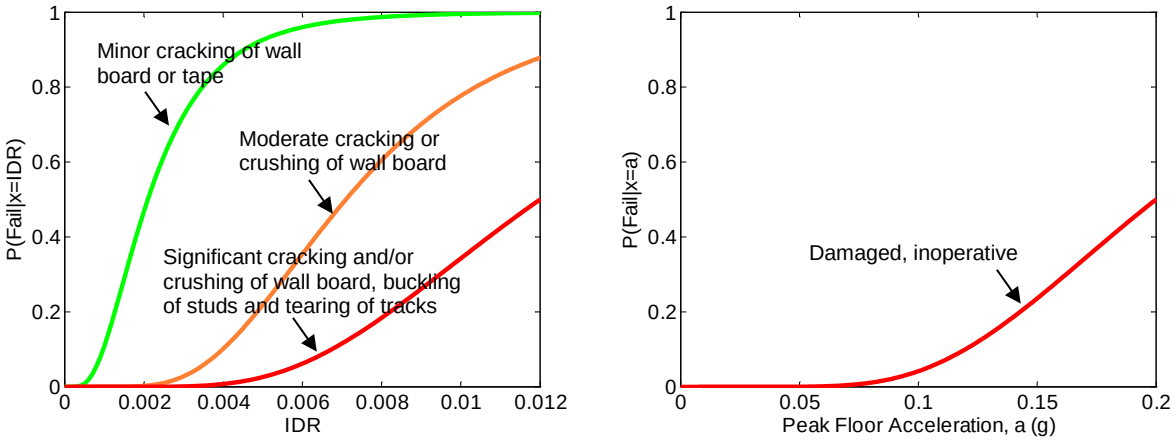

a) Wall partition fragilities **b)** Chiller fragility

Figure 7.3 Selected component fragilities (sensitivity to ground motion).

An implicit assumption of Equation 7.1 was a linear recovery "trajectory" (relationship between recovery time and functionality). The linear trajectory was intended to represent an average post-earthquake response, but the equation could easily be re-derived for trigonometric and exponential recovery trajectories, representative of a below or above average post-earthquake response, respectively (e.g. Cimellaro et al. 2010).

Table 7.3 Serviceability (10% of MCE) performance of Type I non-ductile buildings

Archetype Model	Repair		Prob. of Unsafe Placards	Resilience *R*
	Cost ($)	Time (days)		
1-story				
MF	277,500	50	0.49	0.82
MF+GF	220,000	32	0.26	0.93
+LL (ζ=10%)	108,500	19	0.10	0.98
+TB (ζ=10%)	115,000	20	0.10	0.98
2-story				
MF	330,000	36	0.21	0.94
MF+GF	266,250	32	0.15	0.96
+LL (ζ=10%)	181,250	23	0.05	0.99
+TB (ζ=10%)	172,000	23	0.05	0.99
4-story				
MF	666,667	40	0.19	0.94
MF+GF	490,000	27	0.09	0.98
+LL (ζ=10%)	211,000	14	0.01	1.00
+TB (ζ=10%)	196,875	14	0.01	1.00
8-story				
MF	1,192,000	48	0.10	0.95
MF+GF	775,000	29	0.03	0.99
+LL (ζ=10%)	458,333	18	0.01	1.00
+TB (ζ=10%)	445,000	18	0.01	1.00

The repair costs embedded in *PACT* and the FEMA P-58 documentation reflect costs for northern California in 2011 (FEMA 2012b). The cost data was adjusted to reflect the national average commercial construction costs by computing the national average cost (RSMeans 2013) relative to the average cost of ten population centers in northern California (ranging from Santa Rosa in the north, to San Jose in the south). A result, for use with *PACT* the region cost multiplier was 0.867 and the date cost multiplier was 1.064. The repair time for the building was estimated using typical construction schedules based advice from practitioners and the number of stories (Jarrett et al. 2015), ranging from 357 days for 1-story and 2-story buildings, 392 days for 4-story buildings, and 462 days for 8-story buildings.

Table 7.4 Serviceability (10% of MCE) performance of Type I ductile buildings

Archetype	Repair		Prob. of Unsafe Placards	Resilience
	Cost ($)	Time (days)		
1-story				
MF	1,510,000	228	0.96	0.28
MF+GF	1,310,000	181	0.94	0.47
2-story				
MF	1,540,000	137	0.87	0.68
MF+GF	1,560,000	142	0.87	0.67
4-story				
MF	2,585,714	148	0.93	0.65
MF+GF	2,388,889	139	0.88	0.69
8-story				
MF	4,100,000	162	0.87	0.65
MF+GF	3,800,000	156	0.85	0.68

Table 7.5 Design-level (67% of MCE) performance of Type I ductile buildings

Archetype	Repair		Prob. of Unsafe Placards	Resilience
	Cost ($)	Time (days)		
1-story				
MF	1,510,000	228	0.96	0.28
MF+GF	1,310,000	181	0.94	0.47
2-story				
MF	1,540,000	137	0.87	0.68
MF+GF	1,560,000	142	0.87	0.67
4-story				
MF	2,585,714	148	0.93	0.65
MF+GF	2,388,889	139	0.88	0.69
8-story				
MF	4,100,000	162	0.87	0.65
MF+GF	3,800,000	156	0.85	0.68

The maximum number of workers per square foot (used to calculate repair time) was one worker per 1,000 square feet (the default value in *PACT*). The ratio of repair cost to building replacement cost, or "total loss threshold" was taken as 1.0 (the default value in *PACT*). A single random seed value equal to 5 was used so that the analysis was repeatable. (Using a random seed value equal to zero would lead to a unique simulation for each analysis that was not repeatable.)

For the serviceability performance, the lateral strength in shear tab connections and the collapse prevention system with energy dissipation devices contributed to a significant reduction in both repair cost and downtime. The improvement was most dramatic in the 1-story building. For the 1-story, 2-story, and 4-story buildings, the probability of an unsafe placard ("red tag") for the conventional building (moment frame only) is primarily due to the probability of structural damage to the non-ductile moment frame connections. Collapse prevention systems were highly resilient compared to the conventional building.

For the Type I ductile moment frame 8-story building designed for SDC D_{min}, most repair costs were caused by damage to the gypsum wall partitions. The reserve lateral strength from the gravity framing reduced repair costs by 22%. The time required for repairs is correlated to repair costs, and was dominated by repair time for the gypsum wall partitions. Figure 7.4 contrasts the repair times considering only the moment frame and including the reserve lateral strength in the gravity framing. The bar colors indicate different component performance groups. Interestingly, including the gravity framing actually increased the probable repair time for some components (chiller). Placarding was caused due to prefabricated steel stair systems with steel treads and landings without seismic joints. Reserve strength reduced the probability of placarding from 9% to 3%.

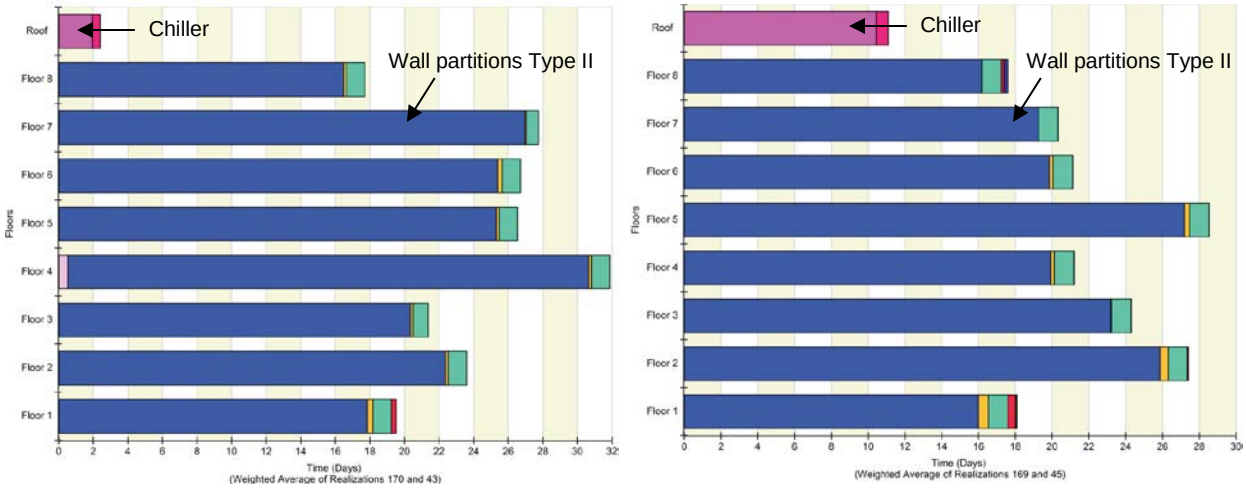

a) Moment-frame only **b)** With reserve lateral strength

Figure 7.4 Serviceability level performance for Type I ductile moment frame 8-story building

For the Type I ductile moment frame 8-story building designed for SDC D_{max}, most repair costs were caused by damage to the gypsum wall partitions, as before, but there were other significant contributions to repair costs, such as bolted shear tab gravity connections, and unanchored chiller and air handling units. The reserve lateral strength from the gravity framing reduced repair costs by 13%.

Repair time was dominated by gypsum wall partitions, but many other fragility performance groups were significant contributors. The reserve lateral strength from the gravity framing reduced the predicted mean repair time by 6 days (4%).

Unsafe placarding was mostly due to the prefabricated steel stair systems without seismic joints, but there were several other components that contributed to the probability of unsafe placards. Reserve strength slightly reduced the probability, with most improvement in reducing placard associated with unbraced fire sprinkler water piping.

7.2.2 Type II Non-ductile 4-story Moment Frame Building

A sub-set of 7 ground motion component pairs was selected from the FEMA P-695 Far-Field Suite. To investigate serviceability-level performance the ground motions were scaled to 5% and 10% of the spectral acceleration corresponding to the MCE ground motion level. As previously discussed, these intensity levels generally correspond to a 43-year MRI and a 72-year MRI, respectively, for the central and eastern United States. For comparison, similarly occurring intensities would generically be 13% and 20% for the western United States.

Figure 7.5 displays average peak inter-story drift ratio (IDR) and acceleration profiles. For these intensity levels, the relationship between ground acceleration, drift, and acceleration is essentially linear. The 5% of MCE response is below the threshold for visual damage (0.003). Accelerations exceed the threshold for human comfort (0.025 g) at high-frequency motion in an office building (Griffis 1993; Murray et al. 2003; Griffis et al. 2012) at both intensity levels, as expected. However, this is probably not an issue for the short duration of shaking.

Compared to the moment-frame direction, the performance of the building in the braced-frame direction is less robust and highly sensitive to even small drifts (on the order of 0.2%). This observation matches a previous comparison of braced frames and moment frames (Nelson et al. 2006) and a related study (Hines et al. 2009) that concluded that braced frames are particularly sensitive to variations in ground motion as well as building system characteristics.

Figure 7.6 shows typical component performance fragility curves documented in FEMA P-58. Performance is judged in terms of “damage” consequences. For example, there are three damage states and associated consequences for non-ductile beam-to-column connections (Deierlein and Victorsson 2008), but only one damage state for braced frames and chillers.

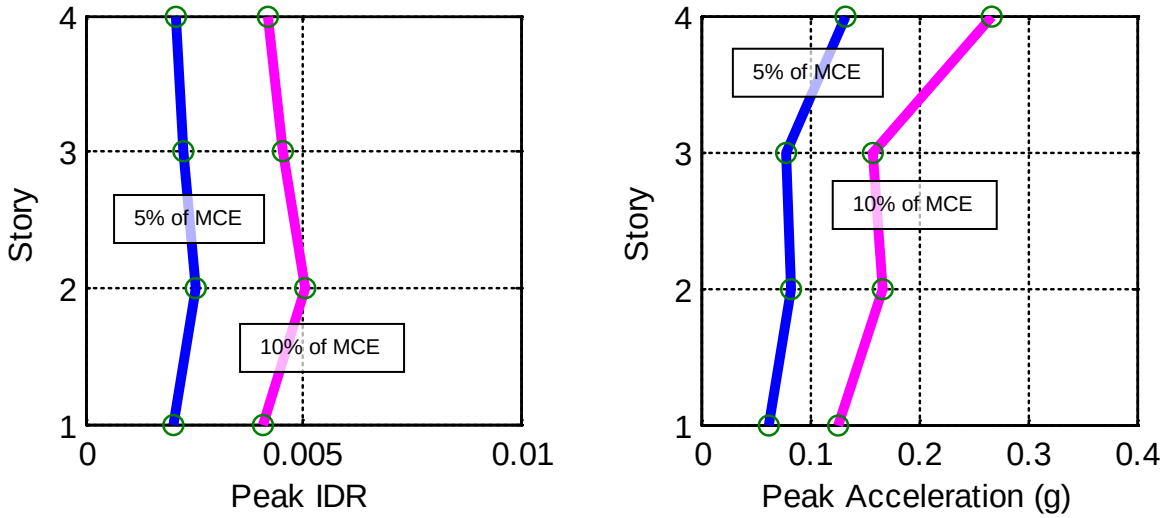

Figure 7.5 Profiles of peak IDR and peak floor/roof acceleration.

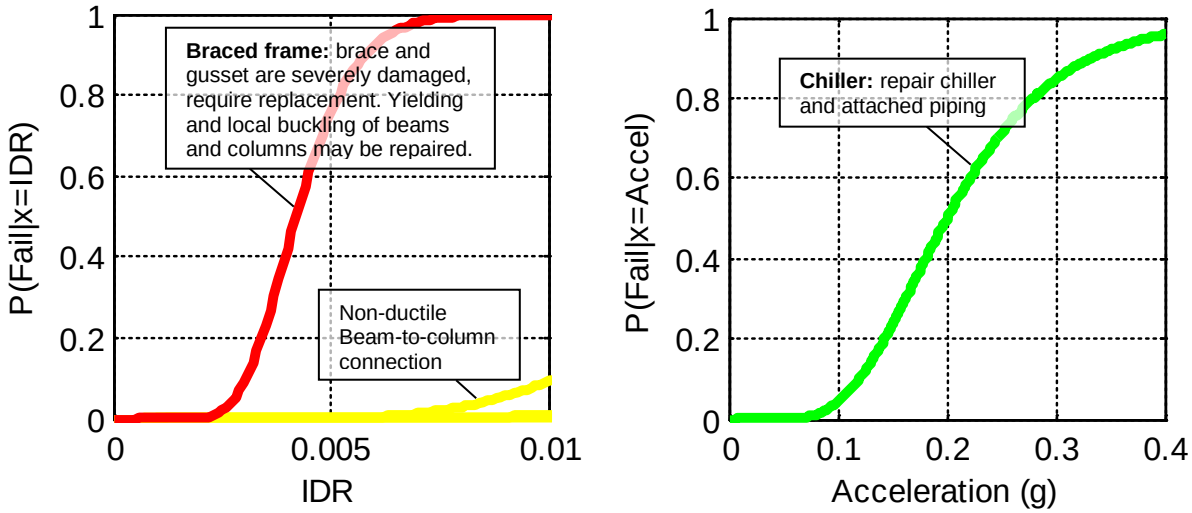

Figure 7.6 Typical component fragility curves.

Based on comparing the fragility curves with the average IDR and acceleration profiles, damage to non-ductile connections is unlikely to be important, but serious damage to the braced frame and chiller are expected. For reference, exterior cladding damage fragility (not shown) has a median demand, θ = 0.04 IDR and dispersion, β = 0.4. Thus, no damage to glazing is expected.

Comprehensive building performance was predicted in *PACT*, and the *PACT* analysis was run twice (component directions are switched in the second run). The average results of the *PACT* analyses are summarized in Table 7.6. The color shading in the table correlates with performance objectives in terms of the tolerable level of damage (see Table 1.1 in Chapter 1). Repair cost is expressed as a percent of the total replacement cost. As before, in this study the focus is on steel-framed buildings constructed in a low or moderate seismic area in the central and eastern United States, so the total replacement cost for the prototype building was estimated at 230 dollars/sf with 30% attributed to the core and shell (building cost excluding tenant improvements). The impact of damages and losses is suggested by color: mild impact (green), moderate impact (yellow), and high impact (orange).

Sample contributions to median cost and downtime are shown in Figure 7.7. Note that contributions to repair costs change for each realization in the *PACT* Monte Carlo simulation. Generally speaking, common contributors are wall partitions, chillers, and air handling units that are not anchored. Similarly, downtime can often be attributed to the elevators, pendant lighting, chillers, and air handling units.

Table 7.6 Summary of average performance assessment for Type II non-ductile 4-story building

	Median Response (PACT)		
Seismic Performance Level	**Repair Cost (% of Total Replacement Cost)**	**Downtime (days)**	**Probability of Unsafe Placards**
Small event (43-year MRI, 5% of MCE)	2%	10	11%
Medium event (72-year MRI, 10% of MCE)	5%	33	65%

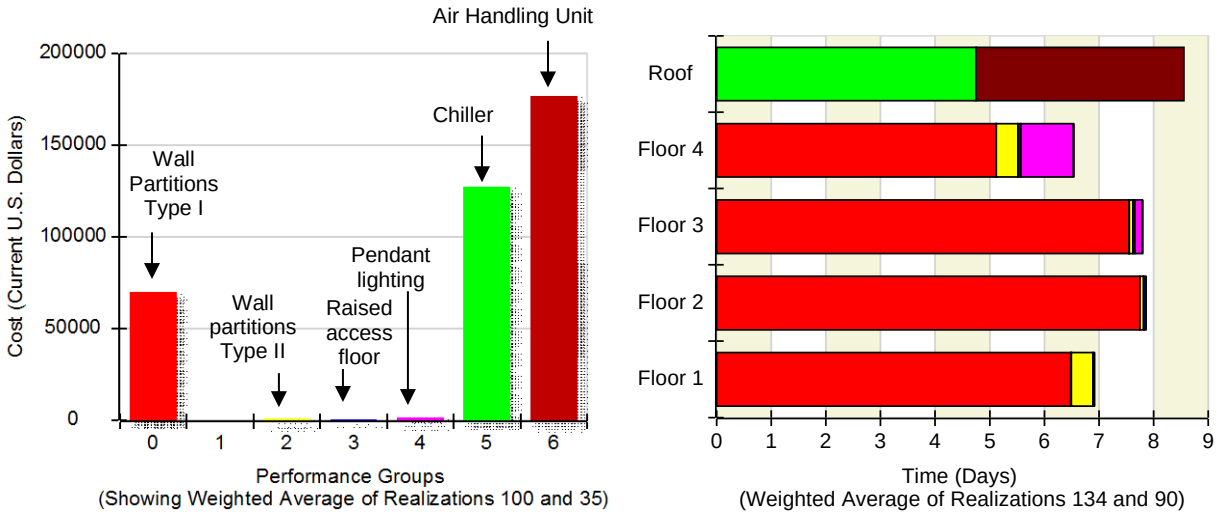

Figure 7.7 Typical contributions to repair cost and downtime at 5% of MCE ground motion

The probability of an unsafe placard during small events is due to the non-seismically detailed braced frames. During medium events, the braced frame contributes the most. (A 5% contribution is from prefabricated stairs without seismic joints, and a 1% contribution is from non-ductile beam-to-column connections.)

For the small event (43-year MRI), repair cost is fairly minimal (mild impact), although there is likely to be some delay in re-occupancy (moderate impact). For the medium event (72-year MRI), there is likely to be moderate repair costs and significant delays (high impact). Thus, relative to SDC D_{max}, the building is probably adequate for small events, but not for medium events. For low and moderate seismic areas (i.e. SDC C_{max} and lower), improved performance (reduced impact in terms of lower costs and usage delays) is probable.

7.3 Resiliency Contours

The repair cost plus the non-functionality loss caused by unsafe placarding, normalized with respect to the replacement cost of the building, or the "initial loss index," *L* associated with a given level of resilience, *R* was computed using Equation 7.2 in terms of normalized repair (recovery) time, *T*.

$$\begin{aligned} R &= \int_{t_0}^{t_c} [1 - Q(t)]dt \\ &= 1 - \frac{1}{2}\left(\frac{C_{Repair} + P_{Placard}C_{Tenant}}{C_{Total}}\right)\left(\frac{t_{Repair}}{t_c}\right) \\ &= 1 - LT/2 \\ L &= \frac{2(1-R)}{T} \end{aligned} \tag{7.2}$$

Using Equation 7.2, resilience contours are plotted in Figure 7.8 for the non-ductile and ductile moment frame buildings. Each contour in the plots represents a constant value of resilience. Mathematically, each contour is described by an equilateral hyperbola (Equation 7.2), and each point on the plot represents a unique scenario of recovery time and loss (Zobel and Khansa 2014). The simulated resilience (the values in Table 7.3 and Table 7.4) of archetype buildings without reserve strength is indicated by points designated with empty symbols; resilience of buildings with reserve lateral strength is indicated by points with filled symbols.

The utility of the contour plots is twofold. First, the relative magnitude of improvement in resilience is readily identified. For example, at the serviceability intensity level the reserve lateral strength was a significant factor for archetype buildings with non-ductile moment frames or with SMF designed for SDC D_{min}, but it was insignificant for buildings with SMF designed for SDC D_{max}. At the design intensity level, the reserve lateral strength was only effective for

the 1-story building. The second advantage of the contour plots is that the optimal direction to improve resilience can be discerned, i.e. orthogonal to the contour lines (green arrows). For example, it is apparent at the serviceability level intensity that an improvement in the initial loss index is the most effective way to increase resilience. In other words, the gradient represented by the contour lines could be used to determine how to get the most benefit for the least cost. Of course, Equation 7.1 relies on the method used to incorporate the probability of unsafe placarding, and this method needs to be carefully evaluated.

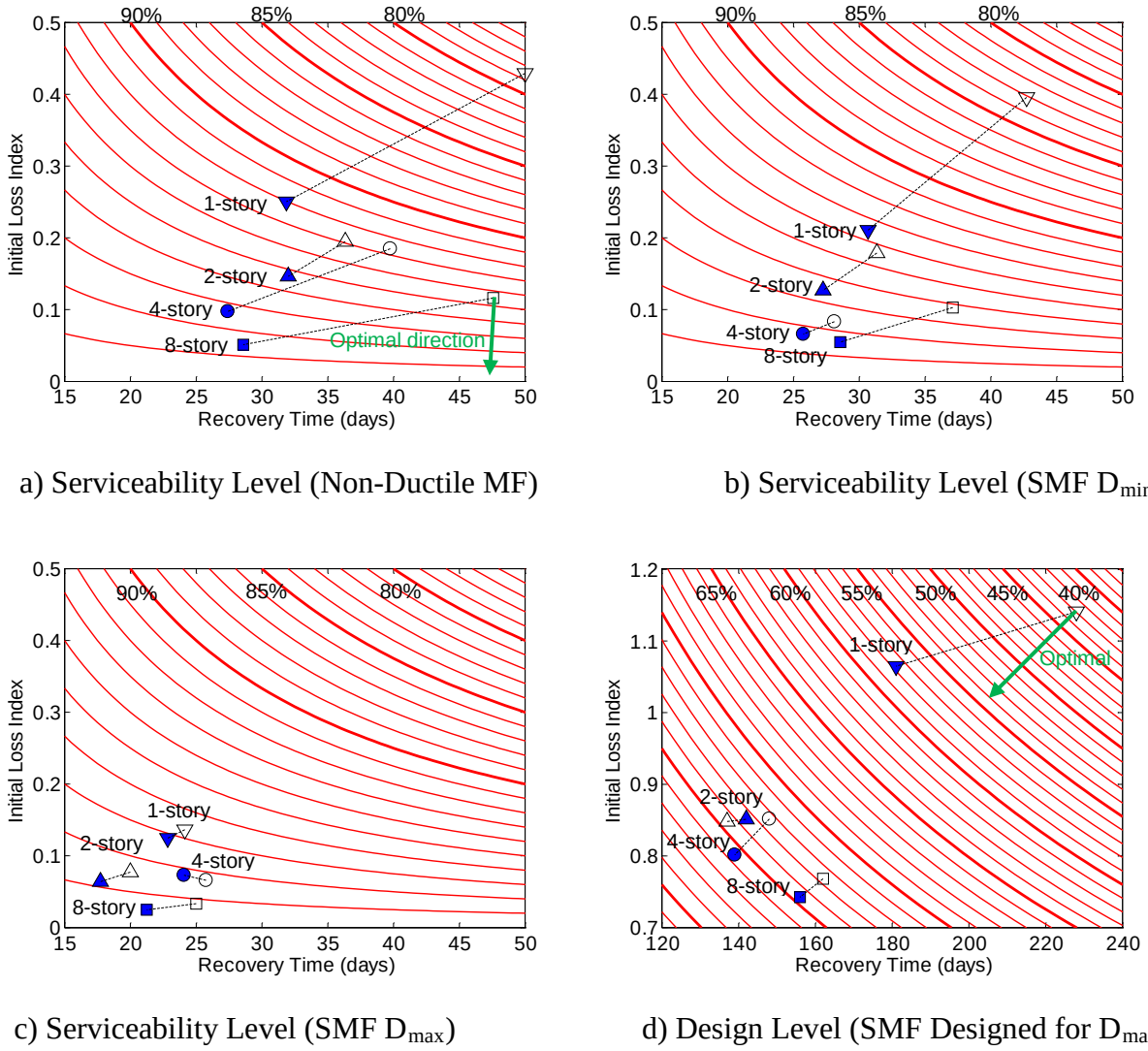

a) Serviceability Level (Non-Ductile MF)

b) Serviceability Level (SMF D_{min})

c) Serviceability Level (SMF D_{max})

d) Design Level (SMF Designed for D_{max})

Figure 7.8 Seismic resilience contour plots

7.4 Discussion

The seismic resilience of Type I archetype buildings generally increased when considering the reserve lateral strength contributed by the shear tab connections (in the gravity framing), but the improvement depended on the type and design of the lateral-force resisting system and the number of stories. For archetype buildings with non-ductile moment frames and special moment frames designed for SDC D_{min}, reserve lateral strength in the shear tab connections was a significant factor in improving resilience. Reserve lateral strength from shear tab connections was less significant as the design strength of the lateral-force resisting system increased.

The results suggest that Type II steel moment-frame buildings designed for wind may provide adequate performance under frequent and occasional ground motions in many areas of the central and eastern United States. The performance is attributed in part to reserve strength in both wind and gravity systems, ductility in the column panel zone, and the relative insensitivity of non-ductile connections to service-level seismic hazard. Further research is needed to examine the seismic performance of braced-frame buildings designed for wind, and to evaluate the effects of building irregularity.

Collapse prevention systems with energy dissipation devices contributed to a significant reduction in both repair cost and downtime. The resilience contour plots showed that for Type I buildings the reserve lateral strength was most effective at improving (reducing) recovery time, but less effective at reducing the associated economic losses. The comparison also illustrated the usefulness of resiliency contours in identifying optimal strategies for improving resilience [see also Judd and Charney (2014e)]. Thus, resilience contour plots could provide a pragmatic approach to visualize the tradeoff between improving robustness (reducing loss) and speeding recovery time, and to easily identify the best path to develop resilience.

Chapter 8

MULTI-HAZARD COLLAPSE ASSESSMENT

This chapter assesses the multi-hazard (combined seismic and wind) risk of collapse. The multi-hazard risk was calculated by assuming that the cumulative seismic risk and the cumulative wind risk are statistically independent. The acceptable level of risk, including social amplification of acceptable risk, is discussed. The results for selected archetype structural system are used to illustrate a multi-hazard assessment.

8.1 General

8.1.1 Background

Multi-hazard risk analysis may be thought of as encompassing four basic elements: hazard, exposure, vulnerability, and consequence (World Bank 2010). Hazard refers to the likelihood of a natural phenomenon that can produce damaging impacts (NAP 2012), but it may also be expanded to include the potential for blasts and technological threats (terrorism). In this study, the focus is on performance-based structural engineering, and hazards were defined as the potential for strong ground motions (caused by earthquakes) and strong wind pressure (caused by

extreme winds, such as hurricanes and tornados). Other events that cause structural hazards (such as fire, for example) are not considered in this study.

Exposure refers to people and assets subject to the damaging impacts from a hazard (NAP 2012). In structural engineering, the focus is on the people and infrastructure that are exposed. The degree of exposure involves the type, quantity, and location of assets and the distribution in terms of both space and time of occupants. Vulnerability refers to the sensitivity of buildings, bridges, and other structures to hazards (NAP 2012). Structural vulnerability is a function of the structural design and construction methods. Vulnerability is generally described in terms of one or more consequences, but in this study the focus is on side-sway collapse of buildings.

8.1.2 Literature Review

In the literature, collapse assessments of building structures have been almost exclusively concerned with a single hazard—usually seismic hazard. To date, there are few collapse assessments for a wind hazard, or multi-hazard collapse assessments or performance assessments (e.g. Li 2012).

Freeman et al. (2005) studied the structural efficiency and life-cycle costs of tall (49-story) buildings subjected to multiple hazards. Crosti and Duthinh (2011) and Duthinh and Simiu (2010) proposed a "risk-consistent" approach to the design of steel moment-frame buildings designed in accordance with AISC specifications and ASCE 7-10. The results showed that for the 10-story building studied by these researchers, the risk of exceeding the MCE level lateral drift limit was not significantly reduced by employing ductile (reduced beam section) beam-to-column connections, compared to welded-unreinforced-flange bolted connections.

Chen (2012) determined the structural response of mid-rise and high-rise steel-frame buildings subjected to earthquake and wind hazards using two-dimensional nonlinear static (pushover) and dynamic response history analyses. The buildings were a combination of moment frames and eccentrically braced frames. The analyses indicated that the seismically designed buildings have an inherent wind resistance for wind speeds up to 127 mph, while the wind designed buildings have inherent seismic resistance for spectral accelerations up to 0.34 g.

8.2 Procedure

8.2.1 Calculation of Multi-Hazard Risk

Risk (the probability of side-sway building collapse considering the likelihood of wind or seismic hazards) was calculated by integrating the respective collapse fragility and hazard curves and calculating the cumulative risk for a given exposure time, t.

Annual seismic hazard failure rate:

$$\lambda_{F,Seismic} = \int_0^{+\infty} \lambda_{a,Seismic}\, f_{Seismic}(a)\, da \tag{8.1}$$

Cumulative seismic risk for exposure time:

$$P_{F,Sesimic} = 1 - e^{(-\lambda_{F,Seismic} t)} \tag{8.2}$$

Annual wind hazard failure rate:

$$\lambda_{F,Wind} = \int_0^{+\infty} \lambda_{a,Wind}\, f_{Wind}(a)\, da \tag{8.3}$$

Cumulative wind risk for exposure time:

$$P_{F,Wind} = 1 - \left(1 - \lambda_{F,Wind}\right)^t \tag{8.4}$$

The total (aggregate) collapse risk was calculated by combining the cumulative seismic and wind collapse risks for a given exposure time.

$$P_F = P_{F,Sesimic} + P_{F,Wind} - \left(P_{F,Sesimic}\right)\left(P_{F,Wind}\right) \quad (8.5)$$

It was assumed in Equation 8.5 that the cumulative seismic risk and the cumulative wind risk are uncorrelated (statistically independent).

8.2.2 Acceptable Level and Social Amplification of Risk

Background

Society's acceptance of risk is constantly changing due to various factors. Uncertainty in the acceptable level of risk may be categorized as being a reflection of at least three factors: irrationality, prior experience, and perception of risk. The use of alternative histories and (to some extent) risk management provides ways to control expectations. The interaction of hazards and vulnerability and the corresponding calculated risk may be amplified or attenuated by public response. In other words, in addition to quantifying risk, an assessment of total risk must also include political, psychological, sociological, and cultural factors (Kasperson 2012; Robinson 2012).

Political factors usually amplify risk. When structures or systems are "messy," scientific knowledge and calculated risk "become unavoidably enmeshed in political disputes" (Metlay and Sarewitz 2012). For example, in recent years, government budget cuts in the United States led to significant flight delays for commercial airliners (Wald 2013). Seismic risk is compounded by megacities, which have a "concentration and buildup of populations and infrastructure in cities" (Aster 2012) that portends magnification of risk (Bilham 2009) including significant casualties (Holzer and Savage 2013). Wind risk has similar complications.

Compared to the western United States, a large-magnitude earthquake is possible in most the central and eastern United States (Chapman 2014), but such an event is rare. The rarity of the such events increases the uncertainty of the seismic hazard (see Stein and Stein 2013). Thus, one researcher has concluded, "All told, we should expect that globally we will experience more such surprising (and even astounding) low-probability and potentially very high-impact Black Swan" events (Aster 2012; see also Taleb 2007). In this study, a preliminary target collapse risk was established with these factors in mind.

Target Collapse Risk

In Chapter 4, the ASCE 7-10 target collapse risk of 1% in 50 years was used to evaluate structural safety under seismic loads. In Chapter 5, the target of 0.15% in 50 years was applied to structural collapse and used to evaluate structural safety under wind loads. The target risk in ASCE 7-10 Table C.1.3.1a was originally established based on the threshold of human risk acceptance (see commentary to ASCE 7-10, Pate-Cornell 1994), and therefore its application to structural collapse assessment was considered reasonable.

In this research, a target multi-hazard collapse risk of 1% in 50 years is suggested. The target risk was established based on lowering a combined risk of 1.15% (seismic and wind) to account for social amplification of risk, and specifically for perception of risk. This value is much larger than the minimum risk generally considered by society, 0.00005% (Ellingwood and Dusenberry 2005). Moreover, recent studies have shown that targets of acceptable risk may need to be revisited in light of modern data regarding risk aversion of building owners, code-enforcement organizations, and other stakeholders (Cha and Ellingwood 2014).

8.3 Results

The multi-hazard collapse risk of the Type I non-ductile moment frame 4-story and 8-story buildings were assessed. Multi-hazard collapse risk was calculated using Equation 8.5. Seismic collapse fragility was determined using parameters from Table 4.4. Seismic hazard was based on 2008 USGS data, adjusted for site amplification based on a correlation between shear wave velocity V_{s30}, and bedrock motion using NGA relationships. Wind collapse fragility was determined using parameters from Table 5.2. Wind hazard was based on the ASCE 7-10 wind speed data, and was extrapolated for extreme wind speeds. This integration was calculated for every 0.5-degree latitude and longitude to generate a map of risk values in the conterminous United States.

Figure 8.1a (upper map) shows shaded contours regions where the multi-hazard collapse risk exceeds 1% in 50 years for the 4-story building, assuming soil site class D (V_{s30} = 180 m/s) everywhere, and not including tornado wind hazards. Blue shaded areas in the central and eastern United States indicate (for this particular building archetype) where the enhanced shear tab collapse prevention system is needed, compared to the moment frame alone. Red shaded areas indicate where the enhanced shear tab collapse prevention system is not sufficient to meet the acceptable multi-hazard risk target (set at 1%). Major metropolitan areas (dots) are shown based on 2011 population estimate using 2010 census data. The upper map shows that the building is effective for a large portion of the central and eastern United States, but not for hurricane prone locations.

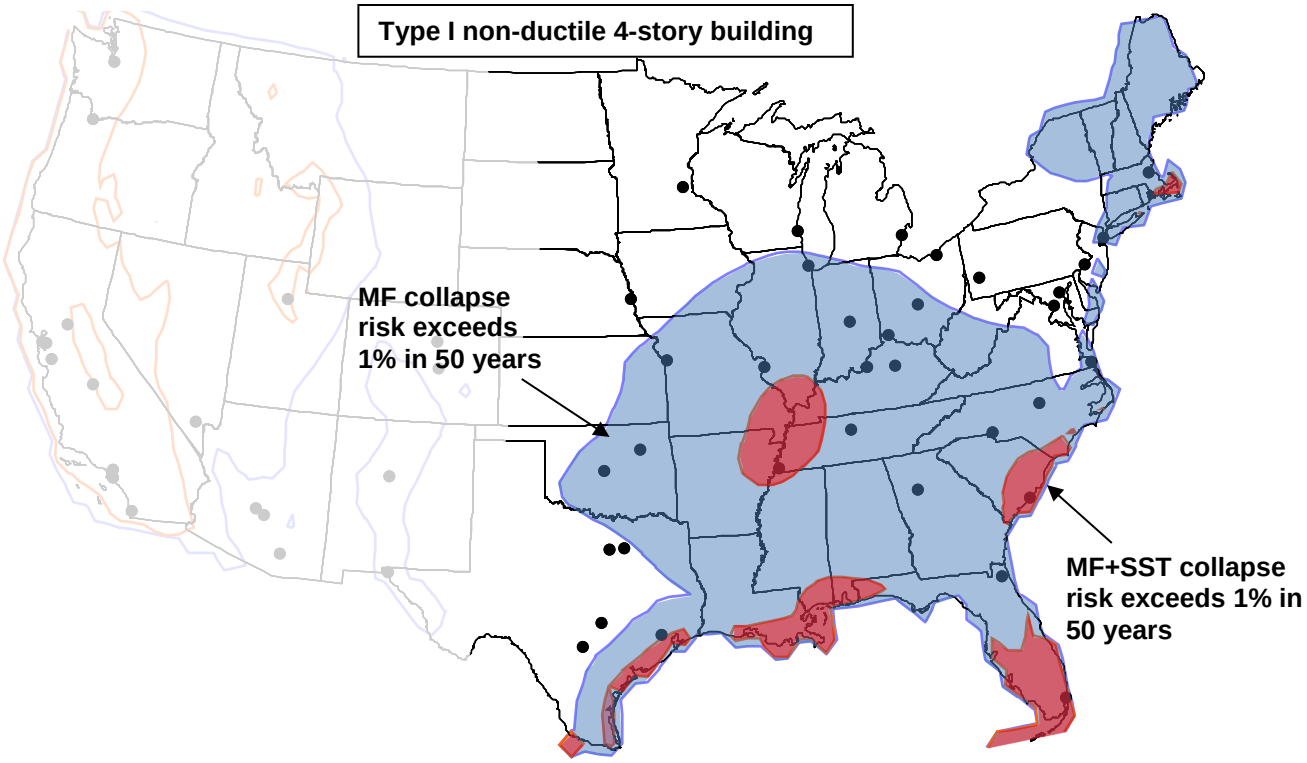

a) assuming soil site class D and extrapolated ASCE 7-10 wind hazards

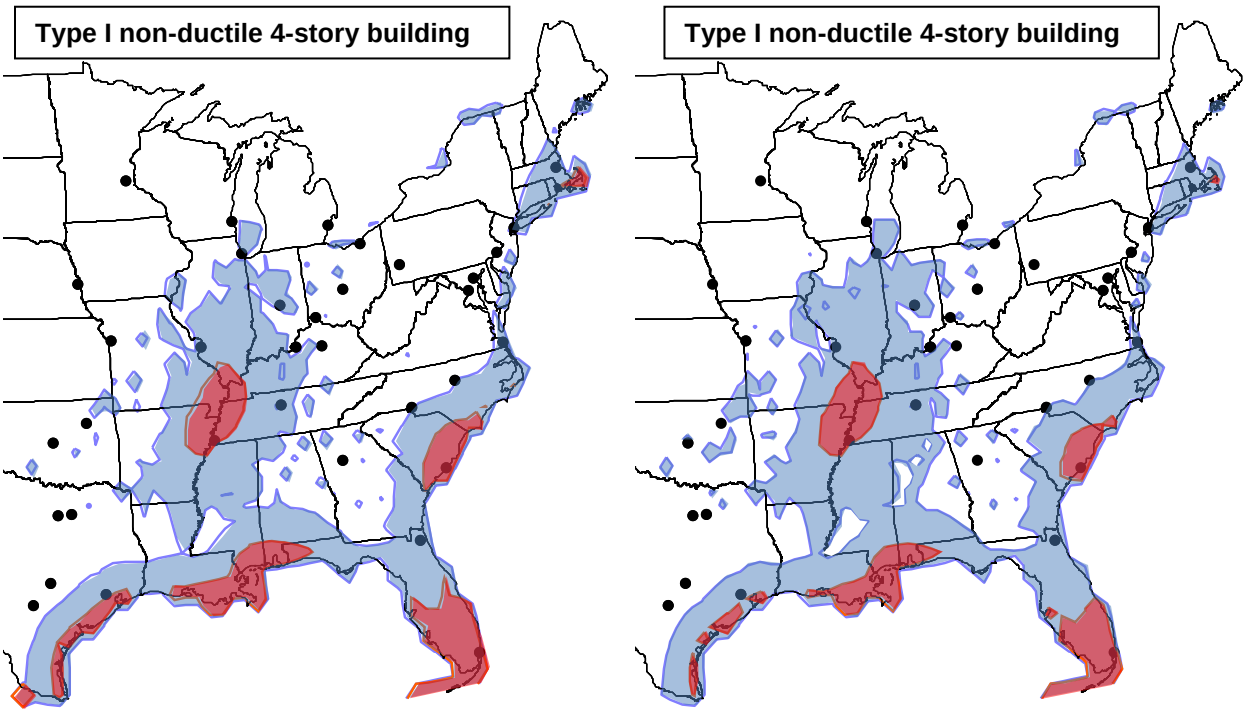

b) Site response using topographic proxy

c) Inclusion of tornado wind hazards with proxy

Figure 8.1 Regions where multi-hazard collapse risk exceeds 1% in 50 years

Figure 8.1b and Figure 8.1c (lower maps) show regions where the risk exceeds 1% in 50 years, using topographic data as a proxy for the average shear wave velocity to estimate site response, and considering synoptic wind hazards (left map) or including tornado wind hazards (right map). The collapse prevention system is shown to be viable for many locations in the central and eastern United States.

Figure 8.2a (upper map) shows where the multi-hazard collapse risk exceeds 1% in 50 years for the 8-story building, assuming soil site class D (V_{s30} = 180 m/s), and not including tornado wind hazards. The upper map shows that, for this particular collapse prevention system and building type, the applicable area is more restricted for the 8-story building compared to the 4-story building. The risk exceeds the target for large swaths of the southern and eastern coastlines of the United States.

Figure 8.2b and Figure 8.2c (lower maps) show regions where the risk exceeds 1% in 50 years, using topographic proxy data and considering synoptic wind hazards (left map), or including tornado wind hazards (right map). Although the banded region is much smaller for the collapse prevention system, the area still contains several major metropolitan areas, extending from Atlanta in the south, to Chicago in the north.

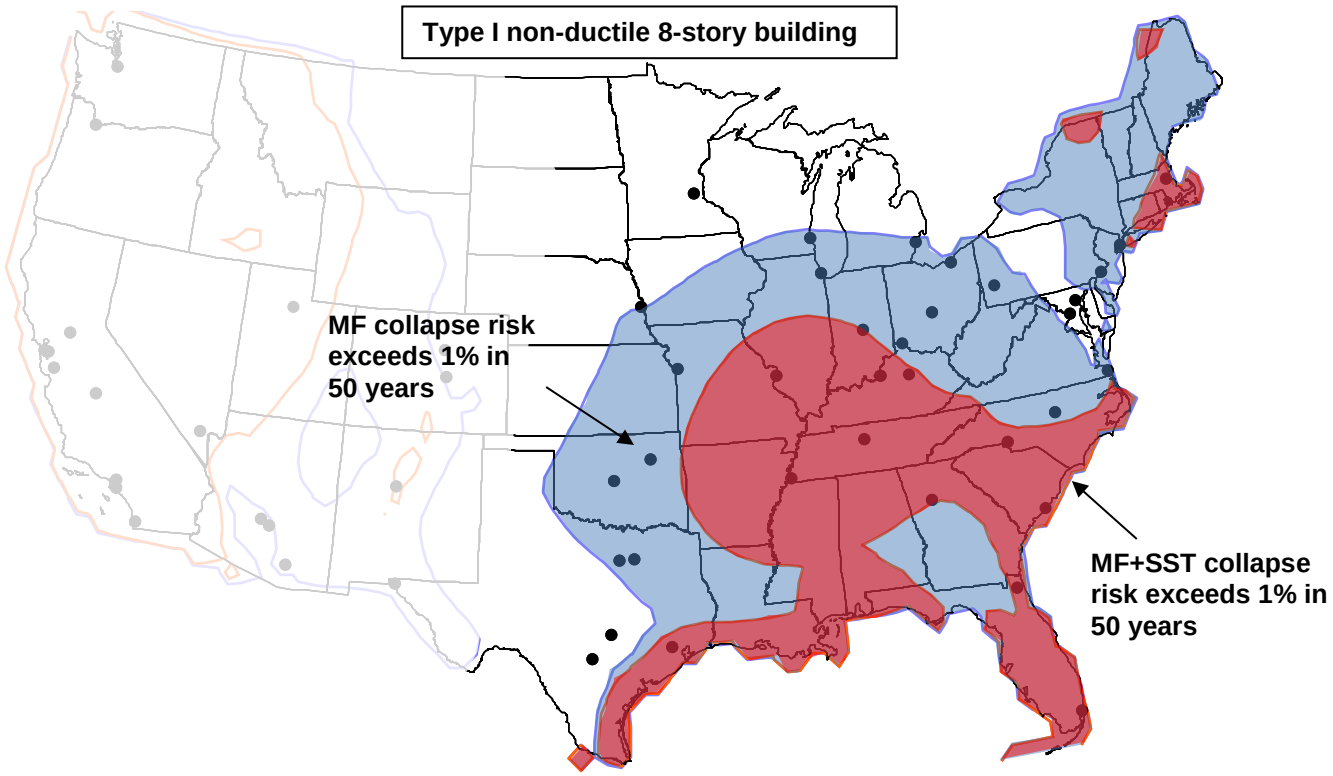

a) assuming soil site class D and extrapolated ASCE 7-10 wind hazards

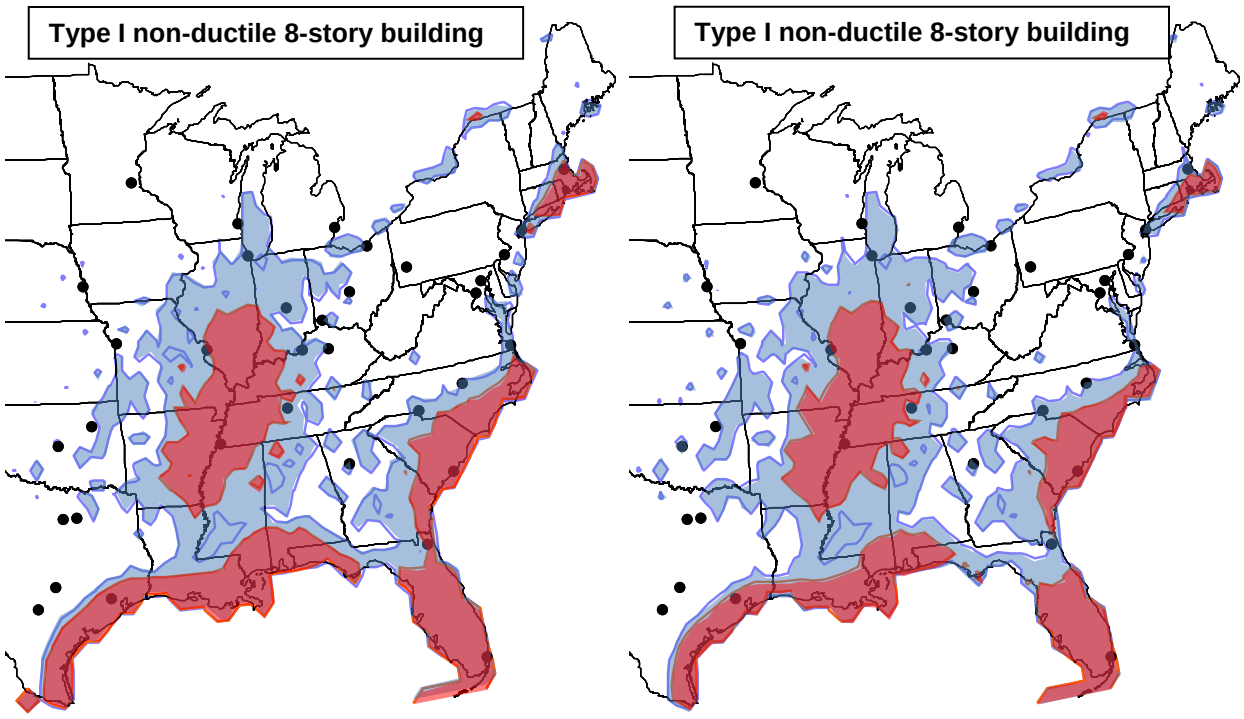

b) Site response using topographic proxy

c) Inclusion of tornado wind hazards with proxy

Figure 8.2 Regions where multi-hazard collapse risk exceeds 1% in 50 years

8.4 Discussion

Multi-hazard collapse assessments suggested that the probability of collapse due to seismic and wind hazards is significant in much of the United States. Enhanced shear tab collapse prevention systems dramatically improve (reduce) the collapse risk for the Type I non-ductile moment frame building, depending on the number of stories. Collapse prevention systems are needed and viable in much of the interior of the United States, but a ductile moment frame designed for high seismic demands or a conventional lateral resisting system would be necessary in regions of high seismicity (such as the in much of the western United States), or a high-wind designed main wind-force resisting system would be necessary along segments of the hurricane-prone southeastern United States.

The quantification of risk predicted in this Chapter should be tempered by considering the uncertain nature of both of the hazards, structural vulnerability, and the acceptable level of risk. The calculation of multi-hazard risk is like the following gambling strategy (Taleb 2005). Suppose one has a 999/1,000 probability of wining one dollar, and a 1/1,000 probability of losing $10,000 dollars. Here the probability is analogous to multiple hazards, and the amount of dollars won or lost is analogous to the tolerable impact of those hazards when combined with structural fragility. The expected result can be obtained by multiplying each probability by each outcome. Thus, the expectation would be that one will lose nine dollars. But the frequency or probability, in and by itself, is totally irrelevant. The probability needs to be judged in connection with the magnitude of the outcome. In the same way, calculating multi-hazard risk in structural engineering needs to be evaluated in the context of disproportionate impact. An examination of the acceptable level of multi-hazard risk is warranted.

Chapter 9

CONCULSIONS

This chapter summarizes the findings of this research study. Conclusions and recommendations based on the results are discussed, and areas for future research are identified. The potential impact of the research is discussed.

9.1 Summary

An examination of seismic and wind hazards in the United States confirmed that extensive regions of the United States are at risk from both hazards. However, the examination revealed that in many locations of the central and eastern United States, wind performance was most crucial for frequently occurring events, and the only seismic limit state of consequence was life safety. The spectral accelerations associated with the 43-year and 72-year events in the central and eastern United States were approximately 5% and 10% of the MCE-level spectral accelerations, respectively, roughly half of the comparable demands in the western United States. The collapse prevention system concept explored in this study may provide a cost-effective solution for these locations. The collapse prevention system concept relies on components that, working together with the primary lateral force-resisting system and gravity framing, are specifically intended to prevent collapse.

The seismic and wind collapse safety of archetypical buildings with and without collapse prevention systems was evaluated. For wind analysis, ensembles of wind load records for nonlinear response history analyses were based on wind tunnel testing. Variability in the wind load records was generated by wind directionality, and this provided a convenient way to incorporate epistemic uncertainties in the analysis. A straight-line wind and a reasonable duration of the wind event were assumed. These aspects of wind collapse analysis differ significantly from the procedures used to select ground motions for seismic collapse analysis.

For the buildings in this study, collapse prevention systems were effective at reducing the conditional probability of seismic collapse (during MCE-level ground motion) and at lowering the seismic collapse risk of a building with moment frames not specifically detailed for seismic resistance. The results indicated that the wind collapse risk was acceptably low for most of the buildings considered in this study if located in the interior (and west coast) of the United States, and if reserve strength in the shear tab connections was included. Taller buildings, however, had a higher wind collapse risk, and the non-ductile moment frame 10-story building did not pass the suggested target of 0.15% chance of collapse in 50 years. Compared to using only the main wind force resisting system, collapse prevention systems were needed and viable in the interior of the United States, but were not sufficient for some locations along the southeastern coast, depending on the location and type of archetype structural system.

Buildings with collapse prevention systems using non-ductile moment frames with fully-rigid flange welded connections passed the FEMA P-695 seismic criteria for SDC D_{min}. Buildings with collapse prevention systems were adequate for many regions in the central and eastern United States, but a conventional lateral force resisting system or a collapse prevention system with a ductile moment frames with reduced beam section connections would be required

for regions of higher seismicity (such as the New Madrid and Charleston areas) and for some regions exposed to high hurricane wind speeds.

Reserve lateral strength in the gravity framing, specifically in the shear tab connections, was a significant factor in the success of the collapse prevention system. In most buildings, simply utilizing the reserve strength in the shear tab connections significantly reduced the probability of seismic or wind collapse. The pattern of collapse prevention component failure depended on the type of loading, archetype building, and type of collapse prevention system, but most story collapse mechanisms formed in the lower stories of the building. Collapse prevention devices usually did not change the story failure mechanism of the building, compared to the primary moment frame alone, except for the "holistic" collapse prevention systems: reserve lateral strength in the gravity framing and enhanced shear tab connections, which in some cases did alter the story failure mechanism for the building.

Collapse prevention systems were highly resilient. Collapse prevention systems with energy dissipation devices contributed to a significant reduction in both repair cost and downtime. Resilience contour plots showed that reserve lateral strength was effective at reducing recovery time, but less effective at reducing the associated economic losses.

Seismic and wind collapse assessments were sensitive to hazard and analytical modeling parameters. The inclusion of gravity column splices, for example, changed the predicted static collapse story mechanism. The seismic collapse assessment was also sensitive to the ground motion variability, relative to the target response spectrum, due to the inevitability of uncaptured frequency content in the spectral matching process. The method used to represent column panel zones and to account for second-order effects in the analytical model had a significant impact on the collapse assessments. Using the centerline modeling approach stiffened the structure

compared to the Krawinkler and scissors approaches. Stiffening the structure then increased the spectral acceleration associated with the median collapse spectral acceleration. Changing from a second-order analysis to a first-order analysis in the non-ductile frame also had a large effect on the collapse response. The first-order approach was incapable of modeling the destabilizing effects of the gravity loads, and thus predicted reduced interstory drift ratios and increased collapse resistance. Such an effect was less pronounced with non-ductile moment frame buildings, because these systems were typically not able to sustain large, repeated interstory drift ratios. This behavior prevented the non-ductile buildings from reaching large interstory drift ratios where the differences between the corotational and P-Δ approximation are amplified before the building collapses.

The method used to integrate seismic or wind hazard and the respective collapse fragility significantly affected both the contribution of different hazards to the annual risk rate, and the calculated cumulative value of collapse risk. When applied in seismic analysis, collapse risk was sensitive to the method used to incorporate site response.

Steel moment-frame buildings designed for wind may provide adequate seismic performance under frequent and occasional ground motions in many areas of the central and eastern United States. The performance was attributed in part to reserve strength in both wind and gravity systems, ductility in the column panel zone, and the relative insensitivity of non-ductile connections to service-level seismic ground motion intensity.

9.2 Conclusions and Recommendations

The research leads to four general recommendations for performance-based analysis and design in earthquake and wind engineering.

- The first recommendation is that gravity framing should be included in structural analysis when feasible. The inherent added stiffness and strength have profound effects on collapse capacity behavior.

- A thorough understanding of the sensitivity of modeling aspects is needed when analyzing steel moment frame buildings to collapse. For example, the collapse responses from analytical models with the Krawinkler and scissors panel zone representations were quite different for the ductile frame buildings with high interstory drift ratios, but the differences were minimal for the ductile frame with low interstory drift ratios. The results suggest that employing the scissors model may be a valid way to reduce the number of degrees of freedom in the model and the analysis run time for some structural systems (i.e. non-ductile systems).

- It is recommended to use the derivative of the collapse fragility curve when calculating collapse risk. Using the derivative of the hazard curve to calculate risk is more computationally expensive, unstable, inaccurately determines the contribution of hazard, and, depending on the method used, may lead to grossly inaccurate values of risk.

- For performance-based wind engineering, adding a limited degree of ductility to the moment frame system, similar in magnitude to that provided by intermediate moment frames in seismic design, could justify the use of a response modification factor for wind and inelastic design for strength-level wind speeds.

The research leads to two specific observations for the collapse prevention system concept.

- It is expected that collapse prevention systems are applicable principally in the central and eastern United States and are not likely to be amenable to the western United States.

- Reserve lateral strength provided by the shear tab beam-to-column connections was a significant factor in the success of the collapse prevention system. This conclusion reflects the fact that shear tab connections can contribute in a significant way to the stiffness, strength, and ductility of the building, depending on the number of connections compared to the number of fully-restrained moment connections.

9.3 Areas for Future Research

Several aspects of the research are important areas for future research. It should be stressed that the results discussed herein are preliminary in nature. Similar to collapse analyses for seismic loads, a detailed study is required that involves a variety of multi-degree of freedom archetypical models representative of actual buildings, as well as consideration of taller buildings and other building shapes. Further research is needed to examine the seismic performance of braced-frame buildings designed for wind, and to evaluate the effects of building irregularity.

Wind collapse analyses exhibit special challenges compared to seismic collapse analyses. In order to meet these challenges, a comprehensive database of wind loads, a method to incorporate the non-stationary, long-term nature of wind loads (a sustained wind load was used in this research), rational methods for estimating the non-explicitly modeled part of damping, and calibration epistemic uncertainties are needed to advance the state-of-the-art.

The effect of the gravity framing on the response leads to the recommendation that three-dimensional modeling, including torsional effects, may be needed to realistically predict collapse behavior of buildings. Data mining procedures need to be developed for collapse assessments in order to glean from the numerical results and promote an understanding of the behavior of building components.

The procedures used to show applicable areas for collapse prevention systems should be reviewed and compared to studies that concentrate on central and eastern United States geology and seismicity, particularly in the highest hazard regions (Charleston and Memphis), and that focus on the windstorms of those areas (especially tornados and hurricanes). Eventually, regions outside the United States for which the collapse prevention system is viable should be identified, and the applicability of the method to those regions should be assessed.

Incremental dynamic analyses and ground motion sets should be developed that reflect the hazard and fault mechanisms likely found in central and eastern United States. A central and eastern United States companion for the FEMA P-695 Far-Field Set should be developed to better understand the vulnerability of structures outside the western United States.

Incremental dynamic wind analysis procedures need to be continued to be developed. The ramping of wind loads needs to be investigated. Reference wind speeds and wind durations need to be established.

Collapse prevention systems need to be optimized. In this research, the strength of the collapse prevention systems was limited by the size of the gravity frame beams and columns, and future research should investigate collapse prevention systems with slightly larger gravity framing members (especially column sizes). This research also revealed that ductility may have a larger impact than strength on the collapse performance of the collapse prevention system.

Accordingly, it may be advantageous to utilize other aspects of buildings that are inherently ductile (such as panel zone yielding). Collapse prevention systems with distributed forms of damping (such as friction dampers) could also be investigated.

The focus of this research was primarily a proof-of-concept. Essential aspects related to the design and the behavior of collapse prevention systems need to be addressed before implementation of the concept. For example, except for the enhanced shear tab connections, the proposed collapse prevention devices (and their connecting elements) need to be detailed. Similarly, the demands imposed on the gravity framing (such as increased base shear forces) need to be addressed.

A comprehensive cost-benefit analysis should look at material, labor, and inspection costs for deployed collapse prevention mechanisms. Collapse prevention systems are not expected to be implemented in actual construction until it is demonstrated that the new system is economically viable, improves performance, and produces reliable expectations of that performance.

A "Design Guide" should be developed for steel structures where the main gravity and wind system is either a moment frame or a braced frame (instead of just a moment frame). The methodology for assessing the strength of the system without the collapse prevention mechanism should be provided along with procedures for designing the collapse prevention mechanism and assessing the performance of the complete collapse prevention system.

It is likely that current retrofit methodologies as outlined in ASCE 41-13 will not be applicable to buildings with collapse prevention systems. This arises from differences identified in the seismic and wind hazards of the central and eastern United States compared to the western United States, and is a result of the concept that the main lateral force-resisting system and

gravity framing is expected to provide adequate performance at all limit states except life-safety and collapse. This lack of applicability should be assessed and recommendations should be made for the future development of guidelines for implementation in existing buildings.

An approach similar to the FEMA P-58 framework used to assess seismic performance needs to be developed in order to better understand the risk of life, as well as occupancy and economic losses that could occur during a wind event. Unlike seismic performance, wind performance encompasses a host of concerns besides building motions that need to be addressed, such as habitability, aero-acoustics, and water infiltration.

9.4 Potential Impact of Research

It is possible that buildings designed for wind can provide adequate multi-hazard performance in many regions. In in the central and eastern United States, where very large, rare earthquakes are possible, a structural system (i.e. a collapse-prevention system) could be devised to exploit the unique shape of seismic and wind hazard curves.

Resilience contour plots could provide a pragmatic approach for practicing structural engineers to visualize the tradeoff between improving robustness (reducing loss) and speeding recovery time, and to easily identify the best path to develop resilience. The approach explored in this research also has the potential to minimize design office errors introduced by implementing ever-evolving seismic code provisions (Cheever and Hines 2010), that were envisioned for use in high-seismic areas, in low-seismic high-wind areas.

The focus of this study was steel moment-frame structures, however the results suggest that reinforced concrete and masonry shear wall structures could be viable primary systems for a secondary collapse prevention system. The demands imposed on the gravity framing columns

suggest that composite gravity frame columns could provide necessary capacity to meet the demands imposed by the collapse prevention system on the gravity framing.

The collapse prevention system concept is equally relevant (and perhaps more attractive) for the repair and retrofit of existing buildings. An important advantage in using collapse prevention systems for rehabilitation (compared to a traditional retrofit) is that the collapse prevention mechanism need not be part of the main lateral load resisting system. A related advantage is that the collapse prevention system concept has less reliance on added deformation capacity, which is a key factor in older construction. For that reason, collapse prevention systems could likewise be used to prevent collapse of a damaged building during a strong aftershock.

This research has the potential to facilitate a "technology transfer" from seismic performance-based design, to wind performance-based design, and to multi-hazard performance-based design. The potential impact of this research will be best realized if the collapse prevention concept becomes part of a larger effort to mitigate the impact of disasters. Instead of a silver bullet, the goal of the collapse prevention concept is to improve, in a cost-effective way, community preparedness for seismic and wind risk by improving the structural performance of older construction and implementing resilient new construction.

REFERENCES

A

Abrahamson, N., and Shedlock, K. M. (1997). Overview: special issue on ground motion attenuation relations. *Seismological Research Letters* 68(1): 9–23.

Adekristi, A. (2013). *Algorithm for spectral matching of earthquake ground motions using wavelets and Broyden updating*. M.S. thesis, Civil Engineering. Virginia Polytechnic Institute and State University, Blacksburg, Virginia.

AISC (2010a). *Specification for structural steel buildings*. ANSI/AISC 360-10, American Institute for Steel Construction (AISC), Chicago, Illinois.

AISC (2010b). *Seismic provisions for structural steel buildings.* ANSI/AISC 341-10, American Institute for Steel Construction (AISC), Chicago, Illinois.

AISC (2011a). *Steel construction manual,* 14th edition. American Institute for Steel Construction (AISC), Chicago, Illinois.

AISC (2011b). *Prequalified connections for special and intermediate steel moment frames for seismic applications, including supplement No. 1*. ANSI/AISC 358-10, American Institute for Steel Construction (AISC), Chicago, Illinois.

AISC (2012). *Seismic design manual, second edition*. American Institute of Steel Construction (AISC), Chicago, Illinois.

AISC (2013). *Design examples*, version 14.1. American Institute of Steel Construction (AISC), Chicago, Illinois.

Aki, K., and Richards, P. G. (1980). *Quantitative seismology: theory and methods, vol. 1*. W. H. Freeman, San Francisco, California.

Allen, T. I., and Wald, D. J. (2009). "On the use of high-resolution topographic data as a proxy for seismic site conditions (Vs30)." *Bulletin of the Seismological Society of America*, 99(2A): 935–943.

Amine, M. S., Godfrey, E. A, Olgun, C. G., Martin, J. R., and Chapman, M. C. (2012). "Region specific site amplification factors for central and eastern United States." Meeting of the Eastern Section of the Seismological Society of America, October 29–30, Blacksburg, Virginia.

Ang, A. H.-S., and Tang, W. H. (2006). *Probability concepts in engineering: emphasis on applications to civil and environmental engineering*, second edition. John Wiley and Sons, Inc., Hoboken, New Jersey.

ANSS (2013). Advanced National Seismic System catalog, www.ncedc.org/anss. Advanced National Seismic System (ANSS), University of California, Berkeley, California.

Ariyaratana, C., and Fahnestock, L. A. (2011). "Evaluation of buckling-restrained braced frame seismic performance considering reserve strength." *Engineering Structures*, 33: 77–89.

ASCE (1986). "Structural serviceability: a critical appraisal and research needs." *Journal of Structural Engineering*, 112(12): 2646–2664.

ASCE (2002). *Design loads on structures during construction*. ASCE/SEI 37-02, American Society of Civil Engineers (ASCE), Reston, Virginia.

ASCE (2005). *Minimum design loads for buildings and other structures*. ASCE/SEI 7-05, American Society of Civil Engineers (ASCE), Reston, Virginia.

ASCE (2006). *Seismic rehabilitation of existing buildings*. ASCE 41-06, American Society of Civil Engineers (ASCE), Reston, Virginia.

ASCE (2010). *Minimum design loads for buildings and other structures*. ASCE/SEI 7-10, American Society of Civil Engineers (ASCE), Reston, Virginia, 2010.

ASCE (2014). *Seismic evaluation and retrofit of existing buildings*. ASCE 41-13, American Society of Civil Engineers (ASCE), Reston, Virginia.

Astaneh-Asl, A., Shen, J., and D'Amore, E. (1998). "Stability of damaged steel moment frames in Los Angeles — engineering structures." *Journal of Earthquake, Wind, and Ocean Engineering*, 20: 4–6.

Aster, R. (2012). "Expecting the unexpected: black swans and seismology." *Seismological Research Letters*, 83(1): 5–6.

Aswegan, K., Charney, F., and Jarrett, J. (2015). "Recommended procedures for damage based serviceability design of steel buildings under wind load." *Engineering Journal*, 52(1): 1–25.

ATC (1978). *Tentative provisions for the development of seismic regulations for buildings*. ATC-3-06, Applied Technology Council (ATC), Redwood City, California, 1978.

ATC (1984). *Tentative provisions for the development of seismic regulations for buildings*. ATC-3-06 Amended, Applied Technology Council (ATC), Redwood City, California.

ATC (2011). Wind speed website, www.atcouncil.org/windspeed. Applied Technology Council (ATC), Redwood City, California.

Atlayan, O., and Charney, F. A. (2011). “Lightly damped moment-resisting steel frames: a design-based approach.” *Engineering Journal*, 48(3): 183–197.

Atlayan, O., and Charney, F. A. (2014). “Hybrid buckling-restrained braced frames.” *Journal of Constructional Steel Research*, 96: 95–105.

B

Baker, J. W. (2011). “Conditional mean spectrum: tool for ground-motion selection.” *Journal of Structural Engineering*, 137(3): 322–331.

Baker, J. W. (2013). “Trade-offs in ground motion selection techniques for collapse assessment of structures.” Proceedings, *Vienna Congress on Recent Advances in Earthquake Engineering and Structural Dynamics 2013 (VEESD 2013)*, August 28–30, Vienna, Austria.

Baker, J. W., and Cornell, C. A. (2005). “A vector-valued ground motion intensity measure consisting of spectral acceleration and epsilon.” *Earthquake Engineering & Structural Dynamics*, 34(10): 1193–1217.

Baker, J. W., Lin, T., Shahi, S. K., and Jayaram, N. (2011). *New ground motion selection procedures and selected motions for the PEER transportation research program*. PEER Report 2011/03, Pacific Earthquake Engineering Research Center (PEER), University of California, Berkeley.

Balling, R.J., and Lyon, J.W. (2011). “Second-order analysis of plane frames with one element per member.” *Journal of Structural Engineering*, 137(11):1350–1358.

Barbato, M., Petrinib, F., Unnikrishnana, V. U., and Ciampolib, M. (2013). “Performance-based hurricane engineering (PBHE) framework.” *Structural Safety*, 45: 24–35.

Barber, M. A. (2011). *Contribution of shear connections to the lateral stiffness and strength of steel frames*. M.S. thesis, Civil Engineering, University of Cincinnati. Cincinnati, Ohio.

Bathe, K.-J. (1996). *Finite element procedures*. Prentice-Hall, Inc., Upper Saddle River, New Jersey.

Bathe, K.-J. (2007). "Conserving energy and momentum in nonlinear dynamics: a simple implicit time integration scheme." *Computers & Structures*, 85: 437–445.

Bathe, K.-J., and Cimento, A. P. (1980). "Some practical procedures for the solution of nonlinear finite element equations." *Computer Methods in Applied Mechanics and Engineering*, 22: 59–85.

Batoz, J.-L., and Dhatt, G. (1979). "Incremental displacement algorithms for nonlinear problems." *International Journal for Numerical Methods in Engineering: short Communications*, John Wiley and Sons, Ltd, 14: 1262–1267.

Batt, D. P., and Odeh, D. J. (2005). "A discussion and analysis of ductile detailing requirements for seismic design in moderate seismic regions." Proceedings, *Structures Congress*, April 20–24, New York, New York, 1–9.

Belytschko, T., Liu, W. K., Moran, B., Elkhodary, K. (2014). Nonlinear finite elements for continua and structures. John Wiley and Sons, Ltd., United Kingdom.

Bernal, D. (1994). "Viscous damping in inelastic structural response." *Journal of Structural Engineering*, 120(4): 1240–1254.

Berton, S. and Bolander, J. E. (2005). "Amplification system for supplemental damping devices in seismic applications." *Journal of Structural Engineering*, 131(6): 979–983.

Bilham, R. (2009). "The seismic future of cities." *Bulletin of Earthquake Engineering*, 7(4): 839–887.

Bleich, F. (1952). *Buckling strength of metal structures*. McGraw-Hill Book Company, Inc., New York, New York.

Boggs, D. W., and Dragovich, J. (2006). "The nature of wind loads and dynamic response." *Performance-based design of concrete buildings for wind loads*, American Concrete Institute, Farmington Hills, Michigan.

Boggs, D. W., and Peterka, J. A. (1992). "Wind speeds for design of temporary structures." Proceedings, *Structures Congress*, April 13-15, San Antonio, Texas.

Bommer, J. J., and Pinho, R. (2006). "Adapting earthquake actions in Eurocode 8 for performance-based seismic design." *Earthquake Engineering and Structural Dynamics*, 35(1): 39–55.

Boore, D. (2003). "Prediction of ground motion using the stochastic method." *Pure and Applied Geophysics*, 160: 635–676.

Borcherdt, R. D. (1994). "Estimates of site-dependent response spectra for design (methodology and justification)." *Earthquake Spectra*, 10: 617–653.

Borcherdt, R. D. (2002). "Empirical evidence for site coefficients in building code provisions." *Earthquake Spectra*, 18(2): 189–217.

Bowland, A., and Charney, F. (2010). "New concepts in modeling damping in structures." *Proceedings*, 19th Analysis & Computation Specialty Conference, American Society of Civil Engineers, Reston, Virginia.

Bozorgmehr, A. (2012). *Collapse assessment of PR composite connections*. M.S. thesis, Civil and Environmental Engineering, Chalmers University of Technology, Göteborg, Sweden.

Bozorgmehr, A., and Leon, R. T. (2012). Collapse assessment of partial restraint composite connection (PR-CC) moment resisting frames using FEMA P695 (ATC-63)

methodology. *Proceedings*, 15th World Conference on Earthquake Engineering, September 24–28, Lisbon, Portugal.

Bradley, B. A., and Dhakal, R. P. (2008). "Error estimation of closed-form solution for annual rate of structural collapse." *Earthquake Engineering and Structural Dynamics*, 37(15): 1721–1737.

Bruneau, M., and Reinhorn, A. (2007). "Exploring the concept of seismic resilience for acute care facilities." *Earthquake Spectra*, 23(1): 41–62.

Bruneau, M., Uang, C.-M., and Sabelli, R. (2011). *Ductile design of steel structures*, second edition. The McGraw-Hill Companies, Inc., New York, New York.

Buyco, K. (2014). "A new framework for quantifying ground motion intensity to estimate collapse vulnerability of buildings." Proceedings, *15th US-Japan Workshop on the Improvement of Structural Engineering and Resiliency*, December 3–5, Kohala Coast, Hawaii.

C

Carr, A. J. (2004). *Ruaumoko Manual Volume 1: theory and user guide to associate programs*. Department of Civil Engineering, University of Canterbury, Christchurch, New Zealand.

Carter, C. J., Murray, T. M., and Thornton, W. A. (2000). "Cost-effective steel building design." *Progress in Structural Engineering and Materials*, 2(1): 16–25.

Celik, O. C. (2007). *Probabilistic assessment of non-ductile reinforced concrete frames susceptible to mid-America ground motions*. Ph.D. dissertation, Civil Engineering, School of Civil and Environmental Engineering, Georgia Institute of Technology.

Cha, E. J., and Ellingwood, B. R. (2014). “Attitudes towards acceptance of risk to buildings from extreme winds.” *Structure and Infrastructure Engineering*, 10(6), 697–707.

Chai, H. (1998). “The post-buckling response of a bi-laterally constrained column.” *Journal of the Mechanics and Physics of Solids*, 46(7): 1155–1181.

Chai, H. (2001). “Contact buckling and postbuckling of thin rectangular plates.” *Journal of the Mechanics and Physics of Solids*, 49(2): 209–230.

Chai, H. (2002). “On the post-buckling behavior of bilaterally constrained plates.” *International Journal of Solids and Structures*, 39(11): 2911–2926.

Chandramohan, R., Lin, T., Baker, J. W., and Deierlein, G. G. (2013). “Influence of ground motion spectral shape and duration on seismic collapse risk.” *Proceedings*, 10th International Conference on Urban Earthquake Engineering, Tokyo, Japan.

Chapman, M. C. (1995). “A probabilistic approach to ground-motion selection for engineering design.” *Bulletin of the Seismological Society of America*, 85(3): 937–942.

Chapman, M. C. (2014). Personal communication.

Chapman, M.C. (2015). “Magnitude, recurrence interval, and near-source ground-motion modeling of the Mineral, Virginia, earthquake of 23 August 2011.” In Horton, J. W., Jr., Chapman, M. C., and Green, R. A., editors, *The 2011 Mineral, Virginia, earthquake, and its significance for seismic hazards in eastern north America*. Geological Society of America Special Paper 509.

Charney, F. A. (2008). “Unintended consequences of modeling damping in structures.” *Journal of Structural Engineering*, 134(4): 581–592.

Charney, F. A. (2010). *Nonlin*, version 8. Advanced Structural Concepts, Inc., Blacksburg, Virginia.

Charney, F. A. (2014). *Seismic loads: guide to the seismic load provisions of ASCE 7-10*. American Society of Civil Engineers, Reston, Virginia.

Charney, F. A. (2015). "The state of the art and practice for assessing seismic performance of new buildings using nonlinear response history analysis." Proceedings, *XI Congreso Chileno de Sismología e Ingeniería Sísmica*, Santiago, Chile.

Charney, F. A., and Horvilleur, J. F. (1995). "A technique for evaluating the effect of beam-column joint deformation on the lateral flexibility of steel frame building structures." *The structural design of tall buildings*, 4(1): 3–13.

Charney, F. A., and Johnson, R. (1986). "The effect of joint deformation on the drift of steel-framed structures." *Proceedings*, ASCE Structures Congress, New Orleans, Louisiana.

Charney, F. A., and Marshall, J. A. (2006). "Comparison of the Krawinkler and Scissors models for including beam–column joint deformations in the analysis of moment resisting frames." *Engineering Journal*, 43(1): 31–48.

Charney, F. A., and McNamara, R. J. (2008). "Comparison of methods for computing equivalent viscous damping ratios of structures with added viscous damping." *Journal of Structural Engineering*, 134(1): 32–44.

Charney, F. A., and Pathak, R. (2007). "Sources of elastic deformation in steel frame and framed-tube structures: part 1: simplified subassemblage models." *Journal of Constructional Steel Research*, 64(1): 87–100.

Charney, F. A., Darling, S., and Eatherton, M. (2012). Seismic performance of very short period buildings. *Proceedings*, 15th World Conference on Earthquake Engineering, Lisbon, Portugal.

Chen, D. (1999). *Vulnerability of tall buildings in hurricanes*. M.S. thesis, Civil Engineering, University of Western Ontario, Canada.

Chen, D. and Davenport, A.G. (2000). "Vulnerability of tall buildings in typhoons." *International Conference on Advances in Structural Dynamics*, 2: 1455–1462.

Chen, E. Y. (2012). *Multi-hazard design of mid- to high-rise structures*. M.S. thesis, Civil Engineering. University of Illinois at Urbana-Champaign, Urbana, Illinois.

Chen, W. F., and Lui, E. M. (1987). *Structural stability: theory and implementation*. Elsevier Science Publishing Co., Inc., New York, New York.

Cheever, P. J. (2013). Personal communication, 15 December 2013.

Cheever, P. J., and Hines, E. M. (2010). "How not to design for moderate seismic regions." *Proceedings*, Structures Congress, May 12–15, Orlando, Florida, 1342–1349.

Chittur Krishna Murthy, A. N. (2005). *Application of visco-hyperelastic devices in structural response control*. M.S. thesis, Civil Engineering. Virginia Polytechnic Institute and State University, Blacksburg, Virginia.

Chopra, A. K. (2012). *Dynamics of structures: theory and applications to earthquake engineering*, fourth edition. Prentice Hall, Upper Saddle River, New Jersey.

Christoph, A., Ibarra, L. F., and Krawinkler, H. (2004). "Evaluation of P-Delta effects in non-deteriorating MDOF structures from equivalent SDOF systems." *Proceedings*, 13th World Conference on Earthquake Engineering.

Ciampoli, M., Petrini, F., and Augusti, G. (2011). "Performance-based wind engineering: towards a general procedure." *Structural Safety*, 33(6): 367–378.

Cimellaro, G. P., Reinhorn, A. M., and Bruneau, M. (2010). "Framework for analytical quantification of disaster resilience." *Engineering Structures*, 32(11): 3639–3649.

Conn, A. (2013). *Q models for Lg wave attenuation in the central United States*. M.S. thesis, Department of Geosciences, Virginia Tech, Blacksburg, Virginia.

Constantinou, M. C., Tsopelas, P., Hammel, W., and Sigaher, A. N. (2001). "Toggle-brace-damper seismic energy dissipation systems." *Journal of Structural Engineering*, 127(2): 105–112.

Cornell, C. A., and Winterstein, S.R. (1988). "Temporal and magnitude dependence in earthquake recurrence models." *Bulletin of the Seismological Society of America*, 78(4): 1522–1537.

Council on Tall Buildings and Urban Habitat (CTBUH) (2014). *Roadmap on the future research needs of tall buildings*. Oldfield, P., Trabucco, D., and Wood, A., editors. Council on Tall Buildings and Urban Habitat, Chicago, Illinois.

Crosti, C., Duthinh, D., and Simiu, E. (2011). "Risk consistency and synergy in multihazard design." *Journal of Structural Engineering*, 137(8): 884–849.

Crowley, H., Colombi, M., Borzi, B., Faravelli, M., Onida, M., Lopez, M., Polli, D., Meroni, F., and Pinho, R. (2009). "A comparison of seismic risk maps for Italy." *Bulletin of Earthquake Engineering*, 7(1): 149–180.

D

Dassault Systèmes (2011a). *ABAQUS/Standard*, version 6.11. Dassault Systemes Simulia Corp. (Dassault Systèmes), Providence, Rhode Island.

Dassault Systèmes (2011b). *Abaqus 6.11 Analysis User's Manual*. Dassault Systèmes Simulia Corp. (Dassault Systèmes), Providence, Rhode Island.

Deierlein, G. G., and Victorsson, V. (2008). *Fragility curves for components of steel SMF systems*. FEMA P-58/BD-3.8.3 Background Document, Federal Emergency Management Agency, Washington, D. C.

Deierlein, G. G., Reinhorn, A. M., and Willford, M. R. (2010). "Nonlinear structural analysis for seismic design," *NEHRP Seismic Design Technical Brief No. 4*, produced by the NEHRP Consultants Joint Venture, a partnership of the Applied Technology Council and the Consortium of Universities for Research in Earthquake Engineering, for the National Institute of Standards and Technology, Gaithersburg, MD, NIST GCR 10-917-5.

Denavit, M. D., and Hajjar, J. F. (2013). *Description of geometric nonlinearity for beam-column analysis in OpenSees*. Department of Civil and Environmental Engineering Reports. Report No. NEU-CEE-2013-02. Department of Civil and Environmental Engineering, Northeastern University, Boston, Massachusetts.

Der Kiureghian, A. (2005). "Non-ergodicity and PEER's framework formula." *Earthquake Engineering and Structural Dynamics*, 34: 1643–1652.

Douglas, J., Ulrich, T., and Negulescu, C. (2013). "Risk-targeted seismic design maps for mainland France." *Natural Hazards*, 65(3): 1999–2013.

Duthinh, D., and Simiu, E. (2010). "Safety of structures in strong winds and earthquakes: multi-hazard considerations." *Journal of Structural Engineering*, 136(3): 330–333.

E

Eads, L., Miranda, E., Krawinkler, H., and Lignos, D. G. (2013). "An efficient method for estimating the collapse risk of structures in seismic regions." *Earthquake Engineering and Structural Dynamics*, 42(1): 25–41.

Eatherton, M. R., and Hajjar, J. F. (2011). “Residual drifts of self-centering systems including effects of ambient building resistance.” *Earthquake Spectra*, 27(3): 719–744.

Elkady A., and Lignos, D. G. (2013). “Effect of composite action on the dynamic stability of special steel moment resisting frames designed in seismic regions.” Proceedings, *Structures Congress*, Pittsburgh, Pennsylvania.

Elkady A., and Lignos, D. G. (2014). “Modeling of the composite action in fully restrained beam-to-column connections: implications in the seismic design and collapse capacity of steel special moment frames. *Earthquake Engineering & Structural Dynamics*, 43(13): 1935–1954.

Ellingwood, B. R., and Dusenberry, D. O. (2005). “Building design for abnormal loads and progressive collapse.” *Computer-Aided Civil and Infrastructure Engineering*, 20: 194–205.

Elnashai, A. S., and Di Sarno, L. (2008). *Fundamentals of earthquake engineering*. John Wiley and Sons, Ltd. United Kingdom.

Engelhardt, M. D., Venti, M. J., Fry, G. T., Jones, S. L., and Holliday, S. D. (2000). *Behavior and design of radius cut reduced beam section connections*. Report No. SAC/BD-00/17, SAC Joint Venture, Sacramento, California.

ENR (2011). *Square foot costbook*. Engineering News Record (ENR), Design and Construction Resources, Vista, California.

F

FEMA (2000a). *State of the art on systems performance of steel moment frames subjected to earthquake ground shaking*. FEMA 355C, prepared by the SAC Joint Venture for the Federal Emergency Management Agency (FEMA), Washington, D. C.

FEMA (2000b). *State of the art report on connection performance*. FEMA-355D, Federal Emergency Management Agency, Washington, D. C.

FEMA (2003). *NEHRP recommended provisions and commentary for seismic regulations for new buildings and other structures*. FEMA P-450, Federal Emergency Management Agency (FEMA), Washington, D. C.

FEMA (2006). *Next-generation performance-based seismic design guidelines: program plan for new and existing buildings*. FEMA P-445, Federal Emergency Management Agency (FEMA), Washington, D. C.

FEMA (2008a). *Taking shelter from the storm: building a safe room for your home or small business*. FEMA P-320, Federal Emergency Management Agency (FEMA), Washington, D.C.

FEMA (2008b). *Design and construction guidance for community safe rooms*. FEMA P-361, Federal Emergency Management Agency (FEMA), Washington, D.C.

FEMA (2009a). *Quantification of building seismic performance factors*. FEMA P-695, Federal Emergency Management Agency (FEMA), Washington, D. C.

FEMA (2009b). *Effects of strength and stiffness degradation on seismic response*. FEMA P-440A, Federal Emergency Management Agency (FEMA), Washington, D. C.

FEMA (2009c). *NEHRP Recommended provisions for seismic design of new buildings and other structures*. FEMA P-750, Federal Emergency Management Agency (FEMA), Washington, D. C.

FEMA (2012a). *Seismic performance assessment of buildings, volume 1—methodology* (FEMA P-58-1). Federal Emergency Management Agency (FEMA), Washington, D. C.

FEMA (2012b). *Seismic performance assessment of buildings, volume 2—implementation guide* (FEMA P-58-2). Federal Emergency Management Agency, Washington, D. C.

FEMA (2012c). *Seismic performance assessment of buildings, volume 3—spreadsheet tools*. Federal Emergency Management Agency (FEMA), Washington, D. C.

FEMA (2012d). *Seismic performance assessment of buildings, volume 3—Performance Assessment Calculation Tool (PACT), version 2.9.65*. Federal Emergency Management Agency (FEMA), Washington, D. C.

FEMA (2012e). *2009 NEHRP Recommended Seismic Provisions Design Examples*. FEMA P751, prepared by the Applied Technology Council for the Federal Emergency Management Agency (FEMA), Washington, D. C.

Fernández, J. A. (2007). *Numerical simulation of earthquake ground motions in the upper Mississippi embayment*. Ph.D. dissertation, Civil Engineering, School of Civil and Environmental Engineering, Georgia Institute of Technology.

Flores, F. X. (2015). *Influence of the gravity system on the seismic performance of special steel moment frames*. Ph.D. dissertation, Civil Engineering. Virginia Polytechnic Institute and State University, Blacksburg, Virginia.

Flores, F. X., and Charney, F. A. (2014). “The influence of gravity system framing on the seismic performance of special steel moment frames.” Proceedings, *10th National Conference in Earthquake Engineering*, Anchorage, Alaska.

Flores, F. X., Jarrett, J. A., and Charney, F. A. (2012). “The influence of gravity-only framing on the performance of steel moment frames.” Proceedings, *15th World Conference on Earthquake Engineering*, Lisbon, Portugal.

Foutch, D. A., and Yun, S.-Y. (2002). “Modeling of steel moment frames for seismic loads.” *Journal of Constructional Steel Research*, 58: 529–564.

Freeman, G., Lee, J. C., and Ettouney, M. M. (2005). “Multihazard design of tall buildings.” *Proceedings*, Council on Tall Buildings and Urban Habitat, New York World Congress.

G

Ghafory-Ashtiany, M, Mousavi, M., Azarbakht, A. (2011). “Strong ground motion record selection for the reliable prediction of the mean seismic collapse capacity of a structure group.” *Earthquake Engineering and Structural Dynamics*, 40(6): 691–708.

Galambos, T. V, and Ellingwood, B. (1986). “Serviceability limit state: deflection.” *Journal of Structural Engineering*, 112(1): 67–84.

Gani, F. and Légeron, F. (2012). “Relationship between specified ductility and strength demand reduction for single degree-of-freedom systems under extreme wind events.” *Journal of Wind Engineering and Industrial Aerodynamics*, 109: 31–45.

Gere, J. M., and Timoshenko, S. P. (1990). *Mechanics of materials*, third edition. PWS-KENT Publishing Company, Boston, Massachusetts.

GEER Team (2012). “Geotechnical reconnaissance of the 2011 Central Virginia earthquake: report of the National Science Foundation sponsored Geotechnical Extreme Events Reconnaissance (GEER) Team.” J. R. Martin, (editor).

Genna, F., and Bregoli, G. (2014). “Small amplitude elastic buckling of a beam under monotonic axial loading, with frictionless contact against movable rigid surfaces.” *Journal of mechanics of materials and structures*, 9(4): 441–463.

Genna, F., and Gelfi, P. (2012a). “Analysis of the lateral thrust in bolted steel buckling-restrained braces. I: experimental and numerical results.” *Journal of Structural Engineering*, 138(10): 1231–1243.

Genna, F., and Gelfi, P. (2012b). “Analysis of the lateral thrust in bolted steel buckling-restrained braces. II: engineering analytical estimates.” *Journal of Structural Engineering*, 138(10): 1244–1254.

Ghafory-Ashtiany, M., Mousavi, M., and Azarbakht, A. (2011). “Strong ground motion record selection for the reliable prediction of the mean seismic collapse capacity of a structure group.” *Earthquake Engineering and Structural Dynamics*, 40(6): 691–708.

Giardini, D., Woessner, J., Danciu, L., Crowley, H., Cotton, F., Grünthal, G., Pinho, R., Valensise, G., Akkar, S., Arvidsson, R., Basili, R., Cameelbeeck, T., Campos-Costa, A., Douglas, J., Demircioglu, M. B., Erdik, M., Fonseca, J., Glavatovic, B., Lindholm, C., Makropoulos, K., Meletti, C., Musson, R., Pitilakis, K., Sesetyan, K., Stromeyer, D., Stucchi, M., and Rovida, A. (2013b). Seismic Hazard Harmonization in Europe (SHARE): Online Data Resource. http://www.efehr.org.

Giardini, D., Woessner, J., Danciu, L., Crowley, H., Cotton, F., Grünthal, G., Pinho, R., Valensise, G., and the SHARE consortium (2013a). *SHARE European seismic hazard*

map for peak ground acceleration, 10% exceedance probabilities in 50 years. http://www.share-eu.org, 2013.

Godfrey, E., Olgun, C. G., Martin, J. R., Amine, M. S. (2012). "Site amplification in Washington metropolitan area during the 2011 Virginia earthquake." Meeting of the Eastern Section of the Seismological Society of America, October 29–30, Blacksburg, Virginia.

Grant, D. N., and Diaferia, R. (2012). "Assessing adequacy of spectrum-matched ground motions for response history analysis." *Earthquake Engineering and Structural Dynamics*, 42(9): 1265–1280.

Griffis, L. (1993). "Serviceability limit states under wind." *Engineering Journal*, 30: 1–16.

Griffis, L., Patel, V., Muthukumar, S., and Baldava, S. (2012). "A framework for performance-based wind engineering." *Advances in Hurricane Engineering*, Applied Technology Council and Structural Engineering Institute.

Gupta, A., and Krawinkler, H. (1999). "Seismic demands for performance evaluation of steel moment resisting frame structures." *Technical Report 132*, The John A. Blume Earthquake Engineering Research Center, Department of Civil Engineering, Stanford University, Stanford, California.

Gupta, A., and Krawinkler, H. (2000). "Dynamic P-Delta effects for flexible inelastic steel structures." *Journal of Structural Engineering*, 126(1): 145–154.

Gutenberg, R., and Richter, C.F. (1944). "Frequency of earthquakes in California." *Bulletin of the Seismological Society of America*, 34: 185–188.

H

Hall, J. F. (2006). "Problems encountered from the use (or misuse) of Rayleigh damping." *Earthquake Engineering and Structural Dynamics*, 35: 525–545.

Hamburger, R. O., Krawinkler, H., Malley, J. O., and Adan, S. M. (2009). “Seismic design of steel special moment frames: a guide for practicing engineers,” *NEHRP Seismic Design Technical Brief No. 2*, NIST GCR 09-917-3, produced by the NEHRP Consultants Joint Venture, a partnership of the Applied Technology Council and the Consortium of Universities for Research in Earthquake Engineering, for the National Institute of Standards and Technology, Gaithersburg, Maryland.

Hamburger, R. O., Rojahn, C., Heintz, J. A., and Mahoney, M. G. (2012). “FEMA P58: Next-generation building seismic performance assessment methodology.” *Proceedings*, 15th World Conference on Earthquake Engineering, Lisbon, Portugal.

Hanks, T., and McGuire, R. (1981). “The character of high-frequency strong ground motion.” *Bulletin of the Seismological Society of America*, 71: 2071–2095.

Hann, F. L., Balaramudu, V. K., and Sarkar, P. P. (2010). “Tornado-induced wind loads on a low-rise building.” *Journal of Structural Engineering*, 136(1): 106–116.

Hardyniec, A. (2014). *An investigation of the behavior of structural systems with modeling uncertainties*. Ph.D. dissertation, Civil Engineering. Virginia Polytechnic Institute and State University, Blacksburg, Virginia.

Hardyniec, A., and Charney, F. A. (2015). “A new efficient method for determining the collapse margin ratio using parallel computing.” *Computers and Structures*, 148: 14–15.

Hart, G. C., and Jain, A. (2013). “Performance based wind design of tall concrete buildings in the Los Angeles region utilizing structural reliability and nonlinear time history analysis.” Proceedings, *12th Americas Conference on Wind Engineering (12ACWE)*, June 16-20, Seattle, Washington.

Haselton, C., and Churapalo, T. (2012). *PACT beta test overview: example buildings, sites, and ground motions*. FEMA P-58/BD-3.7-13 Background Document, Federal Emergency Management Agency, Washington, D. C

Hashash, Y., and Moon, S. (2011). *Site amplification factors for deep deposits and their application in seismic hazard analysis for central U. S*. Technical Report, United States Geological Survey, Reston, Virginia.

Hibbeler, R. C. (1995). *Structural analysis*, 3rd edition. Prentice-Hall, Inc. Englewood Cliffs, New Jersey.

Hines, E. M., and Fahnestock, L. A. (2010). "Design philosophy for steel structures in moderate seismic regions." *Proceedings*, 9th US National and 10th Canadian Conference on Earthquake Engineering, Toronto, Canada.

Hines, E. M., Appel, M. E., and Cheever, P. J. (2009). "Collapse performance of low-ductility chevron braced steel frames in moderate seismic regions." *Engineering Journal*, Q3, 149–180.

Hines, E. M., Baise, L. G., and Swift, S. S. (2011). "Ground-motion suite selection for eastern North America." *Journal of Structural Engineering*, 137(3): 358–366.

Hoffman, D. (2001). *Classification of soils for amplification induced by earthquake ground motions of the Cape Girardeau 7.5' quadrangle, Cape Girardeau County, Missouri*. Missouri Department of Natural Resources, Division of Geology and Land Survey, Open-File Map OFM-01-400-GS, scale 1:24,000.

Holzer, T. L., and Savage, J. C. (2013). "Global earthquake fatalities and population." *Earthquake Spectra*, 29(1): 155–175.

Hong, H. P. (2004). “Accumulation of wind induced damage on bilinear SDOF systems.” *Wind and Structures*, 7(3): 145–458.

Horton, J. W. (2012). “The 2011 Virginia Earthquake: what are scientists learning?” *Eos*, 93(33): 317–324.

Hsiao, P.-C., Lehman, D. E., and Roeder, C. W. (2013). “Evaluation of the response modification coefficient and collapse potential of special concentrically braced frames.” *Earthquake Engineering and Structural Dynamics*, 42(10): 1547–1564.

Huang, G., and Chen, X. (2007). “Wind load effects and equivalent static wind loads of tall buildings based on synchronous pressure measurements.” *Engineering Structures*, 29: 2641–2653.

Huang, H. C. (2004). “Parametric study for motion amplification device with viscous damper.” Proceedings, *13th World Conference on Earthquake Engineering*, August 1–6, Vancouver, B. C., Canada.

Huang, Y.-N., Whittaker, A. S., and Luco, N. (2008). Maximum spectral demands in the near-fault region. *Earthquake Spectra* 24(1): 319–341.

Huang, Y.-N., Whittaker, A. S., and Luco, N. (2010a). “Establishing maximum spectral demand for performance-based earthquake engineering: collaborative research with the University at Buffalo and the USGS.” Technical Report: United States Geological Survey, Reston, Virginia. USGS Award Number 08HQGR0017.

Huang, Y.-N, Whittaker, A. S., and Luco, N. (2010b). “NEHRP site amplification factors and the NGA relationships.” *Earthquake Spectra*, 26(2): 583–593.

Humar, J., Mahgoub, M., and Ghorbanie-Asl, M. (2000). “Effect of second-order forces on seismic response.” *Canadian Journal of Civil Engineering*, 33(6): 692–706.

Hwang, J.-S., Huang, Y.-N., and Hung, Y.-H. (2005). “Analytical and experimental study of toggle-brace-damper systems.” *Journal of Structural Engineering*, 131(7): 1035–1043.

Hwang, J.-S., Huang, Y.-N., Yi, S.-L., and Ho, S.-Y. (2008). “Design formulations for supplemental viscous dampers to building structures.” *Journal of Structural Engineering*, 134(1): 22–31.

Hwang, J.-S., Wang, S.-J., Huang, Y.-N., and Tsai, C.-H. (2006). “Experimental study of a RC structure with toggle-brace-dampers.” *4th International Conference on Earthquake Engineering*, October 12–13, Taipei, Taiwan.

I

Ibarra, L. F., and Krawinkler, H. (2005). *Global collapse of frame structures under seismic excitations*. Report 152, Department of Civil and Environmental Engineering, Stanford University, Stanford, California.

Ibrahim, Y. E.-H. (2005). *A new visco-plastic device for seismic protection of structures*. Ph.D. dissertation, Civil Engineering. Virginia Polytechnic Institute and State University, Blacksburg, Virginia.

ICC (2012a). *International building code*. International Code Council (ICC), Country Club Hills, Illinois.

ICC (2012b). *International performance code*. International Code Council (ICC), Country Club Hills, Illinois.

ICC-ES (2013). *Simpson Strong-Tie® Strong Frame® steel special moment frame connection*. Evaluation report ESR-2802, International Code Council (ICC) Evaluation Service (ES), Country Club Hills, Illinois.

J

Jarrett, J. A. (2013). *Performance assessment of seismic resistant steel structures*. Ph.D. dissertation, Civil Engineering. Virginia Polytechnic Institute and State University, Blacksburg, Virginia.

Jarrett, J. A., Judd, J. P., and Charney, F. A. (2015). "Comparative evaluation of innovative and traditional seismic-resistant systems using FEMA P-58." *Journal of Constructional Steel Research*, 105: 107–118.

Jehel, P., Leger, P., and Ibrahimbegovic, A. (2011). "Modeling energy dissipation: a paradigm for performance-based engineering of RC moment-resisting frame in seismic loading." *Proceedings*, Computational Methods in Structural Dynamics and Earthquake Engineering (COMPDYN), May 26–28, Corfu, Greece.

Jin, C. (2003). *Use of hyperelastic devices to control the seismic response of structures*. M.S. report, Civil Engineering, Virginia Polytechnic Institute and State University, Blacksburg, Virginia.

Judd, J. P. (2005). *Analytical modeling of wood-frame shear walls and diaphragms*. M.S. thesis, Civil Engineering, Brigham Young University, Provo, Utah.

Judd, J. P. (2006). *Quick*, version 1.5. Department of Civil and Environmental Engineering, Brigham Young University, Provo, Utah.

Judd, J. P., and Charney, F. A. (2014a). "Performance-based design in the central and eastern United States." Proceedings, *45th Structures Congress*, Boston, Massachusetts.

Judd J. P., and Charney, F. A. (2014b). "Seismic performance of buildings designed for wind." Proceedings, *45th Structures Congress*, Boston, Massachusetts.

Judd J. P., and Charney, F. A. (2014c). “Earthquake risk analysis of structures.” Proceedings, *9th International Conference on Structural Dynamics (Eurodyn)*, European Association for Structural Dynamics (EASD) and the Faculty of Engineering of the University of Porto (FEUP), June 30–July 2, Porto, Portugal.

Judd J. P., and Charney, F. A. (2014d). “Seismic collapse prevention systems.” Proceedings, *10th National Conference on Earthquake Engineering (NCEE)*, Earthquake Engineering Research Institute, July 21–25, Anchorage, Alaska.

Judd J. P., and Charney, F. A. (2014e). “Resilience of steel moment-frame buildings with reserve lateral strength.” Proceedings, *15th US-Japan Workshop on the Improvement of Structural Engineering and Resiliency*, December 3–5, Kohala Coast, Hawaii.

Judd J. P., and Charney, F. A. (2015a). “Inelastic building behavior and collapse risk for wind loads.” Proceedings, *46th Structures Congress*, American Society of Civil Engineers, April 23–25, Portland, Oregon.

Judd J. P., and Charney, F. A. (2015b). “Analytical design methodology for the buckling restraint mechanism in the Strong-Frame® special moment frame connection system.” Report No. CE/VPI-ST-15/02, Department of Civil and Environmental Engineering, Virginia Polytechnic Institute and State University, Blacksburg, Virginia.

Judd, J. P., and Fonseca, F. S. (2006). “Equivalent single degree of freedom model for wood shearwalls and diaphragms.” *Proceedings, 9th World Conference on Timber Engineering*, August 6–10, Portland, Oregon.

K

Kalkan, E., and Chopra, A. K. (2011). “Modal-pushover-based ground-motion scaling procedure.” *Journal of Structural Engineering*, 137(3): 298–310.

Kanvinde, A. M., and Deierlein, G. G. (2004). *Micromechanical simulation of earthquake-induced fracture in steel structures*. Report 145, Dept. of Civil and Environmental Engineering, Stanford University, Stanford, California.

Kareem, A., Spence, S. M. J., and Bernardini, E. (2013). “Performance-based design of wind-excited tall and slender structures.” Report, NatHaz Modeling Laboratory, University of Notre Dame.

Kasperson, R. E. (2012). “A perspective on the social amplification of risk.” *The Bridge*, 42(3): 23–27.

Kelly, J. M. (2004). “Seismic isolation.” *Earthquake engineering: from engineering seismology to performance-based engineering*, Bozorgnia, Y. and Bertero, V., eds., CRC Press, Boca Raton, Florida.

Kennedy, R. P. (2011). “Performance-goal based (risk informed) approach for establishing the SSE site specific response spectrum for future nuclear power plants.” *Nuclear Engineering and Design*, 241(3): 648–656.

Kottke, A. R., Hashash, Y. M-A., Stewart, J. P., Moss, C. J., Nikolaou, S., Rathje, E. M., Silva, W. J., and Campbell, K. W. (2012). “Development of geologic site classes for seismic site amplification for central and eastern North America.” *Proceedings*, 15th World Conference on Earthquake Engineering, Lisbon, Portugal.

Kramer, S. L. (1996). *Geotechnical earthquake engineering*. Prentice-Hall, Inc., Upper Saddle River, New Jersey.

Krawinkler, H. (1978). “Shear in beam-column joints in seismic design of frames.” *Engineering Journal*, American Institute of Steel Construction, 15(3): 82–91.

Kwok, K. C. S., Burton, M. D., and Abdelrazaq, A. (2015). *Wind-induced motion of tall buildings: designing for habitability*. American Society of Civil Engineers, Reston, Virginia.

L

LADBS (2014). *Reevaluation — Simpson Strong-Tie® Strong Frame Special Moment Frame Connection*. Research Report No. 25957. Los Angeles Department of Building and Safety (LADBS), Los Angeles, California.

Lee, K. (2000). Performance prediction and evaluation of steel special moment frames for seismic loads. Ph.D. dissertation, Civil Engineering, University of Illinois at Urbana-Champaign, Urbana, Illinois.

Lee, K., and Foutch, D. A. (2002). “Seismic performance evaluation pre-Northridge steel frame buildings with brittle connections.” *Journal of Structural Engineering*, 128(4): 546–555.

Lee, K. S. (2003). *Seismic behavior of structures with dampers made from ultra high damping natural rubber*. Ph.D. dissertation, Structural Engineering, Lehigh University, Bethlehem, Pennsylvania.

Lee, S.-H., Min, K.-W., Chung, L., Lee, S.-K., Lee, M.-K., Hwang, J.-S., Choi, S.-B., and Lee, H.-G. (2007). “Bracing systems for installation of MR dampers in a building structure.” *Journal of Intelligent Material Systems and Structures*, 18: 1111–1120.

Leon, R. T. (1998). “Composite connections.” *Progress in Structural Engineering and Materials*, 1(2): 159–169.

Leyendecker, E. V., Hunt, R. J., Frankel, A. D., and Rukstales, K. S. (2000). “Development of maximum considered earthquake ground motion maps.” *Earthquake Spectra*, 16(1): 21–40.

Li, Y. (2012). “Assessment of damage risks to residential buildings and cost-benefit of mitigation strategies considering hurricane and earthquake hazards.” *Journal of Performance of Constructed Facilities*, 26(1): 7–16.

Li, Y., Yin, Y., Ellingwood, B. R., and Bulleit, W. M. (2010). “Uniform hazard versus uniform risk bases for performance-based earthquake engineering of light-frame wood construction.” *Earthquake Engineering and Structural Dynamics*, 39(11): 1199–1217.

Liel, A. B., Haselton, C. B., Deierlein, G. G., and Baker, J. W. (2009). “Incorporating modeling uncertainties in the assessment of seismic collapse risk of buildings.” *Structural Safety*, 31: 197–211.

Lignos, D. (2008). *Sidesway collapse of deteriorating structural systems under seismic excitations*. Ph.D. dissertation, Civil Engineering, Stanford University, Stanford, California.

Lignos, D., Chung, Y., Nagae, T., and Nakashima, M. (2011). “Numerical and experimental evaluation of seismic capacity of high-rise steel buildings subjected to long duration earthquakes.” *Computers and Structures* 89: 959–967.

Lignos, D., Hikino, T., Matsuoka, Y., and Nakashima, M. (2013). “Collapse assessment of steel moment frames based on E-Defense full-scale shake table collapse tests.” *Journal of Structural Engineering*, 139(1): 120-132.

Lignos, D. G., and Krawinkler, H. (2011). “Deterioration modeling of steel components in support of collapse prediction of steel moment frames under earthquake loading.” *Journal of Structural Engineering*, 137(11): 1291–1302.

Lignos, D. G., and Krawinkler, H. (2012). “Development and utilization of structural component databases for performance-based earthquake engineering.” *Journal of Structural Engineering*, American Society of Civil Engineers, posted online ahead of print August 10, 2012.

Lin, T., Haselton, C. B., and Baker, J. W. (2013). “Conditional-spectrum-based ground motion selection. Part II: intensity-based assessments and evaluation of alternative target spectra.” *Earthquake Engineering and Structural Dynamics*, 42(12): 1867–1884.

Liu, J., and Astaneh-Asl, A. (2000). “Cyclic testing of simple connections including effects of slab.” *Journal of Structural Engineering*, 126(1): 32–39.

Liu, J., and Astaneh-Asl, A. (2004). “Moment-rotation parameters for composite shear tab connections.” *Journal of Structural Engineering*, 130(9): 1371–1380.

Lowes, L. N. (2004). *A beam-column joint model for simulating the earthquake response of reinforced concrete frames*. PEER Report 2003/10, Pacific Earthquake Engineering Research Center, College of Engineering, University of California, Berkeley, California.

Lowes, L. N., Mitra, N., and Altoonash, A. (2004). “A beam-column joint model for simulating the earthquake response of reinforced concrete frames.” *PEER Report 2003/10*, Pacific Earthquake Engineering Research Center, University of California, Berkeley, California.

Luco, N. (2006). *Towards risk-targeted ground motion maps*. USGS central and eastern United States Workshop, May 9, Boston, Massachusetts.

Luco, N., Ellingwood, B. R., Hamburger, R. O., Hooper, J. D., Kimball, J. K., and Kircher, C. A. (2007). Risk-targeted versus current seismic design maps for the conterminous United States. *Proceedings*, SEAOC 76th Annual Convention. Structural Engineers Association of California, Sacramento, California.

M

Magistrale, H., Rong, Y., Silva, W., and Thompson, E. (2012). A site response map of the continental U. S. *Proceedings*, 15th World Conference on Earthquake Engineering, September 24–28, Lisbon, Portugal.

Marshall, J. D. (2008). *Development, analysis and testing of a hybrid passive control device for seismic protection of framed structures*. Ph.D. dissertation, Civil Engineering. Virginia Polytechnic Institute and State University, Blacksburg, Virginia.

Marshall J. D., and Charney, F. A. (2010a). "A hybrid passive control device for steel structures I: development and analysis." *Journal of Constructional Steel Research*, 66(10): 1278–1286.

Marshall J. D., and Charney, F. A. (2010b). "A hybrid passive control device for steel structures II: physical testing." *Journal of Constructional Steel Research*, 66(10): 1287–1294.

Marshall J. D., and Charney, F. A. (2012). "Seismic response of steel frame structures with hybrid passive control systems." *Earthquake Engineering and Structural Dynamics*, 41(4): 715–733.

Massey, F. J. (1951). "The Kolmogorov-Smirnov test for goodness of fit." *Journal of the American Statistical Association*, 46(253): 68–78.

MATLAB (2011). *MATLAB*, version 7.12.0.635 (R2011a). The MathWorks Inc., Natick, Massachusetts.

Matthews, M. V., Ellsworth, W. L., and Reasenberg. (2002). "A Brownian model for recurrent earthquakes." *Bulletin of the Seismological Society of America*, 92(6): 2233–2250.

Mazzoni, S., McKenna, F., Scott, M. H., and Fenves, G. L. (2010). Open system for earthquake engineering simulation user command language manual. Pacific Earthquake Engineering Research Center, University of California, Berkeley, California. < http://opensees.berkeley.edu/wiki/index.php/Command_Manual > (12 Oct. 2011).

McGuire, R. K., Silva, W. J., and Constantino, C. J. (2001). *Technical basis for revision of regulatory guidance on design ground motions*. Report NUREG/CR-6728, U. S. Nuclear Regulatory Commission.

McKenna, F., Fenves, G. L., Scott, M. H., Haukaas, T., Kiureghian, A. D., M. de Souza, R., Filippou, F. C., Mazzoni, S., and Jeremic, B. (2000–2011). *Open Systems for Earthquake Engineering Simulation (OpenSees)*, version 2.3.1. Pacific Earthquake Engineering Research Center, University of California, Berkeley, California. < http://opensees.berkeley.edu/OpenSees > (20 Aug. 2011).

Medina R. A., and Krawinkler H. (2003). *Seismic demands for nondeteriorating frame structures and their dependence on ground motions*. PEER Report 2003/15, Pacific Earthquake Engineering Research Center, University of California, Berkeley, California.

Metlay, D., and Sarewitz, D. (2012). "Decision strategies for addressing complex, 'messy' problems." *The Bridge*, 42(3): 6–16.

Milburn, T. W. (2009). *A comparison of the structural response to synthetic earthquake ground motions compatible with central eastern United States attenuation models*. Ph.D. dissertation, Civil Engineering. University of Louisville, Louisville, Kentucky.

Murray, T. M., Allen, D. E., and Ungar, E. E. (2003). *Floor vibrations due to human activity*. AISC Design Guide No. 11, 2nd printing. American Institute for Steel Construction, Chicago, Illinois.

Muthukumar, S., Baldava, S., and Garber, J. (2012). "Performance-based evaluation of an existing building subjected to wind forces." *Advances in Hurricane Engineering*, Applied Technology Council and Structural Engineering Institute.

N

Naga, P., and Eatherton, M. R. (2014). "Analyzing the effect of moving resonance on seismic response of structures using wavelet transforms." *Earthquake Engineering & Structural Dynamics*, 43: 759–768.

NAP (2012). *Disaster resilience: a national imperative*. National Academies Press (NAP), The National Academies, Washington, D. C.

Nassar, A. A., and Krawinkler, H. (1991). *Seismic demands for SDOF and MDOF systems*. Report 95, Department of Civil and Environmental Engineering, Stanford University, Stanford, California.

Nelson, T. A., Gryniuk, M. C., and Hines, E. M. (2006). "Comparison of low-ductility moment resisting frames with chevron braced frames under moderate seismic demands." *Proceedings*, 8th U. S. National Conference on Earthquake Engineering, April 18–22, San Francisco, California.

Newmark, N. M. (1959). “A method for computation for structural dynamics.” *Journal of the Engineering Mechanics Division*, 85: 67–94.

Nikolaou, S., Go, J. E., Beyzaei, C. Z., Moss, C., and Deming, P. W. (2012). “Geo-seismic design in the eastern United States: state of practice.” Geotechnical Engineering State of the Art and Practice, *Proceedings* from Geo-Congress, March 25–29, Oakland, California.

NIST (2010a). *Evaluation of the FEMA P-695 methodology for quantification of building seismic performance factors*. NIST GCR 10-917-8, National Institute of Standards and Technology (NIST), Gaithersburg, Maryland.

NIST (2010b). *Applicability of nonlinear multiple-degree-of-freedom modeling for design: supporting documentation*. NIST GCR 10-917-9, National Institute of Standards and Technology (NIST), Gaithersburg, Maryland.

NIST (2011). *Selecting and scaling earthquake ground motions for performing response-history analysis*. NIST GRC 11-917-15, National Institute of Standards and Technology (NIST), Gaithersburg, Maryland.

NIST (2012a). *Soil-structure interaction for building structures*. NIST GCR 12-917-21, National Institute of Standards and Technology (NIST), Gaithersburg, Maryland.

NIST (2012b). *Tentative framework for development of advanced seismic design criteria for new buildings*. NIST GCR 12-917-20, National Institute of Standards and Technology (NIST), Gaithersburg, Maryland.

NIST (2012c). Seismic analysis and design procedures in existing standards project, www.nist.gov/el/nehrp. National Institute of Standards and Technology (NIST), Gaithersburg, Maryland.

NIST (2014a). *Technical investigation of the May 22, 2011 tornado in Joplin, Missouri*. NIST NCSTAR 3, National Institute of Standards and Technology (NIST), Gaithersburg, Maryland.

NIST (2014b). *Measurement Science R&D Roadmap for Windstorm and Coastal Inundation Impact Reduction*. NIST GRC 11-973-13, National Institute of Standards and Technology (NIST), Gaithersburg, Maryland.

O

Oesterle, M. (2002). *The use of nonlinear fluid viscous dampers in nonlinear dynamic analysis*. M.S. thesis, Civil Engineering, Virginia Polytechnic Institute and State University, Blacksburg, Virginia.

Olsen, A. H., Heaton, T. H., and Hall, J. F. (2014). "Characterizing ground motions that collapse steel, special moment-resisting frames or make them unrepairable." *Earthquake Spectra*, Published Online: January 14.

Olshansky, R., Wu, Y., and French, S. (2003). *Evaluating earthquake risk in mid-American communities*. Final Report, Project SE-5 (Earthquake Loss Estimate Methods for Essential Facilities), Mid-America Earthquake Center, University of Illinois at Urbana-Champaign, Urbana, Illinois.

P

Pate-Cornell, E. (1994). "Quantitative safety goals for risk management of industrial facilities." *Structural Safety*, 13, 145–157.

PEER (2012). *Open Systems for Earthquake Engineering Simulation (OpenSees)*, version 2.4.0. Pacific Earthquake Engineering Research Center (PEER), University of California, Berkeley, California.

PEER (2013). PEER NGA East Technical Updates: 2013, Second Quarter, http://peer.berkeley.edu/ngaeast/technical-updates/2013-second. Pacific Earthquake Engineering Research Center (PEER), University of California, Berkeley, California.

PEER / ATC (2010). *Modeling and acceptance criteria for seismic design and analysis of tall buildings*. ATC-72-1, prepared by Applied Technology Council (ATC) in collaboration with Building Seismic Safety Council, National Institute of Building Sciences, and Federal Emergency Management Agency. Pacific Earthquake Engineering Research Center (PEER), University of California, Berkeley, California.

Petersen, M. D., Frankel, A. D., et al. (2008). *Documentation for the 2008 update of the United States national seismic hazard maps*. U.S. Geological Survey Open-File Report 2008–1128.

Petrini, L., Maggi, C., Priestley, M. J. N., and Calvi, G. M. (2008). "Experimental verification of viscous damping modeling for inelastic time history analyzes." *Journal of Earthquake Engineering*, 12 (Supplement No. 1): 125–145.

Pitilakis, K., Riga, E., and Anastasiadis, A. (2012). "Design spectra and amplification factors for Eurocode 8." *Bulletin of Earthquake Engineering*, 10(5): 1377–1400.

Pitilakis, K., Riga, E., and Anastasiadis, A. (2013). "New code site classification, amplification factors and normalized response spectra based on a worldwide ground-motion database." *Bulletin of Earthquake Engineering*, 11(4): 925–966.

Powell, G. (2008). Damping Models for Nonlinear Dynamic Analysis: Survey Results, Analyses and Conclusions – Including Addendums 1–4, unpublished papers, April to November, 2008.

Prakash, V., Powell, G. H., and Campbell, S. (1993). *Drain-2DX*, version 1.10. Department of Civil Engineering, University of California, Berkeley, California.

Priestley, M. J. N., and Grant, D. N. (2005). "Viscous damping in seismic design and analysis." *Journal of Earthquake Engineering*, 9(2): 229–255.

Priestley, M. J. N., Calvi, M., Petrini, L., and Maggi, C. (2007). *Effects of damping modelling on results of time-history analysis of RC bridges*. Report, Centre of Research and Graduate Studies in Earthquake Engineering and Engineering Seismology (Rose School), Pavia, Italy.

Pryor, S. E., and Murray, T. M. (2013). "Next generation partial strength steel moment frames for seismic resistance." *Research, Development, and Practice in Structural Engineering and Construction*, 27–32.

Puthanpurayil, A. M., Dhakal, R. P., and Carr, A. J. (2011). "Modelling of in-structure damping: a review of the state-of-the-art." *Proceedings*, Ninth Pacific Conference on Earthquake Engineering, Building an Earthquake-Resilient Society, April 14–16, Auckland, New Zealand, Paper Number 091.

R

Ramm, E. (1981). "Strategies for tracing the nonlinear response near limit points." *Nonlinear finite element analysis in structural mechanics, proceedings of the Europe–U. S. Workshop*, Springer-Verlag, New York, New York, 63–89.

Ramsdell, J. V., and Rishel, J. P. (2007). *Tornado climatology of the contiguous United States*. NUREG/CR-4461, Rev. 2, Office of Nuclear Regulatory Research, U. S. Nuclear Regulatory Commission, Washington, D. C.

Rassati, G. A., Leon, R. T., and Noe, S. (2004). "Component modeling of partially restrained composite joints under cyclic and dynamic loading." *Journal of Structural Engineering*, 130(2): 343–351.

Ricles, J.M., Zhang, X., Lu, L.W., and Fisher, J. (2004). *Development of seismic guidelines for deep-column steel moment connections*. Report No. 04-13, Advanced Technology for Large Structural Systems, Lehigh University, Bethlehem, Pennsylvania.

Rix, G. J., and Fernandez, J. A. (2006). "Probabilistic ground motions for selected cities in the upper Mississippi embayment," http://www.ce.gatech.edu/~geosys/soil_dynamics/research/groundmotionsembay, 31 July 2006, Georgia Institute of Technology, Atlanta, Georgia.

Robinson, A. (2012). *Earthquake: nature and culture*. Reaktion Books, London, United Kingdom.

Rodriguez-Marek, A., Bray, J. D., and Abrahamson, N. A. (2001). "An empirical geotechnical seismic site response procedure." *Earthquake Spectra*, 17(1): 65–87.

Rojas, P. (2003). *Seismic analysis and design of post-tensioned friction damped connections for steel moment resisting frames*. Ph.D. dissertation, Civil Engineering, Lehigh University, Bethlehem, Pennsylvania.

RSMeans (2013). *Light commercial cost data*. Reed Construction Data, Norwell, Massachusetts.

Ryan, J. C. (2006). *Analytical and experimental investigation of improving seismic performance of steel moment frames using synthetic fiber ropes*. Ph.D. dissertation, Civil Engineering. Virginia Polytechnic Institute and State University, Blacksburg, Virginia.

S

Salmon, G., Johnson, J., Malhas, F. (2009). *Steel structures: design and behavior*, fifth edition. Pearson Prentice Hall, Upper Saddle River, New Jersey.

Sato, A., and Uang, C.-M. (2013). "A FEMA P695 study for the proposed seismic performance factors for cold-formed steel special bolted moment frames." *Earthquake Spectra*, 29(1): 259–282.

Saunders, R. A. (2004). *Nonlinear dynamic analysis of structures with hyperelastic devices*. M.S. thesis, Civil Engineering. Virginia Polytechnic Institute and State University, Blacksburg, Virginia.

Schnabel, P., Seed, H. B., and Lysmer, J. (1972). "Modification of seismograph records for effects of local soil conditions." *Bulletin of the Seismological Society of America*, 62(6): 1649–1664.

Scott, M., and Fenves, G. (2010). "Krylov subspace accelerated Newton algorithm: application to dynamic progressive collapse simulation of frames." *Journal of Structural Engineering*, 136(5): 473–480.

Seligson, H. A., and Eguchi, R. T. (2005). "The true cost of earthquake disasters: an updated tabulation of losses for the 1994 Northridge earthquake." *Proceedings*, International Symposium on Earthquake Engineering, Kobe, Japan.

Seyhan, E., and Stewart, J. P. (2012). “Site response in NEHRP provisions and NGA models.” Geotechnical Engineering State of the Art and Practice, Proceedings, *Geo-Congress*, March 25–29, Oakland, California.

Shanley, F. R. (1947). “Inelastic column theory.” *Journal of the Aeronautical Sciences*, 14(5): 261–267.

Shi, S. (1997). *Evaluation of connection fracture and hysteresis type on the seismic response of steel buildings*. Ph.D. dissertation, Civil Engineering, University of Illinois at Urbana-Champaign, Urbana, Illinois.

Shi, S., and Foutch, D. A. (1997). *Connection element (type 10) for Drain-2DX*. Civil Engineering Report, University of Illinois at Urbana-Champaign, Urbana, Illinois.

Smyrou, E., Priestley, M. J. N., and Carr, A. J. (2011). “Modelling of elastic damping in nonlinear time-history analyses of cantilever RC walls.” *Bulletin of Earthquake Engineering*, 9: 1559–1578.

Somerville, P. G., Collins, N. Abrahamson, N., Graves, R., and Saikia, C. (2001). *Ground motion attenuation relations for the central and eastern United States*. Final Report, United States Geological Survey, Reston, Virginia.

Song, S. (2014). *A new ground motion intensity measure, peak filtered acceleration (PFA), to estimate collapse vulnerability of buildings in earthquakes*. Ph.D. dissertation, California Institute of Technology, Pasadena, California.

Southern California Earthquake Center (SCEC) (2007). Uniform California earthquake rupture forecast. www.scec.org/ucerf. Southern California Earthquake Center, University of Southern California.

Stein S., and Stein, J. L. (2013). “Shallow versus deep uncertainties in natural hazard assessments.” *Eos*, 94(14): 133–140.

Stewart, J. P., Seed, R. B., and Fenves, G. L. (1999). “Seismic soil-structure interaction in buildings II: empirical findings.” *Journal Geotechnical and Geoenvironmental Engineering*, 125(1): 38–48.

Stoakes, C. D., and Fahnestock, L. A. (2011). “Cyclic flexural testing of concentrically braced frame beam-column connections.” *Journal of Structural Engineering*, 137(7): 739–747.

Stojadinovic, B., Goel, S. C., Lee, K.-H., Margarian, A. G., and Choi, J.-H. (2000). “Parametric tests on unreinforced steel moment connections.” *Journal of Structural Engineering*, 126(1): 40–49.

Symans, M. D., Charney, F. A., Whittaker, A. S., Constantinou, M. C., Kircher, C. A., Johnson, M. W., and McNamara, R. J. (2008). “Energy dissipation systems for seismic applications: current practice and recent developments.” *Journal of Structural Engineering*, 134(1): 3–21.

T

Taleb, N. N. (2005). *Fooled by randomness: the hidden role of chance in life and in the markets*, second edition. Random House, New York, New York.

Taleb, N. N. (2007). *The black swan: the impact of the highly improbable*. Random House, New York, New York.

Tamura, Y., Suganuma, S., Kikuchi, H., and Hibi, K. (1999). “Proper orthogonal decomposition of random wind pressure field.” *Journal of Fluids and Structures*, 13: 1069–95.

Tedesco, J. W., McDougal, W. G., and Ross, C. A. (1999). *Structural dynamics: theory and applications*. 1st edition, Addison Wesley Longman, Inc., Meno Park, California.

Tremblay, R., Tchebotarev, N., and Filiatrault, A. (1997). "Seismic performance of RBS connections for steel moment resisting frames: Influence of loading rate and floor slab." *Behavior of Steel Structures in Seismic Areas*, Proceedings of the Second International Conference, STESSA '97, Kyoto, 664–671.

Tsujita, O., Hayabe, Y., and Ohkuma, T. (1997). "A study on wind-induced response for inelastic structure." *Proceedings*, 7th International Conference on Structural Safety and Reliability (ICOSSAR 97), Kyoto, Japan.

U

Uang, C.M., Chi B., Gilton, C. (2000). *Cyclic response of RBS moment connections: weak-axis configuration and deep column effects*. Report No. SSRP-99/13, Department of Structural Engineering, University of California, San Diego, California.

USGS (2010). 2009 Earthquake Probability Mapping. United States Geological Survey (USGS), Reston Virginia, http://geohazards.usgs.gov/eqprob/2009/.

USGS (2012). "New evidence shows power of east coast earthquakes." News release, November 6, http://www.usgs.gov/newsroom. United States Geological Survey (USGS), Reston, Virginia.

USGS (2013). Earthquake hazards program. United States Geological Survey (USGS), Reston, Virginia, http://earthquake.usgs.gov/hazards/.

USGS – Oklahoma Geological Survey (2014). “Record number of Oklahoma tremors raises possibility of damaging earthquakes.” Joint Statement updated May 2, United States Geological Survey (USGS), Reston, Virginia, http://earthquake.usgs.gov/contactus/golden/newsrelease_05022014.php

V

Vamvatsikos, D. (2011). “Performing incremental dynamic analysis in parallel.” *Computers and Structures*, 89(1–2): 170–180.

Vamvatsikos, D., and Cornell, C. A. (2004). “Applied incremental dynamic analysis.” *Earthquake Spectra*, 20(2): 523–553.

van de Lindt, J. W., and Dao, T. N. (2009). “Performance-based wind engineering for wood-frame buildings.” *Journal of Structural Engineering*, 135(2): 169–177.

Vigil, J. F., Pike, R. J., and Howell, D. G. (2000). “A tapestry of time and terrain.” http://pubs.usgs.gov/imap/i2720. United States Geological Survey, Reston, Virginia.

W

Wald, D. J., and Allen, T. I. (2007). “Topographic slope as a proxy for seismic site conditions and amplification.” *Bulletin of the Seismological Society of America*, 97(5): 1379–1395.

Wald, M. L. (2013). “F.A.A. says furloughs delayed 1,200 flights.” *The Wall Street Journal*, April 23.

Wang, Z. (2011). “Seismic hazard assessment: issues and alternatives.” *Pure and Applied Geophysics*, 168(1–2): 11–25.

Wen, R., Akbas, B., and Shen, J. (2013). “Practical moment–rotation relations of steel shear tab connections.” *Journal of Constructional Steel Research*, 88: 296–308.

Wen Y. K., and Wu, C. L. (2001). “Uniform hazard ground motions for mid-America cities.” *Earthquake Spectra*, 17(2): 359–384.

Whittaker, A., and Constantinou, M. (2004). “Seismic energy dissipation systems for buildings.” *Earthquake engineering: from engineering seismology to performance-based engineering*, Bozorgnia, Y. and Bertero, V., eds., CRC Press, Boca Raton, Florida.

World Bank (2010). *Natural hazards, unnatural disasters: the economics of effective prevention*. International Bank for Reconstruction and Development (World Bank), Washington, D.C.

Y

Yang, Z., Sarkar, P., and Hu, H. (2011). “An experimental study of a high-rise building model in tornado-like winds.” *Journal of Fluids and Structures*, 27(4): 471–486.

Yeo, D., Lin, N., and Simiu, E. (2014). “Estimation of hurricane wind speed probabilities: application to New York City and other coastal locations.” *Journal of Structural Engineering*, 140(6): 04014017-1–5.

Yun, S.-Y., Hamburger, R. O., Cornell, C. A., and Foutch, D. A. (2002). “Seismic performance evaluation of steel moment frames.” *Journal of Structural Engineering*, 128(4): 534–545.

Z

Zareian, F. (2012). *PACT Beta Test Example: building A steel special moment frame building*. FEMA P-58/BD-3.7.14 Background Document, Federal Emergency Management Agency, Washington, D. C.

Zareian, F., and Medina, R. A. (2010). "A practical method for proper modeling of structural damping in inelastic plane structural systems." *Computers and Structures*, 88: 45–53.

Zhang, W. (2012). *Study of the influence of gravity connections on the lateral response of steel-concrete composite moment frames*. M.S. thesis, Civil Engineering, University of Cincinnati. Cincinnati, Ohio.

Zobel, C. W., and Khansa, L. (2014). "Characterizing multi-event disaster resilience." *Computers and Operations Research*, 42: 83–94.

Appendix A

ANALYSIS VALIDATION

This appendix contains analysis examples used to evaluate the performance of computer software and the analysis procedures used in this research. All examples used the Open Systems for Earthquake Engineering Simulation (*OpenSees*) software (McKenna et al. 2000-2011; PEER 2012). For some examples and problems, additional software was used, including *Nonlin* (Charney 2010), *Quick* (Judd 2006), and *Abaqus* (Dassault Systèmes 2011a), depending on the problem considered and software capabilities.

A.1 Computer Software

The primary software used in this study was *OpenSees* (PEER 2012). There were a number of advantages to using *OpenSees*. First, *OpenSees* was computationally powerful. It was amenable to a variety of structural configurations, and included various material behaviors, a wide selection of phenomenological models, element types, as well as a good selection of possible analyses and solution algorithms. Part of this power is owed to the engaged community of users that also play the role of developers. Many aspects of the software have been user added. Implied here is that the software is accurate, and the subsequent example and benchmark problems in part support this assertion.

The second advantage to using *OpenSees* was that the software has been used by many researchers in the earthquake engineering field at the time of this study. The open source code and the low cost (at least in terms of purchase price) was probably the primary driver behind the usage. Using the same software, in this case *OpenSees*, facilitates collaborative work and speeds the creative process.

There were also disadvantages to using *OpenSees*. It may have been as expensive, or more expensive, than comparable finite element software, in terms of labor costs. The man-hours required to climb the steep learning curve and endure the bug-de-bug development cycle create a high cost, despite the initial purchase price. Three factors contribute to these costs. The first factor is that the software was not WYSIWYG. Pre- and post-processing was text based or handled by other software, namely *MATLAB* (2011). The second factor is that the software was not made in a for-profit environment. Much of the code and functionality is ad-hoc, ongoing, and made by a turn-over of temporary student code writers. Documentation suffers in addition to code. Compared to commercially maintained software, both the implementation and the documentation were clunky. The third factor is that *OpenSees* required the use of the TCL script language. The choice of script language was unfortunate because modern script languages, such as PYTHON—used by *Abaqus* (Dassault Systèmes 2011a) software, for example—avoid many of the pitfalls that must be traversed using TCL.

For this study, the advantages of using *OpenSees* were judged to outweigh the disadvantages. *OpenSees* worked well for structures where a GUI was not essential, such as framed structures with regular and repeated geometry, or other structures that were relatively simple (e.g. portal frames).

Additional software was used for comparison with *OpenSees*. For dynamic analysis of single degree of freedom (SDOF) structural systems, *Nonlin* software (Charney 2010) was used. *Nonlin* was developed primarily as educational software for earthquake engineering, and has the capability to model nonlinear structural behavior including damping, ductility, and energy dissipation. Also used for dynamic analysis of SDOF systems, *Quick* (Judd 2006) has the capability to include various hysteresis models. *Quick* was originally developed to study the dynamic response of light-frame wood shear walls and diaphragms (Judd 2006; Judd and Fonseca 2006). For some problems, *Abaqus* (Dassault Systèmes 2011) was used. *Abaqus* is a commercially developed multi-purpose finite element software.

A.2 Static Analysis

Standard analyses examples are discussed in this section to verify some of the basic capabilities of *OpenSees*. Not all analysis capabilities were verified or demonstrated. The software documentation (Mazzoni et al. 2011) provides a more comprehensive introduction to *OpenSees* and its use of the TCL script language. This section also includes a second order analysis [see Charney (2015)] and an eigenvalue buckling analysis example.

A.2.1 Cantilever Beam

A 2D cantilever beam with a point load at the end (Hibbeler 1995) was analyzed using *OpenSees*. The input file is shown below.

```
# DESCRIPTION: OpenSees2.3.1 input file for analysis of a 2D cantilever beam
#              with a point load at the end from Example 8-3 (Hibbeler 1995).
#
wipe
model basic -ndm 2 -ndf 3
# nodal coordinates
```

```
node 1 0 0
node 2 360 0
# bondary conditions
fix 1 1 1 1
fix 2 0 0 0
# transformation
geomTransf Linear 1
#
# elements
element elasticBeamColumn 1 1 2 38.5 29000 600 1
# recorders
recorder Node -file Node2.out -time -node 2 -dof 1 2 3 disp
recorder Element -file Element1.out -time -ele 1 force
#
# gravity loads
pattern Plain 1 Linear {
  load 2 0.0 2.0 0.0
}
# analysis
constraints Plain
numberer Plain
system BandGeneral
algorithm Linear
integrator LoadControl 1.0
analysis Static
#
analyze 1
#
puts "Finished analysis"D
```

The analysis results in two output files: displacements at node 2, and forces in element 1. The displacement results are shown below (time value followed by displacements).

```
1 0 1.78759 0.00744828
```

The calculate slope at the end of the cantilevered beam matches the theoretical slope at the end of the beam using the moment-area analysis method.

$$\theta_{AB} = \int_A^B \frac{M}{EI} dx$$

$$= \frac{(-900\ k*ft)(144\ in.^2/ft)}{(29{,}000\ ksi)(600\ in.^4)}$$

$$= -0.00745\ rad$$

A.2.2 Second-order effects

The effect of the approach used to include second-order effects on a static analysis was determined by examining a typical (W14x82) gravity column. For purposes of illustration, the height of the column is 12.5 feet, and the boundary conditions of the column are idealized as fixed at the base and free at the top. A lateral load *V* of 10 kips was applied.

The columns was analyzed with a vertical load P equal to 15%, 80%, or 99.9% of the elastic critical buckling load, P_{cr} of the column. The column was modeled using *OpenSees* and using a MATLAB routine. The model consisted of one or four elements, depending on the analysis.

Figure A.1 shows the column behavior for the various methods used to model second-order effects. In a first order analysis of the column the displacement, Δ is equal to $Ph^3/3EI$ = 2.62 inches. An estimate of the second-order effect was determined using a linearized geometric stiffness matrix, $K_{geo}. = -P/h$, based on a straight-line deformed column configuration. This assumption in the configuration of the deformed shape causes an incorrect increase in the stiffness the system.

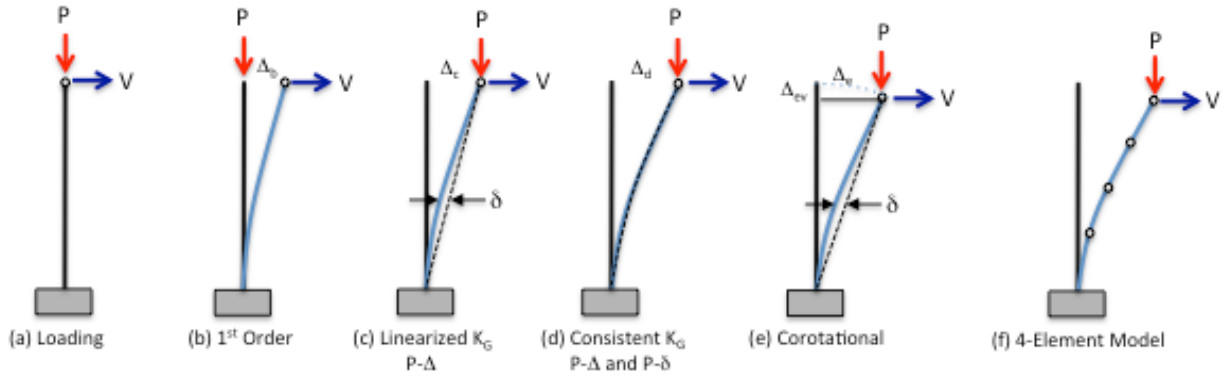

Figure A.1 Column behavior for second-order analysis methods

The second-order effect was more accurately determined using a consistent geometric stiffness matrix, K_{geo}, based on a cubic shape function for both the elastic stiffness and geometric stiffness. Lastly, the second-order effect was determined using the corotational formulation, where the system stiffness is updated to reflect the deformed shape. Such an analysis will report a vertical deflection of the column. However, the corotational formulation does not include the P-δ effect unless more than one element is used to model the column.

The predicted lateral displacement is summarized in Table A.1. The linearized geometric stiffness with 15% of P_{cr} corresponded to an increase in displacement compared to the first order displacement. Using four elements to model the column resulted in larger displacements compared to modeling the column using one element. There was a small increase in displacements when the consistent geometric stiffness model is used, but interestingly, the results for the correlational model are the same as with linearized geometric stiffness because the corotational model using one element does not include the P-δ effect, and because the column rotation is small.

Table A.1 Predicted lateral displacement (in.) of typical gravity frame column

P/Pcr	Number of Elements	1st Order	Second-order method		
			Linear K_{geo}	Consistent K_{geo}	Corotational
0.15	1	2.62	2.97	3.05	2.97
	4	2.62	3.04	3.05	3.04
0.8	1	2.62	7	10.7	6.97
	4	2.62	10.4	10.8	10.3
0.999	1	2.62	12.3	51.0+	12.1+
	4	2.62	46.1	58.8*	34.0**

+ Vertical displacement =0.0 in.
* Vertical displacement = -0.1 in.
** Vertical displacement = -4.88 in.

When the axial load is 80% of P_{cr}, the increase in displacements was significant, and the predicted lateral displacements differ widely. As before, the results from the corotational model are similar to those obtained using linearized geometric stiffness. As the axial P approaches P_{cr}, the choice of analytical model and the level of discretization of the model has a profound effect.

Note that the one-element corotational model was inaccurate at this level of axial load due to the inability to represent P-δ . However, the four-element corotational model was more accurate because the vertical displacement (-4.88 inches) was captured. The smaller lateral displacement (34 inches) for the correctional model relative to that obtained for the consistent geometric stiffness model (58.8 inches) was due to the fact that the length of the column using the corotational model was constant. A study by Denavit and Hajjar (2013) reached similar conclusions.

A.2.3 Buckling Analysis

The critical buckling load of a two-story single-bay frame was analyzed using MATLAB routines, *OpenSees*, and *Abaqus*. (Input scripts and files are shown on the following pages.) Two analysis approaches were used. In the first analysis approach, a constant transverse load V = 0.001 k and a gradually increasing axial load P were applied until reaching the critical buckling load, P_{cr}. In the second analysis approach, P_{cr} was determined using the first mode of an eigenvalue analysis.

The nonlinear response is summarized in Table A.2. Using a consistent geometric stiffness formulation, both analysis approaches accurately predict the critical buckling.

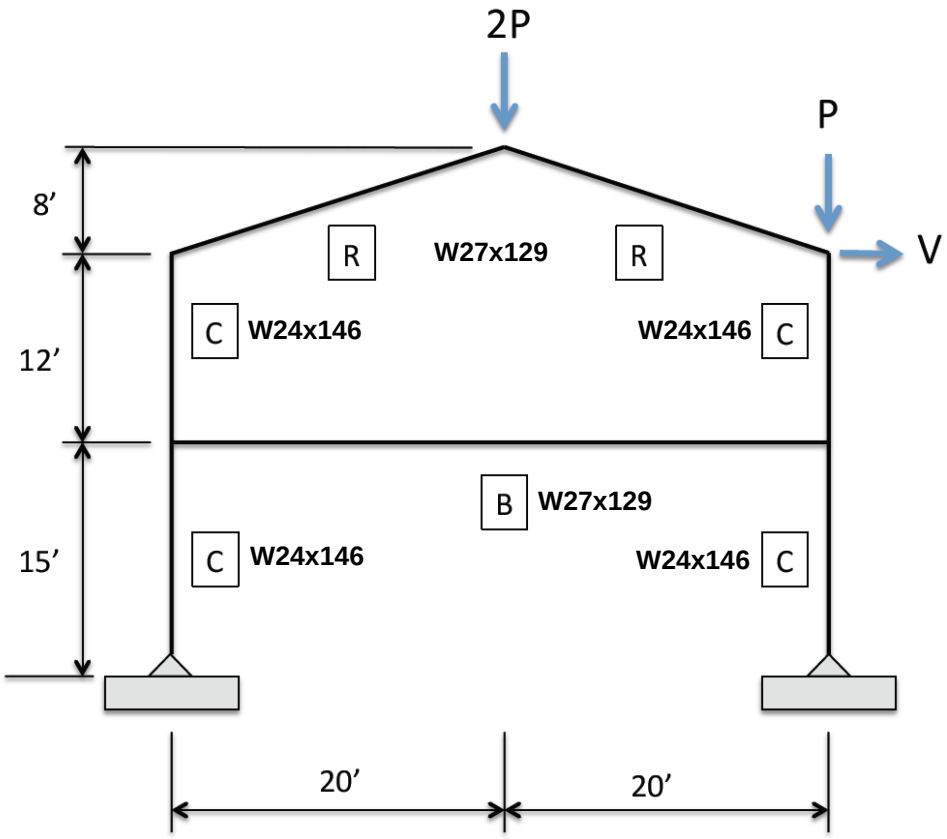

Figure A.2 Two-story single-bay frame

Table A.2 Critical buckling load (k)

Analysis Approach	P_{cr} (k)
Constant *V*=0.001, gradually increase *P* until reaching P_{cr}	3,770
OpenSees using corrotational formulation	3,829
Eigen analysis: *V*=1, and *P* = 1. Solve for *P* times lambda (P_{cr})	3,800
Abaqus	3,790

OpenSees input script:

```
wipe
model basic -ndm 2 -ndf 3
# Input parameters
# Vertical (P) and lateral (V) loads
set P 10.0
set V 0.001
# Material (steel)
set E 30000.0
# Column section (W24x146)
set Ac 43.0
set Ic 4580.0
# Beam and rafter section (W27x129)
set Ab 37.8
set Ib 4760.0
# Node coordinates
node 1  -240.0  0.0
node 2  -240.0  90.0
node 3  -240.0  180.0
node 4  -240.0  252.0
node 5  -240.0  324.0
node 6  -120.0  372.0
node 7  0.0     180.0
node 8  0.0     420.0
node 9  120.0   372.0
node 10 240.0   0.0
node 11 240.0   90.0
node 12 240.0   180.0
node 13 240.0   252.0
node 14 240.0   324.0
# Boundary conditions
fix 1   1 1 0
fix 10  1 1 0
# Transformation
geomTransf Corotational 1
# Element material, type, and connectivity
element elasticBeamColumn 1 1 2 $Ac $E $Ic 1
element elasticBeamColumn 2 2 3 $Ac $E $Ic 1
element elasticBeamColumn 3 3 4 $Ac $E $Ic 1
element elasticBeamColumn 4 4 5 $Ac $E $Ic 1
element elasticBeamColumn 5 5 6 $Ab $E $Ib 1
element elasticBeamColumn 6 6 8 $Ab $E $Ib 1
element elasticBeamColumn 7 8 9 $Ab $E $Ib 1
element elasticBeamColumn 8 9 14 $Ab $E $Ib 1
element elasticBeamColumn 9 3 7 $Ab $E $Ib 1
element elasticBeamColumn 10 7 12 $Ab $E $Ib 1
element elasticBeamColumn 11 10 11 $Ac $E $Ic 1
element elasticBeamColumn 12 11 12 $Ac $E $Ic 1
element elasticBeamColumn 13 12 13 $Ac $E $Ic 1
element elasticBeamColumn 14 13 14 $Ac $E $Ic 1
# Recorders
recorder Node -file Node14.out -time -node 14 -dof 1 2 3 disp
# Loads
timeSeries Linear 1
pattern Plain 1 1 {
# load $nodeTag (ndf $LoadValues)
        load 8  0.0     [expr -$P*2]   0.0
        load 14 0.0     -$P            0.0
        load 14 $V      0.0            0.0
}
# Analysis parameters
constraints Plain
numberer Plain
system BandGeneral
test NormDispIncr 1.0e-8 10
algorithm Newton
integrator LoadControl 0.1
analysis Static
analyze 3829
```

Abaqus input file:

```
*HEADING
**  NODE DEFINITIONS
**
*RESTART,WRITE,FREQUENCY=999
*NODE, NSET=FRAME_NODES
 1, -240.0, 0.0, 0.0
 2, -240.0, 90.0, 0.0
 3, -240.0, 180.0, 0.0
 4, -240.0, 252.0, 0.0
 5, -240.0, 324.0, 0.0
 6, -120.0, 372.0, 0.0
 7, 0.0, 180.0, 0.0
 8, 0.0, 420.0, 0.0
 9, 120.0, 372.0, 0.0
 10, 240.0, 0.0, 0.0
 11, 240.0, 90.0, 0.0
 12, 240.0, 180.0, 0.0
 13, 240.0, 252.0, 0.0
 14, 240.0, 324.0, 0.0
*ELEMENT,TYPE=B21, ELSET=FRAME_ELEMENTS_1
 1,1,2
 2,2,3
 3,3,4
 4,4,5
*ELEMENT,TYPE=B21, ELSET=FRAME_ELEMENTS_2
 5,5,6
 6,6,8
 7,8,9
 8,9,14
 9,3,7
*ELEMENT,TYPE=B21, ELSET=FRAME_ELEMENTS_3
 10,7,12
 11,10,11
 12,11,12
 13,12,13
 14,13,14
*BEAM GENERAL SECTION, SECTION=GENERAL, ELSET=FRAME_ELEMENTS_1
 43.0, 4580.0
 0.0,0.0,-1.0
 30000.0
*BEAM GENERAL SECTION, SECTION=GENERAL, ELSET=FRAME_ELEMENTS_2
 37.8, 4760.0
 0.0,0.0,-1.0
 30000.0
*BEAM GENERAL SECTION, SECTION=GENERAL, ELSET=FRAME_ELEMENTS_3
 43.0, 4580.0
 0.0,0.0,-1.0
 30000.0
*BOUNDARY
 1, 1
 1, 2
 10, 1
 10, 2
*STEP
*BUCKLE
 1,
*CLOAD
 8, 2, -2.0
 14, 2, -1.0
*END STEP
```

A.3 Dynamic Analysis

In this section the time-history response of an elastoplastic SDOF system (Chopra 2012) was compared to the responses of three computer programs: *Nonlin*, *OpenSees*, and *Quick*.

The maximum and permanent displacements are summarized in Table A.3 and Table A.4. The SDOF system is defined with T_n = 0.5 sec, 5% damping, and various bilinear elastoplastic behaviors, defined using the response modification factor, *R*. The SDOF system was subjected to the El Centro ground motion record (a_{max} = 0.32 g) as described by Chopra (2012).

Table A.3 Maximum absolute displacement (in.)

Method	Response modification factor, R			
	R=1	R=2	R=4	R=8
Chopra (Fig. 7.4.2)	2.25	1.62	1.75	2.07
Nonlin	2.24	1.62	1.74	2.06
OpenSees	2.24	1.63	1.77*	2.07
Quick	2.24	1.63	1.76*	2.07
Duhamel's (MATLAB)	2.26			
*Reached at a different time, compared to Chopra.				

Table A.4 Permanent displacement (in.) at time equal to 30 seconds

Method	Response modification factor, R			
	R=1	R=2	R=4	R=8
Chopra (Fig. 7.4.2)	0	0.17	1.1	1.13
Nonlin	0.02	0.17	1.1	1.13
OpenSees	0.04	0.2	1.14	1.1
Quick	0.04	0.2	1.14	1.1

A.4 Nonlinear Multi-Degree-of-Freedom Analysis

In this section the nonlinear response of the 4-story ductile moment frame building designed for SDC D_{max} is compared to the response for a similar building model reported in NIST (2010b).

The models differ in at least the following aspects:

- *OpenSees* was used in this research, whereas the comparison model used Drain-2DX (Prakash et al. 1993).

- In this research, the gravity framing was explicitly modeled and includes gravity columns and beams, whereas the comparison model employed a single leaning column to account for second-order effects.

- The beam-to-column joint model was geometrically accurate in this research (the top of adjacent beams was at the same elevation), whereas it was not in the comparison model.

- The comparison model story elevations were based on beam centerlines, except the first story height was measured from the ground to the top of a trial beam used to establish the first story elevation (not necessarily the actual beam size).

The vibration response is shown in Figure A.3. The reference study's first four periods of vibration were 1.56, 0.50, 0.27, and 0.17 seconds/cycle. The nonlinear static seismic pushover response is shown in Figure A.4. (The red dashed line is the response of the comparative model.)

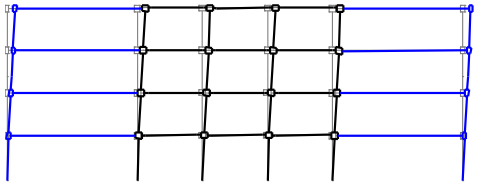

a) Mode 1 (T_1 = 1.46 seconds/cycle)

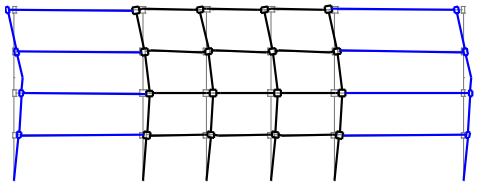

b) Mode 2 (T_2 = 0.47 seconds/cycle)

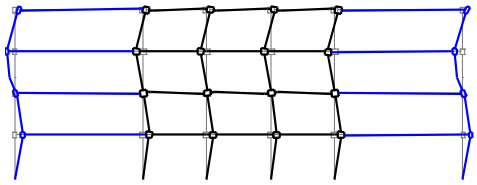

c) Mode 3 (T_3 = 0.22 seconds/cycle)

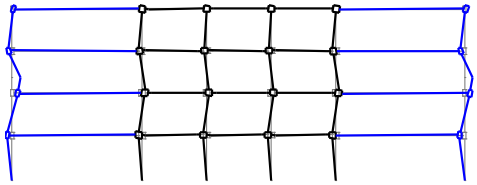

d) Mode 4 (T_4 = 0.14 seconds/cycle)

Figure A.3 Periods of vibration and mode shapes for the model used in this research

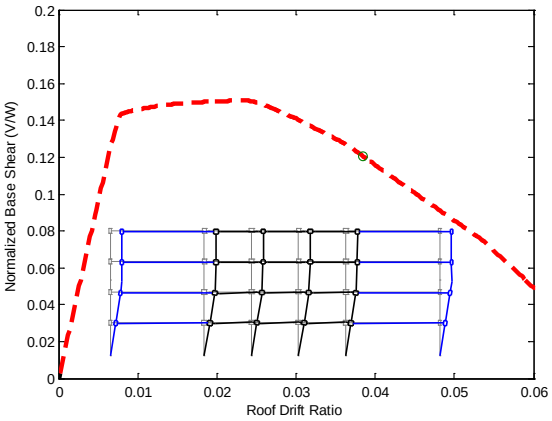

a) Model used in this research

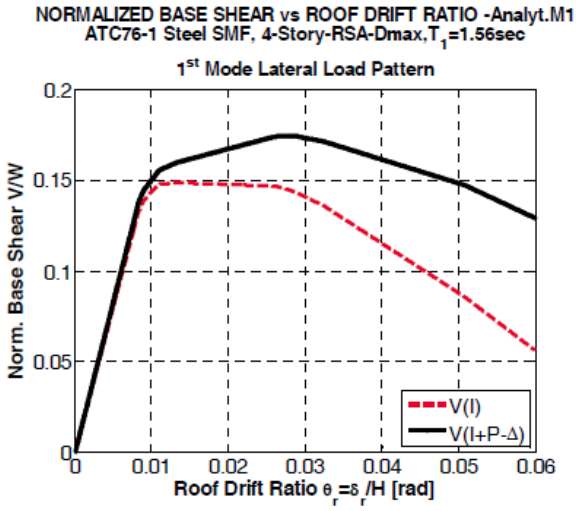

b) Comparative model (from NIST 2010b)

Figure A.4 Nonlinear static seismic pushover response

Figure A.5 shows the results from a free vibration analysis to verify the inherent (non-explicitly modeled) damping in the finite element analysis. (The comparative study did not conduct a free vibration analysis.) In the analysis, the building was subjected to the first 2 seconds of the 1941 El Centro ground motion record (Chopra 2012), scaled to 10% of the original record intensity, followed by 58 seconds of free vibration. The equivalent damping ratio was approximately 2.5% (the target damping ratio was 2.5%).

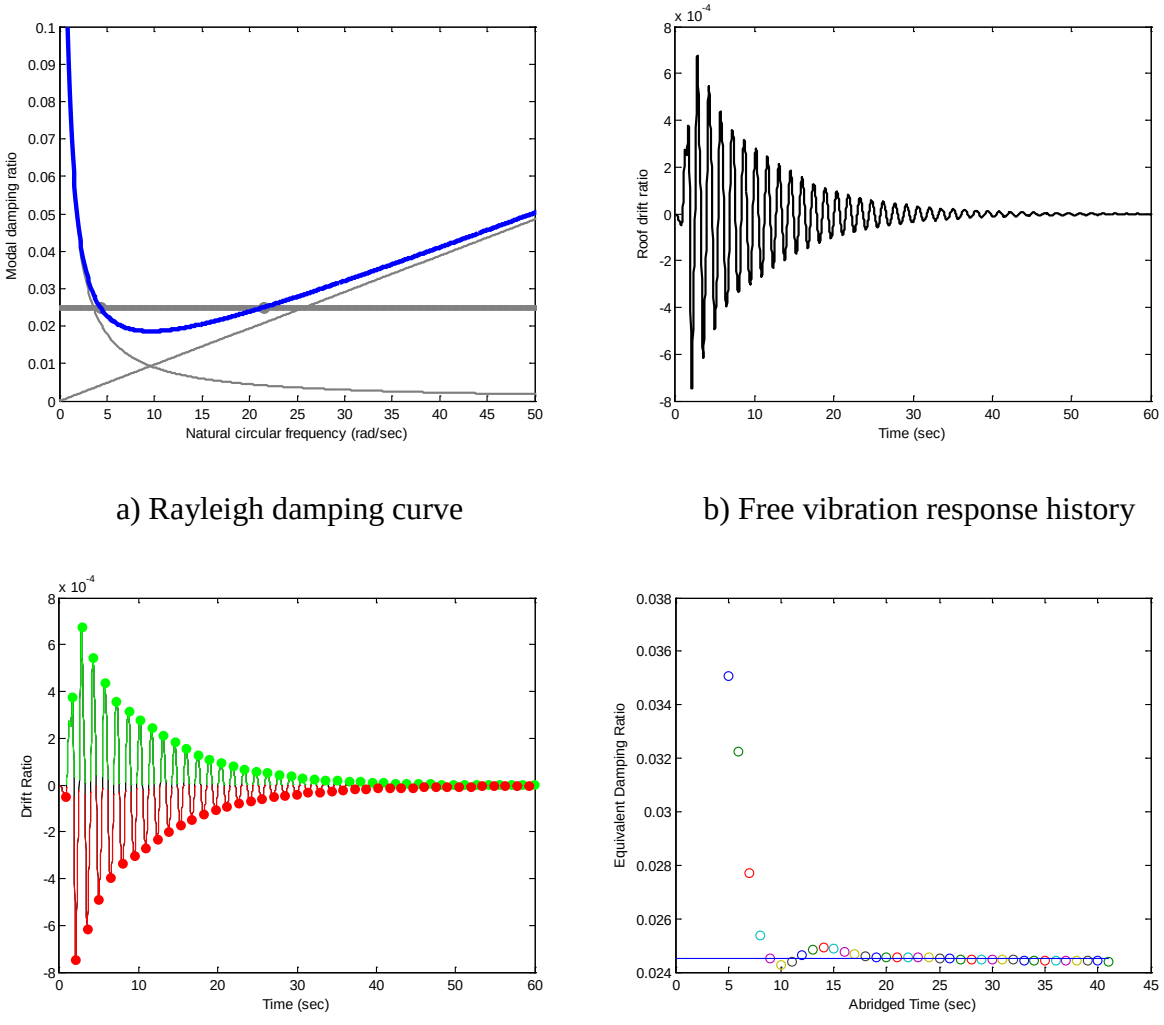

a) Rayleigh damping curve

b) Free vibration response history

c) Half-cycle response history

d) Equivalent damping ratio

Figure A.5 Free vibration analysis response

A.5 Collapse prevention systems

In this section the potential effect of a collapse prevention system is demonstrated through analysis of a portal frame. The portal frame (Figure A.6) was idealized as shear-structure (rigid beam relative to the columns). Inelastic column behaviour was modelled using a concentrated plasticity approach. Members were rigid elastic beam-column elements, and beam-to-column connections were zero-length rotational elastic-plastic springs. The spring stiffness was calculated such that the lateral stiffness of the frame was equal to a frame with fixed columns and a rigid beam. Columns were pinned (free to rotate) at the base and a lean-on column (not shown in Figure A.6) was used to incorporate gravity load columns that are indirectly stabilized by the frame.

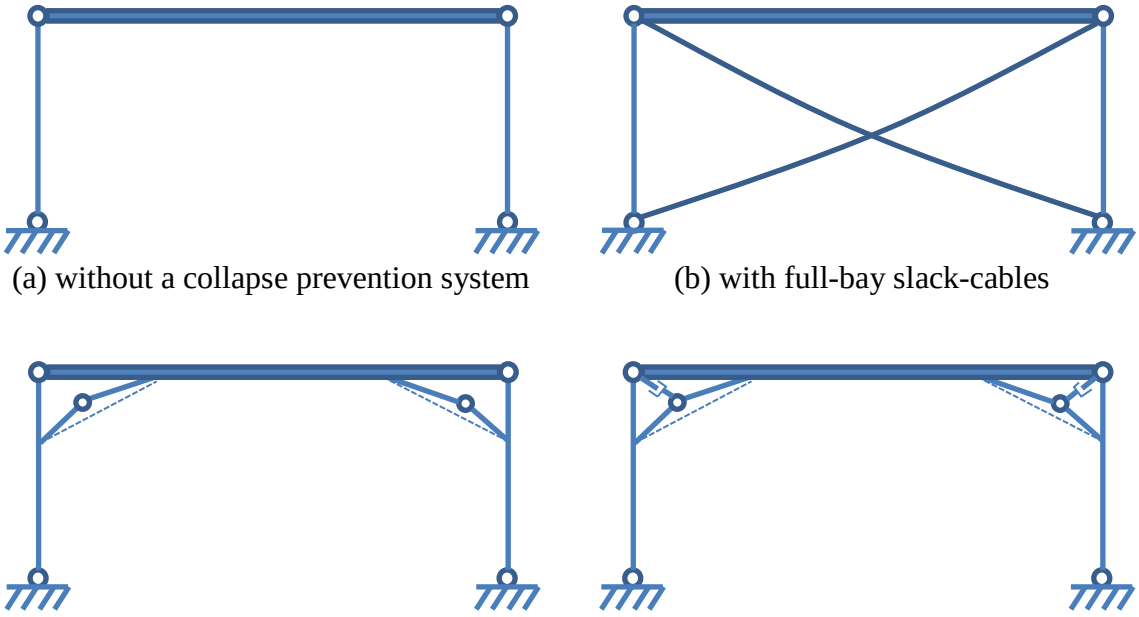

(a) without a collapse prevention system (b) with full-bay slack-cables

(c) with loose linkages (d) loose linkages, viscous fluid dampers

Figure A.6 Idealized configurations of collapse prevention systems

The portal frame height, H, was 10 feet and the frame length (bay length) was 20 feet. The frame weight, W and lateral stiffness, K were selected such that the fundamental period of vibration was 0.5 seconds. The gravity load stabilized was 1.0 times the load directly supported by the frame. The ductility supply to demand ratio was 8, and the inherent damping was estimated to be 5% of critical damping.

Nonlinear dynamic response history analysis was performed using *OpenSees* (PEER 2012). The portal frame was subjected to the Imperial Valley (1940) El Centro ground motion record, scaled to match various hazard intensity values (spectral acceleration) at the fundamental period of vibration. For a structure located in Charleston, South Carolina (with 32.8° latitude, -80.0° longitude) the damped 0.5-sec. spectral acceleration values are, respectively 0.02 g, 0.29 g, and 1.43 g for serviceability (50% probability of being exceeded in 30 years), life safety (10% probability of being exceeded in 50 years), and collapse prevention (2% probability of being exceeded in 50 years).

The collapse-level drift ratio history is shown in Figure A.7 for the portal frame with and without slack-cables. The slack in the cable was selected so that the peak drift ratio was 3%. Similarly, the geometry of the loose linkages was configured to limit the peak drift to 3%. The hybrid collapse prevention system using viscous dampers was selected such that 5% or 10% of equivalent damping was added to the overall structure.

Table A.5 summarizes the potential benefit of incorporating a collapse prevention system in the portal frame. An earthquake hazard level equal to 2/3 of the maximum considered earthquake (MCE) ground motion level was included for comparison of the design basis earthquake (DBE) ground motions. The results show that for this portal frame structure and this location (Charleston, South Carolina), life safety and collapse prevention were the most relevant

performance objectives for seismic design. Employing a collapse prevention system to meet the predetermined limit (3% drift ratio) reduced residual drifts by about half, while only increasing the base shear ratio (base shear divided by frame weight) by 10% to 30%, depending on the collapse prevention system. Viscous fluid dampers reduced residual drift. For this particular frame and analysis, adding 10% compared to 5% of equivalent damping to the system did not improve the performance.

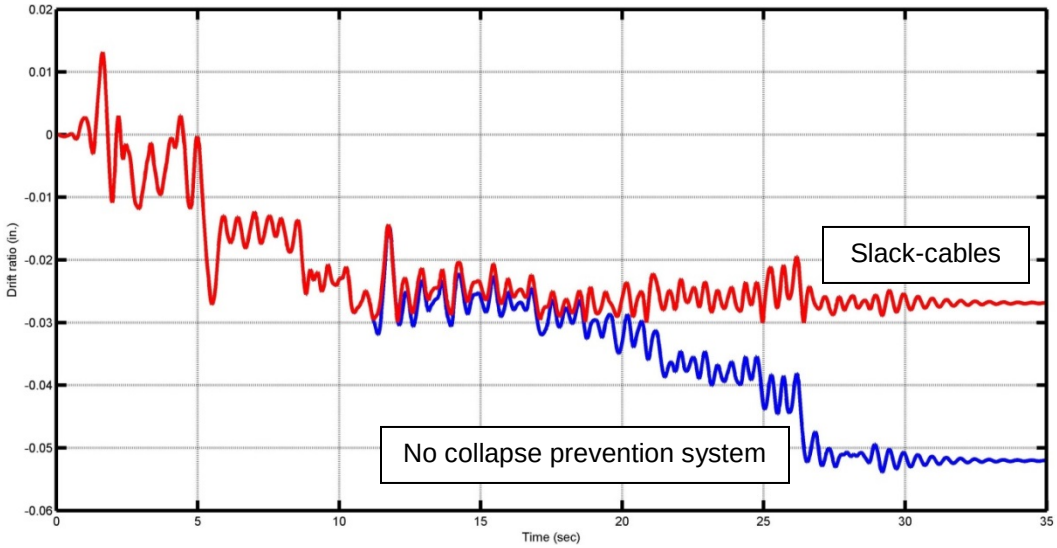

Figure A.7 Collapse-level drift ratio history for portal frame

Table A.5 Nonlinear dynamic response history analysis results for portal frame

Frame Description	Seismic Hazard level	Ratio (%)		
		Δ_{peak} /H	$\Delta_{residual}$/H	V_{base}/W
Without CPS	Serviceability	0.03	0.00002	0.29
	Life safety	0.34	0.03	4.33
	DBE	1.54	1.31	13.5
	MCE	5.39	5.20	20.0
Slack cables	MCE	3.00	2.68	21.9
Loose linkages (LL)		3.00	2.63	25.4
LL with dampers (5% damping)		3.00	2.79	23.1
LL with dampers (10% damping)		3.00	2.79	23.1

Appendix B

DESIGN OF TYPE I NON-DUCTILE MOMENT FRAME BUILDINGS

This appendix discusses the design of the archetype Type I non-ductile moment frame buildings. The archetype buildings were intended to be prototypical building configurations that are representative of possible building configurations to be used with the collapse prevention system concept. The development followed the general procedure recommended in FEMA P695, *Quantification of building seismic performance factors* (FEMA 2009a). Building design criteria was based on current (2015) codes and standards. Design gravity loads (dead loads and live loads) were based on realistic materials and standard occupancy and use. Buildings were evaluated for several hazard levels, considering both wind and seismic hazards. Building configuration was based on common story elevations and plan layouts, and a range of building heights. The intent of archetype development was to reasonably predict general performance of a broad class of buildings based on the performance of the limited set of buildings designed here.

Ordinary moment frame (OMF) buildings were also designed, although these buildings were not used in Chapter 3 and subsequent evaluations. The design of the OMF buildings is included in this appendix because it illustrates the procedures used to design the Type I non-ductile moment frame buildings.

B.1 Design Criteria

The non-ductile buildings were designed to meet the load requirements (including dead, live, wind, and seismic loads) and load combinations provided in ASCE/SEI 7-10, *Minimum design loads for buildings and other structures* (ASCE 2010).

The design of structural steel systems was based on ANSI/AISC 360-10, *Specification for structural steel buildings* (AISC 2010a) and the AISC *Steel construction manual* (AISC 2011a). The design of structural seismic force resisting systems (i.e. the steel moment frames) was based on ANSI/AISC 341-10, *Seismic provisions for structural steel buildings* (AISC 2010b).

Member deflections and building drifts satisfy the performance limits given in Table B.1. Deflections of members under gravity loads were limited to common applications as specified in the *International building code (IBC)* (ICC 2012a). Building drift limit for wind loads was based on a 10-year MRI. Building drift limit for seismic loads was based on 2% allowable drift for Risk Category II steel structures in ASCE/SEI 7-10, Table 12.12-1.

Table B.1 Deflection and drift performance limits

Analysis	Deflection / drift limit
Member live load	L/360
Member total load	L/240
Member construction total load	L/360
Building wind elastic drift (10-year MRI)	H/400
Building seismic inelastic drift (DBE)	H/50

B.2 Design Gravity Loads

The uniform dead and live loads used to design the archetype buildings are given in Table B.2 and Table B.3. The total loads were targeted to match the design loads used in Chapter 6 and Appendix D of the FEMA P-695 evaluation report (NIST 2010a). The dead loads are generally representative of typical design dead loads used in practice, except that a composite steel deck and concrete slab is used instead of a steel-joist and steel-deck system for the roof.

The live loads were representative of the occupancy and use of commercial office buildings. A constant uniform live load was used, matching the live load used in the FEMA evaluation report (i.e. lobby, corridor, stair, and exit area live loads are not used). Construction phase (pre-composite) live load is 25 psf (ASCE 2002). Reduction of roof and floor live loads is applied in accordance with ASCE 7 section 4.7.

Table B.2 Design dead loads

Description	Uniform load (psf)
5.5-inch slab (2-inch normal weight concrete cover on 3-inch steel deck)	51
Partitions (floor) or ballast material (roof)	20
Structural steel members	9
Superimposed dead load (ceiling, mechanical, electrical, plumbing)	10
Total design dead load:	**90**

Table B.3 Design live loads

Use or occupancy	Uniform load (psf)
Roofs (ordinary maintenance)	20
Floors (offices)	50
Construction phase	25

B.3 Seismic Hazard

Archetype buildings were designed for seismic hazard levels described in Table B.4. For each hazard level, the target Seismic Design Category (SDC) design basis earthquake (DBE) spectral acceleration values from ASCE/SEI 7-10, Table 11.6-1 and Table 11.6-2 were used to determine the corresponding risk-based Maximum Considered Earthquake (MCE) ground motion spectral acceleration values (2% probability of being exceeded in 50 years (or 2,475-year MRI), based on soil site class D, and the mapped MCE values.

A hazard level corresponding to SDC D_{max} (shown in FEMA P695 Table 5-1A and Table 5-1B) is included in the design, even though the archetype lateral force resisting system—steel ordinary moment frames (OMF) and steel moment frames not detailed for seismic resistance (so called "R=3" systems)—are not permitted by ASCE/SEI 7-10, Table 12.2-1 in SDC D, for the full range of archetype building height (greater than 65 feet) and material weight (roof and wall dead load in excess of 20 psf). The purpose of including these in the design was to allow for a comparison between the response of non-ductile (OMF and R=3) and ductile (SMF and IMF) frames determined in related studies (Jarrett 2013; Flores 2015).

Table B.4 Seismic design hazards

Seismic Design Category (SDC)	Spectral Acceleration					
	Mapped		MCE		DBE	
	S_S (g)	S_1 (g)	S_{MS} (g)	S_{M1} (g)	S_{DS} (g)	S_{D1} (g)
B_{min}	0.156	0.042	0.25	0.10	0.17	0.07
C_{min}	0.330	0.083	0.51	0.20	0.34	0.13
D_{min}	0.550	0.132	0.75	0.30	0.50	0.20
D_{max}	1.500	0.684	1.50	0.90	1.00	0.60

B.4 Wind Hazard

Archetype buildings are designed for a wind hazard corresponding to non-coastal location in the United States. This provides a typical wind speed for design (avoiding the lower design wind speed on the west coast, and the higher wind speeds along the eastern coast). Service level wind speed (76 mph) and strength level wind speed (115 mph) are based on the 10-year MRI (ASCE 7-10 Figure CC-1) and 700-year MRI (ASCE 7-10 Figure 26.5-1A), respectively.

The buildings are designed for terrain exposure category C (open terrain without obstructions). The effect of wind gust is included based on 1% damping (inherent damping not explicitly modeled) for service level drift, and 2% damping for strength level drift.

B.5 Analyses for Design

For design purposes, story heights were based on beam centerlines, including the first story. This definition of story height differs from the definition of story height in the FEMA P-695 evaluation report (NIST 2010a). In the evaluation report, elevations were based on beam centerlines, except the first story height was measured from the ground to the top of the beam (NIST 2010a Appendix A; NIST 2010b). In that study, the beam size used to establish the first story elevation was not necessarily the final beam size used in the design. (It was likely a trial size). For example, all the 1-story buildings in the evaluation report use a first-story elevation based on a W18X16 first story beam, but only one archetype design actually used that size beam for the first story.

Tributary areas and loads were based on beam and column centerlines. The evaluation report also used beam centerlines when calculating tributary dead loads, but ignored the first story height definition used to determine elevation lines.

Parameters used to design the steel moment frames are summarized in Table B.5. The estimated (empirical) period of vibration for wind analyses is shown. This value differs from the empirical period of vibration used for seismic analyses and is closer to a lower bound on observed data of building periods. The wind base shear force for drift analysis (10-year MRI) and strength analysis (700-year MRI) are shown in Table B.5. For each seismic design category, the base shear force and base shear coefficient, C_s (base shear force normalized by the total weight of the building) is given based on the estimated period of vibration ($T = C_u T_a$).

Table B.5 Design parameters for non-ductile moment frames

Archetype ID	No. of stories	Wind			Seismic			
			V (k)					
		T (s)	10-yr MRI	700-yr MRI	SDC	T (s)	Cs	V (k)
R3-20-1A	1	0.39	8.44	19.3	B_{min}	0.42	0.054	72.8
R3-20-1B					C_{min}	0.40	0.111	150
R3-20-1C					D_{min}	0.37	0.166	224
R3-20-1D					D_{max}	0.34	0.333	450
R3-20-2A	2	0.65	24.8	56.8	B_{min}	0.68	0.033	90.5
R3-20-2B					C_{min}	0.66	0.067	186
R3-20-2C					D_{min}	0.60	0.110	305
R3-20-2D					D_{max}	0.56	0.333	922
R3-20-4A	4	1.10	64.6	149	B_{min}	1.16	0.019	108
R3-20-4B					C_{min}	1.11	0.040	223
R3-20-4C					D_{min}	1.02	0.065	365
R3-20-4D					D_{max}	0.95	0.210	1,175
R3-20-8A	8	1.88	159	369	B_{min}	1.99	0.011	127
R3-20-8B					C_{min}	1.91	0.023	261
R3-20-8C					D_{min}	1.75	0.038	428
R3-20-8D					D_{max}	1.64	0.122	1,378
R3-20-12A	12	2.59	269	624	B_{min}	2.73	0.008	139
R3-20-12B					C_{min}	2.63	0.017	285
R3-20-12C					D_{min}	2.41	0.028	468
R3-20-12D					D_{max}	2.25	0.089	1,505

Table B.6 summarizes the lateral load resisting system drift, strength, and seismic stability analyses used for design. Load combinations and load factors for these requirements were based on ASCE 7-10. Note that in contrast to gravity load combinations, roof live load was not included in the lateral combinations except in a wind strength analysis.

Second-order effects (P-Δ effects) were included in a centerline-model analysis using the Direct Design Method (AISC 360-10). The reduced stiffness that is required by the Direct Design Method was employed only in strength analyses, not in drift or vibration (eigenvalue frequency-determination) analyses (commentary to AISC 2010a; commentary to AISC 2010b).

The equivalent lateral forces used to check the drift requirement was based on the computed fundamental period of vibration from an eigenvalue analysis, per ASCE 7-10 section 12.8.6.2, which are lower compared to the forces used for strength analysis shown in Table B.5. The stability ratio is back-calculated based on first order and second order interstory drift ratios (Charney 2014). The maximum allowable stability ratio is $0.5/C_d$ (story overstrength factor β is taken as 1.0).

Table B.6 Analyses used to design the Type I non-ductile moment frames

Hazard	Analysis	Comments	Load combination
Seismic	Vibration	Centerline joint modeling (rigid joints).	1.0D
	Drift	Lateral forces based on the computed fundamental period from vibration (eigenvalue) analysis.	$(1.2 + 0.2*S_{DS})D + 0.5L + E$
	Strength	Stiffness (modulus of elasticity) reduced 20%.	
	Stability	Stability ratio θ calculated directly based on first and second order drift analyses: $\theta = 1 - \Delta^{1st\ order} / \Delta^{2nd\ order}$.	
Wind	Drift	--	$D + 0.5L + W_{10}$
	Strength	Stiffness (modulus of elasticity) reduced 20%.	$1.2D + L + 0.5L_r + W_{700}$

B.6 Example Calculations

This section provides example calculations for the Type I 4-story non-ductile archetype building with an ordinary moment frame (OMF) system. Included are gravity design calculations for a typical girder, typical column, and lateral design results for the moment frame members.

B.6.1 Gravity Design of Girder

The gravity design included live load reductions and considers composite action between the roof and floor concrete slab and the bare steel beams. Camber (where required) was only used on interior beams. Exterior beams have no camber.

Composite member						
Geometry						
Member span	L =	**40**	ft			
Dist. to adjacent left member	sR =	**20**	ft			
Dist. to adjacent right member	sL =	**20**	ft			
Concrete						
Concrete cover above deck	t =	**4.5**	in.			
Steel deck depth	td =	**3**	in.			
Steel deck orientation	=	**Parallel to steel member**				
Steel						
W-Shape	=	**W24X68**	in.			
Camber	c =	**1 1/4**	in.			
PNA location	=	**5 (BFL)**				

Loads						
Dead Loads						
Pre-composite (construction)	CDL =	**60**	psf			
Composite (service)	DL =	**30**	psf			
Live Loads						
Pre-composite (construction)	CLL =	**25**	psf			
Composite (service)	LL =	**50**	psf			
Live Load Reduction						
Live load type	=	**Floor**				
Tributary area	AT =	800	sf			
Live load reduction factor	=	0.63		ASCE/SEI 7 Section 4.7		
Pre-composite (construction)	CLL =	16	psf			
Composite (service)	LL =	31	psf			

Materials						
Steel						
Yield strength	Fy =	**50**	ksi			
Modulus of elasticity	E =	29,000	ksi			
Concrete						
Concrete	F'c =	**4**	ksi			
Weight	=	**Normal weight**				
Headed stud anchor (HSA)						
Diameter	=	**3/4**	in.			
Single anchor strength	Qn =	**21.5**	k			

Deflection limits					
Pre-composite DL	L/	**360**			AISC Design guide 3
Composite (service) LL	L/	**360**			2009 IBC Table 1604.3

Pre-composite (construction) design					
Required strength					
Uniform load (factored)	wu =	1.94	klf		
Simple-span moment	Mu =	388	k-ft		
Design strength					
Resistance factor	ϕb =	0.90			
Plastic section modulus	Zx =	177	in.3		
Plastic strength	ϕMn =	664	k-ft		
Available strength	ϕMn =	**585**	k-ft	AISCM Table 3-10	
Flexure strength	ϕMn =	585	k-ft	**OK**	Pass by 51%
Deflection					
Moment of intertia	Ix =	1,830	in.4		
DL deflection (unfactored)	ΔDL =	1.30	in.		
DL deflection limit	Δlimit =	1.33	in.		
Required camber	Δc =	0.00	in.		
Provided camber	c =	1.25	in.	**OK**	Pass by1%

Composite design					
Required strength					
Uniform load (factored)	wu =	3.16	klf		
Simple-span moment	Mu =	632	k-ft		
Concrete					
Effective width of concrete	b1 =	120	in.		
	b2 =	240	in.		
	bmin =	120	in.		
Total slab depth	Ycon =	7.5	in.		

Plastic neutral axis					
PNA location	=	5 (BFL)			
Steel flange thickness	tf =	0.585	in.		
Steel flange width	bf =	8.97	in.		
Distance from TFL to PNA	Y1 =	0.5850	in.		
Area of W-shape	As =	20.1	in.2		
Steel web thickness	tw =	0.415	in.		
Lower bound parameters (location 7)					
Lower bound composite action	=	25%		AISCM Page 3-13	
Lower bound horizontal shear fo	ΣQn =	251	k	AISCM Fig. 3-3	
Steel web thickness	tw =	0.415	in.		
Steel shape depth	d =	23.7	in.		
Steel web fillet	k1 =	1.09	in.		
Steel web area	Aw =	8.93	in.^2	AISCM Page 3-13	
	Kdep =	0.505	in.	AISCM Page 3-13	
	Karea =	0.34	in.^2	AISCM Page 3-13	
Lower bound Y1	Y1 (LB) =	5.7958	in.		
Bottom of flange parameters (location 5)					
Bottom of flange Y1	Y1 (BFL) =	0.5850	in.		
Area of W-shape in tension	At =	14.85	in.^2		
Horizontal shear force @ locati	ΣQn =	480	k	AISCM Fig. 3-3	
Location 6 parameters					
Horizontal shear force @ locati	ΣQn =	366	k	AISCM Fig. 3-3	
Steel web thickness	tw =	0.415	in.		
Steel web depth	d =	23.7	in.		
Steel web fillet	k1 =	1.09	in.		
Steel web area	Aw =	8.93	in.^2	AISCM Page 3-13	
	Kdep =	0.505	in.	AISCM Page 3-13	
	Karea =	0.34	in.^2	AISCM Page 3-13	
Location 6 Y1	Y1 (L6) =	3.0367	in.		
Composite W-shape parameters					
Area of W-shape in tension	At =	14.85	in.^2		
Steel tension force	T =	743	k		
Area of W-shape in compresior	Ac =	5.25	in.^2		
Steel compression force	Cs =	262	k		
Horizontal shear force at interfa	ΣQn =	480	k		
Dist. from TOS to conc. flange	a =	1.177	in.	AISCM Eq. 3-7	
Dist. from TFL to conc. force	Y2 =	6.911	in.	AISCM Eq. 3-7	
Conc. compressive force	C =	480	k		
Max steel tension force	T =	1,005	k		

Composite flexure strength	PNA locat	Y1	At	M(-) (k-in)		
	1 (TFL)	0.000	20.1	0.0		
	2	0.146	18.8	9.6		
	3	0.293	17.5	38.4		
	4	0.439	16.2	86.3		
	5 (BFL)	0.585	14.9	153.5		
	6	3.037	13.7	348.4		
	7	5.796	12.6	854.1		
	ϕMp =	1,131	k-ft	OK	Pass by 79%	
Deflection						
Dist. From TFL to conc force	d1 =	6.911	in.			
Dist. From TFL to steel force	d3 =	11.850	in.			
Elastic neutral axis	YENA =	17.916	in.			
Ix, Lower bound	ILB =	4,118	in.4			
DL deflection (unfactored)	ΔDL =	0.30	in.			
DL deflection limit	Δlimit =	1.33	in.	OK	Pass by 342%	
Number of HSA						
Number from zero to Mmax	n1 =	23				
Total number of anchors	n =	46				

Result summary						
Composite member	=	**W24X68 with c=1.25 in. and (46) HSA**				
Pre-composite (construction)						
Strength	=	OK	Pass by 51%			
Deflection	=	OK	Pass by1%			
Composite						
Strength	=	OK	Pass by 79%			
Deflection	=	OK	Pass by 342%			

B.6.2 Gravity Design of Column

Loads			
Dead Loads			
Floor/roof dead load	DL =	**90**	psf
Exterior wall dead load	WDL =	**25**	psf
Live Loads			
Roof live load (construction)	RLL =	**25**	psf
Floor live load	FLL =	**50**	psf

Column factored dead load (k) per level

	Column ID	1	2	3	4	5	6
	Trib A (sf)	**900**	**600**	**400**	**600**	**200**	**400**
Story	Trib W (ft)	**0**	**0**	**20**	**30**	**30**	**20**
4	**6.5**	97	65	47	71	27	47
3	**14**	97	65	52	77	34	52
2	**14**	97	65	52	77	34	52
1	**13**	97	65	51	77	33	51

Column factored live load (k) per level

	Column ID	1	2	3	4	5	6
	Trib A (sf)	**900**	**600**	**400**	**600**	**200**	**400**
Story	Trib W (ft)	**0**	**0**	**20**	**30**	**30**	**20**
4	**6.5**	36	24	21	32	16	21
3	**14**	36	24	27	41	25	27
2	**14**	36	24	27	41	25	27
1	**13**	36	24	26	40	24	26

Column total factored load (Pu, k) per level

	Column ID	1	2	3	4	5	6
	Trib A (sf)	**900**	**600**	**400**	**600**	**200**	**400**
Story	Trib W (ft)	**0**	**0**	**20**	**30**	**30**	**20**
4	**6.5**	133	89	68	102	43	68
3	**14**	133	89	79	118	59	79
2	**14**	133	89	79	118	59	79
1	**13**	133	89	77	116	57	77

Column load (Pu, k) cummulative

	Column ID	1	2	3	4	5	6
	Trib A (sf)	**800**	**400**	**400**	**600**	**200**	**400**
Story	Trib W (ft)	**0**	**0**	**20**	**30**	**30**	**20**
4	**6.5**	133	89	68	102	43	68
3	**14**	266	178	147	221	102	147
2	**14**	400	266	226	339	161	226
1	**13**	533	355	303	455	218	303

Column tributary area (sf)

	Column ID	1	2	3	4	5	6
Story	KLL	**4**	**4**	**4**	**4**	**4**	**4**
4		800	400	400	600	200	400
3		1,600	800	800	1,200	400	800
2		2,400	1,200	1,200	1,800	600	1,200
1		3,200	1,600	1,600	2,400	800	1,600

Column Live Load Reduction factor

	Column ID	1	2	3	4	5	6
Story	KLL	**4**	**4**	**4**	**4**	**4**	**4**
4		0.60	0.80	0.80	0.60	1.00	0.80
3		0.63	1.00	1.00	0.68	1.00	1.00
2		0.52	0.63	0.63	0.56	1.00	0.63
1		0.47	0.56	0.56	0.50	0.68	0.56

Column reduced factored live load (k) per level

	Column ID	1	2	3	4	5	6
	Trib A (sf)	**900**	**600**	**400**	**600**	**200**	**400**
Story	Trib W (ft)	**0**	**0**	**20**	**30**	**30**	**20**
4	**6.5**	22	19	17	19	16	17
3	**14**	23	24	27	28	25	27
2	**14**	19	15	17	23	25	17
1	**13**	17	13	15	20	16	15

Column total load (Pu, k) cummulative including live load reduction

	Column ID	1	2	3	4	5	6
	Trib A (sf)	**800**	**400**	**400**	**600**	**200**	**400**
Story	Trib W (ft)	**0**	**0**	**20**	**30**	**30**	**20**
4	**6.5**	119	84	64	90	43	64
3	**14**	**239**	**173**	143	195	**102**	143
2	**14**	354	253	211	295	161	211
1	**13**	**468**	**331**	277	391	**211**	277

Gravity only columns

		Column	1		2		5	
Story	Hmax (ft)		W-Shape	ϕPn	W-Shape	ϕPn	W-Shape	ϕPn
3 to 4	**13**		W8X31	266	W8X31	266	W8X31	266
1 to 2	**15**		W8X67	523	W8X48	367	W8X31	230

B.6.3 Lateral Design of OMF

Lateral design loads for the 4-story frame are shown below. Figure B.1 shows the MWFRS wind loads (for the 10-year MRI), and Figure B.2 shows equivalent lateral seismic loads (for the OMF

frame in SDC D_{min} / C_{max}). For modeling purposes, the lateral load was applied at each beam-column joint: half load at exterior joints, whole load at interior joints (not entirely at the exterior frame joint as depicted below).

The seismic analysis results using centerline modeling is shown in Table B.7 to Table B.11. Inter-story drift values shown have been amplified to represent inelastic drift values (multiplied by C_d).

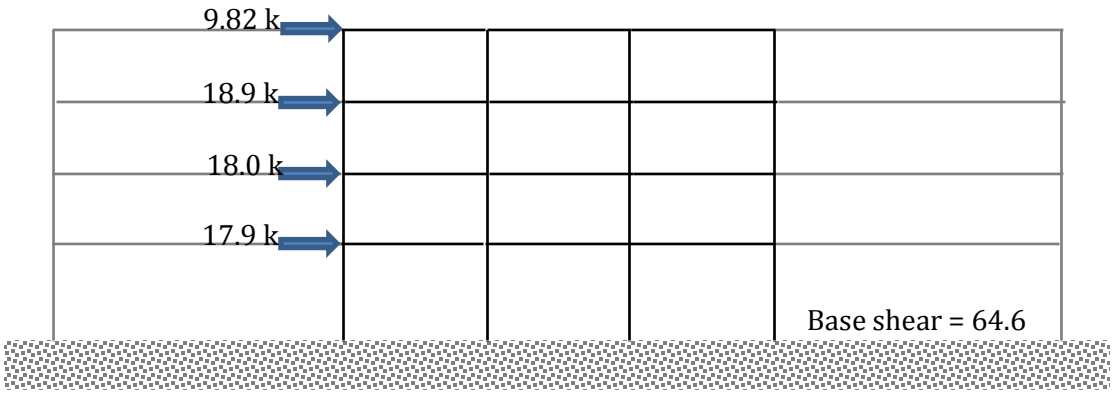

Figure B.1 Lateral MWFRS wind loads (4-story building)

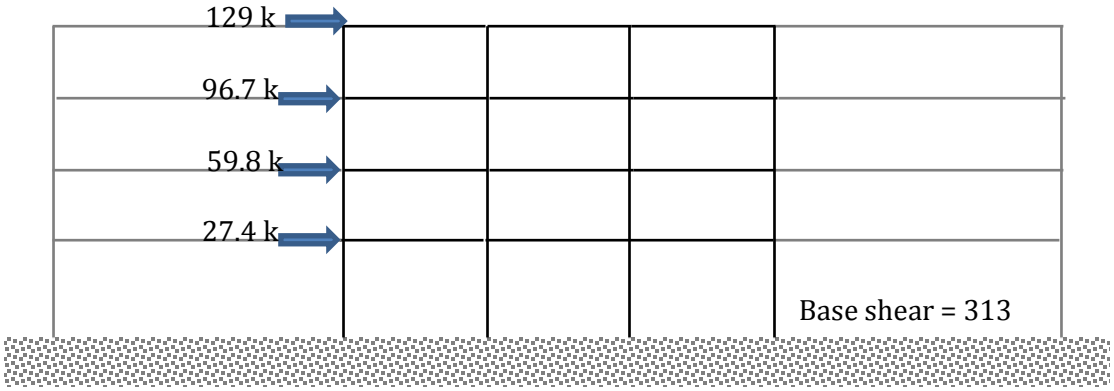

Figure B.2 Lateral equivalent seismic loads (4-story building, OMF, SDC D_{min})

Table B.7 Inter-story drift ratio and stability ratio for seismic drift analysis: 4-story building, OMF SDC D_{min}

Story	Inter-story drift ratio		Stability ratio, θ
	$\Delta^{1st\ order}$	$\Delta^{2nd\ order}$	$(1 - \Delta^{1st\ order} / \Delta^{2nd\ order})$
4	0.0070	0.0077	0.086
3	0.0103	0.0117	0.123
2	0.0093	0.0107	0.134
1	0.0067	0.0077	0.129
Drift limit = 0.0200			θ_{max} = 0.167

Table B.8 Ratio of available / required beam strength for seismic strength analysis: 4-story building, OMF SDC D_{min}

Story	Bay		
	1	2	3
4	0.41	0.36	0.33
3	0.69	0.60	0.61
2	0.89	0.80	0.83
1	0.92	0.84	0.88

Table B.9 Interaction ratio of available and required column flexure and axial strengths for seismic strength analysis: 4-story building, OMF SDC D_{min}

Story	Column			
	1	2	3	4
4	0.41	0.52	0.47	0.37
3	0.82	0.88	0.85	0.90
2	0.39	0.52	0.51	0.55
1	0.80	0.76	0.76	0.97

Table B.10 Ratio of available and required joint (panel zone) shear strength for seismic strength analysis: 4-story building, OMF SDC D_{min}

Story	Column			
	1	2	3	4
4	0.45	0.34	0.30	0.37
3	0.94	0.71	0.67	0.82
2	0.87	0.62	0.61	0.81
1	0.80	0.59	0.59	0.76

Table B.11 Computed periods of vibration: 4-story building, OMF SDC D_{min}

Analytical model	Period (sec/cycle)			
	T_1	T_2	T_3	T_4
Centerline	2.15	0.71	0.39	0.24

For purposes of comparison, the seismic analysis results based on explicit joint modeling (using the Krawinkler panel zone model) are shown in Table B.12 to Table B.16. The archetype designs were not based on explicit joint modeling.

Table B.12 Inter-story drift ratio and stability ratio for seismic drift analysis: 4-story building, OMF SDC D_{min}

Story	Inter-story drift ratio		Stability ratio, θ
	$\Delta^{1st\ order}$	$\Delta^{2nd\ order}$	$(1 - \Delta^{1st\ order} / \Delta^{2nd\ order})$
4	0.0073	0.0080	0.090
3	0.0099	0.0112	0.118
2	0.0092	0.0106	0.131
1	0.0068	0.0078	0.127
Drift limit = 0.0200			$\square_{max}$ = 0.167

Table B.13 Ratio of available / required beam strength for seismic strength analysis: 4-story building, OMF SDC D_{min}

Story	Bay		
	1	2	3
4	0.42	0.34	0.35
3	0.64	0.50	0.58
2	0.84	0.71	0.78
1	0.88	0.76	0.84

Table B.14 Interaction ratio of available and required column flexure and axial strengths for seismic strength analysis: 4-story building, OMF SDC D_{min}

Story	Column			
	1	2	3	4
4	0.41	0.50	0.46	0.38
3	0.76	0.73	0.72	0.85
2	0.34	0.45	0.43	0.51
1	0.80	0.76	0.76	0.98

Table B.15 Ratio of available and required joint (panel zone) shear strength for seismic strength analysis: 4-story building, OMF SDC D_{min}

Story	Column			
	1	2	3	4
4	0.40	0.58	0.54	0.34
3	0.72	0.97	0.97	0.65
2	0.64	0.88	0.85	0.59
1	0.56	0.80	0.78	0.53

Table B.16 Computed periods of vibration: 4-story building, OMF SDC D_{min}

Analytical model	Period (sec/cycle)			
	T_1	T_2	T_3	T_4
Centerline	2.12	0.69	0.35	0.21

A summary of the wind analysis results using centerline modeling is shown in Table B.17 to Table B.19. The wind analysis results (not shown) were based on explicit joint modeling (using the Krawinkler panel zone model) but are not significantly different.

Table B.17 Inter-story drift ratio for wind drift analysis: 4-story building

Story	Inter-story drift ratio	
	$\Delta^{1st\ order}$	$\Delta^{2nd\ order}$
4	0.0005	0.0005
3	0.0010	0.0011
2	0.0011	0.0012
1	0.0009	0.0010
Drift limit = 0.0025 (H/400)		

Table B.18 Ratio of required to provided beam strength for wind strength analysis: 4-story building

Story	Bay		
	1	2	3
4	0.11	0.08	0.04
3	0.22	0.17	0.13
2	0.34	0.29	0.28
1	0.40	0.35	0.36

Table B.19 Interaction ratio of available and required column flexure and axial strengths for wind strength analysis: 4-story building

Story	Column			
	1	2	3	4
4	0.17	0.16	0.11	0.11
3	0.53	0.36	0.32	0.52
2	0.36	0.27	0.25	0.38
1	0.58	0.47	0.47	0.64

B.7 Design Summary

A summary of the design analyses is provided in Table B.20 to Table B.23. For each archetype, the beam and column sizes, the design criteria (strength, drift, or stability) that controlled the overall design, and the computed fundamental period of vibration (based on centerline modeling) used in seismic drift analyses is given.

Table B.20 Archetype design and member sizes for Type I non-ductile 1-story buildings

Design	Story	Beam size	Column size		Controlling criteria	Computed Period, T_1
			Exterior	Interior		
OMF / B_{max}	1	W18X40	W14X90	W14X99	Strength	1.50
OMF / C_{max}	1	W21X44	W14X109	W14X132	Strength	1.27
R=3 / A_{max}	1	W18X35	W14X82	W14X82	Stability	1.67

Table B.21 Archetype design and member sizes for Type I non-ductile 2-story buildings

Design	Story	Beam size	Column size		Controlling criteria	Computed Period, T_1
			Exterior	Interior		
OMF / B_{max}	1	W21X55	W18X71	W18X76	Strength	1.99
	2	W16X31	W18X71	W18X76		
OMF / C_{max}	1	W24X55	W18X97	W18X143	Strength	1.62
	2	W16X31	W18X97	W18X143		
R=3 / A_{max}	1	W21X44	W18X71	W18X76	Stability	2.13
	2	W16X31	W18X71	W18X76		

Table B.22 Archetype design and member sizes for Type I non-ductile 4-story buildings

Design	Story	Beam size	Column size		Controlling criteria	Computed Period, T_1
			Exterior	Interior		
OMF / B_{max}	1	W16X40	W18X76	W18X97	Stability	2.44
	2	W21X44	W18X76	W18X97		
	3	W18X35	W18X40	W18X50		
	4	W16X31	W18X40	W18X50		
OMF / C_{max}	1	W21X44	W18X86	W18X106	Strength	2.15
	2	W21X48	W18X86	W18X106		
	3	W21X44	W18X40	W18X50		
	4	W18X35	W18X40	W18X50		
R=3 / A_{max}	1	W16X40	W18X76	W18X86	Stability	2.49
	2	W21X44	W18X76	W18X86		
	3	W18X35	W18X40	W18X46		
	4	W16X31	W18X40	W18X46		

Table B.23 Archetype design and member sizes for Type I non-ductile 8-story buildings

Design	Story	Beam size	Column size		Controlling criteria	Computed Period, T_1
			Exterior	Interior		
OMF / B_{max}	1	W21X48	W24X146	W24X146	Stability	3.32
	2	W24X68	W24X146	W24X146		
	3	W24X76	W24X76	W24X103		
	4	W24X55	W24X76	W24X103		
	5	W24X55	W24X55	W24X62		
	6	W21X48	W24X55	W24X62		
	7	W18X35	W24X55	W24X55		
	8	W18X35	W24X55	W24X55		
OMF / C_{max}	1	W21X48	W24X131	W24X162	Strength	3.27
	2	W24X76	W24X131	W24X162		
	3	W24X76	W24X76	W24X103		
	4	W24X55	W24X76	W24X103		
	5	W21X55	W24X55	W24X68		
	6	W21X55	W24X55	W24X68		
	7	W18X35	W24X55	W24X55		
	8	W18X35	W24X55	W24X55		
R=3 / A_{max}	1	W21X48	W24X146	W24X146	Wind strength	3.32
	2	W24X68	W24X146	W24X146		
	3	W24X76	W24X76	W24X103		
	4	W24X55	W24X76	W24X103		
	5	W24X55	W24X55	W24X62		
	6	W21X48	W24X55	W24X62		
	7	W18X35	W24X55	W24X55		
	8	W18X35	W24X55	W24X55		

Appendix C

ANALYTICAL MODEL FOR TYPE I NON-DUCTILE MOMENT FRAME 4-STORY BUILDING

This appendix contains excerpts of the *OpenSees* (PEER 2012) scripts and selected modeling results for the Type I non-ductile moment frame 4-story building with enhanced shear tab connections.

C.1 Building and Load Model

The following is an excerpt from the *OpenSees* script used to define the building, materials, connection and plastic hinge behavior, and gravity loads. Figure C.1 shows a perspective view of the finite element model.

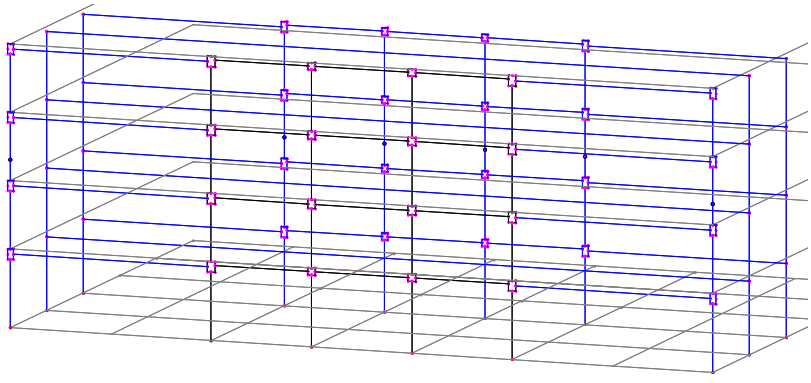

Figure C.1 Finite element model of Type I non-ductile moment frame 4-story building

```
# OpenSees input file generated using MATLAB
#
# General information
wipe
model basic -ndm 2 -ndf 3
geomTransf Linear 1
geomTransf PDelta 2
geomTransf Corotational 3
#
# Frame 1 Base line 1
node 100010100 0.000000 0.000000
fix 100010100 1 1 0
#
# Frame 1 Joint line 1 story 1
node 101020101 6.850000 180.000000
node 101020102 6.850000 180.000000
node 101020103 6.850000 168.150000
node 101020104 6.850000 156.300000
node 101020105 6.850000 156.300000
node 101020106 0.000000 156.300000
node 101020107 -6.850000 156.300000
node 101020108 -6.850000 156.300000
node 101020109 -6.850000 168.150000
node 101020110 -6.850000 180.000000
node 101020111 -6.850000 180.000000
node 101020112 0.000000 180.000000
equalDOF 101020101 101020102 1 2
equalDOF 101020104 101020105 1 2
equalDOF 101020107 101020108 1 2
equalDOF 101020110 101020111 1 2
element elasticBeamColumn 101020101 101020102 101020103 1000.000000
29000.000000 100000.000000 3
element elasticBeamColumn 101020102 101020103 101020104 1000.000000
29000.000000 100000.000000 3
element elasticBeamColumn 101020103 101020105 101020106 1000.000000
29000.000000 100000.000000 3
element elasticBeamColumn 101020104 101020106 101020107 1000.000000
29000.000000 100000.000000 3
element elasticBeamColumn 101020105 101020108 101020109 1000.000000
29000.000000 100000.000000 3
element elasticBeamColumn 101020106 101020109 101020110 1000.000000
29000.000000 100000.000000 3
element elasticBeamColumn 101020107 101020111 101020112 1000.000000
29000.000000 100000.000000 3
element elasticBeamColumn 101020108 101020112 101020101 1000.000000
29000.000000 100000.000000 3
uniaxialMaterial Hysteretic 101020109 2995.671113 0.002855 3199.604513
0.011419 11827.137317 0.285481 -2995.671113 -0.002855 -3199.604513 -0.011419
-11827.137317 -0.285481 1.000000 1.000000 0.000000 0.000000 0.000000
element zeroLength 101020109 101020101 101020102 -mat 101020109 -dir 6
[...]

# Frame 3 Beam bay 5 story 4
equalDOF 101020209 301020209 1
equalDOF 102020209 302020209 1
equalDOF 103020209 303020209 1
```

```
equalDOF 104020209 304020209 1
equalDOF 101020309 301020309 1
[...]

mass 101020109 0.154110 0.000000 0.000000
mass 101020103 0.154110 0.000000 0.000000
mass 101020209 0.154110 0.000000 0.000000
mass 101020203 0.154110 0.000000 0.000000
mass 101020309 0.154110 0.000000 0.000000
mass 101020303 0.154110 0.000000 0.000000
mass 101020409 0.154110 0.000000 0.000000
mass 101020403 0.154110 0.000000 0.000000
mass 101020509 0.154110 0.000000 0.000000
mass 101020503 0.154110 0.000000 0.000000
mass 101020609 0.154110 0.000000 0.000000
[...]

#
# Gravity load time series
timeSeries Constant 1 -factor 1.000000
pattern Plain 101020109 1 {
  load 101020109 0.000000 -16.212500 0.000000
}
pattern Plain 101020104 1 {
  load 101020103 0.000000 -16.212500 0.000000
}
pattern Plain 101020209 1 {
  load 101020209 0.000000 -37.612500 0.000000
}
[...]
```

C.2 Gravity Load Analysis

The following is the script used to define the gravity (pre-load) analysis.

```
# OpenSees input file generated using MATLAB
model basic -ndm 2 -ndf 3
#
# Define source file (finite element model and loads)
source exampleInput.tcl
#
# Analysis parameters
constraints Plain
numberer Plain
system UmfPack
test EnergyIncr 1.000000e-005 20
algorithm Newton
integrator LoadControl 0.100000
analysis Static
set ok [analyze 10 1.000000]
loadConst -time 0.000000
```

C.3 Frequency (Building Period of Vibration) Analysis

The following is the script used to define the frequency analysis. Figure C.2 shows the first four mode shapes and periods of vibration.

```
# OpenSees input file generated using MATLAB
model basic -ndm 2 -ndf 3
#
# Define source file (gravity analysis)
source exampleGravityInput.tcl
#
# Analysis parameters
constraints Plain
numberer Plain
system UmfPack
test EnergyIncr 1.000000e-005 20
algorithm Newton
#
# Define response recorders
recorder Node -file exampleVibrationRecorderNodeeigeni.out -time -dof 1 2 3
eigen i
set lambda [eigen -generalized -fullGenLapack 4]
set fidwrite [open eigenValue.out w]
foreach lam $lambda {
  puts $fidwrite $lam
}
integrator LoadControl 1.000000
analysis Static
set ok [analyze 1 1.000000]
```

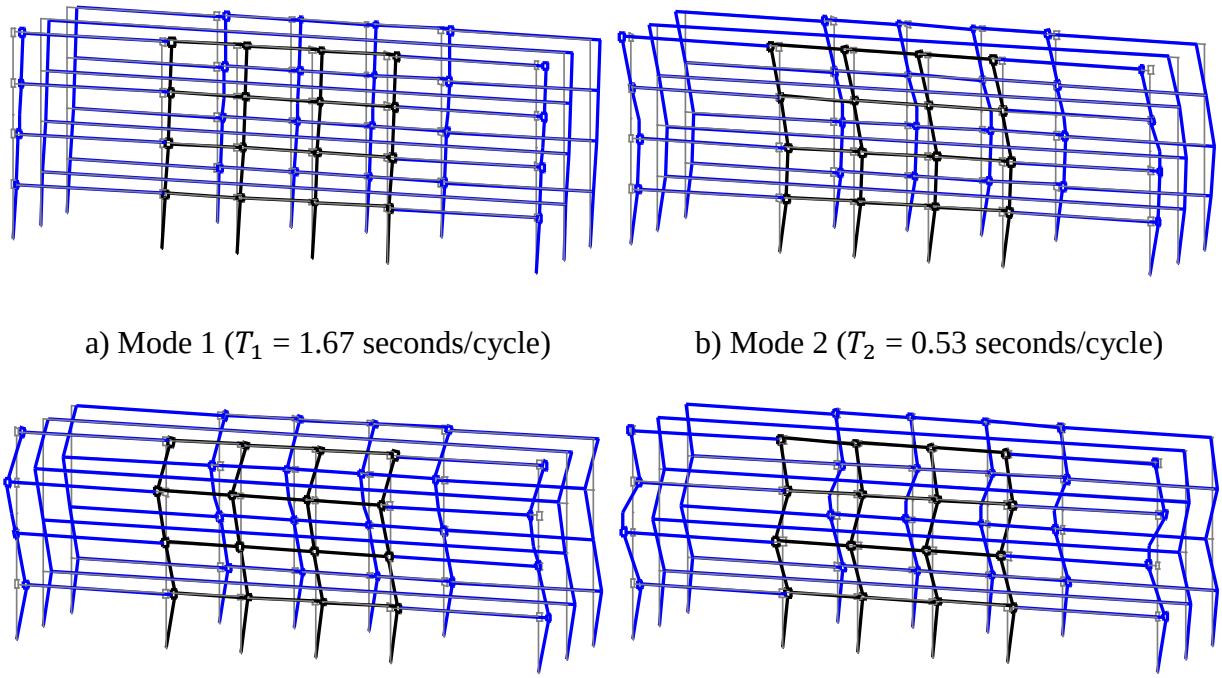

a) Mode 1 (T_1 = 1.67 seconds/cycle)

b) Mode 2 (T_2 = 0.53 seconds/cycle)

c) Mode 3 (T_3 = 0.25 seconds/cycle)

d) Mode 4 (T_4 = 0.17 seconds/cycle)

Figure C.2 Mode shapes and periods of vibration

C.4 Nonlinear Static "Pushover" Analysis

C.4.1 Seismic Pushover

The following is the script used to define the seismic pushover analysis. Figure C.3 shows the seismic pushover response and the deformed shape.

```
# OpenSees input file generated using MATLAB
model basic -ndm 2 -ndf 3
#
# Define source file (gravity analysis)
source exampleGravityInput.tcl
#
# Lateral Seismic pushover profile load time series
timeSeries Linear 2 -factor 1.000000
pattern Plain 101020229 2 {
  load 101020209 0.317256 0.000000 0.000000
}
pattern Plain 102020229 2 {
  load 102020209 0.594542 0.000000 0.000000
}
pattern Plain 103020229 2 {
  load 103020209 0.842210 0.000000 0.000000
}
pattern Plain 104020229 2 {
  load 104020209 0.995724 0.000000 0.000000
}
#
# Analysis parameters
constraints Plain
numberer Plain
system UmfPack
test EnergyIncr 1.000000e-004 20
algorithm Newton
#
# Define response recorders
recorder Node -file exampleSeismicPushoverRecorderNodedisp.out -time -dof 1 2
3 disp
recorder Node -file exampleSeismicPushoverRecorderNodereaction.out -time -dof
1 2 3 reaction
integrator DisplacementControl 104020209 1 0.100000
set fidwrite2Name examplePushoversummary2.out
set fidwrite2 [open examplePushoversummary2.out w]
close $fidwrite2
#
# Solution strategy
set integratorType DisplacementControl
set ok 0
```

```
set step 1
set fidwrite2Name exampleSeismicPushoversummary2.out
set fidwrite2 [open $fidwrite2Name w]
close $fidwrite2
set numIncr 300
set dt 1
set testType EnergyIncr
set tol 0.0001
set maxIter 20
analysis Static
set algorithmType Newton
while {$ok == 0 && $step <= $numIncr} {
   set subStep $dt
   set tempIntegratorType $integratorType
   set ok [analyze 1 $subStep]
   if {$ok != 0} {
       puts "Try 1/4 time step"
       set subStep 0.25
       set ok [analyze 1 $subStep]
       if {$ok == 0} {puts "That worked .. back to regular time step"}
       if {$ok != 0} {
           puts "Try 1/8 time step"
           set subStep 0.125
           set ok [analyze 1 $subStep]
           if {$ok == 0} {puts "That worked .. back to 1/4 time step"}
           if {$ok != 0} {
               puts "Try 1/16 time step"
               set subStep 0.0625
               set ok [analyze 1 $subStep]
               if {$ok == 0} {puts "That worked .. back to 1/8 time step"}
               if {$ok != 0} {
                   puts "Try 1/32 time step"
                   set subStep 0.03125
                   set ok [analyze 1 $subStep]
                   if {$ok == 0} {puts "That worked .. back to 1/16 time
step"}
                   set subStep 0.0625
               }
               set subStep 0.125
           }
           set subStep 0.25
       }
       set subStep $dt
   }
   if {$ok != 0 && $algorithmType != "NewtonLineSearch"} {
       puts "Try Newton Line Search for this step"
       test $testType $tol [expr $maxIter*10]
       algorithm NewtonLineSearch
       set algorithmType NewtonLineSearch
       set ok [analyze 1 $subStep]
       if {$ok == 0} {puts "That worked .. continue with Newton Line Search"}
   }
   if {$ok != 0 && $algorithmType != "KrylovNewton"} {
       puts "Try Krylov-Newton for this step"
       test $testType $tol [expr $maxIter*20]
       algorithm KrylovNewton -initial
       set algorithmType KrylovNewton
```

```
        set ok [analyze 1 $subStep]
        if {$ok == 0} {puts "That worked .. continue with Krylov-Newton"}
    }
    if {$ok != 0 && $algorithmType != "BFGS"} {
        puts "Try BFGS for this step"
        test $testType $tol [expr $maxIter*1]
        algorithm BFGS
        set algorithmType BFGS
        set ok [analyze 1 $subStep]
        if {$ok == 0} {puts "That worked .. continue with BFGS"}
    }
    if {$ok != 0 && $algorithmType != "Broyden"} {
        puts "Try Broyden for this step"
        test $testType $tol [expr $maxIter*1]
        algorithm Broyden 8
        set algorithmType Broyden
        set ok [analyze 1 $subStep]
        if {$ok == 0} {puts "That worked .. continue with Broyden"}
    }
    if {$ok != 0 && $algorithmType != "ModifiedNewton"} {
        puts "Try Modified Newton for this step"
        test $testType $tol [expr $maxIter*20]
        algorithm ModifiedNewton
        set algorithmType ModifiedNewton
        set ok [analyze 1 $subStep]
        if {$ok == 0} {puts "That worked .. continue with Modified Newton"}
    }
    if {$ok != 0 && $algorithmType != "ModifiedNewtonInitial"} {
        puts "Try initial stiffness for this step"
        test $testType $tol [expr $maxIter*50]
        algorithm ModifiedNewton -initial
        set algorithmType ModifiedNewtonInitial
        set ok [analyze 1 $subStep]
        if {$ok == 0} {puts "That worked .. continue with initial stiffness"}
    }
    if {$ok == 0} {set tempTol $tol}
    if {$ok != 0} {
       puts "Try tolerance*10 "
       set tol 0.001
       algorithm NewtonLineSearch
       set algorithmType NewtonLineSearch
       set ok [analyze 1 $subStep]
       if {$ok == 0} {puts "That worked .. continue with Newton Line Search"}
       if {$ok != 0 && $algorithmType != "NetwonLineSearch"} {
           puts "Try Newton Line Search for this step"
           test $testType $tol [expr $maxIter*10]
           algorithm NewtonLineSearch
           set algorithmType NewtonLineSearch
           set ok [analyze 1 $subStep]
           if {$ok == 0} {puts "That worked .. continue with Newton Line
Search"}
       }
       if {$ok != 0 && $algorithmType != "KrylovNewton"} {
           puts "Try Krylov-Newton for this step"
           test $testType $tol [expr $maxIter*20]
           algorithm KrylovNewton -initial
           set algorithmType KrylovNewton
```

```
          set ok [analyze 1 $subStep]
          if {$ok == 0} {puts "That worked .. continue with Krylov-Newton"}
      }
      if {$ok != 0  && $algorithmType != "BFGS"} {
          puts "Try BFGS for this step"
          test $testType $tol [expr $maxIter*1]
          algorithm BFGS
          set algorithmType BFGS
          set ok [analyze 1 $subStep]
          if {$ok == 0} {puts "That worked .. continue with BFGS"}
      }
      if {$ok != 0 && $algorithmType != "Broyden"} {
          puts "Try Broyden for this step"
          test $testType $tol [expr $maxIter*1]
          algorithm Broyden 8
          set algorithmType Broyden
          set ok [analyze 1 $subStep]
          if {$ok == 0} {puts "That worked .. continue with Broyden"}
      }
      if {$ok == 0} {set tempTol $tol}
      if {$ok != 0} {
         puts "Try tolerance*100 "
         set tol 0.01
         algorithm NewtonLineSearch
         set algorithmType NewtonLineSearch
         set ok [analyze 1 $subStep]
         if {$ok == 0} {puts "That worked .. continue with Newton Line
Search"}
         if {$ok != 0 && $algorithmType != "NetwonLineSearch"} {
             puts "Try Newton Line Search for this step"
             test $testType $tol [expr $maxIter*10]
             algorithm NewtonLineSearch
             set algorithmType NewtonLineSearch
             set ok [analyze 1 $subStep]
             if {$ok == 0} {puts "That worked .. continue with Newton Line
Search"}
         }
         if {$ok != 0 && $algorithmType != "KrylovNewton"} {
             puts "Try Krylov-Newton for this step"
             test $testType $tol [expr $maxIter*20]
             algorithm KrylovNewton -initial
             set algorithmType KrylovNewton
             set ok [analyze 1 $subStep]
             if {$ok == 0} {puts "That worked .. continue with Krylov-
Newton"}
         }
         if {$ok != 0 && $algorithmType != "BFGS"} {
             puts "Try BFGS for this step"
             test $testType $tol [expr $maxIter*1]
             algorithm BFGS
             set algorithmType BFGS
             set ok [analyze 1 $subStep]
             if {$ok == 0} {puts "That worked .. continue with BFGS"}
         }
         if {$ok != 0 && $algorithmType != "Broyden"} {
             puts "Try Broyden for this step"
             test $testType $tol [expr $maxIter*1]
```

```
            algorithm Broyden 8
            set algorithmType Broyden
            set ok [analyze 1 $subStep]
            if {$ok == 0} {puts "That worked .. continue with Broyden"}
         }
         if {$ok == 0} {set tempTol $tol}
         if {$ok != 0} {
            puts "Try tolerance*1000 "
            set tol 0.1
            algorithm NewtonLineSearch
            set algorithmType NewtonLineSearch
            set ok [analyze 1 $subStep]
            if {$ok == 0} {puts "That worked .. continue with Newton Line
Search"}
            if {$ok != 0 && $algorithmType != "NetwonLineSearch"} {
                puts "Try Newton Line Search for this step"
                test $testType $tol [expr $maxIter*10]
                algorithm NewtonLineSearch
                set algorithmType NewtonLineSearch
                set ok [analyze 1 $subStep]
                if {$ok == 0} {puts "That worked .. continue with Newton Line
Search"}
            }
            if {$ok != 0 && $algorithmType != "KrylovNewton"} {
                puts "Try Krylov-Newton for this step"
                test $testType $tol [expr $maxIter*20]
                algorithm KrylovNewton -initial
                set algorithmType KrylovNewton
                set ok [analyze 1 $subStep]
                if {$ok == 0} {puts "That worked .. continue with Krylov-
Newton"}
            }
            if {$ok != 0 && $algorithmType != "BFGS"} {
                puts "Try BFGS for this step"
                test $testType $tol [expr $maxIter*1]
                algorithm BFGS
                set algorithmType BFGS
                set ok [analyze 1 $subStep]
                if {$ok == 0} {puts "That worked .. continue with BFGS"}
            }
            if {$ok != 0 && $algorithmType != "Broyden"} {
                puts "Try Broyden for this step"
                test $testType $tol [expr $maxIter*1]
                algorithm Broyden 8
                set algorithmType Broyden
                set ok [analyze 1 $subStep]
                if {$ok == 0} {puts "That worked .. continue with Broyden"}
            }
            if {$ok == 0} {set tempTol $tol}
            puts "Back to tolerance*100 "
            set tol 0.01
         }
         if {$ok == 0} {set tempTol $tol}
         puts "Back to tolerance*10 "
         set tol 0.001
      }
      puts "Back to original tolerance "
```

```
      set tol 0.0001
   }
   if {$ok == 0} {
      puts $step
      set currentTime [getTime]
      set numIteratons [testIter]
      set fidsolutioninfo [open $fidwrite2Name a]
      puts $fidsolutioninfo "$step $tempIntegratorType $currentTime
$algorithmType $numIteratons $tempTol"
      close $fidsolutioninfo
      set step [expr $step + 1]
   }
}
```

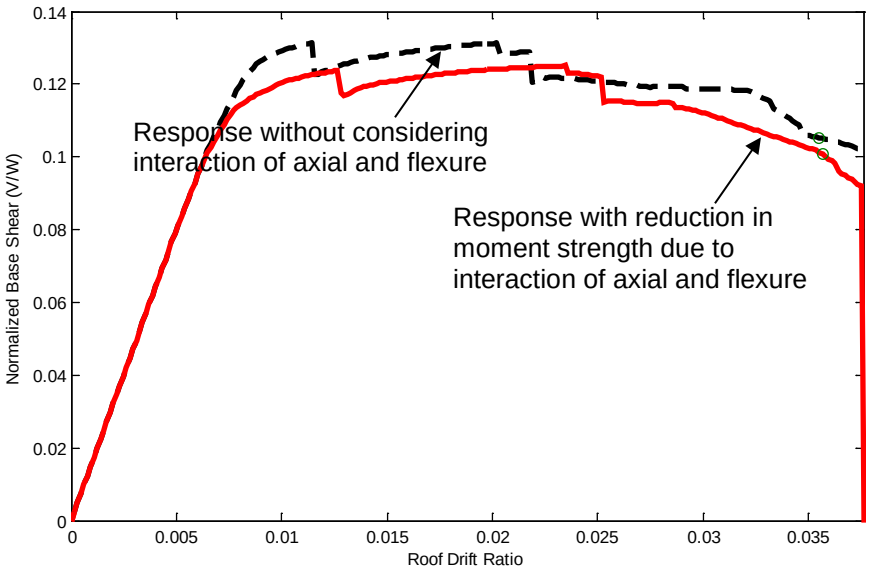

Figure C.3 Seismic pushover response

C.4.2 Wind Pushover

The following is an excerpt from the script used to define the wind pushover analysis. Figure C.4 shows the seismic pushover response and the deformed shape.

```
# OpenSees input file generated using MATLAB
model basic -ndm 2 -ndf 3
#
# Define source file (gravity analysis)
source exampleGravityInput.tcl
#
# Lateral Wind pushover profile load time series
timeSeries Linear 2 -factor 1.000000
pattern Plain 101020229 2 {
  load 101020209 -41.223884 0.000000 0.000000
}
pattern Plain 102020229 2 {
  load 102020209 -41.464717 0.000000 0.000000
}
pattern Plain 103020229 2 {
  load 103020209 -43.627370 0.000000 0.000000
}
pattern Plain 104020229 2 {
  load 104020209 -22.650376 0.000000 0.000000
}
#
# Analysis parameters
constraints Plain
numberer Plain
system UmfPack
test EnergyIncr 1.000000e-004 20
algorithm Newton
#
# Define response recorders
recorder Node -file exampleWindPushoverRecorderNodedisp.out -time -dof 1 2 3
disp
recorder Node -file exampleWindPushoverRecorderNodereaction.out -time -dof 1
2 3 reaction
integrator DisplacementControl 104020209 1 0.050000
set fidwrite2Name examplePushoversummary2.out
set fidwrite2 [open examplePushoversummary2.out w]
close $fidwrite2
#
# Solution strategy
[...]
```

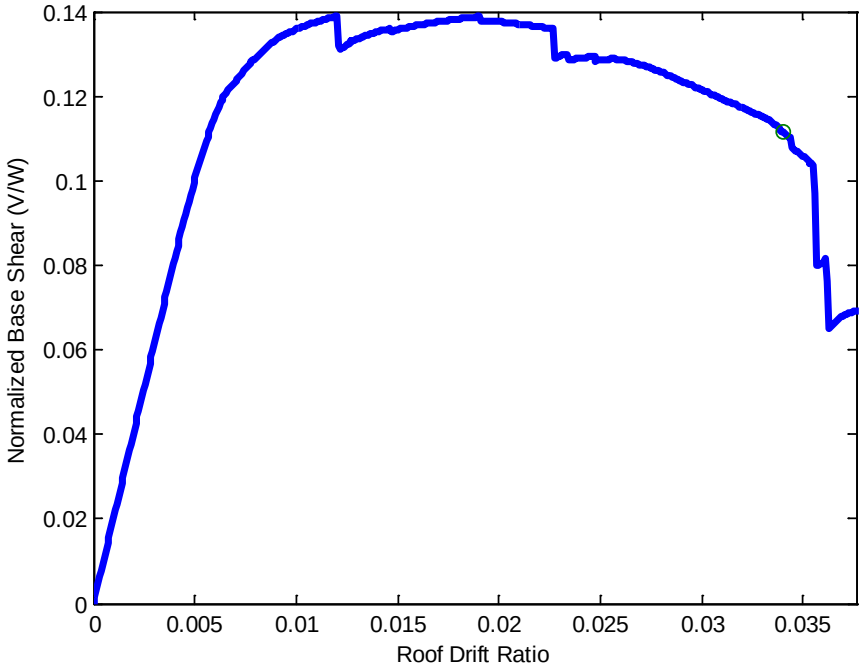

Figure C.4 Wind pushover response

C.5 Nonlinear Response History Analysis

C.5.1 Seismic Incremental Dynamic Analysis (IDA)

The following is an excerpt from the script used to define a typical seismic IDA.

```
# OpenSees input file generated using MATLAB
model basic -ndm 2 -ndf 3
#
# Define source file (gravity analysis)
source exampleGravityInput.tcl
#
# Ground motion
timeSeries Path 3 -dt $dtValue -filePath $filePathValue -factor $factorValue
pattern UniformExcitation 1 1 -accel 3
#
# Inherent non-explicitly-modeled damping
region 101020101 -ele 101020101 -rayleigh 0.156410 0.000000 0.002220 0.000000
region 101020102 -ele 101020102 -rayleigh 0.156410 0.000000 0.002220 0.000000
region 101020103 -ele 101020103 -rayleigh 0.156410 0.000000 0.002220 0.000000
region 101020104 -ele 101020104 -rayleigh 0.156410 0.000000 0.002220 0.000000
region 101020105 -ele 101020105 -rayleigh 0.156410 0.000000 0.002220 0.000000
region 101020106 -ele 101020106 -rayleigh 0.156410 0.000000 0.002220 0.000000
region 101020107 -ele 101020107 -rayleigh 0.156410 0.000000 0.002220 0.000000
region 101020108 -ele 101020108 -rayleigh 0.156410 0.000000 0.002220 0.000000
[...]

# Analysis parameters
constraints Plain
numberer Plain
system UmfPack
test EnergyIncr 1.000000e-004 20
algorithm Newton
# Define response recorders
recorder Node -file
exampleDynamicIDA.$recordName.runNo$runNo.RecorderNode101020209disp.out -time
-node 101020209 -dof 1 2 3 disp
recorder Node -file
exampleDynamicIDA.$recordName.runNo$runNo.RecorderNode102020209disp.out -time
-node 102020209 -dof 1 2 3 disp
recorder Node -file
exampleDynamicIDA.$recordName.runNo$runNo.RecorderNode103020209disp.out -time
-node 103020209 -dof 1 2 3 disp
recorder Node -file
exampleDynamicIDA.$recordName.runNo$runNo.RecorderNode104020209disp.out -time
-node 104020209 -dof 1 2 3 disp
integrator Newmark 0.500000 0.250000
#
# Solution strategy
set integratorType Newmark
set ok 0
set step 1
```

```
set numIncr $points
set dt $dtValue
set minNumSubStep 10
set testType EnergyIncr
set tol 0.0001
set maxIter 20
analysis VariableTransient
set dtMin [expr $dt/$minNumSubStep]
set dtMax $dt
set Jd 1
set algorithmType Newton
while {$ok == 0 && $step <= $numIncr} {
   set subStep $dt
   set tempIntegratorType $integratorType
   set ok [analyze 1 $subStep $dtMin $dtMax $Jd]
   if {$ok != 0} {
       puts "Temporarily try reduced (1/10) dtMin"
       set ok [analyze 1 $subStep [expr $minNumSubStep/10] $dtMax $Jd]
   }
   if {$ok != 0 && $algorithmType != "NewtonLineSearch"} {
       puts "Try Newton Line Search for this step"
       test $testType $tol [expr $maxIter*10]
       algorithm NewtonLineSearch
       set algorithmType NewtonLineSearch
       set ok [analyze 1 $subStep $dtMin $dtMax $Jd]
       if {$ok == 0} {puts "That worked .. continue with Newton Line Search"}
   }
   if {$ok != 0 && $algorithmType != "KrylovNewton"} {
       puts "Try Krylov-Newton for this step"
       test $testType $tol [expr $maxIter*20]
       algorithm KrylovNewton -initial
       set algorithmType KrylovNewton
       set ok [analyze 1 $subStep $dtMin $dtMax $Jd]
       if {$ok == 0} {puts "That worked .. continue with Krylov-Newton"}
   }
   if {$ok != 0 && $algorithmType != "BFGS"} {
       puts "Try BFGS for this step"
       test $testType $tol [expr $maxIter*1]
       algorithm BFGS
       set algorithmType BFGS
       set ok [analyze 1 $subStep $dtMin $dtMax $Jd]
       if {$ok == 0} {puts "That worked .. continue with BFGS"}
   }
   if {$ok != 0 && $algorithmType != "Broyden"} {
       puts "Try Broyden for this step"
       test $testType $tol [expr $maxIter*1]
       algorithm Broyden 8
       set algorithmType Broyden
       set ok [analyze 1 $subStep $dtMin $dtMax $Jd]
       if {$ok == 0} {puts "That worked .. continue with Broyden"}
   }
   if {$ok != 0 && $algorithmType != "ModifiedNewton"} {
       puts "Try Modified Newton for this step"
       test $testType $tol [expr $maxIter*20]
       algorithm ModifiedNewton
       set algorithmType ModifiedNewton
       set ok [analyze 1 $subStep $dtMin $dtMax $Jd]
```

```
        if {$ok == 0} {puts "That worked .. continue with Modified Newton"}
    }
    if {$ok != 0 && $algorithmType != "ModifiedNewtonInitial"} {
        puts "Try initial stiffness for this step"
        test $testType $tol [expr $maxIter*50]
        algorithm ModifiedNewton -initial
        set algorithmType ModifiedNewtonInitial
        set ok [analyze 1 $subStep $dtMin $dtMax $Jd]
        if {$ok == 0} {puts "That worked .. continue with initial stiffness"}
    }
    if {$ok == 0} {set tempTol $tol}
    if {$ok != 0} {
        puts "Temporarily try TRBDF2"
        integrator TRBDF2
        set integratorType TRBDF2
        set ok [analyze 1 $subStep]
        set ok [analyze 1 $subStep $dtMin $dtMax $Jd]
        if {$ok == 0} {puts "That worked .. back to Newmark"}
        if {$ok == 0} {set tempIntegratorType $integratorType}
        integrator Newmark 0.5 0.25
        set integratorType Newmark
    }
    if {$ok != 0} {
       puts "Try tolerance*10 "
       set tol 0.001
       algorithm NewtonLineSearch
       set algorithmType NewtonLineSearch
       set ok [analyze 1 $subStep $dtMin $dtMax $Jd]
       if {$ok == 0} {puts "That worked .. continue with Newton Line Search"}
       if {$ok != 0 && $algorithmType != "NetwonLineSearch"} {
           puts "Try Newton Line Search for this step"
           test $testType $tol [expr $maxIter*10]
           algorithm NewtonLineSearch
           set algorithmType NewtonLineSearch
           set ok [analyze 1 $subStep $dtMin $dtMax $Jd]
           if {$ok == 0} {puts "That worked .. continue with Newton Line
Search"}
       }
       if {$ok != 0 && $algorithmType != "KrylovNewton"} {
           puts "Try Krylov-Newton for this step"
           test $testType $tol [expr $maxIter*20]
           algorithm KrylovNewton -initial
           set algorithmType KrylovNewton
           set ok [analyze 1 $subStep $dtMin $dtMax $Jd]
           if {$ok == 0} {puts "That worked .. continue with Krylov-Newton"}
       }
       if {$ok != 0  && $algorithmType != "BFGS"} {
           puts "Try BFGS for this step"
           test $testType $tol [expr $maxIter*1]
           algorithm BFGS
           set algorithmType BFGS
           set ok [analyze 1 $subStep $dtMin $dtMax $Jd]
           if {$ok == 0} {puts "That worked .. continue with BFGS"}
       }
       if {$ok != 0 && $algorithmType != "Broyden"} {
           puts "Try Broyden for this step"
           test $testType $tol [expr $maxIter*1]
```

```
          algorithm Broyden 8
          set algorithmType Broyden
          set ok [analyze 1 $subStep $dtMin $dtMax $Jd]
          if {$ok == 0} {puts "That worked .. continue with Broyden"}
      }
      if {$ok == 0} {set tempTol $tol}
      if {$ok != 0} {
         puts "Try tolerance*100 "
         set tol 0.01
         algorithm NewtonLineSearch
         set algorithmType NewtonLineSearch
         set ok [analyze 1 $subStep $dtMin $dtMax $Jd]
         if {$ok == 0} {puts "That worked .. continue with Newton Line
Search"}
         if {$ok != 0 && $algorithmType != "NetwonLineSearch"} {
             puts "Try Newton Line Search for this step"
             test $testType $tol [expr $maxIter*10]
             algorithm NewtonLineSearch
             set algorithmType NewtonLineSearch
             set ok [analyze 1 $subStep $dtMin $dtMax $Jd]
             if {$ok == 0} {puts "That worked .. continue with Newton Line
Search"}
         }
         if {$ok != 0 && $algorithmType != "KrylovNewton"} {
             puts "Try Krylov-Newton for this step"
             test $testType $tol [expr $maxIter*20]
             algorithm KrylovNewton -initial
             set algorithmType KrylovNewton
             set ok [analyze 1 $subStep $dtMin $dtMax $Jd]
             if {$ok == 0} {puts "That worked .. continue with Krylov-
Newton"}
         }
         if {$ok != 0 && $algorithmType != "BFGS"} {
             puts "Try BFGS for this step"
             test $testType $tol [expr $maxIter*1]
             algorithm BFGS
             set algorithmType BFGS
             set ok [analyze 1 $subStep $dtMin $dtMax $Jd]
             if {$ok == 0} {puts "That worked .. continue with BFGS"}
         }
         if {$ok != 0 && $algorithmType != "Broyden"} {
             puts "Try Broyden for this step"
             test $testType $tol [expr $maxIter*1]
             algorithm Broyden 8
             set algorithmType Broyden
             set ok [analyze 1 $subStep $dtMin $dtMax $Jd]
             if {$ok == 0} {puts "That worked .. continue with Broyden"}
         }
         if {$ok == 0} {set tempTol $tol}
         if {$ok != 0} {
            puts "Try tolerance*1000 "
            set tol 0.1
            algorithm NewtonLineSearch
            set algorithmType NewtonLineSearch
            set ok [analyze 1 $subStep $dtMin $dtMax $Jd]
            if {$ok == 0} {puts "That worked .. continue with Newton Line
Search"}
```

```
            if {$ok != 0 && $algorithmType != "NetwonLineSearch"} {
                puts "Try Newton Line Search for this step"
                test $testType $tol [expr $maxIter*10]
                algorithm NewtonLineSearch
                set algorithmType NewtonLineSearch
                set ok [analyze 1 $subStep $dtMin $dtMax $Jd]
                if {$ok == 0} {puts "That worked .. continue with Newton Line
Search"}
            }
            if {$ok != 0 && $algorithmType != "KrylovNewton"} {
                puts "Try Krylov-Newton for this step"
                test $testType $tol [expr $maxIter*20]
                algorithm KrylovNewton -initial
                set algorithmType KrylovNewton
                set ok [analyze 1 $subStep $dtMin $dtMax $Jd]
                if {$ok == 0} {puts "That worked .. continue with Krylov-
Newton"}
            }
            if {$ok != 0 && $algorithmType != "BFGS"} {
                puts "Try BFGS for this step"
                test $testType $tol [expr $maxIter*1]
                algorithm BFGS
                set algorithmType BFGS
                set ok [analyze 1 $subStep $dtMin $dtMax $Jd]
                if {$ok == 0} {puts "That worked .. continue with BFGS"}
            }
            if {$ok != 0 && $algorithmType != "Broyden"} {
                puts "Try Broyden for this step"
                test $testType $tol [expr $maxIter*1]
                algorithm Broyden 8
                set algorithmType Broyden
                set ok [analyze 1 $subStep $dtMin $dtMax $Jd]
                if {$ok == 0} {puts "That worked .. continue with Broyden"}
            }
            if {$ok == 0} {set tempTol $tol}
            puts "Back to tolerance*100 "
            set tol 0.01
         }
         if {$ok == 0} {set tempTol $tol}
         puts "Back to tolerance*10 "
         set tol 0.001
      }
      puts "Back to original tolerance "
      set tol 0.0001
   }
   if {$ok == 0} {
      puts $step
      set currentTime [getTime]
      set numIteratons [testIter]
      set fidsolutioninfo [open $fidwrite2Name a]
      puts $fidsolutioninfo "$step $tempIntegratorType $currentTime
$algorithmType $numIteratons $tempTol"
      close $fidsolutioninfo
      set step [expr $step + 1]
   }
}
```

The following is the script used to advance the IDA analysis for a typical ground motion (LOS000 ground motion record). Figure C.5 shows the scaled response spectra, IDA curves, and the measured seismic collapse fragility curve.

```
# OpenSees IDA input file generated using MATLAB
#
# Initialization parameters
set recordName LOS000
set dtValue 0.010000
set points 1999
set filePathValue LOS000.tcl
set g 386.088000
set collapseIDR 0.200000
set collapseFlag 0
set maxCounter 200
set scaleFactor 0.200000
set scaleIncr 0.200000
set scaleTol 0.010000
set runNo 0
set fidwrite [open exampleDynamicIDALOS000summary.out w]
close $fidwrite
#
# Execute and evaluate dynamic response until collapse (IDA)
while {$scaleIncr >= $scaleTol && $runNo <= $maxCounter} {
   #
   # Initialize variables in run
   set runNo [expr {$runNo + 1}]
   set maxIDR 0.0
   set maxIDRstoryNo 0
   set factorValue [expr $scaleFactor*$g]
   #
   # Execute dynamic analysis
   set fidwrite2Name exampleDynamicIDALOS000.runNo$runNo.summary.out
   set fidwrite2 [open $fidwrite2Name w]
   close $fidwrite2
   source exampleDynamicIDAInput.tcl
   wipe
   #
   # Evaluate response for each story
   set prevStoryDisp 0.0
   #
   # Story 1
   set storyHeight1 180.000000
   set fidread1 [open
exampleDynamicIDA.$recordName.runNo$runNo.RecorderNode101020209disp.out r]
   #
   # Extract data from each row of recorder output
   set lineCount 0
   set minX1 0
   set maxX1 0
   while {[gets $fidread1 line] >= 0} {
```

```
      set fields [split $line " "]
      lassign $fields \
      time x y z
      if {$x < $minX1} {set minX1 $x}
      if {$x > $maxX1} {set maxX1 $x}
   }
   #
   # Calculate maximum story displacement
   set absMinX1 [expr abs($minX1)]
   if {$absMinX1 > $maxX1} {
      set storyDisp1 $absMinX1
   } else {
      set storyDisp1 $maxX1
   }
   #
   # Calculate maximum story drift
   set storyDrift1 [expr $storyDisp1 - $prevStoryDisp]
   #
   # Calculate story IDR
   set storyIDR1 [expr $storyDrift1/$storyHeight1]
   #
   # Save if this is the maximum IDR of the building
   if {$storyIDR1 > $maxIDR} {
      set maxIDR $storyIDR1
      set maxIDRstoryNo 1
   }
   #
   # Save this story displacement as the previous story disp
   set prevStoryDisp $storyDisp1
   close $fidread1
   #
   # Story 2
   set storyHeight2 156.000000
   set fidread2 [open
exampleDynamicIDA.$recordName.runNo$runNo.RecorderNode102020209disp.out r]
   #
   # Extract data from each row of recorder output
   set lineCount 0
   set minX2 0
   set maxX2 0
   while {[gets $fidread2 line] >= 0} {
      set fields [split $line " "]
      lassign $fields \
      time x y z
      if {$x < $minX2} {set minX2 $x}
      if {$x > $maxX2} {set maxX2 $x}
   }
   #
   # Calculate maximum story displacement
   set absMinX2 [expr abs($minX2)]
   if {$absMinX2 > $maxX2} {
      set storyDisp2 $absMinX2
   } else {
      set storyDisp2 $maxX2
   }
   #
   # Calculate maximum story drift
```

```
   set storyDrift2 [expr $storyDisp2 - $prevStoryDisp]
   #
   # Calculate story IDR
   set storyIDR2 [expr $storyDrift2/$storyHeight2]
   #
   # Save if this is the maximum IDR of the building
   if {$storyIDR2 > $maxIDR} {
      set maxIDR $storyIDR2
      set maxIDRstoryNo 2
   }
   #
   # Save this story displacement as the previous story disp
   set prevStoryDisp $storyDisp2
   close $fidread2
   #
   # Story 3
   set storyHeight3 156.000000
   set fidread3 [open
exampleDynamicIDA.$recordName.runNo$runNo.RecorderNode103020209disp.out r]
   #
   # Extract data from each row of recorder output
   set lineCount 0
   set minX3 0
   set maxX3 0
   while {[gets $fidread3 line] >= 0} {
      set fields [split $line " "]
      lassign $fields \
      time x y z
      if {$x < $minX3} {set minX3 $x}
      if {$x > $maxX3} {set maxX3 $x}
   }
   #
   # Calculate maximum story displacement
   set absMinX3 [expr abs($minX3)]
   if {$absMinX3 > $maxX3} {
      set storyDisp3 $absMinX3
   } else {
      set storyDisp3 $maxX3
   }
   #
   # Calculate maximum story drift
   set storyDrift3 [expr $storyDisp3 - $prevStoryDisp]
   #
   # Calculate story IDR
   set storyIDR3 [expr $storyDrift3/$storyHeight3]
   #
   # Save if this is the maximum IDR of the building
   if {$storyIDR3 > $maxIDR} {
      set maxIDR $storyIDR3
      set maxIDRstoryNo 3
   }
   #
   # Save this story displacement as the previous story disp
   set prevStoryDisp $storyDisp3
   close $fidread3
   #
   # Story 4
```

```
   set storyHeight4 156.000000
   set fidread4 [open
exampleDynamicIDA.$recordName.runNo$runNo.RecorderNode104020209disp.out r]
   #
   # Extract data from each row of recorder output
   set lineCount 0
   set minX4 0
   set maxX4 0
   while {[gets $fidread4 line] >= 0} {
      set fields [split $line " "]
      lassign $fields \
      time x y z
      if {$x < $minX4} {set minX4 $x}
      if {$x > $maxX4} {set maxX4 $x}
   }
   #
   # Calculate maximum story displacement
   set absMinX4 [expr abs($minX4)]
   if {$absMinX4 > $maxX4} {
      set storyDisp4 $absMinX4
   } else {
      set storyDisp4 $maxX4
   }
   #
   # Calculate maximum story drift
   set storyDrift4 [expr $storyDisp4 - $prevStoryDisp]
   #
   # Calculate story IDR
   set storyIDR4 [expr $storyDrift4/$storyHeight4]
   #
   # Save if this is the maximum IDR of the building
   if {$storyIDR4 > $maxIDR} {
      set maxIDR $storyIDR4
      set maxIDRstoryNo 4
   }
   #
   # Save this story displacement as the previous story disp
   set prevStoryDisp $storyDisp4
   close $fidread4
   #
   # Output information to stdout
   puts "$runNo $scaleFactor $maxIDR $maxIDRstoryNo"
   #
   # IDA output information (runNo,scaleFactor,maxIDR)
   set fidwrite [open exampleDynamicIDALOS000summary.out a]
   puts $fidwrite "$runNo $scaleFactor $maxIDR"
   close $fidwrite
   set fidwrite3 [open exampleDynamicIDALOS000summaryMaxIDRstoryNo.out a]
   puts $fidwrite3 "$runNo $scaleFactor $maxIDR $maxIDRstoryNo"
   close $fidwrite3
   #
   # Check to see if this analysis had a collapse
   if {$maxIDR >= $collapseIDR} {
      set scaleFactor [expr {$scaleFactor - $scaleIncr}]
      set scaleIncr [expr $scaleIncr/2]
      set scaleFactor [expr {$scaleFactor + $scaleIncr}]
      set collapseFlag 1
```

```
    } else {
        # Check to see if previously collapsed
        if {$collapseFlag == 0} {
            set scaleFactor [expr {$scaleFactor + $scaleIncr}]
        } else {
            set scaleIncr [expr $scaleIncr/2]
            set scaleFactor [expr {$scaleFactor + $scaleIncr}]
        }
    }
}
```

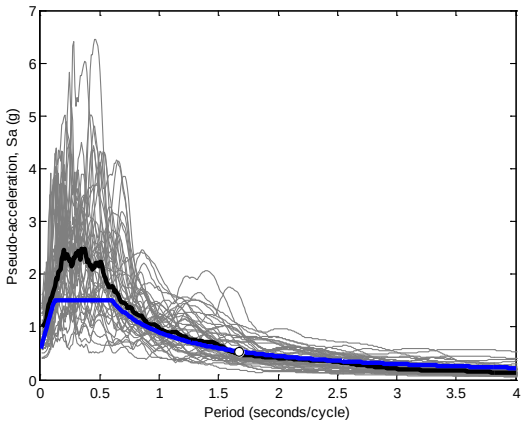

a) Scaled response spectrum: SDC D_{max}

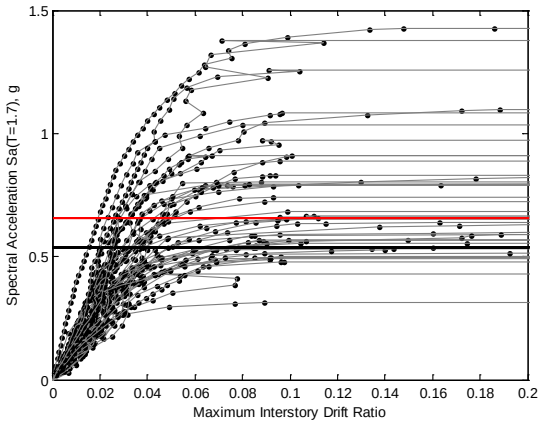

b) IDA curves

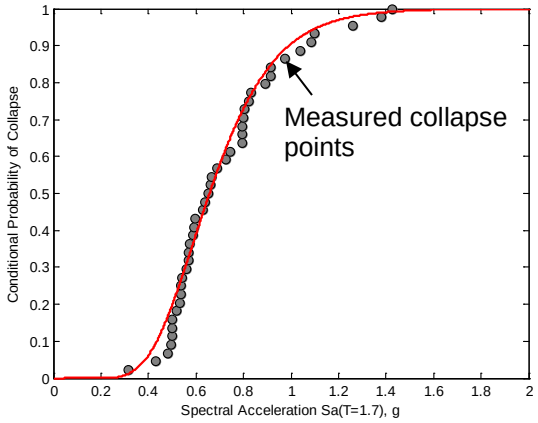

c) Measure seismic collapse fragility

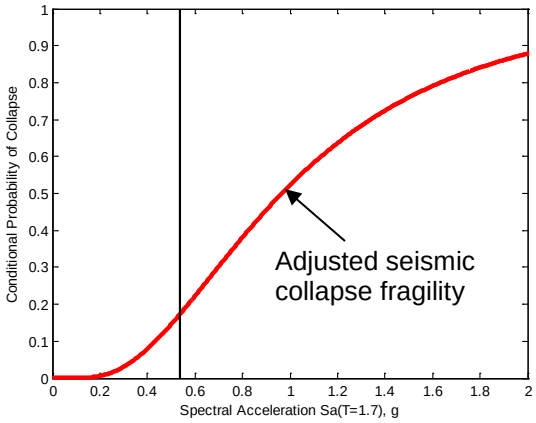

d) Adjusted seismic collapse fragility

Figure C.5 Seismic collapse assessment results

C.5.2 Wind Incremental Dynamic Analysis

The following is the script used to define the wind response history analysis for the along wind direction (90°) and the wind speed intensity at collapse (256 mph). Figure C.5 shows the scaled response spectra, IDA curves, and the measured seismic collapse fragility curve.

```
# OpenSees input file generated using MATLAB
# 15-Apr-2015 by Johnn Judd
# wipe
model basic -ndm 2 -ndf 3
#
# Node coordinates
node 1 0 0
node 2 0 0
#
# Boundary conditions
fix 1 1 1 1
fix 2 0 1 1
#
# SDOF system input parameters
set intensityFactor 1.000000
set Tn 1.673800
set zeta 0.010000
#
set pi 3.14159265359
set omega [expr 2*$pi/$Tn]
set k 10.000000
set m [expr $k/pow($omega,2)]
set c [expr 2*$m*$omega*$zeta]
set fy 1.0
#
# Node masses
mass 2 $m 0. 0.
#
# Node damping
rayleigh $c 0.0 0.0 0.0
#
# Coordinate transformation
geomTransf Linear 1
#
# Materials
set material "atc62_spring2a"
set degflag 1
set i 1
set N 1.000000
source materialList.tcl
set material "atc62_spring1a"
set degflag 1
set i 2
```

```
set N 0.744098
source materialList.tcl
#
# Element type, connectivity, and material
element zeroLength 1 1 2 -mat 1 -dir 1
element zeroLength 2 1 2 -mat 2 -dir 1
#
# Response recorders
recorder Node -file Cp_ts_g12040090.matInput55Node2.out -time -node 2 -dof 1
disp
recorder Element -file Cp_ts_g12040090.matInput55Element1.out -time -ele 1
force
recorder Element -file Cp_ts_g12040090.matInput55Element2.out -time -ele 2
force
recorder EnvelopeNode -file Cp_ts_g12040090.matInput55Node2Denvelope.out -
time -node 2 -dof 1 disp
#
# Loads for forced motion
set normFactor 0.873328
set scaleFactor [expr $normFactor*$intensityFactor]
timeSeries Path 1 -dt 0.008869 -filePath Cp_ts_g12040090.mat.tcl -factor
$scaleFactor
pattern Plain 1 1 {
load 2 1 0 0
}
#
# Analysis parameters
constraints Plain
numberer Plain
system BandGeneral
test NormDispIncr 1.0e-8 10
algorithm Newton
integrator Newmark 0.5 0.25
analysis Transient
#
# Execute analysis
analyze 115201 0.008869
#
puts "Finished nonlinear dynamic response-history analysis:
Cp_ts_g12040090.matInput55"
```

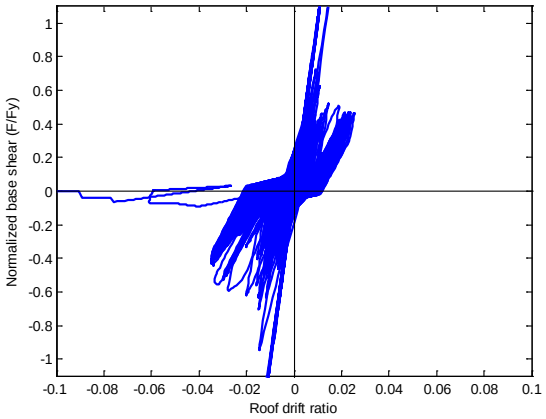

a) SDOF force-deformation

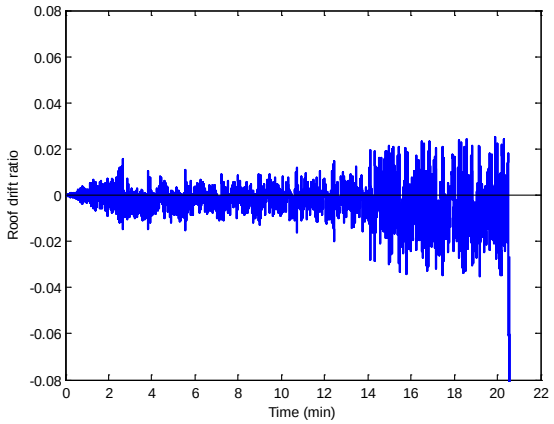

b) Roof drift ratio

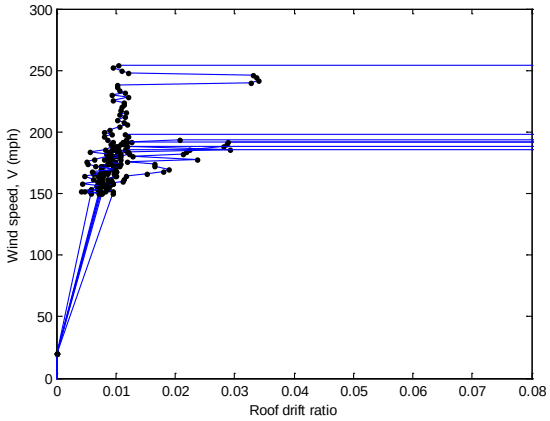

c) Wind IDA curves

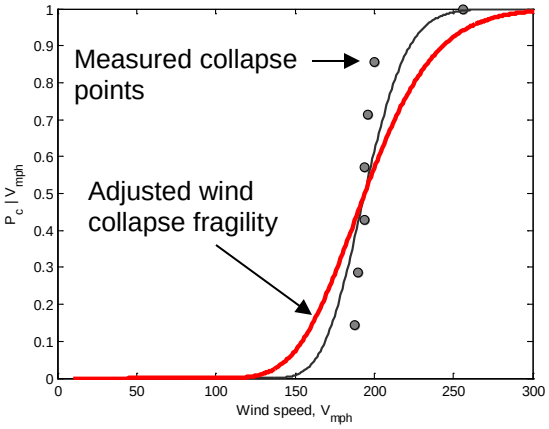

d) Wind collapse fragility

Figure C.6 Wind collapse assessment response for 90° (along-wind) and V_{mph} = 256 mph